LEPTON PAIR PRODUCTION

Moriond Workshop on Lepton Pair Production
Les Arcs - Savoie - France, January 25-31, 1981
LEPTON PAIR PRODUCTION
ISBN 2-86332-008-4
1981 - Editions Frontières, 7, Avenue Kennedy 28100 DREUX - France

Printed in Singapore by Singapore National Printers (Pte) Ltd.

Proceedings of the
FIRST MORIOND WORKSHOP
Les Arcs - Savoie - France, January 25-31, 1981

LEPTON PAIR PRODUCTION

Edited by
J. TRAN THANH VAN

Organizing Committee:

G. ALTARELLI
A.J.S. SMITH
F. VANNUCCI
and J. TRAN THANH VAN

FOREWORD

The first Moriond Workshop was held at Les Arcs, Savoie, (France) from January 25 to January 31, 1981 in the same spirit as the well known Rencontres de Moriond.

The main purpose of the Rencontres de Moriond is to discuss recent developments in contemporary physics and also to promote effective collaboration between experimentalists and theorists in similar fields. By bringing together a relatively small number of participants, the meeting hopes to develop better human relations as well as a more thorough and detailed discussion of the contributions in an informal and friendly atmosphere.

The first Moriond Workshop was focused on the study of lepton pair production. This important process which has been studied ten years ago experimentally by L. LEDERMAN and his group and theoretically by S. DRELL and YAN Tung Mow gave rise to some of the most important discoveries of the last few years : the new particles, ψ , γ and perhaps others in the future. The aim of this workshop is to summarize the important results obtained in this field where the concepts of quarks and colour are most relevant and which provides crucial tests for the only available strong interaction theory : Quantum-Chromo-Dynamics (QCD). It is hoped that this confrontation of ideas in this important field of physics allows the experimentalists to prepare a new generation of experiments with the incoming machines in order to deepen our knowledge on the basic structure of matter.

I would like to thank the organizing committee members : G. ALTARELLI, A.J.S. SMITH and especially the coordinator F. VANNUCCI for the hard work of organizing and preparing the scientific program and the Conference secretaries, M. BAILLY, J. BORATAV and L. NORRY, who have devoted much of their time and energy to the success of the first Moriond Wokshop.

I am also grateful to Mr. ASSIER the hotel director and Mr. TOURAILLE who contributed through their hospitality and cooperation to the well-being of the participants, enabling them to work in a relaxed atmosphere.

J. TRAN THANH VAN

CONTENTS

OPENING TALK: IMPORTANCE OF LEPTON PAIR PRODUCTION

G. Altarelli
Istituto di Fisica dell'Università - Roma
Istituto Nazionale di Fisica Nucleare - Roma

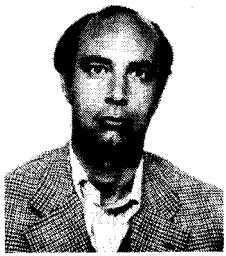

The aim of these introductory remarks is not to give in any sense a review of the growing subject of lepton pair production in hadron-hadron collisions[1,2]. Rather I would like to stress the importance of this class of processes and state their role in the present context of QCD phenomenology. I also want to mention a number of open questions or in general of problematic areas in the field. I am sure that some of these questions shall be answered, in part at least, during this same meeting while progress on some other issues will certainly follow from the information and the impulse gathered in these days of common work.

QCD is the result of two decades of continous development, both experimental and theoretical, in many areas of particle physics from hadron spectroscopy and the phenomenology of deep inelastic phenomena to the theory of relativistic quantum fields. The fundamental notion of fractionally charged quarks, really revolutionary in that it implies confinement, emerged out of hadron spectroscopy and was later established by the success of the (so to say) naive parton model in electron and neutrino scattering. The demise of hadrons from the rank of elementary particles to the more modest status of composite objects brought back the possibility of a description of strong interactions in terms of a basic field theory. A parallel formidable progress in the theory of quantum fields was taking place leading to the formulation, the quantization and the renormalization of non abelian gauge theories, to the development of operator expansion techniques and to the study of the potentiality of the renormalization group equations including the notion of asymptotic freedom and the realization of the unicity of non abelian gauge theories in this respect. At the same time the construction and the impressive success of the gauge theory of electro-weak interactions imposed gauge invariance as the unifiyng principle for the theory of fundamental interactions, gravity included, thus directly pointing to an extension of the same structure to the strong interactions as well. QCD as a gauge theory of coloured quarks and gluons is unique among renormalizable theories in providing a basis for the parton model within the basic principles of quantum field theory. The selection of SU (3) as colour group is also unique in view of a) the fact that the group must admit complex representations because it must be able to distinguish a quark from an antiquark (there are meson states made up of $q\bar{q}$ but not similar qq bound states). b) There must be colour singlet, completely antisymmetric states made up of qqq (baryons). c) The number of colours for each kind of quarks must be in agreement with the data on $\pi^{o} \to 2\gamma$ and on $R_{e^+e^-}$. Within simple groups a) restricts the choice to $SU(n \geq 3)$, $SO(4n+2 \geq 10)$ and E6 and b) and c) directly lead unambigously to SU(3). Thus QCD stands to day as a main building block of the standard model based on $SU(3) \otimes SU(2) \otimes U(1)$ for the hadro-electro-weak interactions (at down to earth energies).

Although QCD emerges as essentially the only possible theory for the strong

interactions within reach of the weapon arsenal of present theoretical physics, yet QCD is far from being established even as a viable theory. Two main questions are in fact pending. First this theory is based on the conjecture that colour symmetry is exact. Second in its present formulation one is not yet able to prove that confinement is contained in the theory as a necessary implication. On this last crucial question some insight has been recently accumulated from the study of gauge theories on a lattice and from the analysis of the structure and the topological properties of non abelian gauge theories[3]. The results are encouraging and make confinement perhaps more believable today than in the past. Yet a real proof is lacking. On the other hand the observation of colour liberation would also impose a radical revision of our views. Therefore QCD must be still considered as a tentative theory.

Thus testing QCD is particularly important in that it represents the less established sector of the standard model. Testing QCD is however difficult. In particular it is more difficult than testing the electroweak sector, because there the interaction is so weak that perturbation theory is always reliable and moreover the leptons are at the same time the fields of the lagrangian and the particles in our detectors. On the contrary QCD is a theory of quarks and gluons while the real world is made up of hadrons. Also perturbative methods, our almost unique tool, are only applicable in particular domains of strong interaction physics, where the freedom, which is only asymptotic, can be reached.

Deep inelastic phenomena immediately emerge as the natural testing ground for QCD. In fact on one hand the hadronic unknowns are reduced to a minimum when restricting to hadron-current interactions. On the other hand the conditions of high energy and deep inelasticity make perturbation theory applicable. The difficulty of testing QCD is reflected in the fact that no single process provides by itself a clear cut and definite experimental proof of the theory. In view of a number of ifs and buts that can be raised against any given experiment it is clear that our confidence on QCD rests at present on the overall picture which is emerging from several processes and many different kinds of tests.

Among the phenomena which could be thought as providing us with gold plated QCD tests the most prominent ones are of course totally inclusive deep inelastic leptoproduction and the total e^+e^- cross section at high energy. In fact the theory of scaling violations in leptoproduction is cristal clear and offers a large set of independent quantities to measure and compare with the theory. The experiments are indeed becoming more and more refined and complete. All data are beautifully consistent with QCD[4]. This is of course of invaluable importance. However critical people may observe, and in fact do, that one cannot really prove from the existing data on structure functions that the mechanism for scaling violations is precisely the one implied by QCD. Indeed, due to the limita-

tions on the available Q^2 range, which makes it difficult to tell logs from powers, and to the onsetting of theresholds, it cannot be strictly excluded that some part or even the totality (as some extremists may say) of the observed scaling violations could be attributed to conventional breakings of the naive parton model or to some other mechanism. Of course these objections could be experimentally settled by looking at the final state and by showing, for example, that the average jet transverse momentum at fixed scaling variables is increasing linearly with the energy scale. This would be a typical signature for a hard parton mechanism of scaling violations. But for this test, which is to some extent supported by the data, one must go out of the light-cone protected domain of gold plated tests.

Similar is the situation for the total cross section of e^+e^- annihilation. The theory is also very clean. The purist's resistance to crossing from negative to positive q^2 values can be subdued. The experimental approximate validity of different asymptotic limits below each threshold is in fact a test of the whole precedure. Also it must be stressed that this is an absolute prediction with no hadronic unknowns. The avaiable energy reaches up to $Q^2 = 10^3$ GeV^2. The experimental success of the really emblematic parton formula $R = 3 \sum_{\text{flavours}} q_f^2$ (q_f = = charge of quarks of flavour f) is striking. Yet one may object that only a single number is measured and that after all the subleading QCD logs are not experimentally disintangled. One could take it as a success for the parton model, seen as a special gift of light cone dominance, rather than a test for a specific, in some sense unique theory, behind it (apart from the fundamental and not questioned experimental proof for the existence of colour). Once more, and in this case in spectacular forms, the best scores for QCD are obtained when the final state is analyzed. The recent work carried on at Petra[5] has shown that in fact the final state looks precisely as QCD had predicted. Even in front of that one may observe that much of the success is merely semiquantitative, that some important aspects are still lacking a precise test, that the quantitative predictions within QCD of some of the measured properties of the final state are not really safe, the importance of non leading corrections in many such cases being still under debate[6]. And of course in any case again one is out of the gold plated, light cone governed domain.

The whole experimental evidence at our disposal, even if taken in the most conservative way, certainly indicates that the validity of parton dynamics extends well beyond the domain of those simplest quantities that are related to the dominant singularities on the light cone. In this respect the importance of Drell-Yan processes as a very stringent probe of parton dynamics is really imposing. In these processes the parton results cannot be linked in any way to light cone or short distance properties. As one considers a completely inclu-

sive quantity (as far as the hadrons in the final state are concerned) the Drell-Yan cross sections only depend on parton densities and not on fragmentation functions. This allows on one hand a direct, absolute computation from the parton densities already measured in leptoproduction of the cross sections in the channels P-Nucleon and $\bar{P}$-Nucleon and, on the other hand, it provides us with a unique possibility of measuring otherwise unaccessible parton densities as those related to pion and kaon structure functions. The experimental proof of the dominance in the pion structure functions of the valence versus sea components, for example, is not at all a trivial result because is can be viewed as a natural expectation only in the parton picture. Moreover the Drell-Yan cross section is quadratic in the parton densities, which means testing the parton model in a particularly complicated dynamical situation. There are effects which may destroy parton results associated with non linear quantities while preserving linear predictions. A possible example, discussed in the literature[7], is associated with instantons.

The strategy in testing QCD must be based on a sequence of natural steps. First one must establish the approximate validity of the naive parton model. Once it has been verified that the parton mechanisms are indeed dominant, then it makes sense to study the structure of the deviations from the naive parton dynamics and to compare these violations with the QCD predictions. Now Drell-Yan processes have the advantage of offering very clear cut signatures for the underlying parton mechanism. We recall the main ones: a) Intensity rules. The cross sections of the valence dominated processes $\pi^{\pm}$ N, K^{-} N, $\bar{P}$ N .. should be much larger, expecially at larger values of τ , than those of the sea dominated processes P N, K^{+}N. Similarly the $\pi^{\pm}$ cross sections on isoscalar targets should approach a ratio of 4 at large values of τ where the sea densities can be neglected. b) The angular distribution of the leptons in their center of mass should be $1 + \cos^2\theta$, that is purely transverse, with respect to a reference line asymptotically coincident with the hadron-hadron direction. c) The dependence on the atomic number of the nuclear target should be linear in the parton regime, because the number of partons in the target increases in proportion to the number of nucleons. d) Scaling should be approximately true and adimensional quantities as for example $Q^3 d\sigma/dQ$ should approach functions of only the variable τ.

The available experimental evidence on lepton pair production at sufficiently large energies and for masses of the pair beyond the J/Ψ confirms the validity of all the previous distinctive features, as amply discussed in these Proceedings. This very neat success of the parton model strenghtens the point that the general theoretical framework for its derivation is not limited to a study of the leading light cone singularities but rather, at the naive scaling level, is

to be found in a diagrammatic analysis of softened field theories. And in fact Drell and Yan proposed[1] their mechanism for lepton pair production precisely on the basis of a field theory model with an external cut off on transverse momentum. The validity of the same type of analysis is carried on to QCD with the only difference that the cut off on transverse momentum is removed (thus giving up exact scaling) and is in a way replaced by asymptotic freedom, its closest analogue in renormalizable field theories.

It is therefore important to refine and extend the experimental analysis in order to precisely determine the domain of validity and the accuracy of the naive parton approximation. The next question is whether or not the QCD effects deviating from the naive parton model are visible in the data. The first and the theoretically most evident of such predictions is the presence of logarithmic scaling violations. In fact the closest analogue to the parton model in QCD is obtained in the leading logarithmic approximation (LLA), that is when all terms down by powers of $\alpha_S(Q^2)$ are neglected. In the LLA all parton formulae keep their validity, as guaranteed by the factorization theorem, provided the naive scaling parton densities are replaced by Q^2 dependent effective parton densities, whose Q^2 dependence is governed, at order $\alpha_S(Q^2)$, by the well known evolution equations. As a consequence it is expected that scaling is broken logarithmically, as in leptoproduction, namely for example that $Q^3 d\sigma/dQ = F(\tau, \ln Q^2)$. The presence of these scaling violations is however not directly visible in the data which cannot, at this stage, be precise enough to show such a delicate effect. This is particularly true in Drell-Yan processes in view of the extremely steep dependence of the cross section on Q^2, which makes all problems of precise normalization quite difficult.

Fortunately there are more efficient ways of detecting the same physical effect in different forms than from scaling violations. As already mentioned in the case of leptoproduction, it is through the observation of a linear increase with energy of the average transverse momentum P_T of the parton jets in the final state that one can detect the hard parton origin of scaling violations. In fact the emission of a hard gluon from a quark (or the production of a hard $q\bar{q}$ pair from a gluon) generates a tail of order α_S in the P_T distribution of the final parton jets, which behaves at large P_T as $1/P_T^2$. The total P_T distribution can then be written schematically as:

$$\frac{d\sigma}{dP_T^2} = \delta(P_T^2) + \alpha_S \frac{1}{P_T^2} + \ldots \qquad (1)$$

The first term corresponds to the naive parton model approximation when the intrinsic p_T component is neglected because, being energy independent, it is not relevant here. Integration of the above distribution over phase space leads to the scaling violation logs in the total cross section:

$$\sigma \sim \int^{\sim Q^2} \frac{d\sigma}{dp_T^2}\, dp_T^2 \sim 1 + \alpha_S \ln Q^2 + \ldots \qquad (2)$$

However this small (because it is of order α_S) but long tail (because it extends up to Q^2) leads to a relatad, computable increase of the average p_T^2:

$$< p_T^2 > \sim \int^{\sim Q^2} p_T^2\, \frac{d\sigma}{dp_T^2}\, dp_T^2 \simeq \alpha_S Q^2 + \ldots \qquad (3)$$

where the dots stand for non calculable constant terms. The above schematic derivation holds both for leptoproduction and Drell-Yan processes. In the latter case the precise result can be cast in the form[8]:

$$< p_T^2 > = \alpha_S(Q^2)\ S\ f\ (\tau, \ln Q^2) + \ldots \qquad (4)$$

and analogue relations for other p_T moments. Of course the increase of p_T^2 with Q^2 or S is only predicted at fixed values of the scaling variable τ.

A remarkable feature of Drell-Yan processes is that the relevant p_T distribution is more easily measured in comparison to other processes. It is in fact determined by the total p_T of the lepton pair. This is to be contrasted to other processes, for example leptoproduction, where this test demands a difficult reconstruction of the parton p_T from the sum of the momenta of all the hadrons in the jet. Thus it is not surprising that, while the direct observation of scaling violations in Drell-Yan processes is not possible, the increase of the average p_T or p_T^2 is instead apparent both in P N collisions (where the very high energy ISR data are extremely useful in this respect) and in $\pi^{\pm}$N data. This is a clear cut deviation from the naive parton model in agreement with QCD expectations.

An important task for the near future is the improvement of the above test from the qualitative to the quantitative stage by precise measurements and comparison to the theory of the slope functions $f(\tau, \ln Q^2)$ in eq. 4 for different p_T moments and different processes. At present there are still gaps to be filled both by theory and experiment before one can be really conclusive on this point. More statistics and more energy binnings are demanded to experiment. On the theoretical side there are still uncertainties in the slope prediction which may amount to factor up to 2-3 or so. This arises mainly from our ignorance of non leading terms. For example we wrote $\alpha_S(Q^2)$ in eq. 4, but we could as well have written $\alpha_S(< p_T^2 >)$. As Q^2 is typically of order 50 - 60 GeV^2 and $< p_T^2 > \simeq 2$ GeV^2, the difference makes about a factor of 2, for reasonable values of Λ. This is because the LLA is strictly justified only in presence of a single energy scale,

namely, in the present case only for $p_T \simeq Q$. A useful result in this connection was the resummation[9)10)] of the leading logs of the form $\ln p_T^2/Q^2$ which are absent when $p_T \simeq Q$ but are instead important when two large scales are present, i. e. in the limit $M^2 << p_T^2 << Q^2$. Such studies indicate that $\alpha_S(< p_T^2 >)$ is presumably a better choice, but the available ranges of Q and p_T values do not really allow a meaningful application of this approximation. On a different line of approach to the problem, the hard computation of the terms of order $\alpha_S^2(Q^2)$ in the slope functions, which is currently being carried on,[14)] will make the issue of the non leading terms hopefully more clear. In P N or K^+N collisions further ambiguities in the slope calculation are added by our relative ignorance of the sea and gluon densities which determine the result in this case. On the other hand estimates of the p_T distributions in π^-N pair production show the dominance of the $q\bar{q}$ term over the $(q+\bar{q})G$ term. Incidentally this fact implies that the recoiling hadronic jet at opposite high p_T is, with large probability produced by a gluon; a good chance to study the gluon hadronization. In conclusion the study of the p_T distributions in Drell-Yan processes well deserves further efforts being one of the main practical approaches to the QCD dynamics.

Besides scaling violations and the increase with energy of the average p_T a third effect which is also of great interest for establishing the relevance of QCD in Drell-Yan processes is the issue of normalization for the cross section, that is the well known K factor problem. We have seen that the parton formulae in terms of effective parton densities are valid in QCD within the LLA and are therefore broken by terms down by powers of $\alpha_S(Q^2)$. In order to evaluate the first order corrections it is preliminarly necessary to precisely specify what is meant by parton densities beyond the LLA. This is for example done by specifing that the quark densities are to be measured from the structure function F_2 of leptoproduction at the same absolute value of the virtual photon mass. Once the parton densities have been specified one can then compute in a non ambiguos way the corrections of order $\alpha_S(Q^2)$ to the parton formulae for all other processes. The explicit evaluation of the first order correction to the parton formula for the cross section of Drell-Yan processes[11)] has led to a surprisingly large result which rescales upward the $q\bar{q}$ term, while all $(q + \bar{q})G$ corrective terms are of normal size and thus negligible in most cases. The physical origin of this result is clear: it can be traced back to the continuation of q^2 from the spacelike region in leptoproduction to the timelike region in lepton pair production and to the difference in phase space between the two processes (the heavy photon is in the initial state in one case and in the final state in the other case). Detailed studies[12)] of the first order correction show that it is approximately a constant in the limited τ range of the data and most of the rapidity range. Taken at face value it should amount at current

energies and τ values to a rescaling of the cross section upward by factor of about 2. The homogeneity of the correction in $q\bar{q}$, its near constancy and the fact that it appears only in the transverse part explains how it is that the tests for the parton mechanism mentioned previously are not affected. The presence of a nearly universal and constant factor of the right sign and magnitude is impressively confirmed by the data in all the available channels. What is most impressive is that the experiments seem to closely reproduce all the quantitative features of the first order result, although its magnitude clearly should correspond to a breakdown of the perturbative expansion in $\alpha_S(Q^2)$. The answer to this puzzle is to some extent provided by the arguments suggesting the resummation and factorization of the largest contributions to this effect[13]. The terms arising from the continuation of the form factor from spacelike to timelike values of q^2 are factorizable provided the double logs of the vertex exponentiate in QCD as they do in abelian theories. The exponentiation of the logs from the phase space effect is implied for the real emission diagrams by the factorization of the $\ln Q^2$ singularities. An obvious task for the theory is to put these arguments on a more solid basis in order to understand the K factor more completely. On the experimental side it is important to study this effect more in detail by detecting its dependence on the scaling variables and on Q^2.

Continuum $\mu^+\mu^-$ production does not exhaust the lines of research of main interest in the field. We mention for example the study of -onia production (the discovery of J/Ψ and of T clearly illustrates the great power of this technique in exploring new territories of physics). The comparison of continuum versus resonance production clearly illustrates the differences in the underlying production dynamics. Much work is still demanded for an understanding of the mechanism of resonance production. Also very important in practice is the extensive work in preparation to the $W^{\pm}$ and Z_0 production experiments at the $P\bar{P}$ collider which shall soon considerably extend the domain of lepton pair production. Finally a particular mention is amply deserved by the analysis of real photon production at large p_T in hadron-hadron collisions. This process, closely related to Drell-Yan production , is also of interest in perturbative QCD in that class of phenomena that starting at order α_S have no naive parton model analogue and can be predicted at present only within uncertainties similar to those encountered in discussing large p_T distributions in Drell-Yan processes. This fact is stated here in that problematic areas are interesting areas as mentioned already at the beginning of this talk.

In conclusion it is clear that Drell-Yan physics is of fundamenal importance in QCD phenomenology because it offers invaluable complementary information to that obtained from deep inelastic leptoproduction and e^+e^- annihilation.

In particular it is a very severe probing of the validity of parton dynamics with clean experimental signatures. It also offers unique possibilities of testing in detail hard parton effects, computable in principle in QCD and also in practice with an accuracy which is increasing with time.

References

1. S. Drell, T. M. Yan, Phys. Rev. Letters 25 (1970) 316; Annals of Phys. 66 (1971) 578.
2. For recent reviews see for example:
   G. Altarelli in "Proceedings of the Int. EPS Conference on High Energy Phys". Geneva 1979, page 727; L. Lyons, Oxford Univ. Preprint 80/80, to appear in "Progress in Particle and Nuclear Physics"; G.Matthiae CERN-EP Preprint 1980.
3. See for example G. Parisi in "Proceedings of the XX Int. Conference on High Energy Physics", Madison, 1980.
4. See for example:
   J. Steinberger CERN-EP/80-222 leectures given at the E. Majorana Int. School of subnuclear Physics, Erice 1980.
   E. Reya Preprint Dortmund Univ. DO-TH 80/27 lectures given at the Int.School of Elementary Particle Physics, Kupari-Dubrovnik, 1980.
5. See for example:
   B. Wiik in "Proceedings of the XX Int. Conference on High Energy Physics, Madison 1980.
6. See for example:
   R. K. Ellis, D. A. Ross, A. E. Terrano Caltech Preprints 68-783 and 68-785, 1980.
7. J. Ellis, M. K. Gaillard, W. J. Zakrzewski Phys Letters 81B (1979) 225
8. See for example the talk by D. Scott in these Proceedings.
9. The first attempt was by Y.L. Dokshitzer, D. I. D'Yakonov, S. I. Troyan Phys. Letters 78B (1978) 290. The correct formula was written down by G. Parisi, R. Petronzio, Nucl. Phys. B154 (1979) 427.
10. See the talks by J. Cleymans, J. C. Collins, M. Greco, G. Pancheri-Srivastava, D. E. Soper; these Proceedings.
11. J. Kubar-Andrè, F. E. Paige, Phys. Rev. D19 (1979) 221 G. Altarelli, R.K. Ellis, G. Martinelli; Nucl. Phys. B143 (1978) 521, E B146 (1978) 544.
12. G. Altarelli, R. K. Ellis, G. Martinelli, Nucl. Phys. B157 (1979) 461
    J. Kubar, M. le Bellac, J. L. Meunier, G. Plaut, Nice Univ. Preprint NTH 80/8, 1980 (see the talk by G. Plaut, these Proceedings).
13. See for example the talk by M. Greco (These Proceedings) and ref. therein.
14. R. K. Ellis, G. Martinelli, R. Petronzio presented by G. Martinelli at this Meeting.

A COMPENDIUM OF FORMULAE FOR LEPTON PAIR PRODUCTION

R.K. Ellis
CERN -- Geneva, Switzerland

A B S T R A C T

I present a collection of theoretical results for the production of lepton pairs in hadron-hadron collisions.

Ten years ago, Drell and Yan[1] proposed a mechanism for the production of lepton pairs in hadron-hadron collisions based on the annihilation of a parton antiparton pair. In the subsequent years our knowledge of the constituents of hadrons and their interactions has grown to such an extent that the original model of Drell and Yan has come to be called naïve. In this appendix I will present some of the formulae of the naïve Drell-Yan model before going on to describe the results of its more sophisticated sibling, the QCD parton model. I will give results for the Drell-Yan total cross-section and the cross-section differential in the rapidity. Special emphasis will be given to the definition of parton densities beyond the leading order in QCD and to the predictions for the transverse momentum distribution of the muon pairs.

The basic interaction of the naïve parton model is shown in Fig. 1, where a quark coming from one hadron and an antiquark coming from the other annihilate to produce a massive photon which subsequently materializes into a muon or electron pair. The corresponding cross-section is given by

$$\frac{d\sigma}{dQ^2} = \frac{4\pi\alpha^2}{9SQ^2} \int_0^1 dx_1 \int_0^1 dx_2 \sum_f e_f^2 \left\{ q_{0f}^{[1]}(x_1)\, \bar{q}_{0f}^{[2]}(x_2) + (1 \leftrightarrow 2) \right\} \delta(x_1 x_2 - \tau) \qquad (1)$$

In this formula $\sqrt{S}$ is the invariant mass of the incoming hadron system, $\tau = Q^2/S$ and Q^2 is the invariant mass squared of the massive photon and hence of the produced lepton pair. The symbol $q_{of}^{[1]}(x_1)$ indicates the probability to find a quark of flavour f inside hadron 1 with a fraction x_1 of the longitudinal momentum of hadron 1 and the subscript "o" indicates that these are naïve (scale independent) parton densities in the sense which will be made more precise below. The reaction is quadratic in α, the electromagnetic coupling constant and the strength of the coupling to various flavours of quarks is determined by e_f, the electric charge of the quark of flavour f, expressed in units of the electron charge. The quark distribution functions are constrained by the conservation of charge,

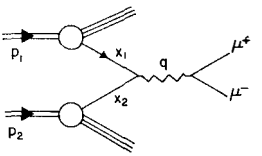

Fig. 1

$$\int_0^1 dx \left[q_{0f}^{[h]}(x) - \bar{q}_{0f}^{[h]}(x) \right] = v_f^{[h]} \qquad (2)$$

where $v_f^{[h]}$ is the valence value of the quark of flavour f inside hadron h. Equation (1) contains a colour factor of $1/3$ which expresses the fact that a coloured quark can only annihilate with a quark of equal and opposite colour.

Certain comments about the range of validity of Eq. (1) are in order. Equation (1) is derived in the impulse approximation which will receive its field theoretic justification when we go on to consider QCD. No account is taken of cooperative effects between quarks within a given hadron which in most kinematic regions are smaller by powers of $1/Q^2$.

In most experimental configurations which have a limited angular acceptance a more differential cross-section is appropriate. These are normally expressed either in terms of the Feynman x_F variable or the rapidity y. These variables are defined in the hadron-hadron centre of mass system where the massive photon (muon pair) has momentum components (hadron beams directed along z direction)

$$q = (E, \vec{q}_\perp, q_z) \qquad (3)$$

In this system the variables mentioned above are given by

$$x_F = \frac{2q_z}{\sqrt{S}} \qquad y = \frac{1}{2} \ln \frac{(E+q_z)}{(E-q_z)} \qquad (4)$$

It is clear from Fig. 1 that specification of the mass and longitudinal momentum of the muon pair completely fixes the values of x_1 and x_2 of the annihilating quarks, since in the naïve parton model the transverse momentum is constrained to be zero and,

$$x_F = x_1 - x_2 \tag{5}$$

The Feynman x_F differential cross-section is hence given by,

$$\frac{d^2\sigma}{dQ^2 dx_F} = \frac{4\pi\alpha^2}{9SQ^2} \frac{1}{(x_1^0+x_2^0)} \sum_f e_f^2 \left\{ q_{0f}^{[1]}(x_1^0)\, \bar{q}_{0f}^{[2]}(x_2^0) + (1\leftrightarrow 2) \right\} \tag{6}$$

where the parton distributions are evaluated at the points,

$$x_1^0 = \frac{1}{2}\left[x_F + \sqrt{(x_F^2+4\tau)} \right] \tag{7}$$

$$x_2^0 = \frac{\tau}{x_1^0} = \frac{1}{2}\left[-x_F + \sqrt{(x_F^2+4\tau)} \right] \tag{8}$$

In terms of the rapidity variable the cross-section has an entirely similar form,

$$\frac{d^2\sigma}{dQ^2 dy} = \frac{4\pi\alpha^2}{9SQ^2} \sum_f e_f^2 \left\{ q_{0f}^{[1]}\left(\sqrt{\tau}\, e^{y}\right) \bar{q}_{0f}^{[2]}\left(\sqrt{\tau}\, e^{-y}\right) + (1\leftrightarrow 2) \right\} \tag{9}$$

In the context of the naïve parton model the differential cross-sections, Eqs (6) and (9) can be used to map out the shapes of the parton distribution functions.

The most positive feature of the naïve Drell-Yan formula was that it allowed the prediction of the lepton pair production cross-section in terms of parton distribution functions derived from deep inelastic scattering (DIS). As we shall see it is precisely this operational definition of parton densities which is the cornerstone of the treatment of the Drell-Yan process in perturbative QCD. It is therefore to the $O(\alpha_s)$ corrections to DIS that we must turn before we can treat the Drell-Yan process.

The lowest order contribution to DIS is shown in Fig. 2a where a spacelike photon scatters off a quark. Radiative corrections to this process are shown in Figs 2b,c,d. In the same order in the strong coupling constant α_s we must also consider the effects of incoming gluons shown in Fig. 3. The value of the structure function F_2 derived from these diagrams is given as follows,

$$\frac{F_2(x,t)}{x} = \int_x^1 \frac{dy}{y} \left\{ \sum_f e_f^2 \left[\delta\left(1-\frac{x}{y}\right) + \frac{\alpha_s}{2\pi} t\, P_{qq}\left(\frac{x}{y}\right) + \alpha_s\, f_q^{DIS}\left(\frac{x}{y}\right) \right] q_{0f}(y) \right.$$

$$\left. + \sum_f e_f^2 \left[\frac{\alpha_s}{2\pi} t\, P_{qG}\left(\frac{x}{y}\right) + \alpha_s\, f_G^{DIS}\left(\frac{x}{y}\right) \right] G_0(y) \right\} \qquad (10)$$

where,

$$t = \ln \frac{Q^2}{\mu^2}, \quad P_{qq}(z) = \frac{4}{3}\left(\frac{1+z^2}{(1-z)_+} + \frac{3}{2}\delta(z-1) \right), \quad P_{qG}(z) = \frac{1}{2}\left(z^2 + (1-z)^2 \right) \qquad (11)$$

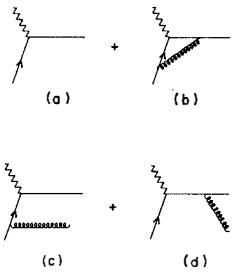

Fig. 2

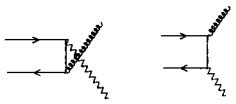

Fig. 3

and the "plus function" is defined in terms of its integral with an arbitrary function f,

$$\int_0^1 dx \frac{f(z)}{(1-z)_+} = \int_0^1 dz \frac{f(z) - f(1)}{(1-z)} \tag{12}$$

The scale μ in Eq. (10) is a cut-off introduced to control the singularity coming from the amplitudes of Figs 2c,d when the gluon is parallel to the incoming quark. The presence of the logarithmic term in Eq. (10) dependent on the scale μ is a potential disaster. Unless we can eliminate the scale μ and the associated large logarithm the asymptotic freedom of the theory will be of no avail; at all values of Q^2, the structure function [Eq. (10)] will be sensitive to the scale μ and hence the low momentum behaviour of the theory about which we have scarse theoretical information.

It turns out that all these large logarithms can be factored out of the perturbative cross-section and into the parton densities in a sensible fashion as first suggested by Politzer[2]. Politzer's observation was that the large logarithms were due to the degeneracy between the state of one parton (e.g., a quark) and the state containing several parallel partons (e.g., a quark and a gluon) and that this energy degeneracy made it clear that the singularities were a feature of the long-time physics of the hadronic wave function rather than the short-time physics of the deep inelastic scattering. The coefficients of the logarithms are independent of the particular hard process and depend only on the parton type. Before proceeding to define the parton densities using this philosophy we note two further features of Eq. (10). Firstly, the constant pieces f beneath the logarithms are ambiguous in any particular regularization scheme. Secondly, the diagrams with incoming gluons (Fig. 3) also contain logarithms. These logarithms will also be absorbed into the quark distribution function since in these diagrams the hard scattering occurs off a quark. This latter is an illustration of the problem of mixing in the definition of the parton densities.

We therefore define our quark densities beyond the leading order[3] in terms of F_2.

$$q(x,t) = \int_x^1 \frac{dy}{y} \left\{ \left[\delta\left(1-\frac{x}{y}\right) + \frac{\alpha_s}{2\pi}\, t\, P_{qq}\left(\frac{x}{y}\right) + \alpha_s\, f_q^{DIS}\left(\frac{x}{y}\right) \right] q_0(y) \right.$$

$$\left. + \left[\frac{\alpha_s}{2\pi}\, t\, P_{qG}\left(\frac{x}{y}\right) + \alpha_s\, f_G^{DIS}\left(\frac{x}{y}\right) \right] G_0(y) \right\} \qquad (13)$$

The quark densities now depend on the scale of the interaction t in a well-defined way given in order $\alpha_s(t)$ by the Altarelli-Parisi equations[4]

$$\frac{dq_f(x,t)}{dt} = \frac{\alpha_s(t)}{2\pi} \int_x^1 \frac{dy}{y} \left[P_{qq}\left(\frac{x}{y}\right) q_f(x,t) + P_{qG}\left(\frac{x}{y}\right) G(y,t) \right] \qquad (14)$$

Moreover, the valence value sum rules, Eq. (2), are still valid,

$$\int_0^1 dx \left[q_f^{[h]}(x,t) - \bar{q}_f^{[h]}(x,t) \right] = v_f^{[h]} \qquad (15)$$

Proceeding to the Drell-Yan process we must calculate the diagrams shown in Fig. 4 involving quark-antiquark annihilation and those in Fig. 5 involving incoming gluons. The result of the perturbative calculation for the total cross-section is given by,

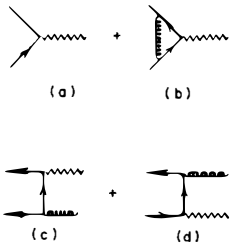

Fig. 4

Fig. 5

$$\frac{d\sigma^{DY}}{dQ^2} \sim \int_0^1 \frac{dx_1}{x_1} \int_0^1 \frac{dx_2}{x_2} \left\{ \sum_f e_f^2 \left[\overset{[1]}{q}_{0f}(x_1)\, \overset{[2]}{\bar{q}}_{0f}(x_2) + (1 \leftrightarrow 2) \right] \right.$$

$$\times \left[\delta(z-1) + \theta(1-z) \left(\frac{\alpha_s}{2\pi} \partial P_{qq}(z) t + \alpha_s f_q^{DY}(z) \right) \right]$$

$$+ \left[\sum_f e_f^2 \left(\overset{[1]}{q}_{0f}(x_1) + \overset{[1]}{\bar{q}}_{0f}(x_1) \right) \overset{[2]}{G}_0(x_2) + (1 \leftrightarrow 2) \right]$$

$$\left. \times \left[\theta(1-z) \left(\frac{\alpha_s}{2\pi} P_{qG}(z) t + \alpha_s f_G^{DY}(z) \right) \right] \right\} . \qquad (16)$$

where the variable z is given by $z = \tau/x_1x_2$. Expressing this result in terms of the structure functions defined by Eq. (13), we obtain the final result for the perturbatively corrected cross-section

$$\frac{d\sigma^{DY}}{dQ^2} = \frac{4\pi\alpha^2}{9SQ^2} \int_0^1 \frac{dx_1}{x_1} \int_0^1 \frac{dx_2}{x_2} \left\{ \left[\sum_f e_f^2 \overset{[1]}{q}_f(x_1,t)\, \overset{[2]}{\bar{q}}_f(x_2,t) + (1 \leftrightarrow 2) \right] \right.$$

$$\times \left[\delta(1-z) + \alpha_s(Q^2)\, \theta(1-z) \left(f_q^{DY}(z) - 2 f_q^{DIS}(z) \right) \right]$$

$$+ \left[\sum_f e_f^2 \left(\overset{[1]}{q}_f(x_1,t) + \overset{[1]}{\bar{q}}_f(x_1,t) \right) \overset{[2]}{G}(x_2,t) + (1 \leftrightarrow 2) \right]$$

$$\left. \times \left[\alpha_s(Q^2)\, \theta(1-z) \left(f_G^{DY}(z) - f_G^{DIS}(z) \right) \right] \right\} . \qquad (17)$$

As indicated above the functions f^{DIS} and f^{DY} by themselves are dependent on the regularization scheme and hence we do not quote them here. However, any such dependence cancels in the differences of the f functions in Eq. (17) which are given by[3),5)]

$$\alpha_s\left(f_q^{DY} - 2f_q^{DIS}\right) = \frac{\alpha_s}{2\pi}\frac{4}{3}\left[-6 - 4z + \frac{3}{(1-z)_+} + 2(1+z^2)\left(\frac{\ln(1-z)}{1-z}\right)_+ + \left(1+\frac{4}{3}\pi^2\right)\delta(z-1)\right] \tag{18}$$

$$\alpha_s\left(f_G^{DY} - f_G^{DIS}\right) = \frac{\alpha_s}{2\pi}\frac{1}{2}\left[\left(z^2 + (1-z)^2\right)\ln(1-z) + \frac{9}{2}z^2 - 5z + \frac{3}{2}\right] \tag{19}$$

Detailed consideration of the size and significance of these terms is given elsewhere in this volume[6]. Suffice it to say that at presently accessible values of Q^2 and τ, the term (18) gives a large positive correction which appears to be substantially independent of τ for reasonable choices of parton distribution functions. The size of this correction casts doubt on the validity of the perturbative expansion retaining only first order terms. It is plausible that these large terms may be resummed giving an improved perturbation series[7].

The transverse momentum distribution of lepton pairs is one of the strongest signals for the departure from the naïve parton model. Since QCD is a theory with a dimensionless coupling constant, if we ignore the intrinsic mass scales associated with the size we have immediately on dimensional grounds

$$q_\perp^2 = S\, f\left(\tau, \alpha_s(Q^2)\right) + \ldots \tag{20}$$

In this formula the dots indicate terms which do not grow with S and may be ascribed to an intrinsic transverse momentum of the partons. The explicit form for the function f to first order in $\alpha_s(Q^2)$ is given below.

In first order QCD this large transverse momentum is due to the diagrams of Figs 4c,d and Fig. 5. Calculating these diagrams we find that the explicit form for the transverse momentum distribution at large values of $q_\perp$, at which the intrinsic transverse spread of the partons may be neglected, is[8]

$$\left.\frac{d\sigma}{dQdq_\perp^2dy}\right|_{y=0} = \frac{8\alpha^2}{27S^2Q}\alpha_s(Q^2)\int_0^1 dx_1\int_0^1 dx_2\,\delta\left(x_1x_2 - \frac{1}{2}(x_1+x_2)\sqrt{(x_\perp^2+4\tau)} + \tau\right)\times$$

$$\times\left[\sum_f e_f^2\left\{q_f^{[1]}(x_1,Q^2)\,q_f^{[2]}(x_2,Q^2) + (1\leftrightarrow 2)\right\}F_{q\bar{q}}(x_1x_2,z,x_\perp)\right]$$

cont.

$$+ \sum_f e_f^2 \left\{ \left(q_f^{[1]}(x_1,Q^2) + \bar{q}_f^{[1]}(x_1,Q^2) \right) G^{[2]}(x_2,Q^2) + (1\leftrightarrow 2) \right\}$$

$$\times F_{qG}^S(x_1x_2,z,x_\perp) + \sum_f e_f^2 \left\{ \left(q_f^{[1]}(x_1,Q^2) + \bar{q}_f^{[1]}(x_1,Q^2) \right) \right.$$

$$\left. \times G^{[2]}(x_2,Q^2) - (1\leftrightarrow 2) \right\} F_{qG}^A(x_1,x_2,z,x_\perp) \Bigg] \qquad (21)$$

where

$$Q = \sqrt{Q^2} \ , \quad x_\perp = \frac{2|q_\perp|}{\sqrt{S}} \ , \quad z = \frac{\tau}{x_1x_2}$$

and

$$F_{q\bar{q}}(x_1x_2,z,x_\perp) = \frac{8}{x_\perp^2}\left(1 + z^2 + \frac{x_\perp^2}{2x_1x_2}\right)$$

$$F_{qG}^S(x_1x_2,z,x_\perp^2) = \frac{3}{8x_\perp^2}\left[\left(\frac{x_\perp^2}{x_1x_2} - (1-z)^2\right)(1+3z) + 4(1-z)^3 + (1-z)(1+z)^2\right] \qquad (22)$$

$$F_{qG}^A(x_1,x_2,z,x_\perp) = \varepsilon(x_1-x_2)\frac{3}{8x_\perp^2}(1-z)\sqrt{1-\frac{x_\perp^2}{x_1x_2(1-z)^2}}\left[\frac{x_\perp^2}{x_1x_2} + 8z - 8z^2 - 4\right]$$

We can also derive from these diagrams the explicit form for the function f in Eq. (20) to lowest order in $\alpha_s(Q^2)$ and we find,

$$\langle q_\perp^2 \rangle \frac{Q^2 d\sigma}{dQ^2} = \frac{\alpha^2\alpha_s(Q^2)}{27}\int_0^1 dx_1 \int_0^1 dx_2\, \theta(1-z)(1-z)^3 \left\{ \left[\sum_f e_f^2 \left\{ q_f^{[1]}(x_1,Q^2) \right.\right.\right.$$

$$\left.\left.\left. \times \bar{q}_f^{[2]}(x_2,Q^2) + (1\leftrightarrow 2) \right\} \right] \left[\frac{16}{3} + \frac{16z}{(1-z)^2} \right] + \left[\sum_f e_f^2 \left\{ \left(q_f^{[1]}(x_1,Q^2) \right.\right.\right.\right.$$

$$\left.\left.\left.\left. + \bar{q}_f^{[1]}(x,Q^2) \right) + (1\leftrightarrow 2) \right\} \right] \left[\frac{3}{2}\frac{1}{(1-z)} + \frac{1}{4}(1-z) - 2z \right] \right\} . \qquad (23)$$

Information about the transverse momentum distributions is particularly interesting because of the importance of the gluons. Indeed in proton-proton collisions we find that at large values of τ, incoming gluons are the dominant producers of lepton pairs at large transverse momentum. However, the size of the corrections to the total cross-section raises doubts about the validity of these lowest order estimates[9].

In the kinematic region in which

$$Q >> |q| >> \sqrt{\Lambda Q} \tag{24}$$

DDT[10] have derived a formula for the transverse momentum distribution of lepton pairs given by

$$\left.\frac{q_\perp^2 d\sigma}{dQ^2 dq_T^2 dy}\right|_{y=0} = \frac{4\pi\alpha^2}{9Q^2 S} \frac{d}{dt_\perp}\left[T^2(t_\perp)\left\{\sum_f e_f^2 \, q_f^{[1]}(\sqrt{\tau}, t_\perp)\, \bar{q}_f^{[2]}(\sqrt{\tau}, t_\perp) + (1\leftrightarrow 2)\right\}\right] \tag{25}$$

where[11]

$$t_\perp = \ln q_\perp^2/\mu^2 \qquad T^2(t_\perp) = \exp - \frac{\alpha_s}{2\pi}\frac{4}{3}(t - t_\perp)^2 \tag{26}$$

Since the kinematic inequalities in Eq. (24) are to be interpreted in a logarithmic sense, the practical utility of this formula at present energies is small. A further improvement of this formula was proposed in Ref. 11) by transforming to impact parameter space which is conjugate in the Fourier transform sense to the transverse momentum space. Calculating the matrix element in the soft approximation, but taking the conservation of transverse momentum into account exactly, the authors of Ref. 11) obtain,

$$\left.\frac{d\sigma}{dQ dq_T^2 dy}\right|_{y=0} = \frac{1}{2}\int b\, db\, J_0(|b||q_\perp|)\, \tilde{\sigma}(b,Q,S) \tag{27}$$

where

$$\tilde{\sigma}(b,Q,S) = \frac{8\pi\alpha^2}{9QS} \sum_f e_f^2 \left[\overset{[1]}{q_f}\left(\sqrt{\tau},\frac{1}{b^2}\right) \overset{[2]}{\bar{q}_f}\left(\sqrt{\tau},\frac{1}{b^2}\right) + (1\leftrightarrow 2) \right] \tilde{T}(Q^2,b^2) \qquad (28)$$

and

$$\tilde{T}(Q^2,b) = \exp \Delta(b), \quad \Delta(b) = \frac{1}{\pi} \int d^2k_T \, \frac{4\alpha_s(k_\perp^2)}{3\pi} \, \frac{\ln(Q^2/k_\perp^2)}{k_\perp^2} \, (\exp ib\cdot k_\perp - 1) \qquad (29)$$

The derivation of the form factor, Eq. (29), is subject to the restriction

$$\Lambda << \frac{1}{b} << Q \qquad (30)$$

whereas the integral in Eq. (27) runs over all values of b. However, inserting the explicit form Eq. (28) into Eq. (27) we find that the contribution from the region $b \sim 1/\Lambda$ is small because of the form factor suppression. Thus, although the chain of approximations is not exactly watertight it is at least self-consistent.

REFERENCES

1) S.D. Drell and T.M. Yan, Phys. Rev. Letters 25, 316 (1970), Ann. of Phys. 66, 578 (1971).

2) H.D. Politzer, Nucl. Phys. B129, 301 (1977).

3) G. Altarelli, R.K. Ellis and G. Martinelli, Nucl. Phys. B143, 521 (1978) [E B146, 544 (1978)], Nucl. Phys. B157,461 (1979).

4) G. Altarelli and G. Parisi, Nucl. Phys. B126, 298 (1977).

5) J. Kubar-André and F.E. Paige, Phys. Rev. D19, 221 (1979).

6) R.K. Ellis "The K factor in lowest order perturbation theory and beyond", these proceedings;
G. Plaut, these proceedings.

7) M. Greco, these proceedings;
G. Pancheri Srivastava, these proceedings and references therein.

8) G. Altarelli, G. Parisi and R. Petronzio, Phys. Lett. 76B, 351, 356 (1978); K. Kajantie and R. Raitio, Nucl. Phys. B139, 72 (1978).

9) G. Martinelli, these proceedings.

10) Yu. Dokshitzer, D. Dyakanov and S. Trojan, Proceedings of the 13th Winter School of the Leningrad Institute of Nuclear Physics, Leningrad (1978).

11) G. Parisi and R. Petronzio, Nucl. Phys. B154, 427 (1979).

NA3 RESULTS ON DIMUON PRODUCTION : TEST OF THE DRELL-YAN MODEL

NA3 Collaboration

Presented by Olivier CALLOT
Laboratoire de l'Accélérateur Linéaire, ORSAY

ABSTRACT

We report here recent results from NA3 Collaboration on dimuon production. Predictions of the Drell-Yan modell are tested. In particular, we present a detailed study of nuclear effects and of angular distributions.

RESUME

Nous présentons ici des résultats récents de la collaboration NA3 sur la production de dimuons. Des prédictions du modèle de Drell-Yan sont testées. En particulier, nous présentons une étude détaillée des effets nucléaires et des distributions angulaires.

1. NA3 EXPERIMENT

This apparatus has been described in detail[2], the main features are the large acceptance and the high rejection trigger[3]. We have taken data during about two years, and the analysis is not yet completely finished. Statistics are given in the following table for continuum events ($4.1 < M < 8.5$ GeV).

Table 1

Number of events ($4.1 < M < 8.5$) in the continuum

Reaction \ Energy	-150	-200	+200	-280
$\pi^{\pm} + p_t$	∿22000	∿5600	∿2000	∿19000
$\pi^{\pm} + H_2$	535	121	40	740
$p,\bar{p} + p_t$	275		1300	
$K^{-} + p_t$	700			

2. NUCLEAR EFFECTS

a) Targets

We use two targets simultaneously (hydrogen and platinum), and can then measure A dependance without any absolute normalization problems. But we must ensure that the identification of the target is clean, and that differences of acceptance are understood. For a platinum target, one must be aware of Fermi motion, which gives a change in the value of S, and of possible production of dimuons by secondary interactions (estimated to be about 5 % of the direct production in our 6 cm target).

So systematic effects in this comparison come from uncertainties on the number of nucleons in each target (< 5 %) and from the above mentioned effects, giving a global systematic error of less than 10 %.

b) Drell-Yan Prediction

The cross section of the Drell-Yan process depends on the quark content of beam and target. Here, the beam particles are π^- and the target particles are proton (hydrogen) or a mixture of .4 p + .6 n (platinum). If we consider only valence-valence processes (i.e $\bar{u}u$ annihilation), we expect a ratio of $\frac{2}{3}$ (hydrogen) over $.4 \times \frac{2}{3} + .6 \times \frac{1}{3}$ (platinum), that is 1.43. Values obtained with a more complete calculation (including valence-sea and sea-sea), and integrated over the 4.1 - 8.5 GeV mass interval, are 1.48, 1.45 and 1.41 at 150, 200, 280 GeV for π^- and .89 for π^+ at 200 GeV. We can also compute variations of this ratio with mass, x_1, x_2,...

c) Global analysis

We measure the ratio of the cross-section per nucleon (hydrogen over platinum) integrated over the mass interval. The ratio of this ratio to the Drell-Yan prediction is then a measurement of the nuclear effects ; using an A^α parametrization of the nuclear cross-section, the ratio is then $\left(\frac{AH_2}{Ap_t}\right)^{1-\alpha}$, and we extract then the value of α. Results are given in table 2 for each set of data :

Table 2

Global measurements of nuclear effects - Systematic errors are included

Reaction	Ratio H_2/p_t per effective nucleon	Drell-Yan prediction	Ratio to prediction	α
π^-, 150 GeV	1.51 ± .15	1.48	1.02 ± .10	1.00 ± .02
π^-, 200 GeV	1.35 ± .20	1.45	.93 ± .15	1.02 ± .03
π^+, 200 GeV	1.13 ± .25	.89	1.27 ± .28	.95 ± .05
$(\pi^- - \pi^+)$ 200 GeV	1.60 ± .40	1.92	.83 ± .21	1.04 ± .04
π^- 280 GeV	1.40 ± .14	1.41	.99 ± .10	1.00 ± .02

d) Variations with x_1, x_2, mass, pt

With our 150 and 280 GeV data, we can study the variation of the hydrogen to platinum ratio as function of some variables. We compare these variations with

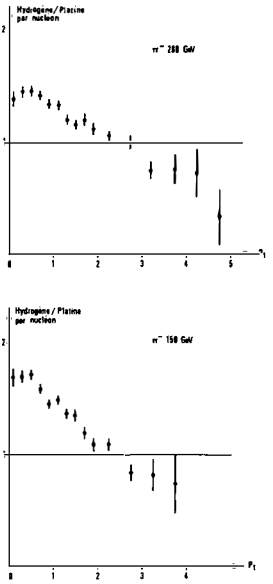

Fig. 3 : Hydrogen to platinum cross section ratio for ψ production as function of transverse momentum.

the prediction of the Drell-Yan model, and results are shown on figure 1 and 2 for the two energies. Agreement is very nice for x_1, x_2 and mass. For P_T dependance, there is no prediction, because the Drell-Yan model ignores P_T. But we expect this P_T to be due to the hard process, and not to nuclear effects. The measured ratio is flat up to large values of P_T, in good agreement with this expectation. Note that, for the J/ψ, there are nuclear effects, as can be seen on fig. 3.

e) Carbon-platinum comparison

Because corrections are important (acceptance and Drell-Yan prediction) when comparing hydrogen and platinum, we have performed a check using simultaneously carbon and platinum target (the Drell-Yan prediction is about the same). We frequently exchanged the target positions, in order to cancel acceptance corrections. We took data during two days, giving about 200 events for each target in each position. The final result is an α value of .97 ± .05 (including systematics), in agreement with previous measurement.

In conclusion, the absence of nuclear effects is clearly established, and measured by the value of α :

$$\alpha = 1.00 \pm .02 \quad \text{(systematics included)}$$

3. PARTICLE RATIOS

The Drell-Yan cross section depends in the nature and distributions of quarks (and antiquarks) in the beam and in the target. Using our data with 6 incident particles, we can measure the cross section ratios, integrated over the mass interval 4.1 to 8.5 GeV in a first stage. We obtain the following numbers.

Table 3

Cross section ratio to π^-, for all beam particles on the platinum target, at 200 GeV, integrated in mass

Particle	K^-	$\bar{P}$	π^+	K^+	p
Ratio to π^- at 200 GeV	.98 ± .10	1.07 ± .20	.51 ± .01	.23 ± .02	.23 ± .02
Valence antiquark	$\bar{u}$	$\bar{u},\bar{d}$	$\bar{d}$	$\bar{s}$	-

As can be seen, this cross-section ratio is very sensitive to the possibility of valence-valence $\bar{q}q$ annihilation. We can measure more precisely the K^- to π^- ratio as a function of x_1, and this is a measurement of the K^- $\bar{u}$ structure function[4].

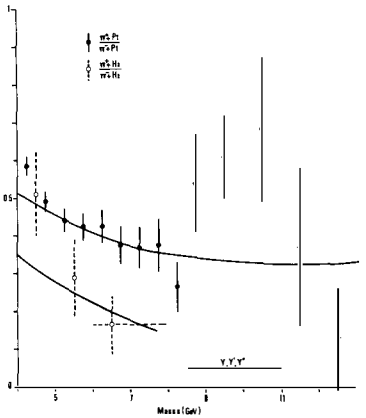

Fig. 4 : π^+ to π^- cross section ratio as function of the mass. Curves are the Drell-Yan model predictions.

For the π^+ to π^- ratio, we can measure it as a function of the mass, and this gives the well known fig. 4, which is related to the electromagnetic coupling in the Drell-Yan formula : the π^- has an $\bar{u}$ valence quark (charge 2/3) and the π^+ an $\bar{d}$ (charge 1/3). For valence-valence annihilation on an isoscalar target, the π^+ to π^- ratio is then expected to be $(1/3)^2/(2/3)^2 = \frac{1}{4}$. On a platinum target, this limit depends on the nucleon structure functions and is between .286 ($d = \frac{u}{2}$) and .375 ($d = \frac{u}{d}(1-x)$). For hydrogen, the limits are respectively .125 and 0.

We cannot distinguish between these two limits, because of the presence of the upsilon family.

4. SCALING

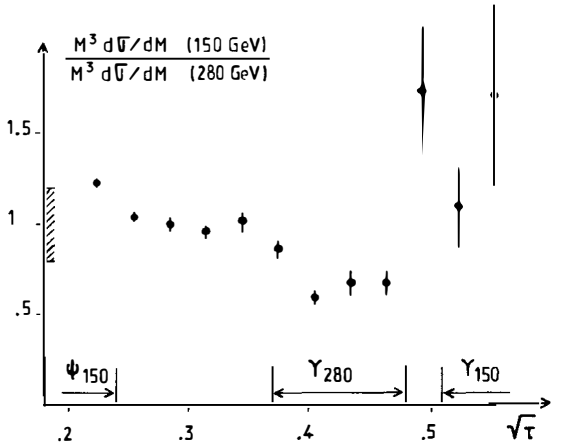

Fig. 5 : Ratio of the invariant cross section $M^3 \frac{d\sigma}{dM}$ at 150 GeV compared to 280 GeV. Resonances regions are indicated. Systematic error is indicated on the vertical axis.

The Drell-Yan model predicts that $M^3 \frac{d\sigma}{dMdx_F}$ is only a function of τ and x_F. By comparing our 3 energies, we can verify this prediction. The standard picture is the curve $M^3 \frac{d\sigma}{dMdx_F}$ for different energies. Here, we show the ratio of these invariant cross sections at 150 and 280 GeV (fig. 5), and we can see that this ratio is compatible with 1 (within systematic error) and doesn't change with $\sqrt{\tau}$ in the continuum region (.25 to .37).

5. TRANSVERSE MOMENTUM

In the Drell-Yan model, the transverse momentum of the lepton pair is only due to the transverse momenta of quarks in the hadrons, that is an intrinsic momentum, of the order of a few hundred MeV. This is well known to be false, $\langle P_T \rangle$ being between 1 and 1.2 GeV and increasing with S. This behaviour can be analysed in the framework of QCD.

We have performed such an analysis, see Jean Badier's contribution to these proceedings. Here, we will only give a phenomenological description of the shape of the P_T distribution. The most simple expression, $\frac{d\sigma}{dP_T^2} \alpha e^{-\lambda P_T^2}$ is known to decrease too fast at large P_T. Our parametrization takes into account the S dependance, and is the following :

$$\frac{d\sigma}{dP_T^2} \alpha \left(1 - \frac{M_T}{\sqrt{S}}\right)^{\gamma} / M_T^{\beta} \quad ; \quad M_T = \sqrt{\mu^2 + 4P_T^2}$$

$$\mu = 4.15 \text{ GeV}, \ \beta = 4.7, \ \gamma = 11.05$$

This parametrization reproduces all our data very well as can be seen in fig. 6.

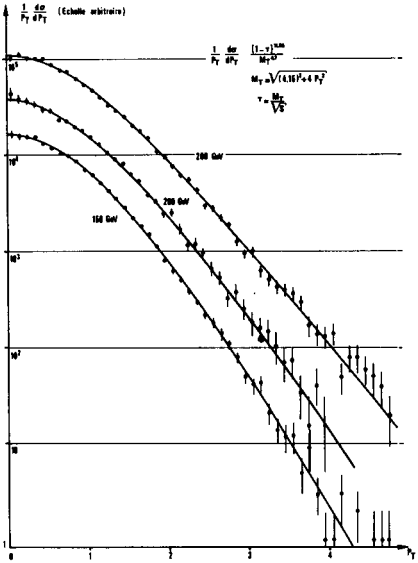

Fig. 6 : $\frac{1}{P_T}\frac{d\sigma}{dP_T}$ parametrization compared to data for our 3 energies

6. ANGULAR DISTRIBUTIONS

In the Drell-Yan model, the polarization of the virtual photon is completely transverse, this means that the angular distribution of the muon in the dimuon rest frame is $1 + \cos^2\theta$, θ being the angle between the muon and the quark direction. We present our analysis only for the 150 GeV data.

a) Reference frames

The quark direction is not accessible to experiment, and we must choose as axis some combination of the hadron directions. If there is no transverse momentum, the beam and the target have the same direction in the dimuon rest frame, and there are no ambiguities (according to the Drell-Yan model).

The most commonly used frames are the following :

. Axis $\vec{L} = \vec{\pi}$ (Gottfried-Jackson, G.J)

. Axis $\vec{L} = \vec{P}$ (u channel)

. Axis $\vec{L}$ = external bisectrix of $\vec{\pi}$ and $\vec{p}$ (Collins Soper, CS)

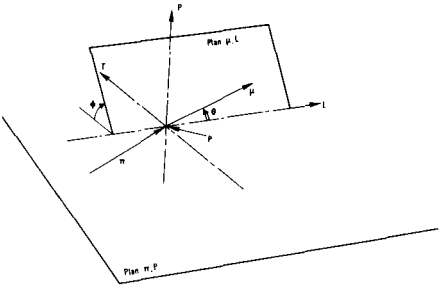

Fig. 7 : Definition of angle and axis in the dimuon rest frame.

The typical angle between these axes is of the order of P_T/M. We define also an angle ϕ between $(\vec{\pi}, \vec{p})$ plane and $(\vec{\mu}, \vec{L})$ plane, positive in the $\vec{\pi} \times \vec{p}$ hemisphere, see fig. 7. Most of the theoretical prediction use the Collins-Soper frame, because in this case the P_T of the dimuon is equaly shared between the two quarks.

b) Global analysis

First, we can look at the cosθ distribution, integrated over all other variables (i.e M, X_F, ϕ, P_T). The result is shown on fig. 8, together with acceptance. A fit of the form $\frac{d\sigma}{d\cos\theta} \alpha 1 + \lambda \cos^2\theta$ gives $\lambda = .91 \pm .08$ in the C.S frame. This is in good agreement with Drell-Yan prediction. Note that the acceptance in cosθ is very poor at large values of $\cos^2\theta$, and this gives us some problems which we will describe now.

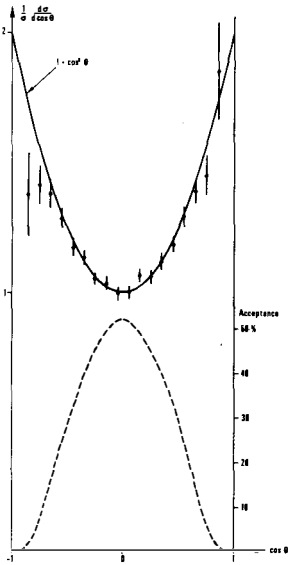

Fig. 8 : Acceptance and data for cos θ distribution. Collins-Soper frame, 150 GeV.

c) Problems

The general expression for this angular distribution is

$W(\theta,\phi) = W_T (1+\cos^2\theta) + W_L \sin^2\theta + W_\Delta \sin 2\theta \cos\phi + W_{\Delta\Delta} \sin 2\theta \cos 2\phi$

W's are functions of all other variables (M, X_F, P_T). Acceptance is a function of M, X_F, P_T, θ, φ, with strong correlation in some regions (eg P_T and θ at large X_F, θ and φ,...). We need a good representation of all other parameters, before analysing angular distribution. We use the Drell-Yan model with the P_T distribution described before.

After the Moriond meeting, we found that the contribution of non continuum events, which is small when integrated over angular variables (less than 1 %), turn out to have a very different behaviour in $\cos\theta$. For example, the same sign dimuons are concentrated at large $\cos\theta$, and this indicates that opposite sign dimuons due to π decays,... (i.e same origin as same sign dimuons) are also at large $\cos\theta$, and we must substract these events before analysing angular distributions. Two other effects were taken into account : reinteraction in the target (cut at a positive X_F to eliminate most of these events) and contamination from badly reconstructed ψ produced in the hydrogen target (cut at mass greater than 4.5 GeV). The main effect of these corrections is a decrease of the value of λ of $\sim$ .2 as compared with the values we have presented at the Moriond meeting.

We determine 3 coefficients of the angular distribution :

$W(\theta,\phi) \propto (1+\cos^2\theta) + A \sin^2\theta + B \sin 2\theta \cos\phi + C \sin^2\theta \cos 2\phi$ and we present the results in terms of λ ($= \frac{1-A}{1+A}$), B and C as functions of some parameters.

d) Influence of P_T

First, we look at the effect of P_T, this variable being the source of the reference axis problem. In the CS frame, and for values of x_1 not too small nor too large ($.4 < x_1 < .8$), we obtain the following results :

Table 4

Dependance in P_T of the angular distribution coefficients in the Collins-Soper frame

P_T	λ	B	C
0 - .5	.81 ± .28	- .11 ± .13	.27 ± .19
.5 - 1.	.89 ± .20	- .05 ± .06	.07 ± .07
1. - 1.5	.87 ± .22	- .15 ± .07	.02 ± .06
1.5 - 2.	.70 ± .30	- .15 ± .10	.27 ± .09
2. - 3.	1.03 ± .45	- .51 ± .13	.27 ± .11

As P_T increases, B and C terms become important. This may be related to the choice of the reference frame. In order to investigate this point, we look for the influence of P_T/M in various frames.

e) Influence of P_T/M

Fig. 9 shows the variation of λ, B and C with P_T/M in the CS frame. Curves are eye-fits for B and C, using linear (for B) and quadratic (for C) dependance. We obtain $B \simeq (-.6 \pm .2) \frac{P_T}{M}$ and $C \simeq (1.5 \pm .5) \frac{P_T^2}{M^2}$. For λ, we use the relation $A = 2C$, together with the parametrization of C to obtain the curve in the figure. Agreement is satisfactory. Note that the value of A is sensitive to systematic effects as explained before.

In the Gottfried-Jackson frame, the same type of parametrization gives the following values : $B \simeq (-1.4 \pm .2) \frac{P_T}{M}$ and $C \simeq (2 \pm .5) \frac{P_T^2}{M^2}$ this means that the ϕ terms are more important. In the u-channel frame, the values are now $B \simeq (0 \pm .2) \frac{P_T}{M}$ and $C \simeq (1 \pm .5) \frac{P_T^2}{M^2}$. This means than the u-channel frame is probably the best frame to describe angular distributions in π^- nucleon interactions.

f) Influence of x_1

We now look at possible variations with x_1, and we give results for two P_T regions. Results obtained in the u-channel axis are shown in fig. 10. We don't see any significant variation with x_1, but we are not very sensitive to small ($\sim .3$) changes in the value of λ.

7. CONCLUSION

Drell-Yan predictions have been tested successfully in our experiment, in particular :

- The cross-section on nucleons is linear with A : $\alpha = 1.00 \pm .02$
- The charge asymmetry is clearly visible in the π^+/π^- ratio
- Scaling is compatible with our data, within systematic errors
- The angular distribution is compatible with $1 + \cos^2\theta$.

But when looking in detail, the angular distributions are more complex, and show variations with $\frac{P_T}{M}$, depending on the choice of the reference frame. The u-channel frame seems to be the "cleanest" frame, because there are no $\cos\phi$ terms. and the $\sin^2\theta \cos 2\phi$ term is of the order of $(1 \pm .5) \frac{P_T^2}{M^2}$.

Transverse momentum is larger than expected by the simple model, and also cross section is larger than predicted (K factor). This may be related to QCD corrections, as discussed in detail during this meeting. (See S. Weisz and J. Badier talk for our results on these points).

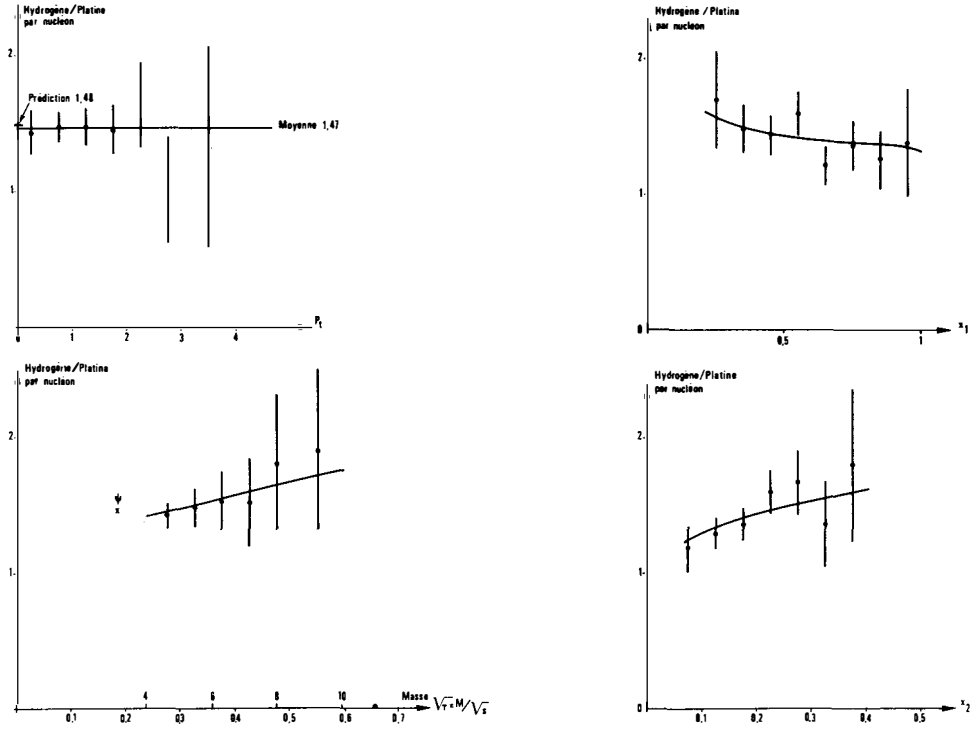

Fig. 1 : Hydrogen to platinum cross section ratio (per nucleon). Curves are the Drell-Yan model predictions. π^- at 150 GeV.

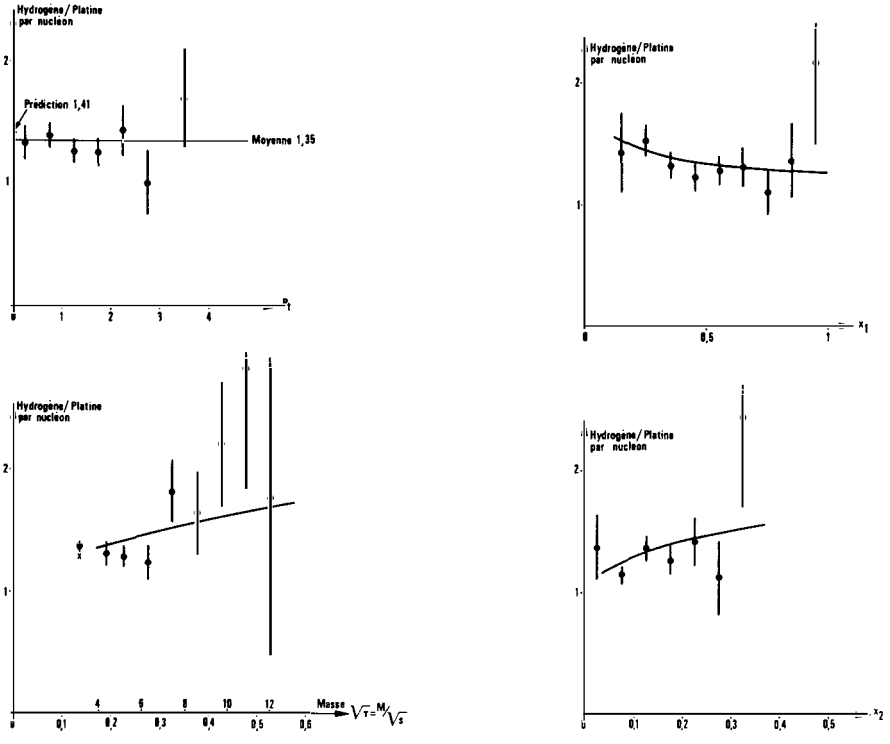

Fig. 2 : Hydrogen to platinum cross section ratio (per nucleon) Curves are the Drell-Yan model predictions. π^- at 280 GeV.

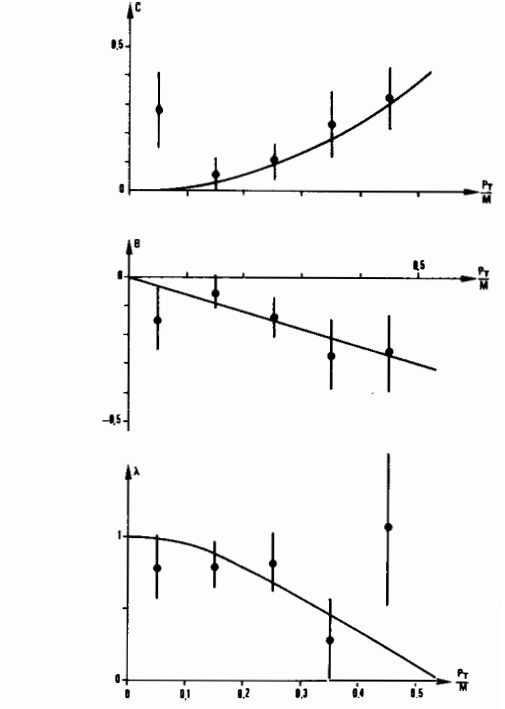

Fig. 9 : Dependance with P_T/M of the angular distribution parameters in the Collins-Soper frame at 150 GeV. Curves are described in the text.

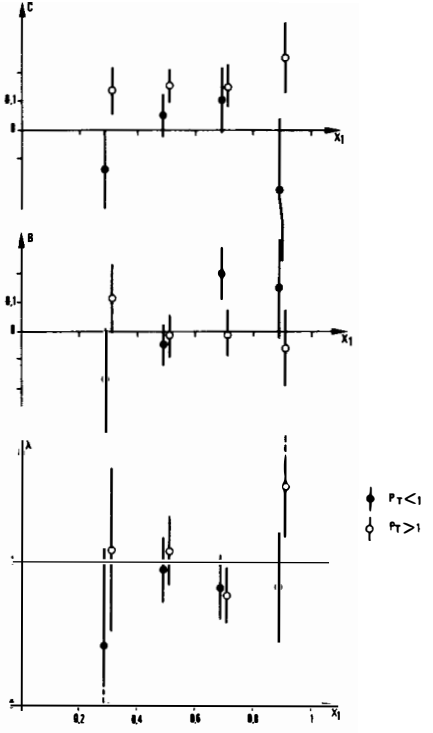

Fig. 10 : Dependance with x_1 of the angular distribution parameters in u-channel frame at 150 GeV.

FIGURE CAPTIONS

Fig. 1 : Hydrogen to platinum cross section ratio (per nucleon). Curves are the Drell-Yan model predictions. π^- at 150 GeV.

Fig. 2 : Hydrogen to platinum cross section ratio (per nucleon). Curves are the Drell-Yan model predictions. π^- at 280 GeV.

Fig. 3 : Hydrogen to platinum cross section ratio for ψ production as function of transverse momentum.

Fig. 4 : π^+ to π^- cross section ratio as function of the mass. Curves are the Drell-Yan model predictions.

Fig. 5 : Ratio of the invariant cross section $M^3 \frac{d\sigma}{dM}$ at 150 GeV compared to 280 GeV. Resonances regions are indicated. Systematic error is indicated on the vertical axis.

Fig. 6 : $\frac{1}{P_T} \frac{d\sigma}{dP_T}$ parametrization compared to data for our 3 energies.

Fig. 7 : Definition of angle and axis in the dimuon rest frame.

Fig. 8 : Acceptance and data for cos θ distribution. Collins-Soper frame, 150 GeV.

Fig. 9 : Dependance with P_T/M of the angular distribution parameters in the Collins-Soper frame at 150 GeV. Curves are described in the text.

Fig. 10 : Dependance with x_1 of the angular distribution parameters in u-channel frame at 150 GeV.

REFERENCES

1. CERN[1] - Collège de France[2] - Ecole Polytechnique[3] - Orsay[4] - Saclay[5] Collaboration.

   J. Badier[3], J. Boucrot[4], J. Bourotte[3], G. Burgun[5], O. Callot[4], P. Charpentier[5], M. Crozon[2], D. Décamp[4], P. Delpierre[2], A. Diop[2], R. Dubé[4], P. Espigat[2], B. Gaudois[5], R. Hagelberg[1], M. Hansroul[1], Y. Karyotakis[4], W. Kienzle[1], A. Lafontaine[5], P. Le Dû[5], J. Lefrançois[4], T. Leray[2], J. Maillard[2], G. Matthiae[1], A. Michelini[1], P. Miné[3], H. Nguyen-Ngoc[4], G. Rahal[5], O. Runolfson[1], P. Siegrist[5], A. Tilquin[2], J. Timmermans[1], R. Vanderhaghen[3], J. Valentin[2] and S. Weisz[3].

2. J. Badier et al., Nucl. Instr. and Meth. 175, 319 (1980).

3. J. Boucrot et al., Nucl. Instr. and Meth. 174, 379 (1980)

4. J. Badier et al., Phys. Lett. 93B, 354 (1980).
   See also S. Weisz contribution in this proceedings.

ANTIPROTON CROSS SECTION FOR DIMUON PRODUCTION AND DETERMINATION OF THE MESON STRUCTURE FUNCTIONS

NA3 Collaboration

presented by S. WEISZ

Physique Nucléaire des Hautes Energies
Ecole Polytechnique 91128 PALAISEAU France

ABSRACT

The NA3 spectrometer has collected dimuon events with incident pions, kaons and nucleons of 150 GeV/c and 200 GeV/c.

We observe cross section significantly larger than what is expected from non perturbative Drell-Yan calculation : this result is unambigous in the case of our anti-proton data, as we know the nucleon structure functions from deep inelastic scattering experiments. We also present a determination of the mesons structure functions.

INTRODUCTION

The analysis presented here has two levels : the first step is to show the coherence between dimuon and deep inelastic scattering measurements using our anti-proton and proton data ; the second step is to extract the mesons structure functions.

THE DATA SAMPLE

A description of the NA3 Spectrometer can be found in ref.(2). We just remind in table I the statistics collected on a platinum target for various projectiles.

Table I : Statistics for $M_{\mu\mu} \in [4.1, 8.5]$

	150 GeV/c	200 GeV/c
π^-	4970	21600
K^-	90	688
$\bar{p}$	32	275
π^+	1750	
K^+	170	
p	1070	35*

Measuring the mass and longitudinal momentum of a dimuon, we define the X_1 and X_2 variables :

$$X_1 \, X_2 = M^2 / s$$
$$X_1 - X_2 = 2 \, P^*_{//} / \sqrt{s}$$

Fig. I shows the $X_1 - X_2$ plane : we see that for masses between 4.1 and 8.5 GeV/c, we explore a region leaning from $X_F = -.3$ up to the kinematical limit.

---

* These 35 events are obtained with an integrated proton luminosity comparable to the one we have for anti-proton at the same energy. It correspond to 2 days of data-taking instead of 70 days in the $\bar{p}$ case.

THE MODEL

The Drell-Yan (3) formulae can be written as :

(1)
$$\frac{d^2\sigma}{dX_1 dX_2} = \frac{\sigma_o}{3} \sum_i \frac{q_i^2}{X_1^2 X_2^2} \left[f_i^P(X_1)\, f_{\bar{i}}^T(X_2) + f_{\bar{i}}^P(X_1)\, f_i^T(X_2) \right]$$

where $\sigma_o = \frac{4}{3} \pi \alpha^2$, and $\frac{1}{3}$ hold for color. $f_i^{p(T)}(X)$ represent the density of the parton i in the projectile (target).

The deep inelastic scattering experiments have measured these structure functions for the nucleons, and we take their results as an input to our analysis : we assume a Buras-Gaemers (4) parametrisation, giving for the proton valence structure function :

$$V^P(X) \propto X^{\alpha_v} (1 - X)^{\beta_v}$$

$$\text{with } \alpha_v = \alpha_{vo} + a\,\bar{S} \quad ; \quad \beta_v = \beta_{vo} + b\,\bar{S}$$

$$\bar{S} = \text{Log} \frac{\text{Log } Q^2/\Lambda^2}{\text{Log } Q_o^2/\Lambda^2}$$

which is a good approximation to the Q^2 dependance predicted by the Altarelli-Parisi (5) evolution equation.

Within our mass range, we can estimate the effect of scaling violation to be $\lesssim 10\%$ on β_v and $\lesssim 5\%$ on α_v : this is small and well beyond our statistical precision. We futhermore take structure functions independant of Q^2, obtained at $Q^2 = 20$, our average squared mass.

The CDHS collaboration (6) gives for XF_3, at $Q^2 = 20$, the exponents:

$$\alpha_v = 0.51 \pm 0.02 \quad ; \quad \beta_v = 3.03 \pm 0.09$$

In fact, we need an expression for the Up and Down distributions. We then have to introduce the relations

$$U^P \propto X^{\alpha u} (1 - X)^{\beta_u}$$
$$D^P \propto X^{\alpha d} (1 - X)^{\beta_d}$$
$$\text{with } \alpha_d = \alpha_u \text{ and } \beta_d = \beta_u + 1$$

We now write for the moments $M(n) = \int X^{n-2} f(X) dX$ the relations

$M^v(n) = M^u(n) + M^d(n)$ for n = 2, 3 assuming the sum rules

$$\int \frac{1}{X} U^P(X)\, dX = 2 \quad ; \quad \int \frac{1}{X} D^P(X)\, dX = 1$$

We then get
$$\left.\begin{aligned} \alpha_u &= 0.52 \pm 0.02 \\ \beta_u &= 2.80 \pm 0.10 \end{aligned}\right\} \quad (3)$$

ANTIPROTON EVENTS

From relation (1), we observe that only valence structure functions contribute to the difference between anti-proton and proton cross section :

$$(4) \quad \left.\frac{d^2\sigma}{dx_1 dx_2}\right|_{\bar{p}N} - \left.\frac{d^2\sigma}{dx_1 dx_2}\right|_{pN} = \frac{\sigma_0}{3} \cdot \frac{1}{9 x_1^2 x_2^2} \cdot f(x_1)\, g(x_2) \; *$$

where $f(x_1) = 4\, U^P(x_1) + D^P(x_1)$

$g(x_2) = .4\, U^P(x_2) + .6\, D^P(x_2)$

on platinum target nucleon (Z/A = .4).

Relation (4) becomes, in terms of number of events :

$$(5) \quad \frac{1}{A(x_1, x_2)} \cdot \left[\frac{1}{\mathcal{L}_{\bar{p}}} \left.\frac{dN}{dx_1 dx_2}\right|_{\bar{p}N} - \frac{1}{\mathcal{L}_p} \left.\frac{dN}{dx_1 dx_2}\right|_{pN}\right] = \frac{\sigma_0}{3} \cdot \frac{1}{9 x_1^2 x_2^2} \cdot f(x_1)\, g(x_2)$$

where $A(x_1, x_2)$ is the acceptance and $\mathcal{L}$ the luminosity.

We define experimentally $F(x_1)$ as :

$$F(x_1) = \frac{\frac{1}{\mathcal{L}_{\bar{p}}} \int \left.\frac{dN}{dx_1 dx_2}\right|_{\bar{p}N} dx_2 - \frac{1}{\mathcal{L}_p} \int \left.\frac{dN}{dx_1 dx_2}\right|_{pN} dx_2}{\frac{\sigma_0}{27 x_1^2} \cdot \int \frac{g(x_2)}{x_2^2} A(x_1, x_2)\, dx_2}$$

---

* We neglect a $.2\, D^P(x_1) \cdot [U^P(x_2) - D^P(x_2)]$ term coming from a non isoscalar target. For realistic values of U^P/D^P, its contribution is less than 2% of expression (4).

We would expect $F(x_1) = f(x_1)$

Figure II shows $F(x_1)$ obtained at 150 GeV/c : we see that the agreement in shape is good, but that the measured cross section is twice higher than expected by the Drell-Yan model.
We then define a K factor as

$$K = \frac{\text{Number of observed events}}{\text{Number of D-Y predicted events}}$$

its numerical value is

$$K = 2.3 \pm .4$$

We can project our data over x_2 in the same way we did for x_1 with $F(x_1)$: this is shown on figure III. Figure IV gives the mass distribution compared to the model.

To conclude, we would say that the cross sections factorise as expressed in relation (5), and that we do not observe any deviation from K = 2.3 with respect of x_1, x_2 or the mass of the dimuon.

MESONS STRUCTURE FUNCTIONS

Relation (1) again tells us that the difference of the cross sections with incident π^- and π^+ should factorise :
(6)

$$\left.\frac{dN}{dx_1 dx_2}\right|_{\pi^-} - \left.\frac{dN}{dx_1 dx_2}\right|_{\pi^+} = \frac{\sigma_o}{3} \cdot \frac{1}{9} \cdot \frac{1}{x_1^2 x_2^2} \; V^{\pi}(x_1) \cdot (U^P(x_2) + 2D^P(x_2))$$

This fact is well suported by our data, and this encourage us to determine the pion structure functions.
We use the folowing parametrisation :

Valence : $V^{\pi}(x) \propto x^{\alpha_V} (1 - x)^{\beta_V}$ with $\frac{1}{x}\int V^{\pi}(x)\, dx = 1$

Sea : $S^{\pi}(x) \propto (1 - x)^{\beta_S}$ SU(3) symetric with $2\langle V\rangle + \langle S\rangle = .5$
(50% of momentum carried by gluon)

A fit on the shape of the distribution then gives for the pion :

$$200\ \text{GeV/c} \quad \begin{cases} \alpha_v = .45 \pm .1 \\ \beta_v = 1.04 \pm .1 \\ \beta_s = 5.4 \pm 2.0 \end{cases}$$

We only have π^- data at 150 GeV/c, and we have to introduce the pion sea measured at 200 GeV/c. We then get

$$150\ \text{GeV/c} \quad \begin{cases} \alpha_v = .40 \pm .1 \\ \beta_v = .90 \pm .1 \end{cases}$$

To plot the results in one dimension, we use the following projection method :

we write the Drell-Yan cross section as :

$$\frac{d^2\sigma}{dx_1 dx_2} = \frac{\sigma_o}{3} \cdot \frac{1}{9} \cdot \frac{1}{x_1^2 x_2^2} \cdot \left[V^\pi(x_1) G(x_2) + S^\pi(x_1)\, H(x_2) \right]$$

with
$$G(x_2) = 1.6\, U^P(x_2) + 2.4\, D^P(x_2) + 5\, S^P(x_2) : \pi^-$$
$$G(x_2) = .6\, U^P(x_2) + .4\, D^P(x_2) + 5\, S^P(x_2) : \pi^+$$
$$H(x_2) = 2.2\, U^P(x_2) + 2.8\, D^P(x_2) + 11\, S^P(x_2) : \pi^\pm$$

The distribution of events along x_1 is of the form :

(7)
$$\frac{dN}{dx_1} = K\, \mathcal{L} \cdot \frac{\sigma_o}{3} \cdot \frac{1}{9\, x_1^2} \cdot \left[V^\pi(x_1)\ I(x_1) + S^\pi(x_1)\ J(x_1) \right]$$

where
$$I(x_1) = \int \frac{1}{x_2^2}\ A(x_1, x_2)\ G(x_2)\, dx_2$$

$$J(x_1) = \int \frac{1}{x_2^2}\ A(x_1, x_2)\ H(x_2)\, dx_2$$

We define $F(x_1)$, directly connected to the data through relation (7):

(8)
$$F(x_1) = K\left[V^{\pi}(x_1) + \frac{J(x_1)}{I(x_1)} \quad S^{\pi}(x_1)\right]$$

$F(x_1)$ is plotted on figure Va : We again have a K factor close to 2 at 150 GEV/c and 200 GeV/c incident energies. Projection on the x_2 axis are plotted on figure Vb.

The K^- and π^- induced dimuons are collected simultanously, so we have very little systematic errors on their ratio (see ref. 7). For $x_1 > .2$, we can neglect terms which are not valence-valence annihilatiion up to an accuracy of 10%, inside our satistical fluctuation. We then write :

(9)
$$\frac{\bar{U}^{k}(x_1)}{\bar{U}^{\pi}(x_1)} = \frac{\mathcal{L}_{\pi}}{\mathcal{L}_{K}} \quad \frac{dN/dx_1}{dN/dx_1}\Big|_{k} \Big|_{\pi}$$

Our data are plotted on figure VI : they are well represented by the form

$$\frac{\bar{U}^{k}(x_1)}{\bar{U}^{\pi}(x_1)} \equiv (1 - x)^{.18 \pm .07}$$

We give comparison with prediction from different model (8-10)

CONCLUSION

We first studied the difference between anti-proton and proton cross sections : we have seen that it factorise as predicted by the Drell-Yan model, but that the total yield of events is a factor $K = 2.3 \pm .4$ higher than expected.

We then turned to the meson data : the difference between π^- and π^+ cross sections also factorise according to the model. The determination of the pion structure function was

$$V^{\pi}(x) \propto x^{\alpha_v} (1 - x)^{\beta_v}$$

$$S^{\pi}(x) \propto (1 - x)^{\beta_s}$$

with :

200 GeV/c	150 GeV/c
α_v = .45 ± .1	α_v = .4 ± .1
β_v =1.04 ± .1	β_v = .90 ± .1
β_s =5.4 ± 2.0	

REFERENCES

(1) CEN, Saclay[1]-CERN, Geneva[2]-Collège de France, Paris [3]- Ecole Polytechnique, Palaiseau[4]-Laboratoire de l'Accélérateur Linéaire, Orsay[5]

J. Badier[4], J. Boucrot[5], J. Bourotte[4], G. Burgun[1], O. Callot[5], Ph. Charpentier[1], M. Crozon[3], D. Decamp[2], P. Delpierre[3], A. Diop[3], R. Dubé[5], P. Espigat[3], B. Gandois[1], R. Hagelberg[2], M. Hansroul[2], J. Karyotakis[5], W. Kienzle[2], A. Lafontaine[1], P. Le Dû[1], J. Lefrançois[5], Th. Leray[3], J. Maillard[3], G. Matthiae[2], A. Michelini[2], Ph. Miné[4], G. Rahal[1], O. Runolfsson[2], P. Siegrist[1], A. Tilquin[3], J. Timmermans*[2],

*) Now at NIKHEF-H, Amsterdam, The Netherlands.

(2) BADIER et al. A large acceptance spectrometer to study muon pairs N.I.M. 175(1980) 319.

(3) S.D. DRELL and T.M. YAN, Phys. Rev. Lett. 25(1970) 316.

(4) A.J. BURAS and K.J.F. GAEMERS, Nucl. Phys. B132 (1978) 249.

(5) G. ALTARELLI and G. PARISI, Nucl. Phys. B126 (1977) 298.

(6) J.G.H. DE GROOT et al. Phys. Lett. B82 (1979) 456.

(7) J. BADIER et al, Phys. Lett. B93 (1980) 354.

(8) P.V. CHLIAPNIKOV et al., Nucl. PHys. B148 (1979) 400.

(9) A.EL HASSOUNI and O. NAPOLY, Dual model for parton densities ; DPHT 10/80 (CEN-Saclay preprint).

(10) F. MARTIN (report on the work with A. de RUJULA and P. SORBA) CERN Preprint TH 2845.

FIGURE CAPTIONS

I x_1-x_2 scatter plot for π^- events at 200 GeV/c

II Valence structure function $F(x_1)$ of the nucleon as determined by the anti-proton data after subtraction of the corresponding proton data at 150 GeV. Data points are compared to the prediction of the Drell-Yan model based on the CDHS determination of the valence nucleon structure functions.

III) Same as fig. II for the x_2 axis

IV) $M^3 \frac{d\sigma}{dM}\Big|_{x>0}$ versus $\sqrt{\tau} = \frac{M\mu\mu}{\sqrt{S}}$

dotted line correspond to the Drell-Yan prediction

V) a : the data points represent $F(x_1)$ as defined by eq (8)

b : $F_N(x_2)$ defined as

$$F_N(x_2)=K[(1.6\ U^p(x_1)+2.4\ D^p(x_2)) \frac{J(x_2)}{I(x_2)} (2.2U^p(x_2)+2.8D^p(x_2)+11S^p(x_2))]$$

where $I(x_2) = \int_{x_1^2}^{1} A(x_1,x_2)\ V^{\pi}(x_1)dx_1$

$J(x_2) = \int_{x_1^2}^{1} A(x_1,x_2)\ S^{\pi}(x_1)dx_1$

dashed curves represent the valence distribution solid curves represent the (valence + sea) distribution.

The curves have been scaled up by a factor K :

K = 2.25 at 150 GeV/c

K = 2.4 at 200 GeV/c

VI) The datapoints represent :

$$\frac{\mathcal{L}_\pi \frac{dN}{dx_1}\Big|_K}{\mathcal{L}_K \frac{dN}{dx_1}\Big|_\pi}$$ as defined by eq.(9)

The dashed curves represent the limits of this ration using $\bar{U}_K/\bar{U}_\pi$ and $S_K/\bar{U}_K$ from ref.(8). The upper (lower) curve corresponds to A = 1/8 (A=1/2) The dotted and solid curves represent $\bar{U}_K/\bar{U}_\pi$ ratio from ref.(9) and (10) respectively. For Ref. (9), one should use $\alpha^\phi = 0.17$ instead of 0. (O. Napoly private communication).

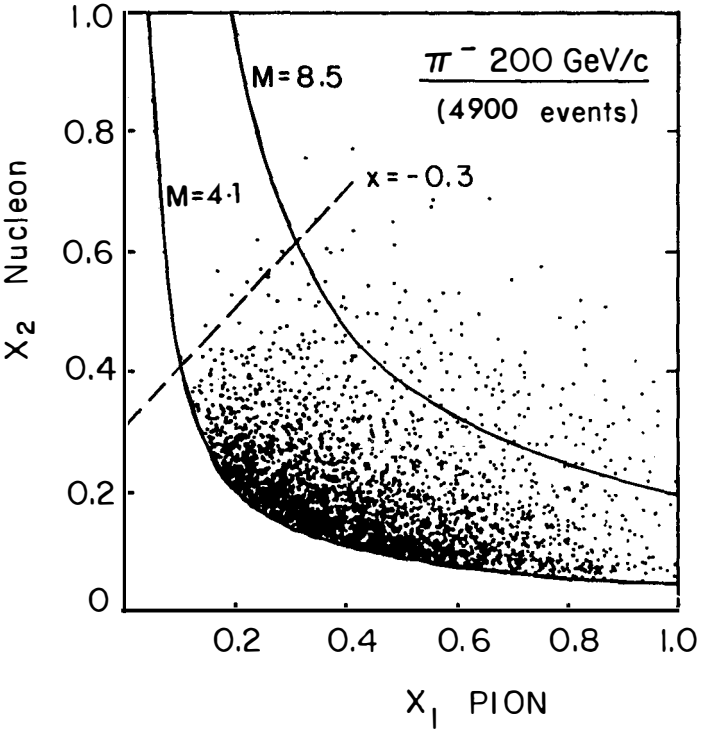
1.0
0.8
0.6
0.4
0.2
0
X_2 Nucleon
M=8.5
M=4.1
π^- 200 GeV/c
(4900 events)
x = -0.3
0.2
0.4
0.6
0.8
1.0
X_1 PION

FIGURE I

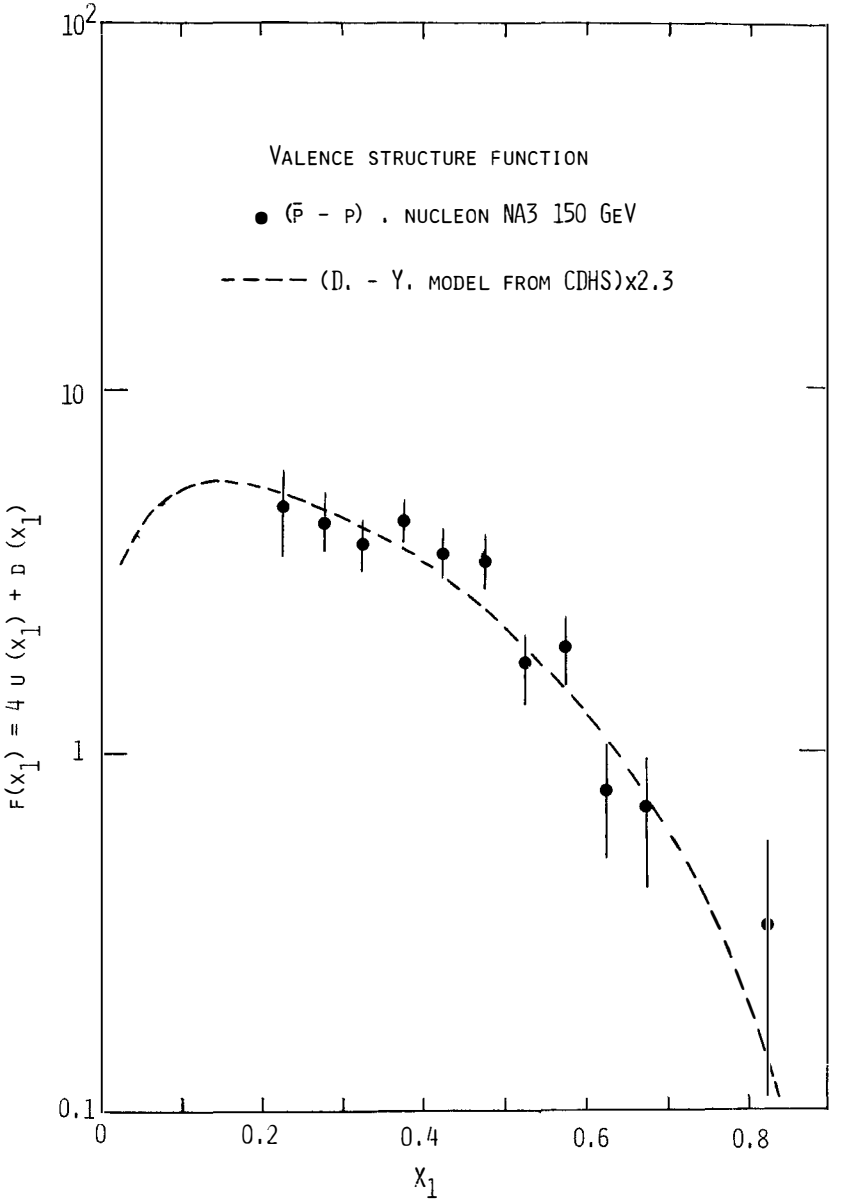
VALENCE STRUCTURE FUNCTION
● (P̄ - P) . NUCLEON NA3 150 GeV
---- (D. - Y. MODEL FROM CDHS)x2.3
10^2
10
1
0.1
$F(x_1) = 4\ u\ (x_1) + D\ (x_1)$
0
0.2
0.4
0.6
0.8
X_1

Figure II

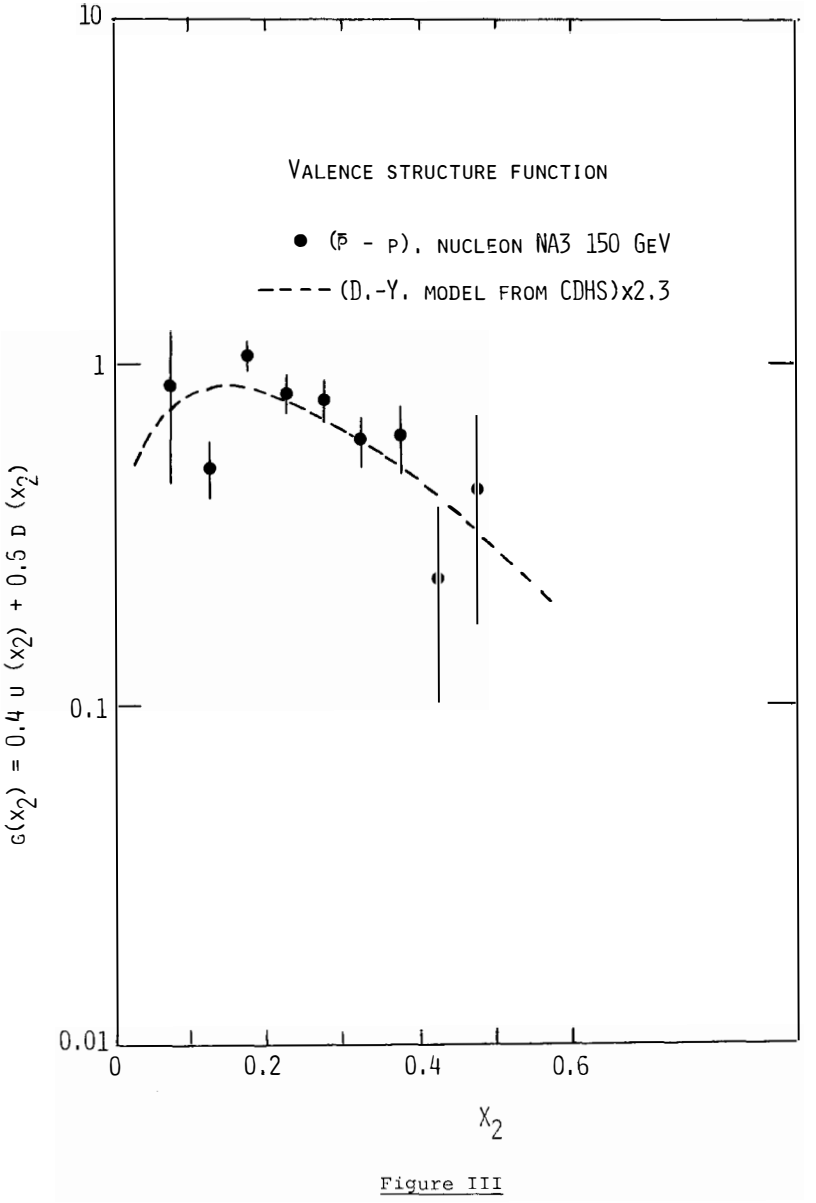
VALENCE STRUCTURE FUNCTION
● ($\bar{p}$ - p), NUCLEON NA3 150 GEV
---- (D.-Y. MODEL FROM CDHS)x2.3
10
1
0.1
0.01
0
0.2
0.4
0.6
X_2
$G(x_2) = 0.4\ u\ (x_2) + 0.5\ D\ (x_2)$

Figure III

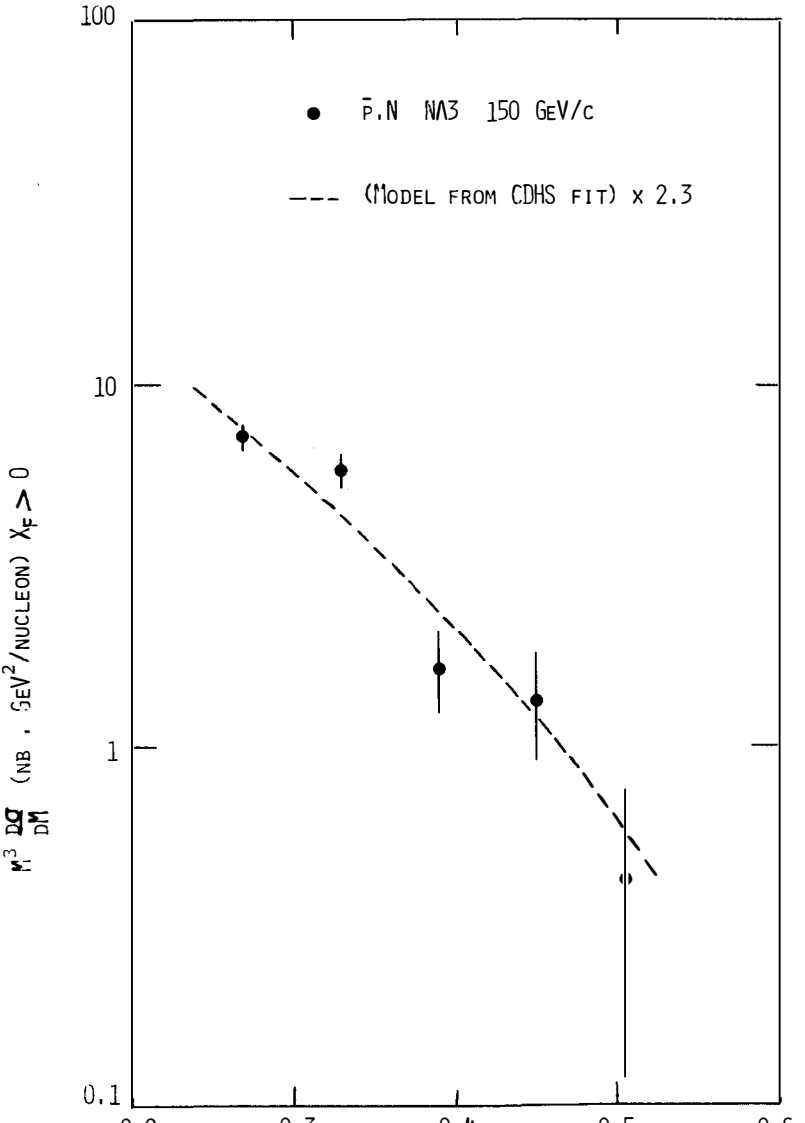
100
10
1
0.1
0.2
0.3
0.4
0.5
0.6
$\bar{P}$.N NA3 150 GeV/c
(Model from CDHS fit) x 2.3
$M^3 \frac{d\sigma}{dM}$ (nb . GeV^2/nucleon) $x_F > 0$
$\sqrt{\tau}$

Figure IV

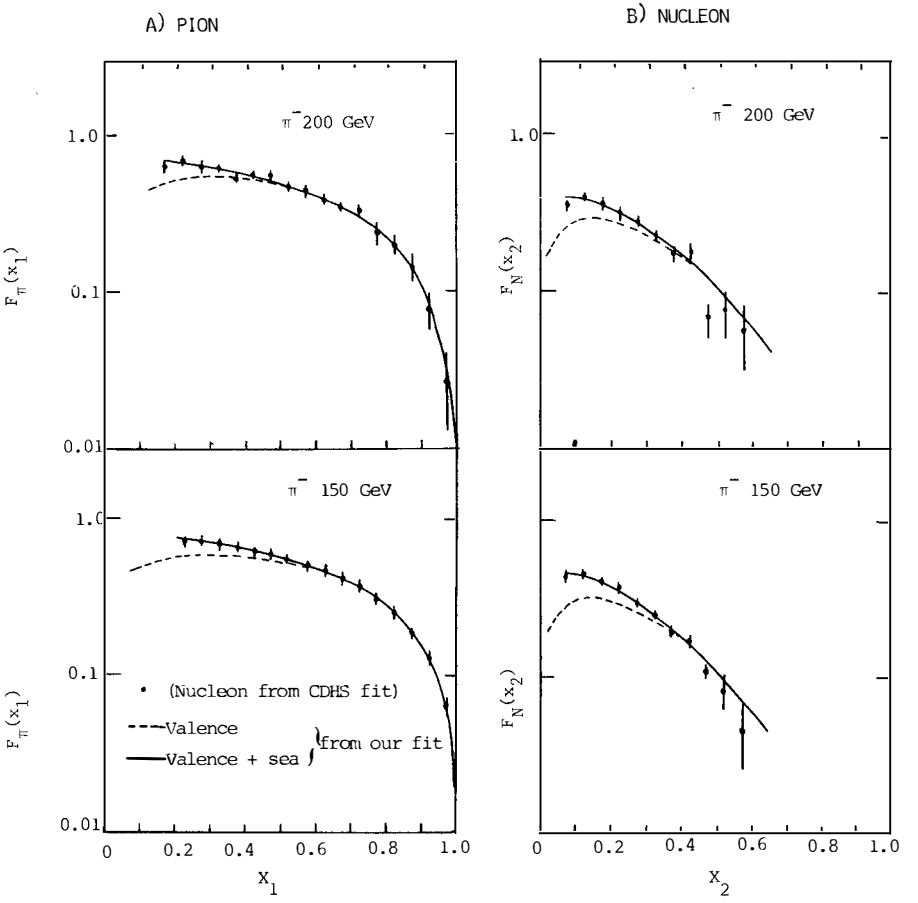
A) PION
B) NUCLEON
π⁻ 200 GeV
π⁻ 150 GeV
1.0
0.1
0.01
$F_\pi(x_1)$
$F_N(x_2)$
• (Nucleon from CDHS fit)
---Valence
—Valence + sea } from our fit
0
0.2
0.4
0.6
0.8
1.0
x_1
x_2

FIGURE V

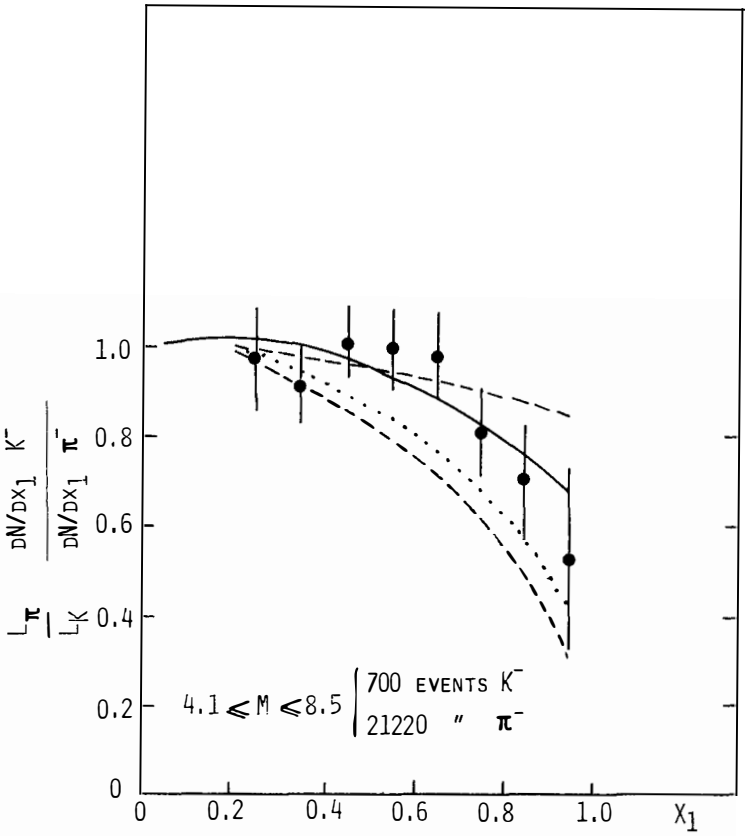
1.0
0.8
0.6
0.4
0.2
0
0
0.2
0.4
0.6
0.8
1.0
X_1
$\frac{L_\pi}{L_K} \frac{dN/dx_1 \; K^-}{dN/dx_1 \; \pi^-}$
$4.1 \leqslant M \leqslant 8.5$
700 EVENTS K^-
21220 " π^-

Figure VI

HADRONIC ψ PRODUCTION IN THE NA3 EXPERIMENT

NA3 COLLABORATION [1]

Presented by Ph. Charpentier
DPhPE/SEE, CEN-Saclay

ABSTRACT

Some qualitative and quantitative results on ψ hadronic production in the NA3 experiment are reported here. Only spots are given on each item. More precise results as well as quantitative comparisons with models are under study.

1) INTRODUCTION

In the same experiment used to measure and study extensively the Drell-Yan continuum [2,3], a large amount of ψ events have been collected, which are studied in order to extract more information about the ψ hadroproduction mechanism.

Data have been obtained with 5 different beams : ±150 GeV, ±200 GeV and -280 GeV/c.

Particle identification at 150 and 200 GeV/c allows us to study ψ production by pions, kaons and protons (or antiprotons) on both our targets (hydrogen and platinum).

This variety of energies, beam particles and targets gives us a total of 26 different data sets with very high statistics for $\pi^{\pm}$ and protons.

The statistics for each data set is given in table 1 and an idea of how a mass spectrum of ψ's looks like can be seen in fig.1

TABLE 1

TARGET		H_2			Pt		
Beam energy	Beam part.	π	K	p	π	K	p
150	+	234	20	150	10 000	550	5 470
	-	18 300	680	300	740 700	29 900	11 900
200	+	2 860	420	2 890	142 740	19 530	131 850
	-	3 580	56	16	172 750	3 200	1 220
280	-	20 100	/	/	516 600	/	/

Statistics of ψ events

2) RESULTS

We present here only the guide lines of some of the studies which have been undertaken on these data, refering the reader to ref.[4] to [13] for theoretical aspects of hadronic ψ production.

A) Nucleus dependence

From our simultaneous use of H_2 and Pt targets, we get directly the nuclear effects. Assuming a A^{α} power law the results are given in table 2.

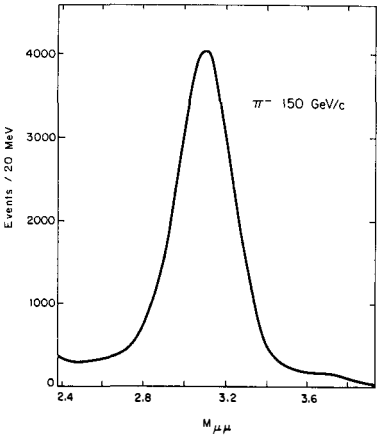

Fig. 1 : $\mu^+\mu^-$ mass spectrum around the ψ mass for π^- at 150 GeV/c.

TABLE 2

Energy of π^- (GeV/c)	α
150	0.935 ± 0.025
200	0.95 ± 0.03
280	0.935 ± 0.025

These values of α are averaged over $x_{\parallel} > 0$ and the whole P_t range. Figures 2a and 2b show however that α varies considerably as a function of P_t and $x_{\parallel}$.

The Pt dependence of α is an effect which is well known for all hadron production mechanisms on nuclei [15]. The quantitative effect is directly related to the ψ-nucleon cross section which can be extracted from both the shape and the magnitude of the P_t distribution. The average value of $\alpha \simeq 0.94$ is not incompatible with measurements of ψ-N cross section by photoproduction experiments [16] ($\sigma_{\psi N} \simeq 3.5$ mb).

The $x_{\parallel}$ dependence has however to be explained. The Fermi motion could have some effect, through the s-dependence of the cross section at large $x_{\parallel}$. Quantitative estimations of this effect are under study.

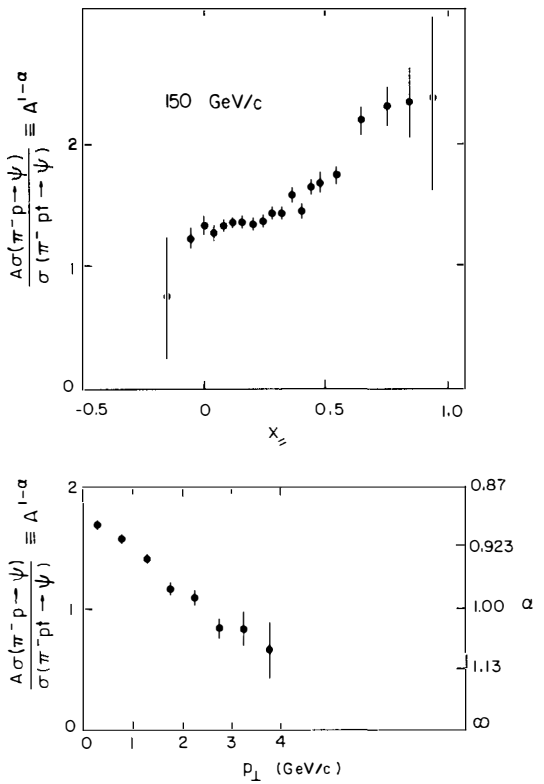

Fig. 2a + b : α as a function of $x_{\parallel}$ and P_t for π^- at 150 GeV/c.

B) Incident particles

We can compare directly our data with π^+ and π^- by using both our targets, in the following way. Let us define

$$R \equiv \frac{\sigma(\pi^+ H_2 \to \psi)}{\sigma(\pi^+ Pt \to \psi)} \Big/ \frac{\sigma(\pi^- H_2 \to \psi)}{\sigma(\pi^- Pt \to \psi)}$$

$$R = r\,\frac{0.4 + 0.6r}{0.6 + 0.4r} \quad \text{where} \quad r = \frac{\sigma(\pi^+ p \to \psi)}{\sigma(\pi^- p \to \psi)}$$

From the measured value of R, one can extract r and the ratio of the cross section on platinum with small errors, as the acceptance and the normalisation do not account. Our results are as follows :

150 GeV/c	200 GeV/c
$R = 0.95 \pm 0.06 \pm 0.04$	$R = 0.97 \pm 0.03 \pm 0.04$
$\downarrow$	$\downarrow$
$r = 0.93 \pm 0.07 \pm 0.04$	$r = 0.96 \pm 0.04 \pm 0.04$
$\downarrow$	$\downarrow$
$\frac{\sigma(\pi^- Pt)}{\sigma(\pi^+ Pt)} = 1.01 \pm 0.02$	$\frac{\sigma(\pi^- Pt)}{\sigma(\pi^+ Pt)} = 1.01 \pm 0.01$

We use the value $\sigma(\pi^- Pt)/\sigma(\pi^+ Pt) = 1.0$ for comparing positive and negative beams.

Table 3 gives the ratio of the cross section for $x_{\parallel} > 0$ at 150 and 200 GeV/c.

TABLE 3

Ratio / P_{beam}	π^-/π^+	K^-/π^-	K^+/π^+	p/π^+	$\bar{p}/p$
150 GeV/c	1.00±0.02	0.97±0.06	1.15±0.12	0.44±0.05	2.02±0.31
200 GeV/c	1.01±0.01	1.08±0.10	0.78±0.08	0.54±0.06	1.57±0.20

Ratio of ψ production cross section

By comparing p and $\bar{p}$ total cross section, one can compute the fraction of ψ's produced by $q\bar{q}$ fusion, since this is the only difference.

At 150 GeV/c 50% of ψ's are produced by valence $\bar{q}q$ fusions in $\bar{p}$-nucleus interaction. Taking into account the effects of the sea, one can calculate that 63±10% of the ψ's are produced by $\bar{q}q$ fusion. In p-nucleus interactions, around 70% are produced by gluon-gluon fusion, since only 30% are due to $\bar{q}q$ fusion (sea-valence and valence-sea).

Quantitative results on a comparison of differential cross sections for different incident particles at various energies are under study [14], and one can hope that they will give some information about $\bar{q}q$-ψ and gg-ψ couplings and gluon contents of the hadrons.

C) Production cross section

Table 4 gives the results of the total production cross section per platinum nucleus (times the branching ratio of ψ into $\mu^+\mu^-$) for the pions at our three energies.

TABLE 4

Energy of π^-(GeV/c)	$\sigma(x_{\parallel} > 0)$
150	850 ± 110 nb
200	1055 ± 130 nb
280	1250 ± 120 nb

Cross section for ψ production by pions at $x_{\parallel} > 0$, per platinum nucleus (A = 195).

3) CONCLUSIONS

By studying high statistics of ψ's produced by different hadrons at various energies on H_2 and platinum targets, we have got evidence for ψ production via $\bar{q}q$ fusion, and we determined with a good precision the α power of the A-dependence.

Further results will become available in a few months.

REFERENCE

[1] J. Badier[4], J. Boucrot[5], J. Bourotte[4], G. Burgun[1], O. Callot[5], Ph. Charpentier[1], M. Crozon[3], D. Decamp[5], P. Delpierre[3], A. Diop[3] R. Dubé[5], P. Espigat[3], B. Gandois[1], R. Hagelberg[2], M. Hansroul[2], J. Karyotakis[5], W. Kienzle[2], A. Lafontaine[1], P. Le Dû[1], J. Lefrançois[5], Th. Leray[3], J. Maillard[3], G. Matthiae[2], A.Michelini[2], Ph. Miné[4], G. Rahal[1], O. Runolfsson[2], P. Siegrist[1], A. Tilquin[3], J. Timmermans[2], J. Valentin[3], R. Vanderhaghen[4], S. Weisz[4].

CEN,Saclay[1]-CERN,Geneva[2],-Collège de France,Paris[3]-Ecole Polytechnique, Palaiseau[4]-Laboratoire de l'Accélérateur Linéaire,Orsay[5]

[2] O. Callot, these proceedings and also Thesis, Orsay 1981.

[3] S. Weisz, these proceedings and Thesis in preparation.

[4] N.B. Green, M. Jacob, P.V.Landshoff, Il Nuovo Cim. 29A (1975) 123.

[5] A. Donnachie, P.V. Landshoff, Nucl. Phys. B112 (1976) 233.

[6] H. Fritzsch, Phys. Lett. 67 B (1977) 217.

[7] M. Glück, J.F. Owens, E. Reya, Phys. Rev. D17 (1978) 2324.

[8] L.M. Jones, H.W. Wild Jr., Phys. Rev. D17 (1978) 2332.

[9] H. Fritzsch, K.H. Streng, Phys. Lett. 78B (1978) 447.

[10] V. Barger, W.Y. Keung, R.J.N. Phillips, Phys. Lett. 91B (1980) 253; Z. Phys. C6 (1980) 169.

[11] M. Glück and E. Reya, Phys. Lett. 94B (1980) 84.

[12] C.E. Carlson and R. Suaya, Phys. Rev. D18 (1978) 760; Phys. Lett 81B (1979) 329.

[13] R. Rückl, these proceedings.

[14] Ph. Charpentier, Thesis in preparation.

[15] J.H. Kühn, Phys. Rev. D13 (1976) 2948 for example.

[16] R.L. Anderson et al., Phys. Rev. Lett. 38 (1977) 263.

TRANSVERSE MOMENTUM OF DILEPTONS

NA3 Collaboration

Presented by J. BADIER

Physique Nucléaire des Hautes Energies

Ecole Polytechnique 91128 PALAISEAU France

ABSTRACT

Transverse momentum produced by π^- et 150, 200 and 280 GeV are compared with QCD predictions.

RESUME

Les impulsions transverses de dimuons produits par des π^- de 150, 200 et 280 GeV, sont comparées aux prédictions de CDQ.

Incident π^- of 150 GeV, 200 GeV and 280 GeV producing muon pairs on a platinum target were studied in the NA3 spectrometer. The distribution of the transverse momentum p_t is expected to be described by the convolution of two functions : the first one is the distribution of the quark intrinsic momentum k_t ; the second is deduced from QCD calculations. In terms of mean squared values, one has :

$$\langle p_t^2 \rangle = \langle k_t^2 \rangle + \langle p_t^2 \rangle_{QCD}$$

Without scaling violations, one expects :

$$\langle p_t^2 \rangle_{QCD} = S\ f(\tau, y),\ \tau = M^2/S$$

y is the rapidity and M the mass of the dimuon.

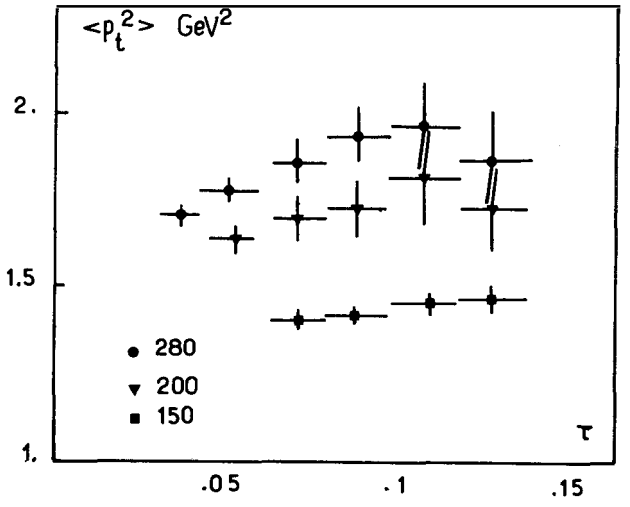

Fig. 1 : $\langle p_t^2 \rangle$ versus $\tau = M^2/S$

The τ dependance of $\langle p_t^2 \rangle$ is presented in figure 1, after integration over y in the range [-.3, 1.1]. The quoted errors are statistical only, but systematic effects of the order of .1 GeV^2 have to be added. They are essentially induced by the beam spread in the target. The data are consistent with the expected form :

$$\langle p_t^2 \rangle = .85 + S\ F\ (\tau)$$

In figure 2, one has plotted the quantity : $(\langle p_t^2 \rangle - .85)/S$. A comparison with QCD calculations may be performed. One calls σ_{DY} the cross section corresponding to the graph :

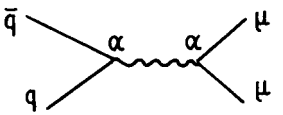

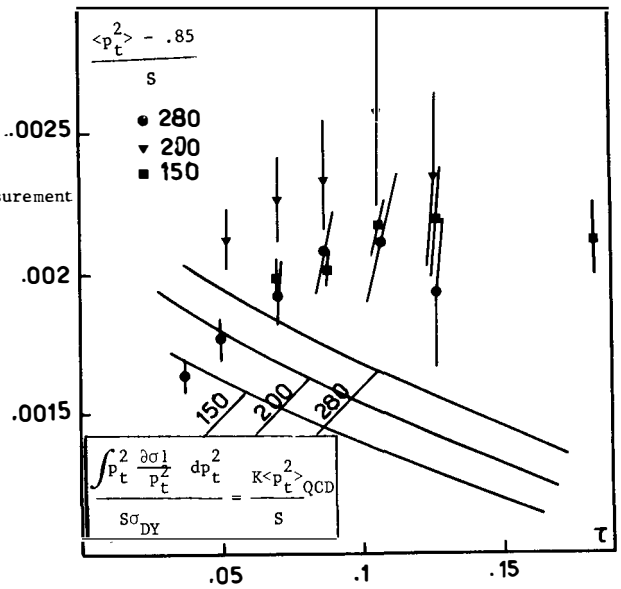

Fig. 2
Experimental measurement compared to QCD calculations.

It is possible to calculate $\frac{d\sigma 1}{dp_t^2}$ corresponding to the first order in α_s. It involves external gluons as in the graphs :

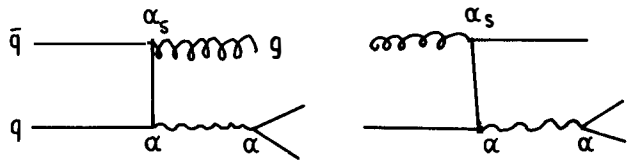

annihilation Compton

In π^- interactions, the annihilation term is predominant contrary to the proton case. The total cross section is related to σ_{DY} by the K factor[2)]

$$\sigma_{tot} = K\ \sigma_{DY}$$

Then, at the first order in αs :

$$\langle p_t^2 \rangle_{QCD} = \frac{\int p_t^2 \frac{d\sigma 1}{dp_t^2} dp_t^2}{K\ \sigma_{DY}}$$

In order to take into account scaling violation, one has choosen :

$$\alpha_s = 12\ \pi / 25\ \text{Log}\ (1 + 4\ Q^2)$$

The quarks structure functions are deduced from deep inelastic [3)] and Drell-Yan [4,5)] experiments :

Proton :

$u = 2A\ (\alpha,\beta)\ x^{\alpha}(1-x)^{\beta} + \bar{u}$

$d = A(\alpha,\beta+1)\ x^{\alpha}(1-x)^{\beta+1} + \bar{d}$

$\bar{u} = \bar{d} = 2\lambda = 2\bar{\lambda} = A(1-x)^{n}$

$\alpha = .52 - .16\ \bar{S}$

$\beta = 2.79 + .77\ \bar{S}$

$A = .26 + .18\ \bar{S}$

$n = 7.80 - .78\ \bar{S}$

$$\bar{S} = \text{Log}\ \frac{\text{Log}\ 4\ Q^2}{\text{Log}\ 80}$$

Pion :

$\bar{u} = d = A(\alpha',\beta')x^{\alpha'} + u$

$u = \bar{d} = 2\lambda = 2\bar{\lambda} = A'(1-x)^{n'}$

$\alpha' = .5 - .1\ \bar{S}$

$\beta' = 1. + .7\ \bar{S}$

$A' = .12 + .7\ \bar{S}$

$n' = 5.$

$$A(\alpha,\beta) = \frac{\Gamma(\alpha + \beta + 1)}{\Gamma(\alpha)\ \Gamma(\beta + 1)}$$

The smaller contribution due to the compton-graphs is computed with gluon structure functions of the form : $Ag(1-x)^{ng}$, with : $Ag = 3.49 + 4.1\ \bar{S}$, $ng = 5.75 \pm 7.5\ \bar{S}$ for the nucleon and $Ag = 2.$, $ng = 3.$ for the pion.

The results of the calculation are displayed in figure 2, where $\langle p_t^2 \rangle_{QCD}$ is multiply by the K factor. The confrontation with experimental values suggests that $\frac{d\sigma 1}{dp_t^2}$ has to be corrected by a factor greater than this K factor. Furthermore, the QCD estimations decrease with τ, whereas experimental values increase. In conclusion, one has :

$$\langle p_t^2 \rangle = \langle k_t^2 \rangle \frac{\int p_t^2 \frac{d\sigma 1}{dp_t^2} dp_t^2 + \int p_t^2 \frac{d\sigma_n}{dp_t^2} dp_t^2}{K\ \sigma_{DY}}$$

with $\langle k_T^2 \rangle = .85 \pm .1$

$$\frac{d\sigma_n}{dp_t^2} > K \frac{d\sigma 1}{dp_t^2}$$

$\frac{d\sigma_n}{dp_t^2}$ represents all the contributions which have to be added to the first order of QCD.

In figure 3, $\langle p_t^2 \rangle$ is displayed as a function of y, after integration over τ, in the range [.06, .14]. Shapes agree with theoretical ones resulting essentially from phase space.

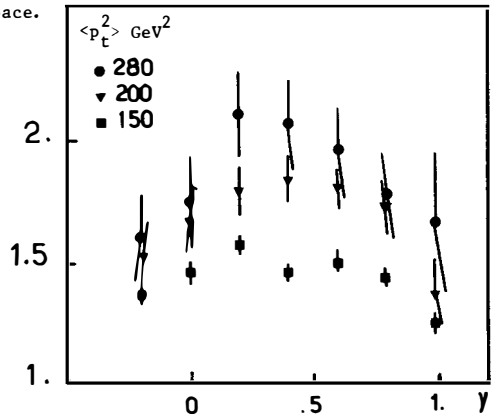

Figure 3
$\langle p_t^2 \rangle$ versus center of mass rapidity

REFERENCES

1) CEN, Saclay[1]-CERN, Geneva[2]-Collège de France, Paris[3]- Ecole Polytechnique, Palaiseau[4]- Laboratoire de l'Accélérateur Linéaire, Orsay[5]

J. Badier[4], J. Boucrot[5], J. Bourotte[4], G. Burgun[1], O. CALLOT[5], Ph. Charpentier[1], M. Crozon[3], D. Decamp[2], P. Delpierre[3], A. Diop[3], R. Dubé[5], P. Espigat[3], B. Gandois[1], R. Hagelberg[2], M. Hansroul[2], J. Karyotakis[5], W. Kienzle[2], A. Lafontaine[1], P. Le Dû[1], J. Lefrançois[5], Th. Leray[3], J. Maillard[3], G. Matthiae[2], A. Michelini[2], Ph. Miné[4], G. Rahal[1], O. Runolfsson[2], P. Siegrist[1], A. Tilquin[3], J. Timmermans*[2], J. Valentin[3], R. Vanderhagen[4], S. Weisz[2].

*) Now at NIKHEF-H, Amsterdam, The Netherlands.

2) Physics Letters 89B (1979) p. 145
J. Badier et al.

3) Physics Letters 82B (1979) p. 456
J.G.H. De Groot et al.

4) Phys. ReV. Letters 42 (1979) p. 951
C.B. Newman et al.

5) Madison
J. Badier et al.

DIMUON PRODUCTION IN A BEAM DUMP DETECTOR BY 400 GeV PROTONS

Paul M. Mockett
Department of Physics, FM-15
University of Washington, Seattle, Washington USA 98195

Abstract: Results from 225,000 dimuon events with mass above 6 GeV obtained in a beam dump detector are presented. The sea quark structure functions are determined from the mass spectrum and are found to be a factor of 1.6±0.3 larger than those obtained from inelastic neutrino scattering. A test of the Drell-Yan model over the Feynman x, x_F, range of -0.2 to 1.0 is made for masses up to 14 GeV. The x_F dependence of the Upsilon family production cross section is given. Also presented is the average P_t of the dimuon pairs versus x_F and the mass. A small increase with mass is indicated, but no significant decrease with x_F is found.

1. Introduction*

The results of the MNTW** collaboration presented in this talk are based on data taken at Fermilab in the spring of 1978. The first data obtained in this experiment were taken at the time of the discovery of the Upsilon family by the CFS group.[1] Confirmation of this meson family was first reported by the MNTW group in D. A. Garelick et al.[2] Approximately 225,000 dimuon pairs with mass above 6 GeV were recorded. These were produced by 400 GeV/c protons on a tungsten target. About 15,000 events in the Upsilon family were contained in this sample.

The experimental technique employed can be characterized as a beam dump detector. The advantages of this device are: (1) a high rate capability of up to 10^{12} protons per pulse; (2) a large overall acceptance of approximately 6% and all Feynman x greater than -0.2; (3) a multi-muon detection capability where three or more muons might be seen, for example, if naked charm or bare bottom mesons were produced in coincidence with the J/ψ or Υ resonances. The detector could also have recorded low mass pairs produced at large P_t had we realized the importance of studying this process at that time.

The disadvantages of the device are: (1) a poor mass resolution of about 7.5%; (2) a contamination from dimuons produced by secondary hadrons in the long target and dump. As an aside we note that an air gap magnet placed downstream of the dump would have enabled this technique to obtain a mass resolution of about 2% at large mass. The Northeastern Group component of this collaboration is proposing to do this in Fermilab Experiment P645.

In this paper we will report on (1) the sea quark structure functions as determined from our dimuon spectrum and K factor; (2) a test of the Drell-Yan model; (3) the Feynman x dependence of the ratio of the Upsilon production to that of the continuum; (4) the average P_t dependence of the dimuon pairs as a function of both Feynman x and dimuon mass.

2. The Detector

Our apparatus is shown in Fig. 1. A 400 GeV/c proton beam is incident from the left and impinges on a 32 cm tungsten target. The target is placed

* This work was supported by the National Science Foundation and the Department of Energy.

** The institutions involved in this collaboration are University of Michigan, Northeastern University, Tufts University, and the University of Washington. The collaborators were S. Childress, D. A. Garelick, P. S. Gauthier, M. J. Glaubman, H. R. Gustafson, L. W. Jones, H. Jonstad, M. J. Longo, M. L. Mallary, P. M. Mockett, J. Moromisato, W. P. Oliver, E. Pothier, T. J. Roberts, J. P. Rutherfoord, S. R. Smith, E. von Goeler, M. R. Whalley, and R. W. Williams.

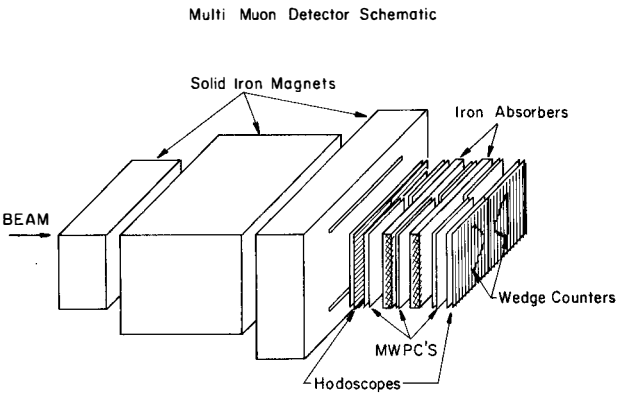

Fig. 1. Beam Dump Detector Schematic. The 400 GeV/c proton beam is incident from the left and impinges on a 32 cm tungsten target. The 5.5m of solid iron magnets have a horizontal field of 2.15T.

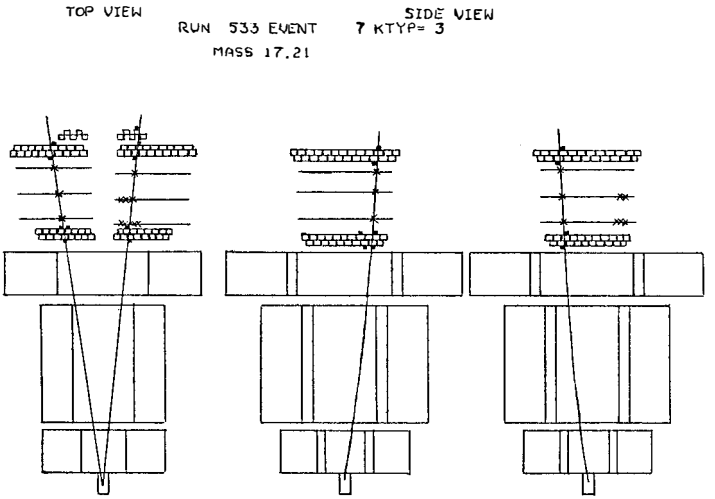

Fig. 2. Typical High Mass Event. The hodoscope and PWC hits of a 17 GeV mass dimuon event are shown along with the reconstructed trajectories.

next to the first dump magnet so that background from pion decays is minimized. The 5.5m of beam dump magnets carry a horizontal field of 2.15T and also serve as the analysis magnets.

Following the iron is the dimuon detector. It is composed of two mirror-image arms whose opening angle can be adjusted for different running conditions. Most of the running was taken with the arms making a minimum angle of 18 mr with respect to the target. Each arm begins with two planes of trigger hodoscopes which give the horizontal and vertical position of muons traversing the magnets. These hodoscopes are followed by 9 planes of proportional wire chambers grouped into three sets. Each set is separated by a 7-inch slab of iron to prevent showers produced near the end of the magnet from penetrating all the planes. Following the proportional wire chambers is another set of horizontal and vertical trigger hodoscopes.

Following these hodoscopes is a final set of vertical hodoscopes which were used to restrict the triggers to the highest mass. These formed a wedge-shaped pattern and were used in the trigger to replace the inner back vertical hodoscopes that they overlapped. The bulk of our high mass data was obtained with this requirement. The fast trigger required hits in the four planes of hodoscopes in each arm. The latched hodoscope hits were then viewed by a matrix logic unit based on the memory chip developed by Brookhaven National Laboratory. This matrix logic imposed a higher momentum cut than was produced by the acceptance of the magnets and hodoscopes, and it required the dimuon trajectories to point back to the target in the non-bend plane. If these requirements were not satisfied the event was aborted. The trigger was very clean and approximately 70% of our triggers were reconstructed to give good dimuon pairs. A typical high mass event is shown schematically in Fig. 2. The hits in the PWC's and the hodoscopes are shown, along with the reconstructed muon trajectories.

3. Acceptance and Systematics.

As a check on background produced by random dimuon coincidences, a scaled sample of events with one arm delayed by two rf buckets with respect to the other was also recorded. These could be compared with the like sign events taken along with the opposite sign events. To make the comparison precise, one of the like sign events was reflected in the horizontal mid-plane before calculating the mass. This corrects for the difference of the acceptance of the opposite and like sign pairs. The reflected like sign data, along with the opposite sign raw data for the high mass trigger is shown in Fig. 3. As can be seen, the background from accidentals is typically 1% or less in the high mass region.

In Fig. 4 we show the acceptance of the apparatus as a function of q^2

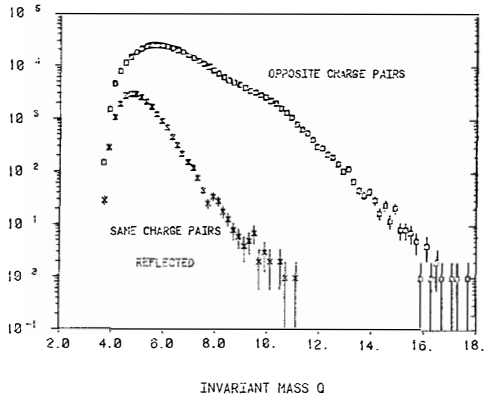

Fig. 3. Accidental Rate. This is a plot of our raw high mass data and the accidental data as evidenced by the like sign pairs.

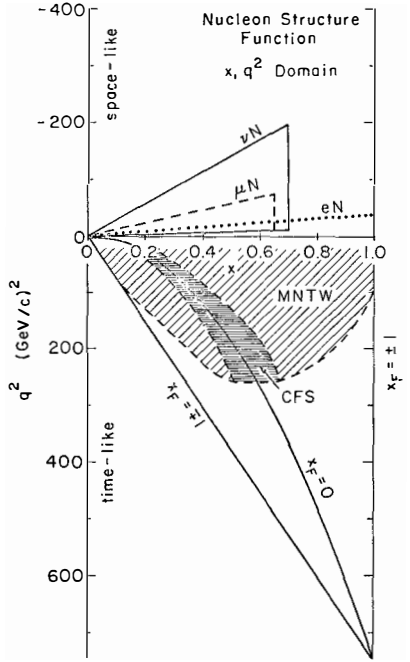

Fig. 4. Apparatus Acceptance. The acceptance of the apparatus is shown for Bjorken x and q^2. Also noted are the acceptances of the deep inelastic lepton scattering experiments in the space-like region and the CFS acceptance at 400 GeV. The dashed boundary is the limit of useful statistics.

versus Bjorken x of the partons. The dashed boundary is not a geometrical cut-off but is determined by the limit of useful statistics. Also noted is the region covered by the CFS group at 400 GeV and by the deep inelastic lepton scattering experiments in the space-like domain.

In order to correct the data for the systematics of the apparatus acceptance and the interaction of muons in iron, a Monte Carlo program was used that simulated the effects, including the fluctuations, of multiple scattering, knock-on electrons, bremmstrahlung, pair production and finite radiative corrections.[3] The finite resolution of the PWC's was also included.

In Fig. 5 we show the corrected dimuon mass spectrum for dimuon events with Feynman x from 0 to 0.2. The three curves labeled (a), (b), and (c) are acceptance functions for the different triggers used and reference the scale at the right. For (a) the two arms were together, for (b) the two arms were separated by 18 mr and for (c) the high mass wedge counter trigger was satisfied as well as the matrix logic conditions. These acceptances are affected by the geometry as well as the resolution because muon pairs can scatter into the acceptance. The dimuon spectra resulting from the three different triggers after correction agreed to better than 5% in the two regions of overlap. A small correction for random coincidences has been made from the like-sign pairs $\mu^+\mu^+ + \mu^-\mu^-$ and for muons produced by pions in the target. The inset shows the events in the Upsilon region on a linear scale after a subtraction of the continuum is made. The shape agrees very well with our Monte Carlo results.

4. Sea Quark Distribution.

To find the sea quark distribution we use the events from the region shown in Fig. 6. These are the events shown in Fig. 5 above 5 GeV in mass and excluding the Upsilon region. Using the value of $F_2^p(x,q^2)$ found in deep inelastic lepton scattering[4], we fit our spectrum with the function

$$C_1F_2^p(x_1,q^2)S(x_2)+C_2S(x_1)F_2^p(x_2,q^2)+C_3S(x_1)S(x_2)$$

where C_1, C_2 and C_3 are known functions of x_1 and x_2 and S(x) specifies the sea quark distribution. We have used the parameterization of F_2^p given by T. Kirk.[5] For the q^2 evolution we have assumed that $q^2 = m^2$ where m is the dimuon mass, and have ignored the sign change. F_2^n was obtained from the SLAC deep inelastic electron scattering[6] and we have assumed that $F_2^n/F_2^p = .807 - .535x$ is independent of q^2.

The $\bar{u}$ $\bar{d}$, $\bar{s}$ and s sea quark distributions have been parameterized in two ways:

A. symmetric sea: $x\bar{d} = x\bar{u} = 2xs = 2x\bar{s} = a(1-x)^b$

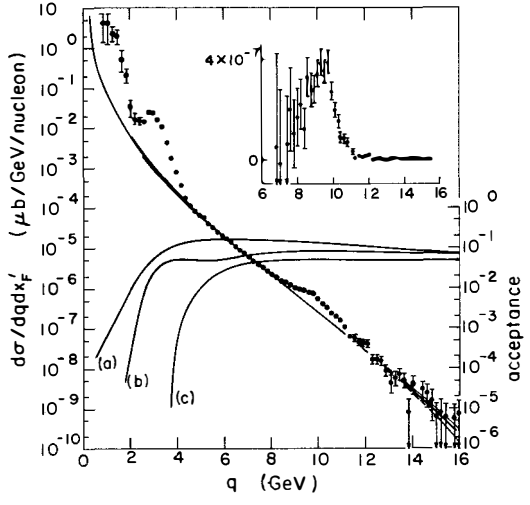

Fig. 5. Dimuon Production Cross Section. This shows the dimuon cross section for events in the region of $0<x_F'<0.2$ versus mass, q. Mass dependent systematic errors are indicated by the spread in the fitted curve and are in addition to an 11% overall error. The fit is the result of the asymmetric sea determination. The curves labeled (a), (b), and (c) are the acceptances for the three triggers used and reference the scale to the right.

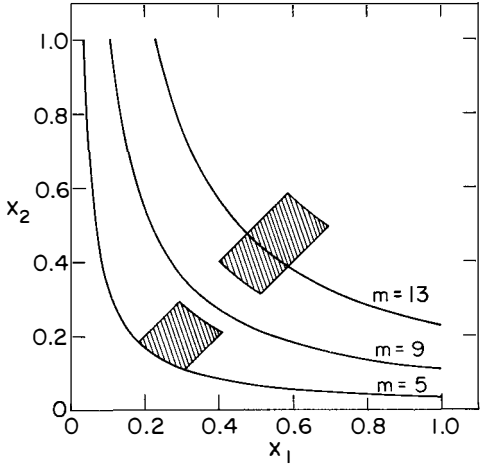

Fig. 6. Sea Quark Fit. x_1 and x_2 are the Bjorken x values of the beam and target partons, respectively. The shaded area is the region from which the sea quark distributions were determined.

B. Asymmetric sea: $x\bar{d} = a(1-x)^b$

$$x\bar{u} + (1-x)^{2.5} x\bar{d}$$

$$xs = x\bar{s} = (x\bar{u}+x\bar{d})/4$$

All higher mass quark flavors are neglected. The asymmetric form is suggested by the results of the CFS group.[7)]

The results of a best fit to the data in Fig. 6 for the parameters a and b are given in the following table.

	A	B
a	.46±.03±.06	.50±.03±.06
b	8.2±.2±.3	7.4±.2±.3

where the first error is statistical and the second an estimate of the systematics. In Fig. 5, the solid curve is the fit using the asymmetric sea and has a chi-square of 35 for 35 degrees of freedom. The broadening of the curve is a measure of the systematics. These are largely due to the uncertainty of the extent of the dimuon production from secondary particles. There is also an overall 11% uncertainty in the normalization of our data.

We emphasize that the q^2 dependence of the sea cannot be obtained from this fit, since each point, x, for the sea quark distribution is essentially measured at a single value of q^2. If the sea quark distributions are compared with those obtained by the CDHS collaboration[8)] (although these were at lower q^2), we find a larger value by a factor of 1.6±0.3 in the region of overlap. This ratio is customarily called the K factor, and is somewhat smaller than that obtained from the pion data,[9)] but the difference may be due to scale breaking.

5. Test of Drell-Yan

Having obtained these sea quark distributions we can then compare the predictions of the Drell-Yan model with the cross section observed in the remainder of phase space detected by our apparatus. To systematically note the edge of phase space we use the variable $x_F' = x_F/(1-\tau)$ where $\tau = m^2/s$. That is, Feynman x is scaled by the maximum possible value for a given mass. In Fig. 7 we show on a linear scale the cross section prediction of the Drell-Yan model vs. x_F' (compared with the data) for dimuon masses in the region of 11.5 GeV. The normalization of the curve comes from the fit in the x_F' region of .0 to 0.2 and the shape depends upon the Drell-Yan model. In Fig. 8 we show the results on a logarithmic scale for 5 different mass bins. The curves show excellent agreement with the data. The chi-square per degree of freedom are as follows:

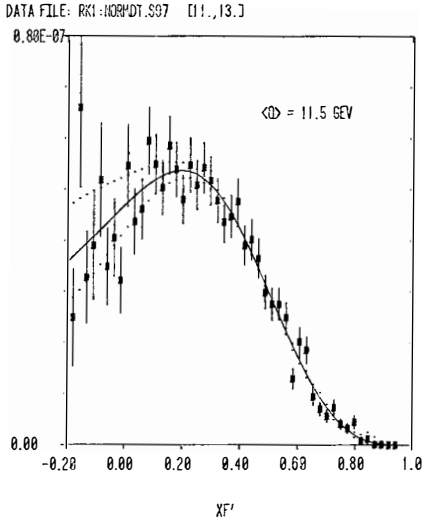

Fig. 7. Test of Drell-Yan. This shows a comparison of the cross section predicted by the Drell-Yan model and our data in the 11.5 GeV mass region. The sea quark distribution was obtained from the asymmetric fit. The dotted curve is a measure of our systematic uncertainty.

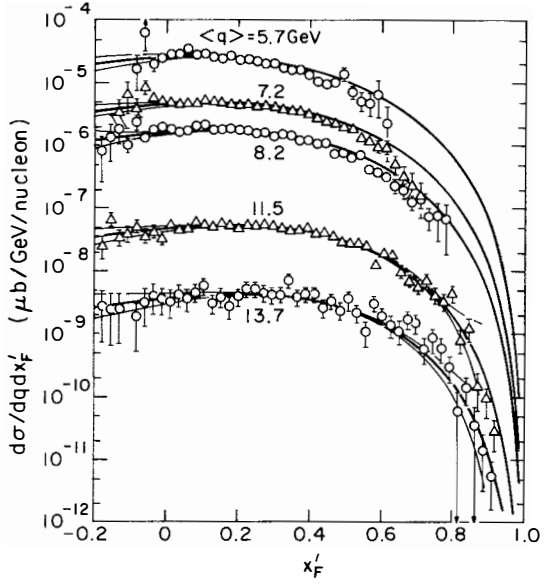

Fig. 8. Test of Drell-Yan. This shows a comparison of the Drell-Yan model predictions for five different mass bins with our data. The lack of events at low mass and large x_F' is due to limited statistics.

mass	chi-square	degree of freedom
5.7 GeV	93.5	30
7.2	73.7	36
8.2	116.5	41
11.5	74.5	47
13.7	37.3	46

The cut-off in the data at large x_F' and low mass is due to the poor acceptance in this region by the high mass trigger and the limited statistics obtained with the low mass trigger. The poorer fits at the lower masses could be due to our parameterization of F_2, a K factor variation or scale breaking in the sea. Scale breaking is expected and could be included to improve the fit to the data.

6. Upsilon Production

The production mechanism for the resonances observed in hadron production of dimuons is as yet uncertain and several mechanisms have been suggested[10]. The ratio of the Upsilon to the continuum as a function of x_F' is clearly sensitive to the production mechanism and a ratio avoids errors introduced by absolute normalization. For example, if the production were mainly due to quark-antiquark annihilation, then the ratio would be expected to be approximately constant for different Feynman x values. Small differences in the behavior of the up and down quark structure functions would prevent the ratio from being precisely constant. On the other hand, a substantial component of gluon production would cause the ratio to decrease with Feynman x. Given the gluon structure function different models can be tested or given a model, the gluon structure can be constrained. We show the ratio of the Upsilon family to continuum production vs. x_F' in Fig. 9.

The ratio plotted in Fig. 9 is given by

$$R = (d\sigma(\Upsilon)/dx_F')/(d^2\sigma(C)/dm dx_F')$$

in units of GeV. The data has not been corrected for absorption in the tungsten nucleus, but this is expected to be small. We have also assumed that the decay angular distribution for the Upsilon family is isotropic. Our results agree well with the point obtained by the CFS group shown on the plot. The decrease in the ratio as a function of x_F is characteristic of substantial production by gluons.

6. P_t Dependence

It is now clear that the Drell-Yan process involves a sizeable amount of gluon radiation. This radiation may be responsible for a large fraction of the

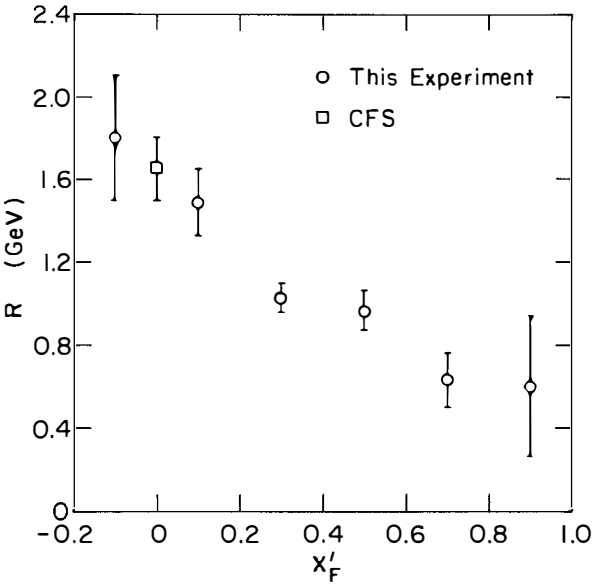

Fig. 9. Upsilon to Continuum Ratio. This shows the ratio of the Upsilon family production cross section to the continuum cross section in the Upsilon region as a function of x'_F.

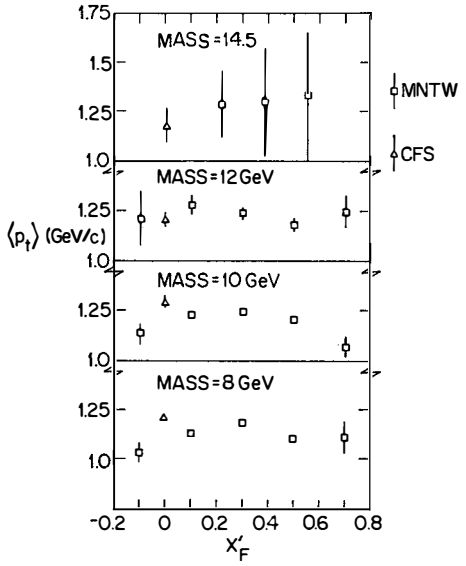

Fig. 10. Average P_t. Plotted here is the average P_t of the dimuon pairs versus x'_F for four mass intervals. No significant decrease in the average P_t with increasing x'_F is indicated, although a slight increase with increasing mass is apparent.

transverse momentum carried by the dimuon pairs. In Fig. 10 we show the mean value of the dimuon P_t as a function of x_F' for several mass bins. The data indicate a mean value that is independent of x_F' and slowly increases with mass. Hopefully QCD will be able to explain the precise nature of this behavior, although the predicted decrease in mean P_t with Feynman x is not observed.[11]

7. Summary

We can summarize our results as follows: We have obtained sea quark structure functions similar to those obtained in other processes but with a K factor of 1.6±0.3. Using the Drell-Yan model, these structure functions are used to predict the behavior of the cross sections for a large range of mass and Feynman x. The agreement with our data is very good.

We have found that the ratio of the Upsilon production to continuum decreases substantially with Feynman x, which indicates a significant amount of the production involves gluons.

The average value of P_t for the continuum is found to be large and independent of Feynman x. The average value does show a small increase with increasing dimuon mass.

References

1) S. W. Herb et al., Phys. Rev. Lett. 39, 252(1977).
2) D. A. Garelick et al., Phys. Rev. D18, 945 (1978).
3) A. Soni, Phys. Rev. D8, 2264 (1973).
4) B. A. Gordon et al., Phys. Rev. D20, 2645 (1979).
5) T. B. W. Kirk, Fermilab Report Number TM-791 (1978).
6) A. Bodek et al., Phys. Rev. D20, 1471 (1979).
7) A. S. Ito et al., FERMILAB-Pub-80/19-EXP(1980).
8) J. G. H. de Groot et al., Zeitschrift fur Physik C1, 143 (1979).
9) For a summary see, for example, G. Matthiae CERN-EP/80-183.
10) J. F. Owens and E. Reya, Phys. Rev. D17, 3003 (1978) and R. Rückl at this conference.
11) F. Halzen and D. M. Scott, Phys. Rev. Lett. 40, 1117 (1978).

THE STATUS OF CFS

(the Columbia-Fermilab-Stony Brook Collaboration)

Charles N. Brown

Fermilab

Abstract:

Some aspects of the final published E-288 data set are examined. Some extrapolations and systematics which plague current phenomenology are emphasized. A description of a planned follow-on experiment, Fermilab E-605, is given.

It is now two years since we took the last dimuon data with the CFS apparatus and one year since we finished the final analysis of all the data. The special calibration runs have been combined with extensive Monte Carlo checks to complete the full analysis of the data. Complete tables of the data, listed in separate bins in the transverse, longitudinal and mass variables (P_t, y, m) are included in the final publication.[1]

In the data we have seen presented to this conference, there are usually correlations between these kinematic quantities which are often forgotten when spectra are integrated over one variable to give better statistics in some other variable. I urge phenomenologists who want to critically examine the ensemble of lepton-pair production data now available to carefully watch for and consider these correlations.

In my short review of our CFS results today I would like to remind the audience of one such complication which makes it difficult to extract a "K-factor" from our data. I would then like to examine our P_t spectra in the manner that Altarelli and Scott have suggested in preceding talks with the object of giving some guidance in designing our future experiment, E-605. Finally I will show the present design plans for E-605.

Contrary to Vannucci's introductory talk at this conference, I do not think of the Drell-Yan effect as a QCD diagram, but rather as a real physical effect. Figure 1 schematically shows the yield of dimuon pairs in proton-nucleus collisions at Fermilab. The vector meson resonances sit on a monotonically falling continuum of massive dilepton states. We now believe that we can understand this yield of virtual photons, over most of the ten decades of cross-section shown, in terms of a simple quark-antiquark annihilation.[2] Indeed, the predictions that follow from this simple explanation: A-dependance, angular distribution of the decay, scaling, dimuon-dielectron equality, universality of the structure functions thus determined, have been investigated and qualitatively confirmed in the many experiments you have heard from this week. In proceeding in the future with further testing of QCD we are now faced with two choices.

Fig. 1. Schematic yield of dilepton pairs in 400 GeV proton-nucleus collisions (from CFS and Chicago-Princeton data at FNAL).

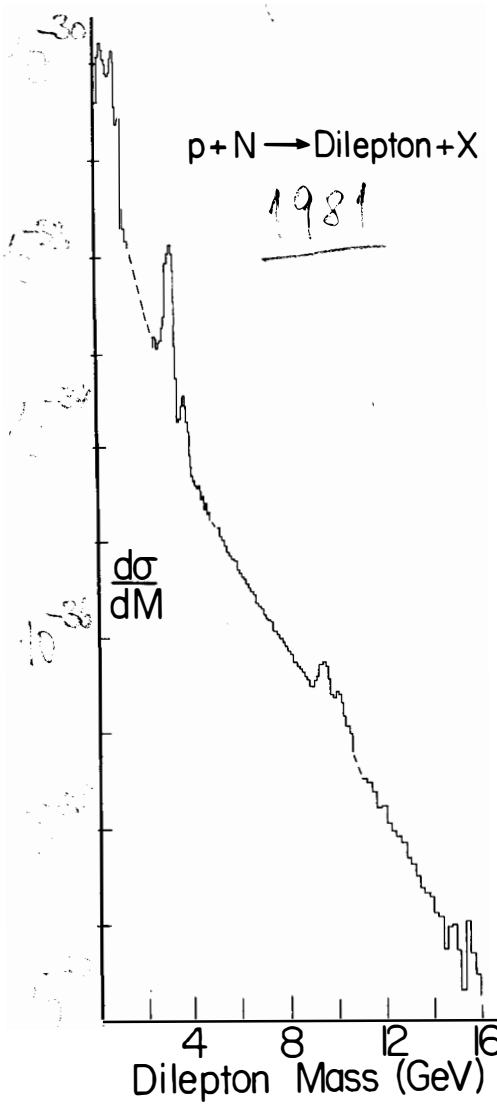

We can try to test the basic Drell-Yan prediction with much higher statistics experiments or we can try to find regions of phase space where terms other than the Born term dominant the cross-section.

Let me first address the question of high-precision tests of Drell-Yan by considering our CFS scaling data shown in Figure 2. The agreement with scaling appears to be better than the quoted ±20% systematic error and shows almost no sign of log Q^2 scale-breaking effects. Figure 3 indicates the magnitude of scale-breaking expected from structure function evolution calculations.[3] Clearly, investigation of any log Q^2 predictions of QCD is going to require large excursions in center-of-mass energy to avoid systematic error problems inherent in any experiment.

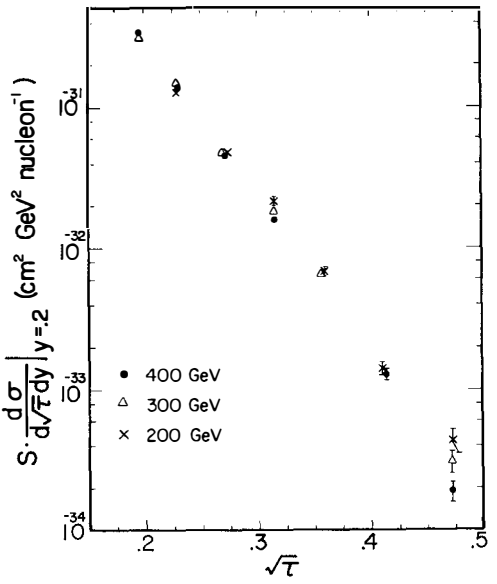

Fig. 2. Scaling form of the cross section for 200, 300, and 400 GeV data.

Figure 4 shows such an attempt to confront scaling over a larger range in energies by comparing our data to ISR data.[4] Since the comparison involves both an extrapolation to smaller values of $\sqrt{\tau}$ and a different reaction, proton-proton instead of proton-nucleus, the comparison must be made to a curve calculated from the structure functions derived from the CFS data. Although the agreement is impressive, the combination of the meager ISR statistics and the extrapolation preclude any stringent test of log Q^2 effects.

Next, one might try to accurately determine the absolute normalization of the dilepton data. The ratio of the measured cross-section to that predicted using structure functions determined in deep inelastic lepton scattering experiments (DIES), the so-called "K-factor", is believed to be a sensitive test of higher order QCD effects. We choose to make the comparison in figure 5 using the combined ocean structure function $\bar{q}(x) = \bar{u}(x) + \bar{d}(x) + \bar{s}(x)$ derived from a fit to our data.

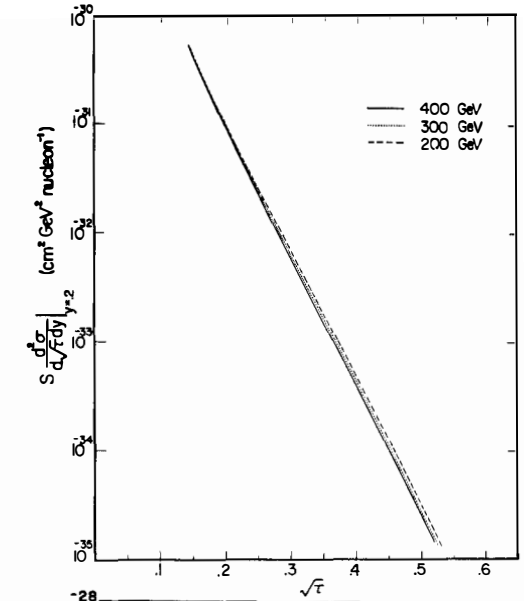

Fig. 3. Cross section at the three different beam energies as predicted by a QCD calculation of Owens and Reya (Ref. 3).

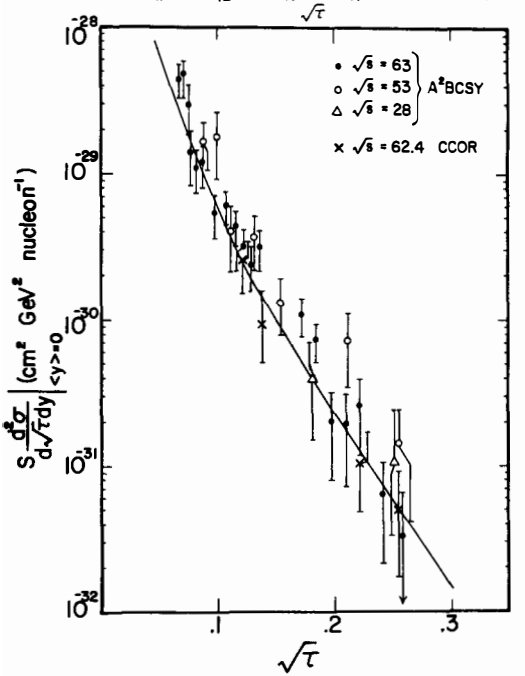

Fig. 4. CERN ISR dilepton data. The solid line is a Drell-Yan model fit to the CFS data extrapolated to the CERN regime.

Unfortunately both the DIES data and the dilepton data have a bad correlation of x and Q^2 as indicated in the figure 5 caption. The overlap in Q^2 occurs at about x = .15, below the CFS data. Thus the determination of the "K-factor" involves an extrapolation (with an unknown functional shape) to lower x for the CFS data, an extrapolation in Q^2, and a neutrino-antineutrino subtraction measurement with its inherent systematic problems. The data are consistent with a K-factor of about 2 but no more accurate statement than this can honestly be made. I urge you to remember this in other determinations of the K-factor; the simple ratio of two large data sets is usually completely dominated by hidden extrapolations and systematics.

I believe one aspect of our data does confront QCD calculations and can lead to more fruitful research in the future. Figure 6 shows our data on the yield of dilepton pairs as a function of the P_t of the pair. The data shows a complicated behavior; for P_t<1 GeV/c the curves look quadratic, i.e. a behavior like $e^{-aP_t^2}$.

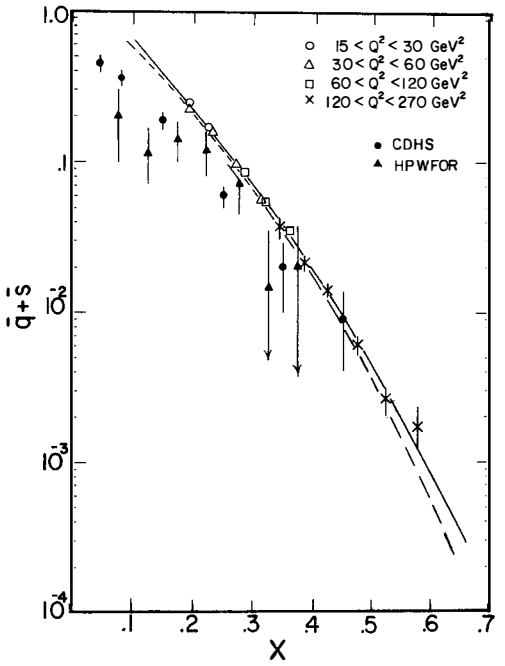

Fig. 5. Sea distribution for this experiment compared with neutrino results. In the dilepton data there is a correlation $\langle Q^2 \rangle \approx 2mx^2E$ and in the neutrino data the correlation is $\langle Q^2 \rangle \approx 2mxyE$. See Reference 1 for details of the comparison and fitted curves.

For P_t>2 GeV/c the curves flatten off and became slightly concave indicating a P_t dependance slower than exponential, a possible sign of power-law dependance. Clearly, quoting an average value of $\langle P_t \rangle$ or $\langle P_t^2 \rangle$ does not do justice this data; the cross section may be reflecting different sub-processes in the low and high P_t region.

Kajantie and Raitio[5]; Altarelli, Parisi and Petronzio[6]; Berger[7]; and other theorists spotted these trends in our data and attempted to calculate second order lepton-production contributions. Briefly, their work involved including contributions due to the gluon bremstrahlung and gluon Compton scattering diagrams shown in Figure 7b and 7c respectively. The Compton scattering diagram especially was found to contribute importantly at high P_t if one assumed that the constituent quarks in a nucleon had a limited intrinsic transverse momentum.

Unfortunately the simple calculation of these second order diagrams diverges at low P_t. Some way must be found to "regularize" the low P_t behavior. A simple procedure involves folding all the calculations with a simple gaussian intrinsic transverse momentum, $e^{-aK_t^2}$. A straightforward procedure can then be followed to fit the data to the sum of the five terms shown in Figure 7.

In order to fit our data, we have assumed a univeral shape for the distribution of gluons in a nucleon, $B(1-x)^m$; a form for the anti-quark distributions in a proton, $d= A(1-x)^n$ and $u= A(1-x)^{n+\beta}$; and a Gaussian intrinsic transverse momentum spectrum for the constituents, $e^{-aK_t^2}$. The valence structure functions u(x) and d(x) are taken from existing deep inelastic scattering data.[8] Since the second order diagrams involve a gluon-quark vertex, the strong coupling constant α_s is also a parameter in the fit.

The convergence of the fit was slow due to a large correlation between the number of gluons, coefficient B, and the strength of their coupling, α_s. In the final fit the integral of the fractional momentum carried by the gluons (i.e. the coefficient B) was fixed at 50%, as seen in deep inelastic scattering. The data were binned in incident energy (200 GeV, 300 GeV, 400 GeV), dilepton mass (excluding the upsilon region), dilepton P_t, and dilepton rapidity y.

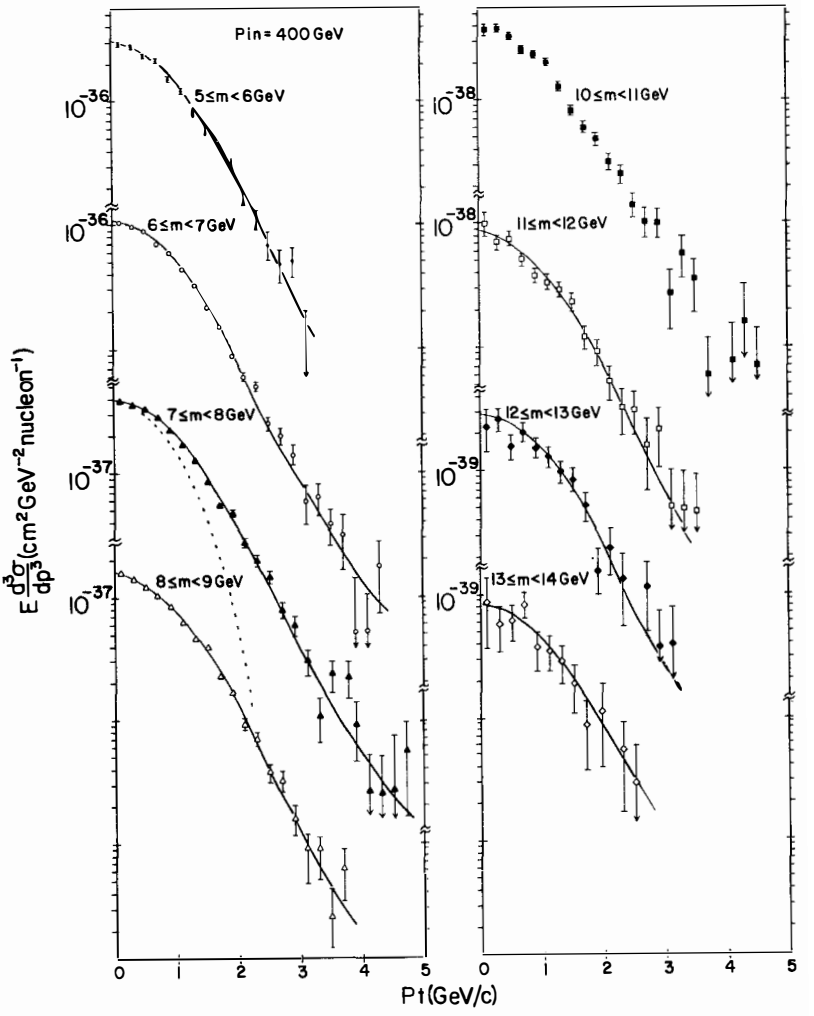

Fig. 6. Invariant yield of dimuons at 400 GeV as a function of the transverse momentum P_t of the muon pair. The solid curves result from the simultaneous fit to all the CFS data as described in the text, the dashed curve indicates the contribution of the Born term alone at 7.5 GeV mass.

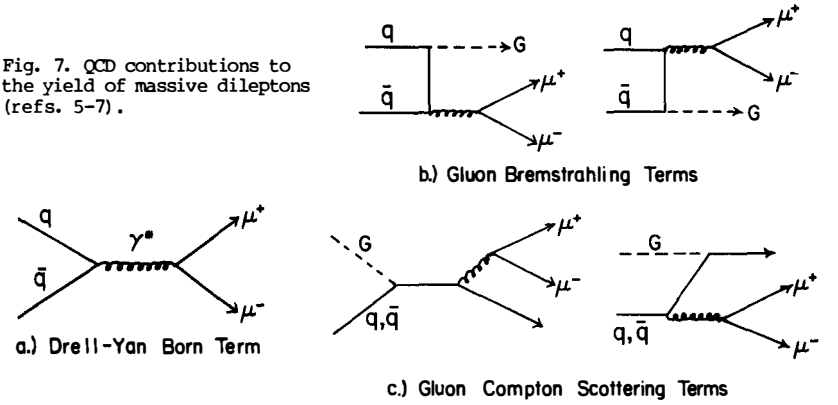

Fig. 7. QCD contributions to the yield of massive dileptons (refs. 5-7).

The 876 separate data points were fit very well (χ^2 per degree of freedom ~ 1) with the parameters shown in Table I.

The solid curves on Figure 6 are a plot of the calculated fit. The dotted curve shows the contribution of the Drell-Yan Born term for one mass bin. At high P_t the fit describes the data very well and is completely dominated by the second order terms. The fit values of the strong coupling constant $\alpha_s = .27$, the intrinsic transverse momentum $\langle K_t \rangle = 580$ MeV, and the gluon structure function shape m = 4.1 appear very reasonable.

Table I

Explicit QCD Fit Parameters

$\bar{d}$	=	$A(1-x)^N$	A	=	0.56 ± 0.01
$\bar{u}$	=	$A(1-x)^{N+\beta}$	N	=	8.1 ± 0.1
$\bar{s}$	=	$(\bar{u} + \bar{d})/4$	β	=	2.6 ± 0.3
g	=	$B(1-x)^m$	B	=	2.55 (fixed by $\int g(x)dx = 0.5$)
f	=	$e^{-ak_T^2}$	m	=	4.1 ± 0.2
			α_s	=	0.27 ± 0.01
			a	=	1.14 ± 0.02 GeV^{-2}
			χ^2/DF	=	805/876

I would not claim that we have in any way determined the values of these second order contributions. Instead, I claim that the fit qualitatively shows that we are probing different physics at high P_t. Instead of studying the log Q^2 behavior of the Born term at low P_t, a more definitive test of QCD might involve studying in more detail, i.e. as a function of both production and decay variables, the behavior of this high P_t dilepton yield. This is indeed one of the goals of our next experiment, E-605.

Two years ago when we began planning for an experiment to follow E-288 we set down a number of design goals:

a.) The apparatus should have a physical aperture stop for all particles with P_T<6 GeV.

b.) It is important to positively identify all particle species: $e^{\pm}$,$\mu^{\pm}$,$\pi^{\pm}$, $k^{\pm}$ and $p^{\pm}$.

c.) The apparatus should be compatible with intensities of 3 x 10^{12} protons per pulse at 1 TeV incident energy.

d.) The acceptance for high P_t pairs should be increased.

e.) The resolution should be better than E-288.

We believe the apparatus shown in Figure 8 more than meets these goals. The large target and dump magnet has a field integral of 30 Tesla-m. A forward particle must have a momentum greater than 70 GeV/c to reach the MWPC detector station 1. The momentum remeasurement in the second magnet and the positive particle identification in the ring-imaging Cerenkov, the electron and hadron calorimeters, and behind the muon wall assure sensitive background rejection. The mass resolution of the apparatus is designed to be .3% FWHM for hadron or lepton pairs in the 10 to 20 GeV mass range.

The calculated acceptance of the apparatus for one sign of the charge (the upper half of the aperture) is shown in Figure 9. The acceptance boundaries shown are determined by the physical location of the magnet coils and the beam dump in the magnet. A trigger processor being built at Columbia University will be used to reject background particles including muons from the dump and hadrons rescattered off the various aperture boundaries.

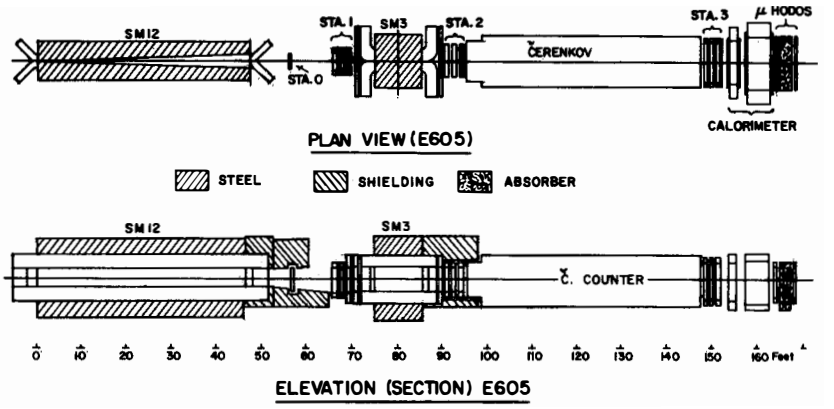

Fig. 8. Schematic of Fermilab Experiment 605, a Columbia, Fermilab, Stony Brook, Univ. of Washington, KEK, Kyoto, Saclay and CERN collaboration. This experiment is currently under construction in the Meson Detector Building at Fermilab.

Note that we are sensitive to a large fraction of the kinematic domain $X_t>.5$. In this unique domain the particle detected, whether it is a lepton or hadron, must be the leading particle. In a constituent scattering picture one would expect an increasing probability of observing an accompanying particle on the other side. This has been observed in our previous experiments[9] for $X_t<.5$. We hope that by studying the kinematic domain $X_t>.5$ in detail we can make sharp tests of QCD constituent scattering predictions.

The experiment is currently under construction and will be set up in the M1 beam line at Fermilab this summer. Hopefully by this time next year we will be getting our first glimpse of very high P_t hadrons and leptons.

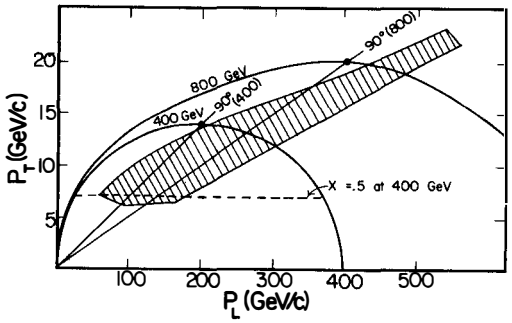

Fig. 9. E-605 acceptance plot. The magnetic field, magnet coils, and absorber placement determine the acceptance (shaded area) for positive particles and for negative particles (passing above and below the dump respectively). The semi-circles indicate the kinematic limit at 400 and 800 GeV incident proton energy.

References

1. A.S. Ito, R.J. Fisk, H. Jostlein, D.M. Kaplan, S.W. Herb, D.C. Hom, L.M. Lederman, H.D. Synder, J.K. Yoh, B.C. Brown, C.N. Brown, W.R. Innes, R.D. Kephart, K. Ueno, T. Yamanouchi, Phys. Rev. D23, 604 (1981).

2. S.D. Drell and T-M. Yan, Phys. Rev. Lett. 25 , 316 (1970); Ann. Phys. 66 , 578 (1971).

3. J.F. Owens and E. Reya, Phys. Rev. D17 , 3003 (1978).

4. J. Pilcher, "Review of Dimuon Production in Hadron Collisions", and A.L.S. Angelis et al., Int. Symp. on Lepton and Photon Int. at High Energies, Batavia (1979). U. Becker et al., EPS Int. Conf. on High Energy Physics, Geneva, (1979).

5. K. Kajantie and R. Raitio, Nucl. Phys. B139 , 72 (1978).

6. G. Altarelli, G. Parisi, R. Petronzio, Phys. Lett. 76B , 351 (1978); Phys. Lett. 76B , 356 (1978).

7. E.L. Berger, "Hadroproduction of Massive Lepton Pairs and QCD" SLAC-PUB-2314, (April 1979).

8. B.A. Gordon et al., Phys. Rev. D20, 2645 (1979); we use the fit for R=.52. W.B. Atwood, Ph.D. thesis, Stanford Univ., SLAC Report No. 185, (1975).

9. H. Jostlein et al., Phys. Rev. D20, 53 (1979).

THE PRODUCTION OF J/ψ IN HADRONIC COLLISION

A. ROMANA, B. CHAURAND and R.A. SALMERON
LPNHE, Ecole Polytechnique, PALAISEAU, France
M.J. CORDEN, J.D. DOWELL, J. GARVEY, R.J. HOMER, M. JOBES,
I.R. KENYON, T. Mc MAHON, R.C. OWEN, K.C.T.O. SUMOROK
R.J. VALLANCE, P.M. WATKINS and J.A. WILSON
University of Birmingham, U.K.
P. SONDEREGGER
CERN, Geneva, Switzerland
Presented by A. ROMANA

ABSTRACT

This paper describes an attempt to take account to the cross-sections of J/ψ's produced by $\pi^{\pm}$, $K^{\pm}$, p and $\bar{p}$ with a common mechanism. We essentially use our Ω results at 39.5 GeV/c [1] and extrapolate the results to higher energy in order to compare to the 200 GeV/c data obtained by the NA3 Collaboration [2].

A. INTRODUCTION

In the parton model, hadrons constituents are quarks (u,d,s,c,b, ...) and gluons, and the J/ψ is considered to be a $c\bar{c}$ bound state. Three main general mechanisms can be considered in the J/ψ production in hadron collision, namely : the light quark-antiquark annihilation, the charmed quark-antiquark annihilation and the gluon-gluon fusion as represented below :

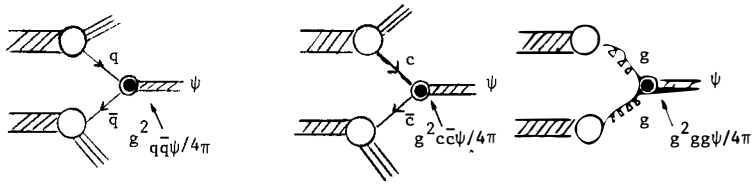

Assuming the knowledge of the structure functions of the constituents in the different hadrons and ignoring the internal structure of the blob at the ve ices, we can express the cross section for each mechanism using simple coupling constants $g^2_{q\bar{q}\psi/4\pi}$, $g^2_{c\bar{c}\psi/4\pi}$ and $g^2_{gg\psi/4\pi}$:

$$\frac{2E^*}{\sqrt{s}}\frac{d\sigma_{q\bar{q}}(A+B \to \psi + X)}{dx_F} = \frac{1}{3}\frac{4\pi^2}{M^2}\frac{g^2_{q\bar{q}\psi}}{4\pi}\sum_{q=u,d,s}\left[F^A_q(x_a)\,F^B_{\bar{q}}(x_b) + F^A_{\bar{q}}(x_a)\,F^B_q(x_b)\right]$$

$$\frac{2E^*}{\sqrt{s}}\frac{d\sigma_{c\bar{c}}(A+B \to \psi + X)}{dx_F} = \frac{1}{3}\frac{4\pi^2}{M^2}\frac{g^2_{c\bar{c}\psi}}{4\pi}\left[F^A_c(x_a)\,F^B_{\bar{c}}(x_b) + F^A_{\bar{c}}(x_b) + F^A_{\bar{c}}(x_a)\,F^B_c(x_b)\right]$$

$$\frac{2E^*}{\sqrt{s}}\frac{d\sigma_{gg}(A+B \to \psi + X)}{dx_F} = \frac{4\pi^2}{M^2}\frac{g^2_{g\bar{g}\psi}}{4\pi}F^A_g(x_a)\,F^B_g(x_b)$$

where E^* and M are the center of mass energy and the mass of the dimuon.

B. STRUCTURE FUNCTIONS

The structure functions which we use in this description are the following, using the conventional notations and the usual symmetry rules :

$V_u^p(x) = V_d^n(x) = 3.0\ x^{0.6}(1-x)^3$ $\qquad$ $V_d^p(x) = V_u^n(x) = 1.72\ x^{0.6}(1-x)^4$

$S^p(x) = 0.2\ (1-x)^8$ $\qquad$ $S_c^p(x) = r_c\ S^p(x)$

$G^p(x) = 3.1(1-x)^5$

$V_{\bar{u}}^{\pi^-}(x) = V_{\bar{d}}^{\pi^-}(x) = 0.75\ x(1-x)$ $\qquad$ $S^\pi(x) = 0.11(1-x)^5$

$S_c^\pi(x) = r_c\ S^\pi(x)$ $\qquad$ $G^\pi(x) = 2.0\ (1-x)^3$

$F^K(x) = F^\pi(x)$

TABLE 1

In this scheme, the charmed sea is supposed to be suppressed relative to the light quark sea but the suppression factor r_c can be taken into account in the effective coupling constant $g'^2_{c\bar{c}\psi} = r_c^2\, g^2_{c\bar{c}\psi/4\pi}$.

C. STUDY OF THE SEPARATED MECHANISMS

The computation of the three mechanisms separately for the six different hadrons and comparison with our data at 40 GeV/c[1] gives us first information that none of the mechanisms would be sufficient by itself to explain ψ production. This is clearly shown with the $p/\bar{p}$ cross section ratio :

data on tungsten at 40 GeV	$\sigma(p)/\sigma(\bar{p}) = 0.12 \pm 0.02$
light quark annihilation	0.05
charmed quark annihilation as well as gluon fusion	1.0

as well as the x_F distribution for π^- induced ψ's which is too flat if we consider the $q\bar{q}$ annihilation and too steep for $c\bar{c}$ annihilation and/or gg fusion mechanisms.

In any case, a $q\bar{q}$ contribution appears to be needed in association of mechanisms, so we will now examine the 3 different possible associations :

$q\bar{q} + c\bar{c}$

$q\bar{q} + gg$

$q\bar{q} + c\bar{c} + gg$

D. ASSOCIATION OF TWO MECHANISMS $q\bar{q} + c\bar{c}$ or $q\bar{q} + gg$

We obtain the two sets of coupling constants ($g^2_{q\bar{q}\psi/4\pi}$ and $g'^2_{c\bar{c}\psi/4\pi}$) and ($g^2_{q\bar{q}\psi/4\pi}$ and $g^2_{gg\psi/4\pi}$) from the fit of the total cross-section induced by π^- and the ratio of the cross-sections of the five other incident hadrons (π^+, $K^\pm$, p and $\bar{p}$) to that of π^- at 40 GeV. This fit gives the following results for the two kinds of association :

$q\bar{q} + c\bar{c}$: $g^2_{q\bar{q}\psi/4\pi} = (2.0 \pm 0.1)10^{-4}$ and $g'^2_{c\bar{c}\psi/4\pi} = 0.09 \pm 0.01$

$q\bar{q} + gg$: $g^2_{q\bar{q}\psi/4\pi} = (2.1 \pm 0.1)10^{-4}$ and $g^2_{gg\psi/4\pi} = (1.2 \pm 0.1)10^{-5}$

From these constants we can recompute the cross-sections at 40 GeV to show the quality of the fit to our data and we compute also the cross sections at 200 GeV to compare with the NA3 results [table 2]. In this table, we have assumed a linear A dependence to derive the cross-section per nucleon from our data on tungsten and the NA3 data on platinium.

The computed percentage of the contribution of the $q\bar{q}$ mechanism is of the order of 75% at 40 GeV and 35% at 200 GeV for the $q\bar{q} + gg$ association.

		$\sigma(\pi^-)$ nb/nucleon	π^+/π^-	K^-/π^-	K^+/π^-	$\bar{p}/\pi^-$	p/π^-
40 GeV	$q\bar{q} + c\bar{c}$	16. ± 1.	1.06± .04	1.01±.04	.32 ± .02	1.10 ±.05	.17 ± .08
	$q\bar{q} + gg$	16. ± 1.	1.06 ± .04	1.01±.04	.38 ± .02	1.15 ± .04	.18 ± .06
	data	16.1±1.4	1.05 ± .06	0.88±.11	.31 ± .06	1.13 ± .14	.14 ± .02
200 GeV	$q\bar{q} + c\bar{c}$	293. ± 30.	1.01 ± .1	1.00±.1	.93 ± .1	1.2 ± .1	.94 ± .1
	$q\bar{q} + gg$	100. ± 10.	1.03 ± .1	1.00±.1	.77 ±.1	1.4 ± .1	.75 ± .1
	data	92. ± 17.	1.01 ± .02	1.1 ±.1	.78 ±.08	.83 ± .12	.59 ± .1

TABLE 2

The first evidence is that the cross-section given by the $q\bar{q}$ + $c\bar{c}$ association grows highly too fast with energy as can be explained with the shape of the structure function of the charmed quarks inside hadrons. If we consider then the $q\bar{q}$ + gg mechanism, we can see that agreement is quite reasonable when we go from $\sqrt{s}$ = 8.6 to $\sqrt{s}$ = 20 GeV for the six different hadrons.

Figure 1 shows the x_F distribution of π^- induced J/ψ's as obtained from our data and from the two associations of mechanisms with the fitted coupling constants. The curves don't agree very well but they give the general trend if we take into account the poor knowledge of the charmed and gluon structure functions and the bad experimental acceptance at low x_F which gives a large error in the overall normalisation.

E. ASSOCIATION OF THE 3 MECHANISMS.

Although the $c\bar{c}$ annihilation contribution has to be very small, we now consider the association of the three mechanisms.

For this, we fit the 3 coupling constants to the data at 40 and 200 GeV/c together : the data involved in the fit are again the total cross-section for π^- and the five cross-section ratios relative to π^- for the other incident particles.

The results are :

$$g^2_{q\bar{q}\psi/4\pi} = (2.0 \pm 0.1)\ 10^{-4}$$

$$g'^2_{c\bar{c}\psi/4\pi} = (1.2 \pm 0.1)\ 10^{-2}$$

$$g^2_{gg\psi/4\pi} = (1.1 \pm 0.2)\ 10^{-5}$$

With these constants, the results of the fit are given in table 3.

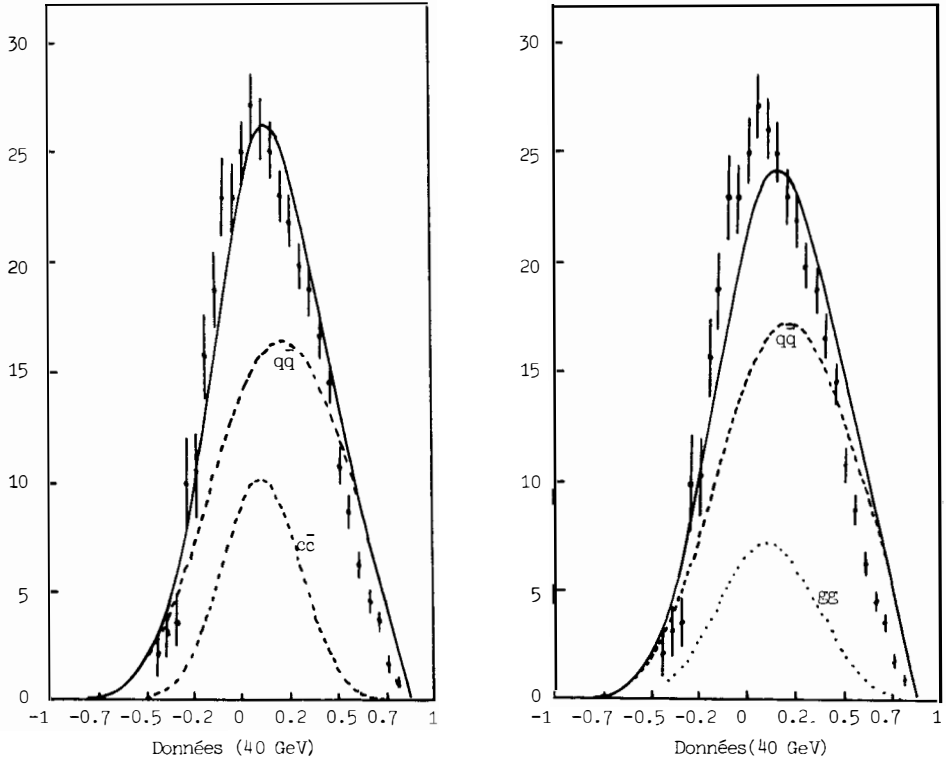

Fig. 1 x_F distribution of π^- induced J/ψ's for the associations $q\bar{q}$ + $c\bar{c}$ and $q\bar{q}$ + gg

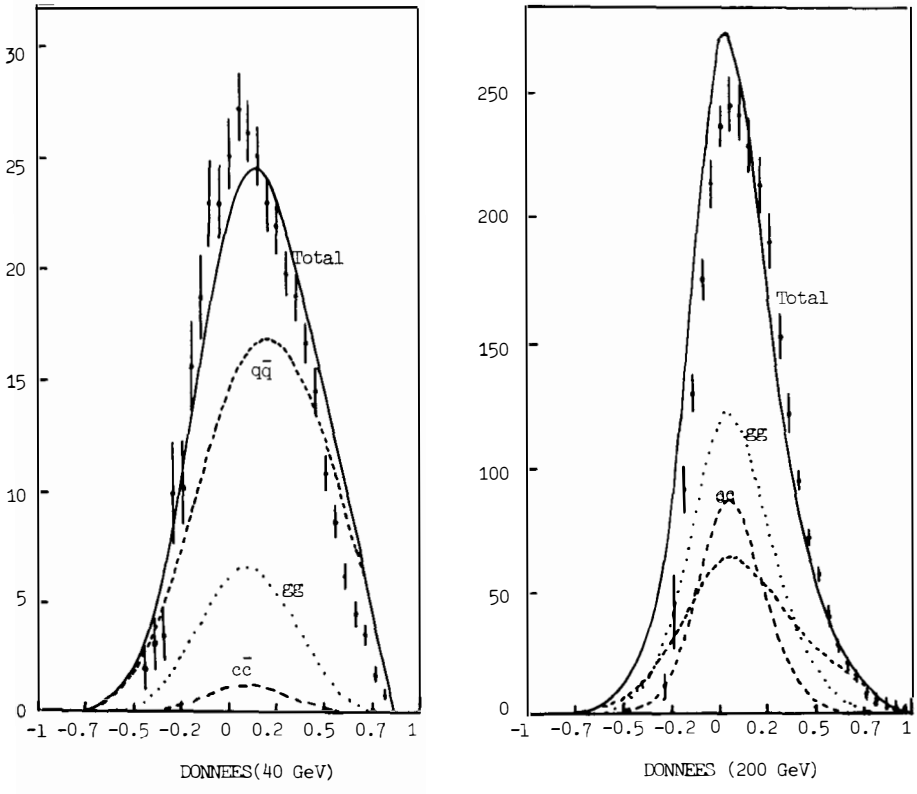

Fig.2 $\frac{d\sigma}{dx_F}$ for $q\bar{q} + c\bar{c} + gg$

$\sqrt{s}$ GeV		π^-	π^+/π^-	K^-/π^-	K^+/π^-	$\bar{p}/\pi^-$	p/π^-
8.6	Fit	16. ± 1.	1.06±.05	1.00±.05	.36±.02	1.1±.1	.18±.01
	Data	16.1± 1.4	1.05±0.05	.88 ±.11	.31±.06	1.13±.14	.14±.02
20	Fit	125. ± 7.	1.03±.03	1.0 ± .05	.83±.04	1.3 ± .1	.81 ±.04
	Data	92 ± 17.	1.01±.02	1.1 ±.1	.78±.08	.83 ±.12	.59 ±.1

TABLE 3

The agreement is quite good except for the $\bar{p}/\pi^-$ and the p/π^- ratios at 200 GeV/c although the $p/\bar{p}$ ratio is correct (fit gives 0.62 ± .06 while data are 0.71 ± .1). In this scheme, the $q\bar{q}$ contribution goes down from 75% at 40 GeV/c to 35% at 200 GeV/c, as expected qualitatively from the shapes of the structure functions.

With the coupling constants given above, we can also determine the cross-sections for the J/ψ production on hydrogen. The results at 40 GeV are given in table 4, where we can only compare at 40 GeV with the π^- and π^+ induced production.

	π^-	π^+/π^-	K^-/π^-	K^+/π^-	$\bar{p}/\pi^-$	p/π^-
computation	15. ± 3.	.61 ± .11	1.0 ± .2	.31 ± .1	.75 ± .14	.12 ± .02
H2 data	13.9 ± 9	.78 ± .1				

TABLE 4

We also have computed the x_F distribution for π^- induced J/ψ on tungsten at 40 GeV and platinium at 200 GeV to compare to the experimental distributions (Fig. 2). The discontinuous curves show the contribution of the different mechanisms.
Agreement is reasonable at both energies.

F. CONCLUSION

Using usual structure functions and a simple parton model where we consider the interaction to be pointlike, we can interpret the J/ψ production as an association of light quark-antiquark annihilation and gluon-gluon fusion and/or charmed quark-antiquark annihilation. The results are quite satisfactory for six different beam particles and a lever arm in energy from 40 to 200 GeV/c($\sqrt{s}$ from 8.6 to 20 GeV).

The coupling constant we find for the $q\bar{q}$ annihilation is of the order of 2.10^{-4}, i.e. roughly larger than what is expected if the only vertex were violating the Zweig rule; this can be an indication for a process where one gluon is produced.

For the $c\bar{c}$ annihilation (if needed), the effective coupling constant is $g'^2_{cc\psi/4\pi} = r_c^2\, g^2_{c\bar{c}\psi/4\pi} \simeq 10^{-2}$ which leads to a suppression factor of about 15% if we assume a real coupling constant of 1/2 as expected from the J/ψ width.

The gg coupling constant is difficult to compute in terms of QCD to compare to our actual value of about 10^{-5}.

The main contribution at 40 GeV/c is due to the light quarks annihilation (75%); this contribution decreases with energy (as expected from the structure functions and the kinematic giving the simple relation : $x_a\, x_b = M_\psi^2/s$) up to 35% at 200 GeV/c.

The results presented give the limits of such a simple model where we neglect the p_T distributions, the QCD corrections and the decay of any $c\bar{c}$-state into the ψ. On the other hand, these results are good enough to have a rather good sensitivity to the validity of the model and to the validity of the chosen structure function for gluons inside hadrons : fits were attempted with different shapes of the gluon structure function which gave results that are worse in the comparison with data.

REFERENCES

1. M.J. Corden et al., Phys. Let. 96B (1980) 411
2. J. Badier et al., CERN/EP 79-68 EPS Inst. Conf. Geneva 79
3. M.J. Corden et al. Phys. Let. 98B(198)220.

CONTINUUM DIMUON PRODUCTION BY 39.5 GEV/C $\pi^{\pm}$, $K^{\pm}$, p AND $\bar{p}$ INCIDENT ON A TUNGSTEN TARGET

Birmingham - CERN - Ecole Polytechnique

J.D. Dowell

Physics Department, University of Birmingham

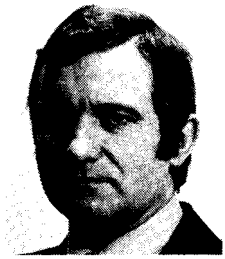

Inclusive dimuon production by 39.5 GeV/c $\pi^{\pm}$, $K^{\pm}$, p and $\bar{p}$ has been studied for masses greater than 2.0 GeV/c^2. The π^-,π^+ and (π^--π^+) cross sections exceed the naive Drell-Yan predictions by a factor $\sim$2.4 and the scaling cross section $M^3/d\sigma/dM$ scales with higher energy data within the systematic errors. The ratios of the cross sections for the different incident particles to π^- agree with Drell-Yan predictions. The pion valence structure function is consistent with that found at 200 GeV/c. Some x_F dependence of the angular distribution is observed with large errors. A comparison of $\langle P_t^2 \rangle$ at fixed τ to higher energy data shows an increase with increasing s at four values of τ.

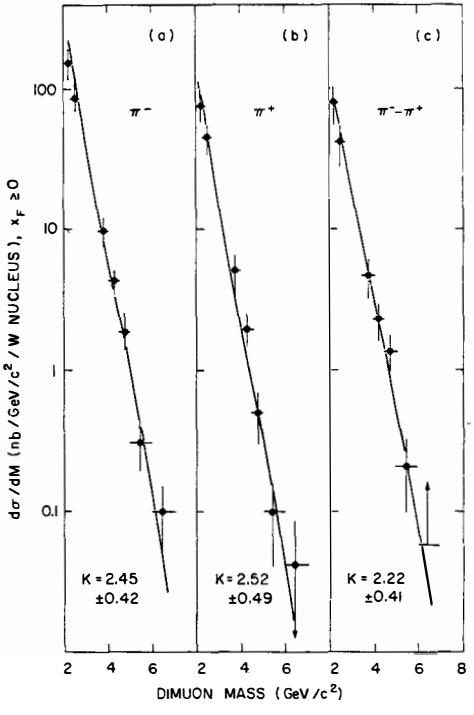

Fig. 1 $d\sigma/dM$ (nb/GeV/c^2/W nucleus) for $x_F>0$ versus mass. The curves are Drell-Yan predictions multiplied by a factor K.

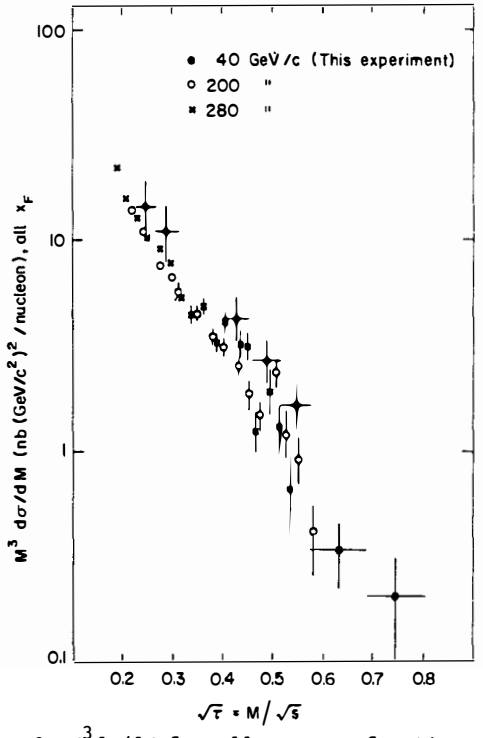

Fig. 2 $M^3 d\sigma/dM$ for all x_F as a function of $\sqrt{\tau} = M/\sqrt{s}$ for incident π^- in this experiment and ref {10}. Overall systematic errors are shown for the 40 GeV data.

The experiment was carried out in the CERN Omega Spectrometer which has a large acceptance ($-0.5<x_F<1.0$) for the produced dimuons. Details of the experimental method may be found in reference {1} and further information about the results discussed here in reference {2}. Data were obtained for dimuon masses from 2.0 to 7.0 GeV/c^2 or $0.23<\sqrt{\tau}<0.80$. Figure 1 shows the differential cross sections ($x_F>0$) as a function of dimuon mass for π^-, π^+ and (π^--π^+). The data are corrected for acceptance but not for Fermi-motion and the errors include all systematic effects. The curves are calculated assuming a linear A-dependence and the simple Drell-Yan formula, using the structure functions of NA3 {3} for the pion and CDHS {4} for the nucleon, but multiplied by a factor K to fit the data. The difference cross section (π^--π^+) is expected to be free from hadronic backgrounds and requires K=2.22±0.41 similar to the value observed in higher energy experiments {5,6,7}. The fact that the K-values obtained for π^+ and π^- separately are only about 10% higher and the good agreement with the curves indicate that dimuon production is dominated by the Drell-Yan mechanism even at the lowest masses.

Figure 2 is a plot of the scaling cross section $M^3 d\sigma/dM$ versus $\sqrt{\tau}$ at all x_F for our data and those of NA3 {10} at 200 and 280 GeV. A linear A-dependence has been used to obtain the cross section per nucleon but this is not critical as the targets (W and P_t) have similar A-values. No Fermi-motion corrections have been applied in either experiment. Our data lie about 20% higher on average but we are compatible with scaling within our errors which include all systematic effects. A small deviation in the direction observed would be expected on the basis of the scaling violations observed in deep inelastic scattering.

Figure 3 shows the cross sections for different incident particles relative to π^- as a function of mass and include our J/ψ results ($2.7<M<3.5$ GeV/c^2). The π^+/π^- ratio is close to unity for J/ψ production while for the continuum it decreases with increasing dimuon mass towards the value of ¼, the ratio of the squares of the annihilating valence quark charges. For the other particles the ratios fall with mass without a discontinuity at the J/ψ. This is consistent with quark model expectations. The small ratios for K^+ and p are consequences of the absence of valence $\bar{u}$ or $\bar{d}$ in these particles. The solid curves are computed from the

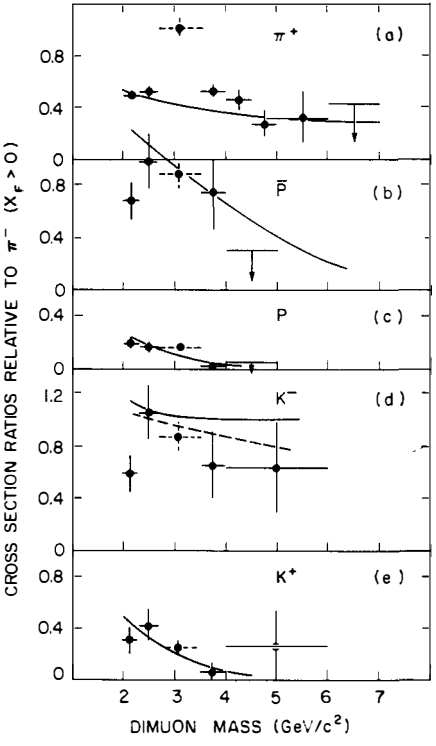

Fig. 3 Ratios for different incident particle cross sections to those for π^-. The curves are Drell-Yan predictions (see text).

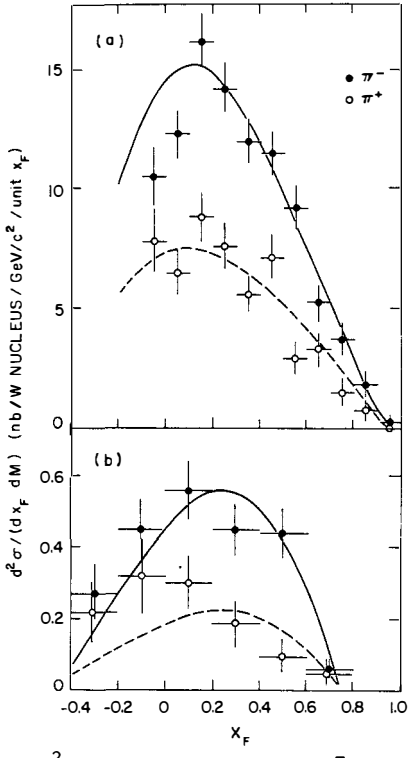

Fig. 4 $d^2\sigma/dMdx_F$ for incident π^- and π^+, a) $2.3<M<2.7$ GeV/c^2, b) $4.0<M<5.0$ GeV/c^2. The curves are Drell-Yan predictions.

Drell-Yan model using the structure functions of references {3,4}. The agreement is generally good. The solid curve for K^-/π^- is where the $\bar{u}$ distribution for the K^- is taken to be the same as for the π^- while the dashed curve uses the results of ref. {9}. for the K^- structure function. The latter agrees better with the data providing further evidence that the $\bar{u}$ distribution in a K^- falls more steeply with x than in a π^-. The variation we observe for the K^-/π^- ratio as a function of x_F is also consistent with this result.

Figure 4a and 4b show the x_F distributions for muon pairs in the mass ranges 2.3-2.7 and 4.0-5.0 GeV/c^2 for incident π^- and π^+. The superimposed curves (normalised to the data for $x_F>0$) are calculated using the structure functions mentioned earlier and reproduce the data reasonably well. At higher masses the predicted x_F distributions are broader and peak further away from zero because of the difference in the valence quark distributions between pions and nucleons and the fact that large quark x-values are required to produce high masses. In order to determine the pion structure function we have fitted the data for π^+ and π^- simultaneously in the mass interval 2.0-2.7 GeV/c^2 for x_F between -0.1 and 0.8 with the pion valence structure function parameterized as $Ax^{\alpha}(1-x)^{\beta}$. The pion sea is fixed as $B(1-x)^{\gamma}$ where $\gamma=5$ and B is such that 6% of the pion momentum is carried by each sea quark flavour while for the nucleon the CDHS parameters have been used {4}. The fitted results give $\alpha=0.44\pm0.12$ and $\beta=0.98\pm0.15$ and a K factor of 2.6 ± 0.5 to be compared with $\alpha=0.40\pm0.06$ and $\beta=0.90\pm0.06$ in ref. {3}. There is no evidence within experimental error of any scaling violation from the shape of the pion structure function between 40 GeV/c and 200 GeV/c; the prescription of Buras and Gaemers {8} applied to the pion predicts that the parameter β would be smaller by $\sim$0.2 at the lower momentum.

The cos θ angular distribution has been studied in the Gottfried-Jackson system for $|\cos\theta|<0.8$ assuming that the azimuthal distribution ϕ is isotropic. The results are critically dependent on the acceptance for which a systematic error has been included. Allowance has also been made for the smearing effect of multiple scattering. The combined π^+ and π^- distributions have been fitted with $1+\alpha\cos^2\theta$. The large $|\cos\theta|$ values have the largest influence on α but are the most poorly determined because the corrections are

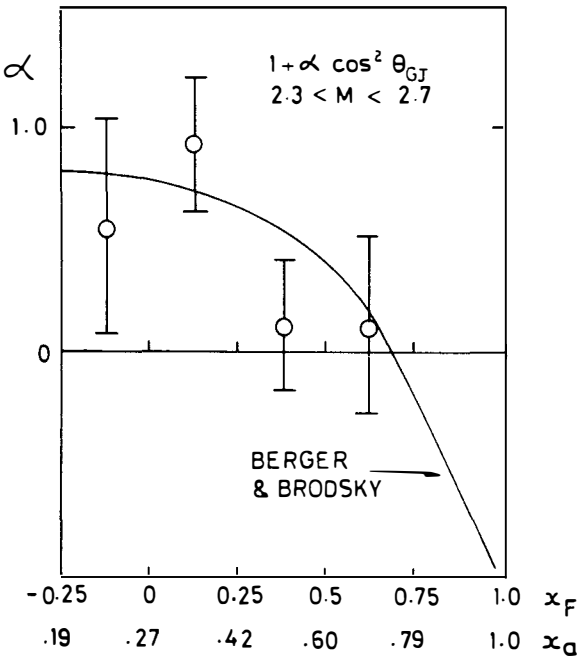

Fig. 5 The angular parameter α versus x_F for $2.3<M<2.7$ GeV/c^2 for π^+ and π^- data. The curve is the prediction of reference 11. The lower scale gives the x of the pion quark.

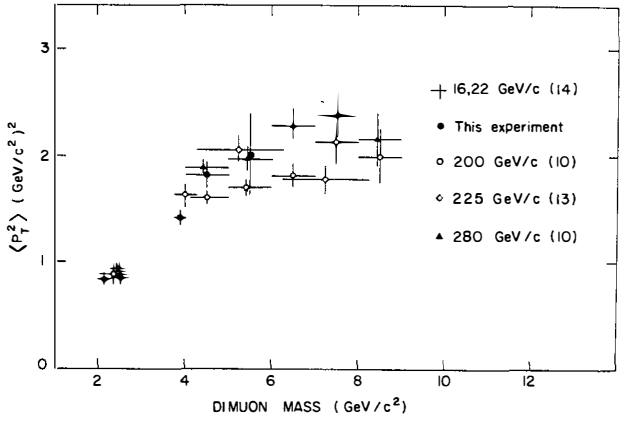

Fig. 6 $\langle p_t^2 \rangle$ versus mass for incident π^- for these and other data.

large and the statistics low. Consequently one should be cautious in interpreting the results. The values of α obtained for $x>-0.25$ are $\alpha=0.44\pm0.17$ (0.44 ± 0.48) for the mass regions 2.3-2.7 GeV/c^2 (4.0-5.0 GeV/c^2). Figure 5 is a plot of α versus x_F for the lower mass range, with the lower scale showing the x-value of the quark in the pion. The curve is the prediction of Berger and Brodsky {11} and the data show the predicted decrease in α with increasing x_F as first observed at 225 GeV/c {12}. However the large errors and systematic uncertainties make it difficult to draw a conclusion.

The P_t^2 distributions for the π^- and π^+ induced dimuons are well fitted by an exponential form for $P_t^2 < 2.0(\text{GeV/c})^2$. At higher P_t^2 the data fall more slowly than the exponential as observed in reference {10}. The $\langle P_t^2 \rangle$ values are similar for all beam particles and show a dependence on mass and x_F. Corrections have been applied to $\langle P_t^2 \rangle$ to allow for the smearing effect of multiple scattering. Figure 6 shows $\langle P_t^2 \rangle$ versus mass compared to other data. Our data have a similar mass dependence to the higher energy data but correspond to much higher values of $\sqrt{\tau}$. Figure 7 shows $\langle P_t^2 \rangle$ versus s at four values of $\sqrt{\tau}$. There appear to be some inconsistencies but the data show that $\langle P_t^2 \rangle$ increases with s at fixed τ. The straight lines are not fits but are to guide the eye and have slopes ranging from .0023 to .0035 with no clear systematic trend. There is not a common intercept on the $\langle P_t^2 \rangle$ axis implying that the primordial $\langle P_t^2 \rangle$ is a function of τ. Our data show a smooth decrease of $\langle P_t^2 \rangle$ with increasing x_F (figure 8) which is particularly striking at high mass where it must at least partly reflect the approach to the kinematic boundary. The acceptance is a slowly varying function of both x_F and P_t and could not, due to error, account for the behaviour.

In conclusion we observe at 40 GeV/c only a small change in the scaled continuum cross section $M^3 d\sigma/dM$ from the values measured at 200 and 280 GeV/c. The cross sections exceed the naive Drell-Yan predictions by a factor $\sim$2.4. The pion valence structure function is consistent with that found at 200 GeV/c. Some evidence of a dependence of the angular distribution parameter α on x_F is observed but the errors are large. Comparing to higher energy data $\langle P_t^2 \rangle$ rises with increasing s at fixed τ but decreases with x_F at our energy.

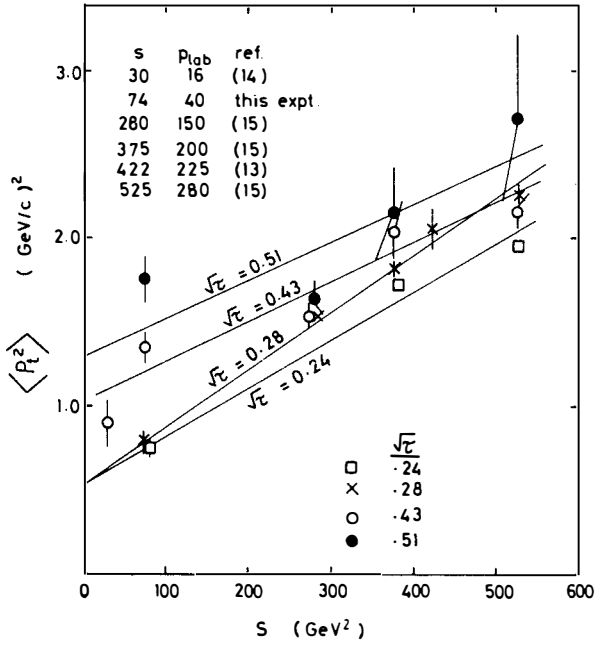

Fig. 7 $\langle p_t^2 \rangle$ versus s for incident π^- at four values of $\sqrt{\tau}$ for these and other data. The lines are to guide the eye.

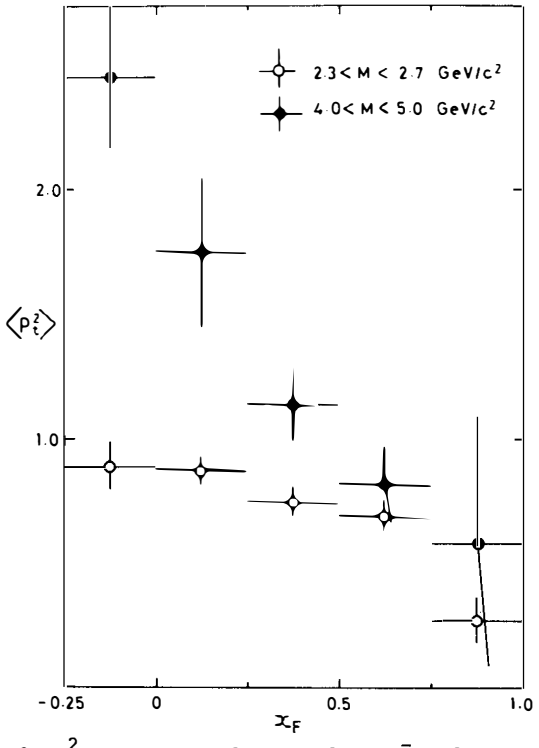

Fig. 8 $\langle p_t^2 \rangle$ versus x_F for incident π^- and two mass intervals.

References

1. M.J. Corden et al., Phys. Lett. 96B (1980) 411.
2. M.J. Corden et al., Phys. Lett. 96B (1980) 417.
and CERN/EP/80-152.
3. J. Badier et al., CERN/EP/79-67.
4. J.G.H. de Groot et al., Phys. Lett. 82B (1979) 456.
5. J. Badier et al., Phys. Lett 89B (1979) 145.
6. R. Barate et al., Phys. Rev. Lett. 43 (1979) 1541.
7. A.S. Ito et al., Fermilab - Pub - 80/19 - Exp.
8. A.J. Buras and K.J.F. Gaemers, Nucl. Phys B132 (1978) 249.
9. J. Badier et al., Phys. Lett. 93B (1980) 354.
10. J. Badier et al., CERN/EP/79-68.
11. E.L. Berger and S.J. Brodsky, Phys. Rev. Lett. 42 (1979) 940.
12. K.J. Anderson et al., Phys. Rev. Lett. 43 (1979) 1219.
13. K.J. Anderson et al., Phys. Rev. Lett. 42 (1979) 944.
14. J. Alspector et al., Phys. Lett. 81B (1979) 397.
15. J. Badier et al., CERN/EP/80-150.

*
M.J. Corden, J.D. Dowell, J. Garvey, R.J. Homer, M. Jobes, I.R. Kenyon, T.J. McMahon, R.C. Owen, K.C.T.O. Sumorok, R.J. Vallance, P.M. Watkins and J.A. Wilson.
University of Birmingham, UK.

P. Sonderegger.
CERN, European Organisation for Nuclear Research, Geneva Switzerland.

B. Chaurand, A. Romana and R. Salmeron.
Ecole Polytechnique, Palaiseau, France.

HIGH-MASS DIMUON PRODUCTION AT THE CERN ISR

F. Vannucci
LAPP, Annecy, France

ABSTRACT

New results from a dimuon production experiment at the ISR are presented for energies of 44 and 62 GeV. Scaling is discussed and some characteristics of the dynamics of the muon pairs are given.

1. INTRODUCTION

Partial results of the R209 experiment at the ISR have already been presented[1], concerning cross-sections for resonance production, a test of scaling, and the two-photon process. Details of the detector, made of magnetized iron toroïds interleaved with scintillation counters and large drift chambers, were also given. Here we will add some final results on scaling, and on the dynamics of dimuons produced at $\sqrt{s}$ = 44 and 62 GeV with about 2500 and 12,000 events, respectively. Results concerning hadrons associated with the lepton pairs are discussed in these proceedings[2].

2. SCALING

Cross-sections for dimuon production at centre-of-mass energies $\sqrt{s}$ = 44 and 62 GeV are shown in Fig. 1. They correspond to an integrated luminosity of 0.42×10^{38} cm^{-2} and 1.11×10^{38} cm^{-2}, respectively.

A test of scaling can be performed by comparing the quantities $m^3 d\sigma/dmdx\big|_{x=0}$ obtained at these two energies. The plots are shown in Fig. 2 together with results at $\sqrt{s}$ = 27.4 GeV [3]. A common fit:

$$m^3 \left.\frac{d\sigma}{dmdx}\right|_{x=0} = (1.01 \pm 0.03) \frac{(1-\sqrt{\tau})^{10}}{\sqrt{\tau}} \times 10^{-32} \text{ cm}^2/\text{GeV}$$

gives a good description of these experimental data in the $\sqrt{\tau}$ range between 0.05 and 0.5 ($\sqrt{\tau}$ is the usual dimensionless parameter $\sqrt{\tau} = m/\sqrt{s}$). Scaling is tested by fixing $\sqrt{\tau}$ and comparing $m^3 d\sigma/dmdx$ obtained at various energies. From Fig. 2 it is apparent that scaling is tested in the region $\sqrt{\tau} \simeq 0.2$ between the Fermilab and ISR energies. This is the region where the ISR points have low statistics and where QCD predicts little scaling violation. One should still keep in mind that the dimuon-production cross-section at the ISR is more than two orders of magnitude larger than at Fermilab for a dimuon mass of 12 GeV. This huge factor disappears completely by the scaling procedure, thus giving good support for this prediction.

It can be emphasized that the ISR results concentrate at low $\sqrt{\tau}$, thus being sensitive to the sea component of the incident hadrons.

3. DYNAMICS

For the resonance-free interval 5 < m < 8 GeV the angular distribution of the 4400 muon events obtained at 62 GeV, relative to the Collins-Soper axis[4], was fitted to a form $(1 + \alpha \cos^2 \theta)$. We find $\alpha = 1.0 \pm 0.5$ consistent with

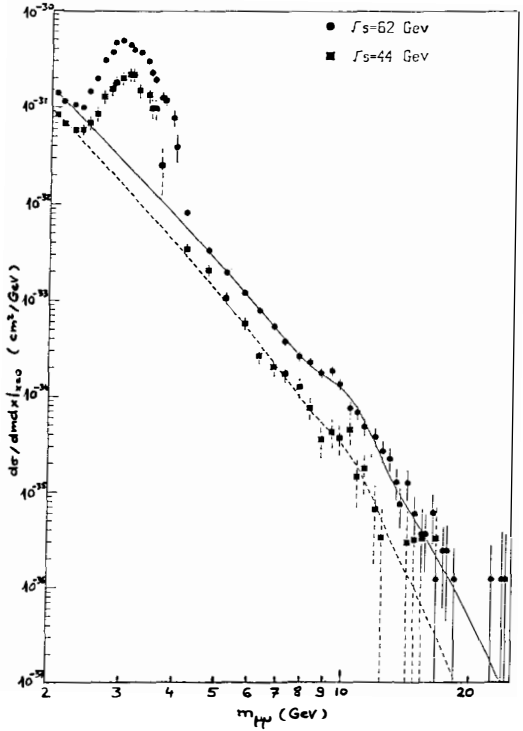

Fig. 1 Dimuon cross-sections at $\sqrt{s}$ = 44 and 62 GeV

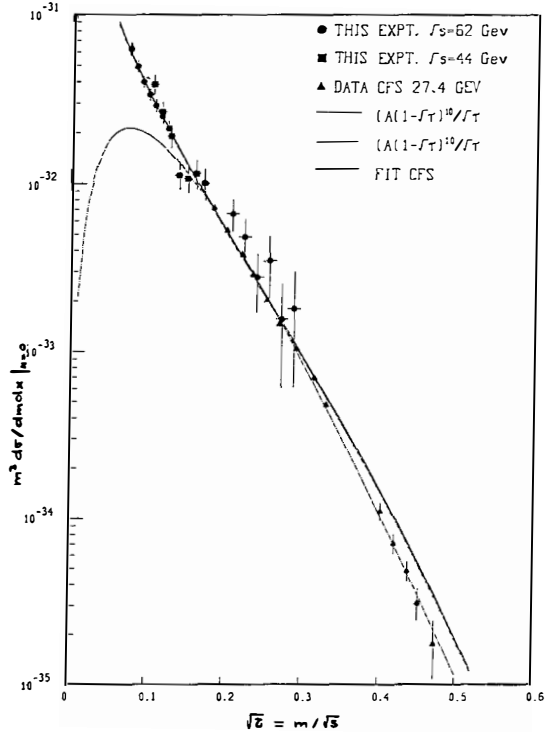

Fig. 2 Scaling plot $m^3 d\sigma/dmdx\big|_{x=0}$ versus $\sqrt{\tau}$

expectations from the Drell-Yan mechanism. The x distribution has also been studied, x being the Feynman parameter $x = 2p_L/\sqrt{s}$. Figure 3 gives the measured distributions for the 62 GeV data and three mass intervals. Their shapes are in good agreement with a Drell-Yan calculation[5] scaled up by a factor 1.6.

Finally the p_T distribution is presented in Fig. 4 for three different mass intervals. Omitting the first bin, we obtain good fits to a simple exponential. The extracted average transverse momenta are substantially higher than predicted by the simple Drell-Yan model. Figure 5 summarizes measurements of dimuon $\langle p_T \rangle$ obtained over a range of c.m. energies extending from 19 to 62 GeV [3,6]. A large increase of $\langle p_T \rangle$ with increasing $\sqrt{s}$ is observed. This is in disagreement with the simple quark-antiquark annihilation graph, but is in qualitative agreement with QCD predictions incorporating gluon interactions. The K factor, found to be 1.7 and which was reported earlier[1] based on the CDHS structure functions[5], also points to the need for QCD corrections for the over-all normalization of the cross-section.

* * *

REFERENCES AND FOOTNOTES

1) F. Vannucci, *in* Proc. 15th Rencontre de Moriond, March 1980.

2) V. Cavasinni, these Proceedings.

3) K. Ueno et al., Phys. Rev. Lett. 42, 486 (1979).
J.K. Yoh et al., Phys. Rev. Lett. 41, 684 (1978).

4) J.C. Collins and D.E. Soper, Phys. Rev. D 16, 2219 (1977).
θ is the angle between μ^+ and the average direction of the incident protons in the dimuon c.m. frame.

5) J.G.H. de Groot et al., Z. Phys. C1, 143 (1979).
J. Badier et al., Phys. Lett. 89B, 145 (1979).
The structure functions used are:
$u_V(x) = 2.13\ \sqrt{x}\ (1-x)^{2.8}$
$d_V(x) = 1.26\ \sqrt{x}\ (1-x)^{3.8}$
$u_S = \bar{u} = d_S = \bar{d} = 2s = 2\bar{s} = 0.27\ (1-x)^{8.1}$.

6) J. Branson et al., Phys. Rev. Lett. 38, 1334 (1977).
K.J. Anderson et al., Phys. Rev. Lett. 42, 944 (1979).
G.E. Hogan et al., Phys. Rev. Lett. 42, 948 (1979).

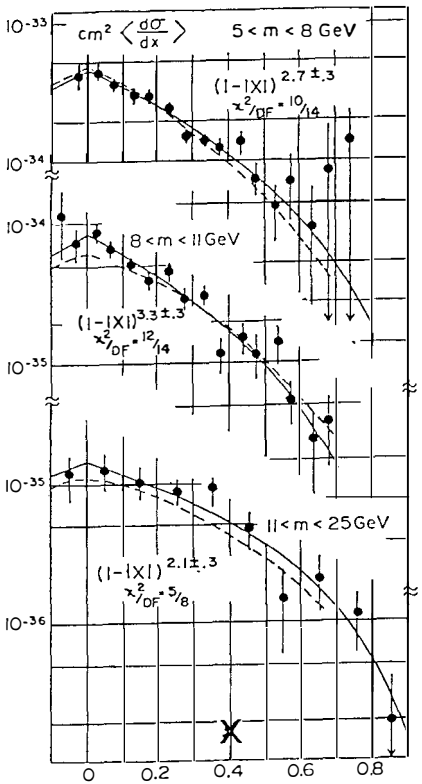

Fig. 3 Distribution of dimuons in x for three mass intervals

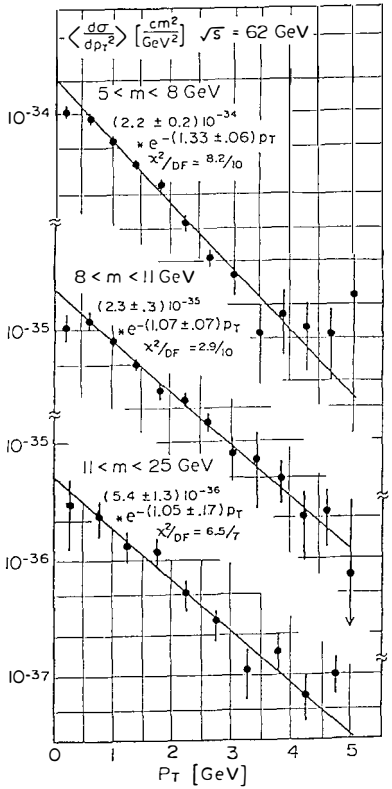

Fig. 4 Distribution in the transverse momentum of the dimuon

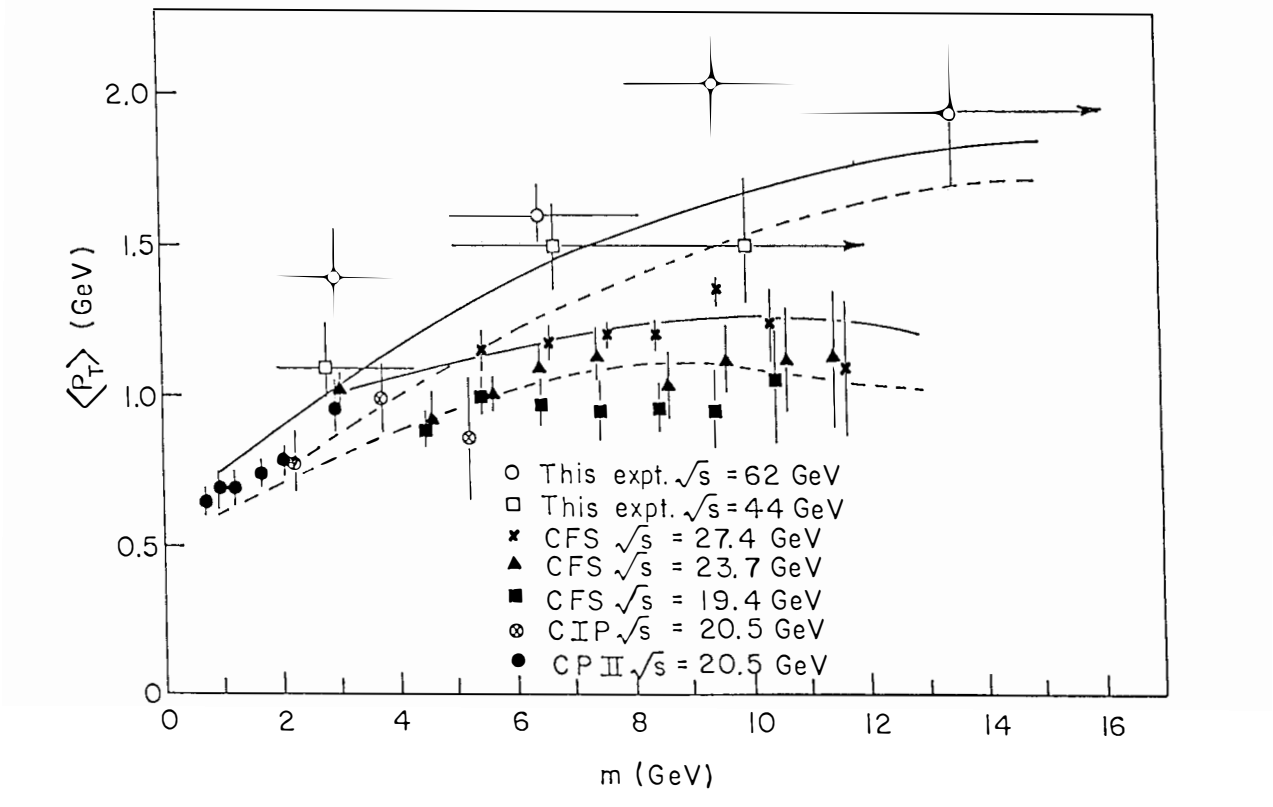

Fig. 5 Average transverse momenta as a function of the dimuon mass

THE PRODUCTION OF HIGH-MASS ELECTRON PAIRS AT THE CERN ISR

C. Kourkoumelis
Physics Laboratory, University of Athens, Greece

ABSTRACT

The production of high-mass electron pairs ($4.5 < m < 19$ GeV/c^2) from proton-proton collisions was studied at the CERN ISR, at c.m. energies in the range $28 \leq \sqrt{s} < 63$ GeV. Our results include measurements of the scaling function down to $m/\sqrt{s} \simeq 0.07$, and measurements of the angular decay distribution as well as a study of the transverse momentum distribution of the pairs.

High-mass electron pairs, $4.5 < m < 19$ GeV/c^2, produced from pp collisions have been studied by our experiment at the CERN ISR. The apparatus included four modules, each consisting of proportional chambers, scintillators, xenon/PWC-lithium transition radiation detectors, and a lead/liquid-argon calorimeter. The last two elements were very essential for the selection of the electrons over the intense background of hadrons, both at the trigger level and at the off-line analysis. More details about the apparatus, the triggers, and the analysis methods used, can be found elsewhere[2].

The integrated luminosities corresponding to each c.m. energy were the following: 0.095, 1.214, and 8.748 ($\times 10^{37}$) cm^{-2} at $\sqrt{s}$ = 30, 53, and 63 GeV, respectively.

Figure 1 shows the cross-section for the production of massive electron pairs as a function of their mass, for the combined data at $\sqrt{s}$ = 53 and 63 GeV. The errors include a 50% uncertainty on the subtraction of the background.

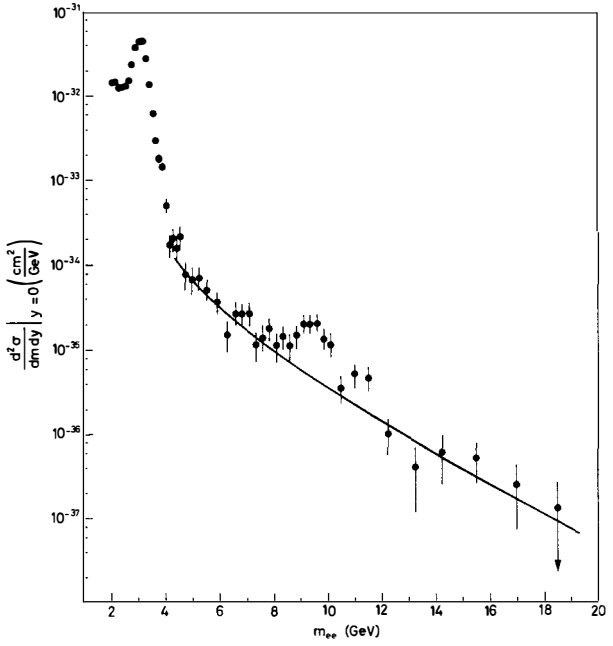

Fig. 1 The cross-section $d^2\sigma/dmdy\Big|_{y=0}$ as a function of m

The dielectron data were further used for the investigation of scaling in $\sqrt{\tau} = m/\sqrt{s}$. Figure 2 shows our data on scaling together with other experimental results for comparison. Scaling seems to hold, within the statistical accuracy of the data, in the range $\sqrt{s}$ = 28-63 GeV down to values of $\sqrt{\tau}$ = 0.07. The region of low values of $\sqrt{\tau}$ is precisely the relevant region for the production of intermediate vector bosons at the new accelerators. Our data can be presented by the form:

$$m^3 \left.\frac{d^2\sigma}{dmdy}\right|_{y=0} = (2.32 \pm 0.12) \times 10^{-32} \times \exp\left[(-11.6 \pm 0.5)\frac{m}{\sqrt{s}}\right] \text{cm}^2\ \text{GeV}^2$$

(with χ^2 = 25 for 30 degrees of freedom). All the data of Fig. 2 covering a wider region of $\sqrt{\tau}$ values can be well parametrized by the form:

$$m^3 \left.\frac{d^2\sigma}{dmdy}\right|_{y=0} = (2.60 \pm 0.13) \times 10^{-32} \times \exp\left[(-2.0 \pm 0.7)\frac{m}{\sqrt{s}}\right]\left(1 - \frac{m}{\sqrt{s}}\right)^{9.7 \pm 0.4} \text{cm}^2\ \text{GeV}^2$$

(with χ^2 = 72 for 57 degrees of freedom). This last function is also shown superimposed on Fig. 1. On Fig. 2 is also shown a parametric fit from lower $\sqrt{s}$ values[3], which fails though to represent well the data at low $\sqrt{\tau}$ values. Summarizing, our data are in good agreement with universal scaling.

We have also studied the angular distribution of the dielectrons for two different mass regions: for the continuum $4.5 < m < 8.7$ GeV/c^2 and for the T region,

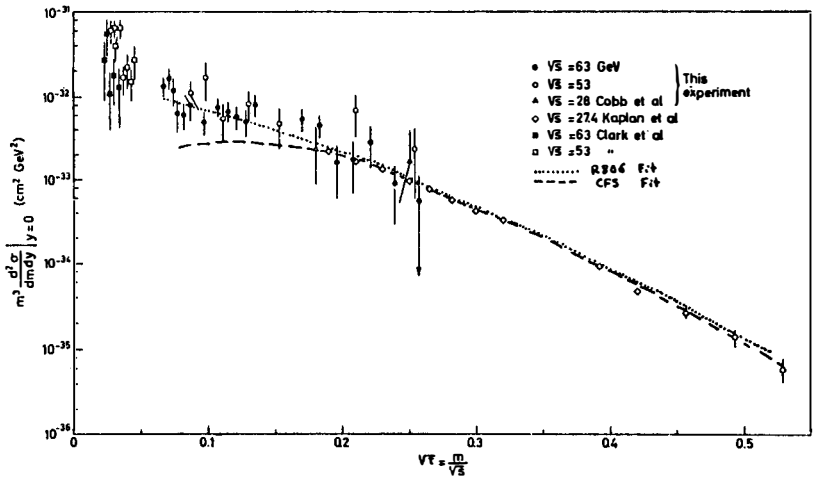

Fig. 2 Plot of the scaling cross-section as a function of $\sqrt{\tau}$

$8.7 < m < 10.3$ GeV/c^2. The corresponding distributions measured in the s-channel helicity system are shown on Figs. 3a and b. We have fitted our data to the form $d\sigma/d\cos\theta = (1 + \alpha \cos^2\theta)$ and found a good fit for $\alpha = 1.15 \pm 0.34$ and $\alpha = 0.79 \pm 0.40$ for the continuum and Υ region, respectively. The value found for the continuum agrees with the virtual photon production picture of the simple Drell-Yan mechanism.

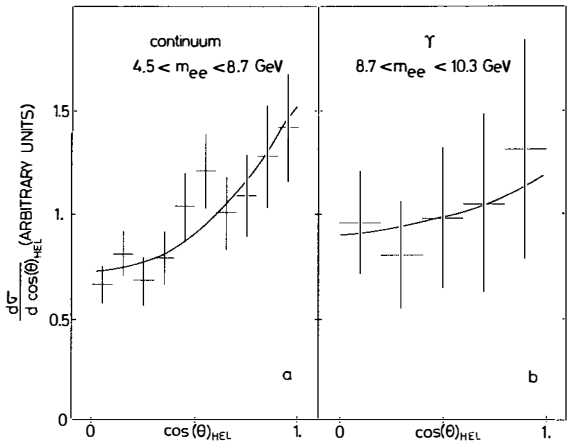

Fig. 3 Angular distribution of the electron pairs

For the study of the average transverse momenta of the dielectrons a requirement on the low multiplicity in the modules containing the electrons was imposed, since the fraction of the background was increasing rapidly with the $\langle p_T \rangle$. The distribution of the $\langle p_T \rangle$ at $\sqrt{s}$ = 63 GeV is shown in Fig. 4 as a function of the dielectron mass, together with other experimental results at different c.m. energies. This figure shows that the $\langle p_T \rangle$ is independent of mass, $\langle p_T \rangle = 1.43 \pm 0.07$ GeV/c, but rises with rising $\sqrt{s}$. The rise of $\langle p_T \rangle$ with $\sqrt{s}$ for fixed τ is in disagreement with the simple Drell-Yan model and in support of the QCD corrections[4].

We have tried to evaluate the size of the departure from the "naïve" Drell-Yan model, measuring the k-factor which is defined as follows:

$$\left.\frac{d^2\sigma^{exp}}{dmdy}\right|_{y=0} = k \left.\frac{d^2\sigma^{naïve\ D.Y.}}{dmdy}\right|_{y=0} .$$

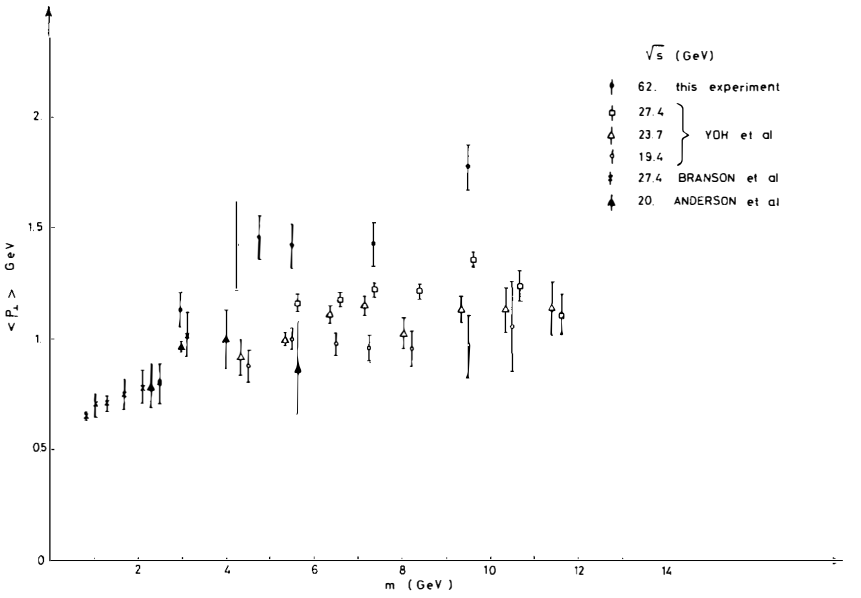

Fig. 4 The average $\langle p_T \rangle$ versus mass for different c.m. energies

We found that k is approximately 1.7, but its value depends both on the assumed sea-quark distribution as well as on $\sqrt{\tau}$, varying between 2.5 and 1.2. A sea distribution of the form $\chi \cdot S(x) \sim (1-x)^{11.5}$ fits well our data and gives a k value independent of $\sqrt{\tau}$ within the measured range.

In conclusion, the only observed departure from the naïve Drell-Yan mechanism is the rise of $\langle p_T \rangle$ with $\sqrt{s}$, as well as the absolute value of the cross-section.

REFERENCES AND FOOTNOTES

1) Work done by the Athens^2-Brookhaven-CERN-Syracuse Collaboration (C. Kourkoumelis, L.K. Resvanis, T.A. Filippas, E. Fokitis, A.M. Cnops, J.H. Cobb, R.Hogue, S. Iwata, R.B. Palmer, D.C. Rahm, P. Rehak, I. Stumer, C.W. Fabjan, T. Fields, D. Lissauer, I. Mannelli, P. Mouzourakis, K. Nakamura, A. Nappi, W. Struczinski, W.J. Willis, M. Goldberg, N. Horwitz, G.-C. Moneti and A.J. Lankford).

2) C. Kourkoumelis et al., Phys. Lett. 91B, 475 (1980).

3) L. Lederman, Physica Scripta 20, 227 (1979).

4) See, for example: G. Altarelli et al., Phys. Lett. 76B, 351 and 356 (1978).

INTERMEDIATE MASS ($1.4 \lesssim M \lesssim 2.6$ GeV/c^2) $\mu^+\mu^-$ PAIRS

A. C. Melissinos
Department of Physics and Astronomy
University of Rochester
Rochester, N.Y., 14627, U. S. A.

Abstract: We discuss results from the hadronic production of $\mu^+\mu^-$ pairs in the interval $1.4 \lesssim M_{\mu^+\mu^-} \lesssim 2.6$ GeV/c^2. It is shown that dimuons are produced not only directly $\mu^+\mu^-$ in accordance with the Drell-Yan model but also indirectly through one or more other mechanisms. Evidence for the scale breaking of the pion structure function is presented; the Q^2-evolution being in good agreement with QCD predictions. Finally we evaluate the magnitude of the intrinsic transverse momentum of the partons and find $\langle k_T \rangle \simeq 320 \pm 40$ MeV.

1. Introduction

Hadronic production of lepton pairs with $M \gtrsim 4.0$ GeV/c^2 is in close agreement with the Drell-Yan (D.Y.) model[1] subject to first order QCD corrections[2]. Below the J/ψ mass dilepton production cannot be accounted for only by the D.Y. model even though it exhibits many similarities to the production of high mass pairs. The intermediate mass region, $1.4 \lesssim M \lesssim 2.6$ GeV/c^2 is of interest because of:

(a) The definite presence of a dilepton production mechanism other than D.Y.

(b) It makes possible the determination of the structure function of the pion at low values of Q^2 and therefore a study of its Q^2-evolution.

(c) The determination of the average intrinsic transverse momentum of the partons is practically independent of dynamic (QCD) effects.

In this report we discuss the above topics based primarily on results obtained with 16 GeV/c $\pi^{\pm}$ and 22 GeV/c π^- beams incident on nuclear targets. The experiments were performed at Brookhaven National Laboratory and details can be found in the literature[3-7]. Similar results have been obtained by the Chicago-Princeton group[8,9], in two experiments using the Omega spectrometer at CERN[10,11] as well as by groups in the USSR[12]

2. Comparison of $\mu^+\mu^-$ pair production with the D.Y. model; indirect dilepton production

Examination of the data indicates that the order of magnitude and the x-dependence of the differential cross-sections $d\sigma/dMdx$ is in reasonable agreement with the D.Y. model. However the data are higher than predicted by a factor of $\sim$2.0, the discrepancy increasing at lower masses. It is unwise to base conclusions about the validity of the model on normalization comparisons alone because the vertex correction[2] (K-factor $\simeq$ 2.0) and the color factor (1/3) are of the same order as the observed differences. Fortunately, the D.Y. model makes definite predictions for other features of the data which are independent of the absolute normalization.

A specific prediction is the ratio of dilepton production by π^+ and π^- beams. This ratio R takes a simple form if the data are restricted to $x_1 > 0.4$ in which case the pion sea can be ignored, so that

$$R = \frac{d\sigma/dM(\pi^+N \to \mu^+\mu^- + \ldots.)}{d\sigma/dM(\pi^-N \to \mu^+\mu^- + \ldots.)} = \frac{[Zd_v(x_2)+Nu_v(x_2)] + 5(Z+N)\lambda(x_2)}{4[Zu_v(x_2)+Nd_v(x_2)] + 5(Z+N)\lambda(x_2)} \qquad (1)$$

Here x_1, x_2 refer to the indicent pion and target nucleon, respectively and $u_v(x_2)$, $d_v(x_2)$ are the proton structure functions for valence "up", "down" quarks. The proton sea quark distribution is $\lambda(x_2) = \bar{u}_s = u_s = \bar{d}_s = d_s$ and we ignore the contribution of other flavors; (Z,N) characterize the target nucleus.

We have used the Q^2-dependent structure functions of Buras and Gaemers[13] to evaluate Eq. (1) as a function of τ for three different energies. The result is given by the solid curve in Fig. 1, to be compared with the dashed curve which is a fit to the data points; the shaded area indicates the range in the error of the fit. We attribute the discrepancy between the data and Eq. (1) to the presence of one or more production mechanisms in addition to the D.Y. model. We shall refer to these mechanisms as <u>indirect</u> production in distinction to the term <u>direct</u> production which we reserve for the D.Y. process.

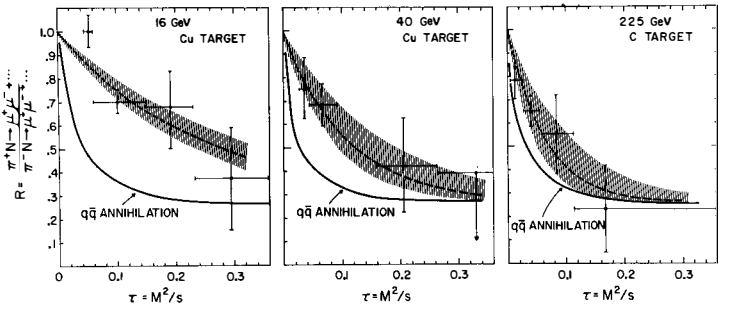

Fig. 1 - Ratio of $\mu^+\mu^-$ yield from π^+N and π^-N interactions.

To interpret the data of Fig. 1 we make the simplest possible assumption, namely that the indirect production is charge independent. We can then evaluate the fraction γ of directly produced pairs to the total production

$$\gamma(s,\tau) = \frac{d\sigma/dM[\pi^-N \to (q\bar{q} \to \mu^+\mu^-) + \ldots]}{d\sigma/dM[\pi^-N \to \mu^+\mu^- + \ldots\ldots\ldots]} = \frac{1-R(s,\tau)_{\text{observed}}}{1-R(s,\tau)_{\text{calculated}}} \qquad (2)$$

The fraction γ is shown in Fig. 2a as a function of τ for different incident energies; and in Fig. 2b as a function of mass. In this case γ appears to be independent of the incident energy. However it can depend on the target as discussed below.

We recall that the D.Y. model does not consider secondary interactions and therefore dilepton production from nuclear targets should be exactly proportional to the target atomic number A. This prediction is fulfilled for high mass pairs but fails for $M \lesssim 3.0$ GeV/c^2. We can account for this observation by making the plausible assumption that indirect production is typical of hadronic processes and has an A^ρ dependence with ρ in the range 2/3 to 0.74. It follows that the observed A-dependence will be of the form A^δ where

$$\delta(M) = 1 - \frac{\log\{\gamma(M,A) + A^{1-\rho}[1 - \gamma(M,A)]\}}{\log A} \qquad (3)$$

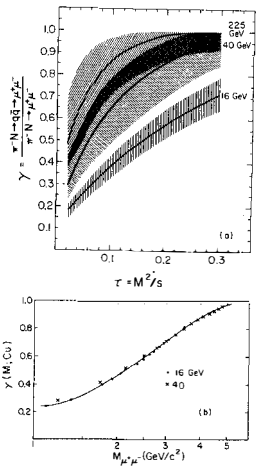

Fig. 2 - The fraction of directly produced dimuons.

The prediction of Eq. (3) is compared with the data in Fig. 3 and shows good agreement.

A further consequence of the D.Y. model is that at sufficiently high energies the virtual photons decaying into $\mu^+\mu^-$ are transversely polarized; therefore the decay angular distribution in the dimuon rest frame must be of the form $(1 + \cos^2\theta^*)$ with respect to the photon spin direction. When the dimuons are produced with significant transverse momentum ($p_T/M \simeq 1$) the polarization axis is not anymore uniquely defined. From the data we find[6] that in the helicity frame the decay distribution can be fit to the form

$$\frac{d\sigma}{d\cos\theta^*} = (1 + \alpha\cos^2\theta^*)$$

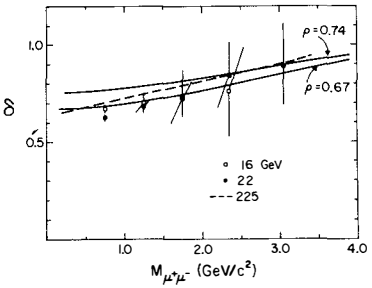

Fig. 3 - The exponent δ when dimuon production from nuclei is parametrized as A^{δ}.

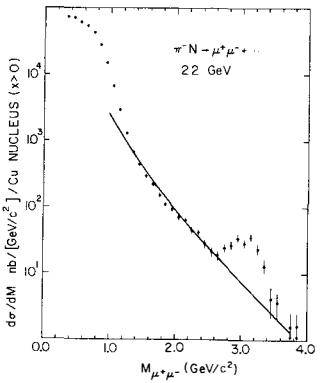

Fig. 4 - Dimuon production by 22 GeV π^- on Cu.

with $\alpha = 0.32 \pm 0.23$. If the indirect production is isotropic it dilutes the asymmetry and the observed value of α becomes

$$\alpha_{observed} = \frac{3\gamma}{4 - \gamma} \tag{4}$$

For $\gamma \simeq 0.4$ Eq. (4) reproduces the asymmetry of the data.

We can now address the question of the absolute normalization. The x-dependence of the indirect production is unknown but in deriving Eq. (2) it has been implicitly assumed that it is similar to that predicted by the D.Y. model. We can then use the pion structure function derived from the data (see following section) and the values of $\gamma(M)$ from Fig. 2b to calculate the observed cross-section $d\sigma/dM$. The result is shown by the solid curve in Fig. 4, in excellent agreement with the data.

The conclusion of this analysis is that when indirect production is taken into account there is no need to introduce the vertex renormalization K-factor. Of course our data agree with those of the other groups as can be easily realized by noting that in this mass range $1/\gamma \simeq K$. The difference is in interpretation of the data and the fact that γ is mass-dependent and tends to unity for $M \geq 4$ GeV/c^2. In contrast, the K-factor is generally taken as mass independent; however because of the increase of $\alpha_s(Q^2)$ as $Q^2 \to 0$, the K-factor should increase at low masses.

Several mechanisms for indirect dilepton production have been proposed but at present it is not possible to differentiate between them. For instance Bjorken and Weissberg[14] suggest that in the final state interactions following hard qq scattering a number of secondary $q\bar{q}$ annihilations take place leading to the production of low mass pairs. David and Barbara Schrempp[15] have considered the two photon exchange (Bethe-Heitler) electromagnetic production of very low mass pairs. Shuryak[16] and Domokos[17] have proposed a thermodynamic model whereby low mass pairs are produced in the short space-time region of a hadronic collision. If this process does indeed take place, low mass dileptons can be used as a signature of phase transitions from nuclear to quark matter especially in the collision of heavy nuclei[17].

3. Scale breaking of the pion structure function

The consideration of indirect lepton production allows us to establish the observed cross section due to the D.Y. process. We can then extract the pion structure function either by using the known nucleon structure functions or by the factorization method[5]. Both methods lead to the same results which are indicated by the solid points in Fig. 5. Since our data probe the structure

function only for $x_1 > 0.4$ we fix the dependence at $x \to 0$ and fit them to the form

$$F^{\pi}(x_1) = A\sqrt{x_1}\ (1 - x_1)^n \tag{5}$$

with A, n free parameters. The result is

$$n = 0.47 \pm 0.05 \qquad A = 0.72 \pm 0.05$$

Integration of Eq. (5) with the above fitted values for n, A gives

$$\int_0^1 F^{\pi}(x_1)\,\frac{dx_1}{x_1} = 1.10 \pm 0.10 \quad \text{and} \quad \int_0^1 F^{\pi}(x_1)dx_1 = 0.29 \pm 0.04$$

for the probability of finding a $\bar{u}$ (or d) quark in the π^- and for the momentum fraction carried by each quark.

Structure functions obtained from deep inelastic scattering (DIS) depend on Q^2, their evolution being described by the Altarelli-Parisi equation[18] Presuming that this formalism remains valid in the time-like domain the pion structure function (determined from dilepton production) should evolve as

$$F^{\pi}(x_1,Q^2) = \frac{1}{B(\eta_1,\eta_2+1)}\,(x_1)^{\eta_1}(1 - x_1)^{\eta_2} \tag{6}$$

We used the QCD calculation of Owens and Reya[19] and our own structure function as input to determine

$$\eta_1 = 0.5 - 0.104\bar{s} \qquad \eta_2 = 0.47 + 0.69\bar{s}$$

with

$$\bar{s} = \ln\left[\frac{\ln(Q^2/\Lambda^2)}{\ln(Q_o^2/\Lambda^2)}\right]$$

where $Q_o^2 = 3.17\ \text{GeV}^2$ corresponds to the mean value of M^2 for our data and we have set $\Lambda \simeq 0.5$ GeV. The lower curve in Fig. 5 is the prediction of Eq. (6) evaluated at $Q^2 = 36\ \text{GeV}^2$, the mean value of M^2 for the Chicago-Princeton data[9] at 225 GeV. We note that the data points are in agreement with the theoretically predicted evolution of $F^{\pi}(x_1)$.

It can be argued that the observed agreement is fortuitous in view of the difficulty of establishing the structure function at low values of Q^2; and of course depends on the value of Λ. On the other hand there is little doubt that the pion structure function at $Q^2 \simeq 36$ (i.e. for $4.5 \lesssim M \lesssim 9.5$) is of the form indicated by the lower curve. It therefore follows that for smaller values of M, $F^{\pi}(x_1)$ is much flatter and is inconsistent with a $(1-x_1)^{1.0}$ dependence as $x_1 \to 1.0$. This argument can be used to support the conclusions reached in the previous section. More generally, a study of scale breaking effects whether in DIS or in dilepton production must by necessity make use of data at low values

of Q^2; in this domain QCD corrections are subject to larger uncertainties both in the space-like and time-like domain. The advantage of dilepton data over DIS data is that they probe the region $x \simeq 1.0$ where scale breaking effects are large and free of contributions from the sea.

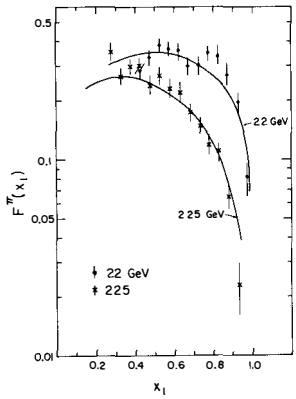

Fig. 5 - Q^2-Evolution of the pion structure function.

4. Intrinsic transverse momentum of the partons

In the simple D.Y. model the dileptons are produced with no transverse momentum. First order QCD corrections involving the emission of, or scattering from, a gluon allow the dilepton to acquire transverse momentum. The magnitude of this effect does not suffice to account for the observed distributions and one must assign an intrinsic (primordial) transverse momentum to the quarks confined in the colliding hadrons. From purely dimensional arguments the mean p_T generated by QCD grows as $\sqrt{s}$ and therefore becomes the dominant effect at high energies. At low energies the p_T distribution is due primarily to the intrinsic k_T.

To calculate the expected transverse momentum distribution[7] we use the regularization procedure of Altarelli et al[20], where

$$\left.\frac{d^2\sigma}{dMdp_T^2dy}\right|_{reg.} = \sigma_{DY}(\tau,s,y)f(p_T^2) + \frac{1}{\pi}\int d^2\vec{k}_T\sigma_{QCD}(k_T,\tau,s,y)[f((\vec{p}_T-\vec{k}_T)^2) - f(p_T^2)] \quad (7)$$

and $f(k_T^2)$ is a steeply falling function representing the effective contribution due to the intrinsic transverse momentum of <u>both</u> partons. We have chosen a Gaussian

$$f(k_T^2) = Ae^{-Ak_T^2} \qquad A = \frac{\pi}{8\langle k_T\rangle^2} \quad (8)$$

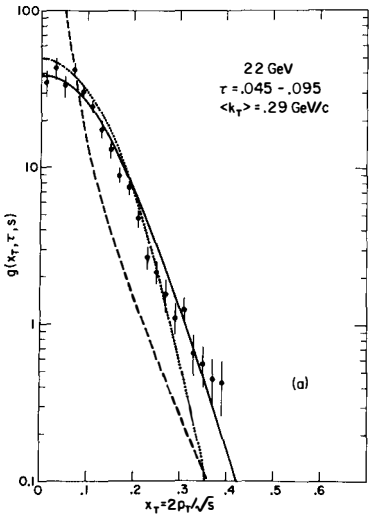

Fig. 6 - Transverse momentum distribution of dimuons.

with a width corresponding to $\sqrt{2}\ \langle k_T \rangle$.

Equation (8) has been evaluated numerically for different values of $\langle k_T \rangle$ and fitted to the data. In this process we have taken account of the fact that the indirect dilepton production is completely determined by the intrinsic distribution of Eq. (8) alone; details of this procedure can be found in ref. (7). A typical result is shown in Fig. 6: the dashed curve is the infrared-divergent QCD cross-section; the dotted curve the intrinsic Gaussian; and the solid curve the convolution of these two contributions as indicated by Eq. (7). The intrinsic transverse momentum dominates the distribution whereas the inclusion of QCD effects decreases $\langle k_T \rangle$ by $\sim$20%.

We find that $\langle k_T \rangle$ is independent of the incident energy but grows slowly with τ. Averaging over the mass interval $1.4 \leq M \leq 2.6$ GeV/c^2

$$\langle k_T \rangle = .370 \pm 0.030 \text{ GeV/c}$$

When the effects of Fermi motion and experimental resolution are unfolded one obtains

$$\langle k_T \rangle = 0.320 \pm 0.040 \text{ GeV/c}$$

We note that $\langle k_T \rangle$ as defined in Eq. (8) refers to the intrinsic transverse momentum of <u>one</u> of the colliding quarks. Therefore the mean p_T of the dileptons due to intrinsic effects alone is $\langle p_T \rangle = \sqrt{2}\ \langle k_T \rangle$. Finally, our results can be parametrized as a function of s and τ by the approximate form

$$\langle p_T \rangle = \begin{Bmatrix} 0.40 & (\sqrt{\tau} = 0.24) \\ 0.50 & (\sqrt{\tau} = 0.34) \\ 0.57 & (\sqrt{\tau} = 0.45) \end{Bmatrix} + 0.038\sqrt{s} \qquad (9)$$

Equation (9) even though only of qualitative nature, is in reasonable agreement with the $\langle p_T \rangle$ observed for dilepton production in 150 and 280 GeV π^-N collisions[21].

REFERENCES

1. S. D. Drell and T. M. Yan, Phys. Rev. Lett. 25 (1970) 316; Ann. Phys. (N.Y.) 66 (1971) 578.
2. R. K. Ellis, Appendix to these proceedings.
3. J. Alspector et al., Phys. Lett. 81B (1979) 397; J. LeBritton et al., Phys. Lett. 81B (1979) 401.
4. C. Reece et al., Phys. Lett. 85B (1979) 427.
5. D. McCal et al., Phys. Lett. 85B (1979) 432.
6. R. Youngquist et al., Phys. Lett. 95B (1980) 457.
7. W. Metcalf et al., Phys. Lett. 91B (1980) 275.
8. J. G. Branson et al., Phys. Rev. Lett. 39 (1977) 1388; 38 (1977) 1331,1334.
9. C. B. Newman et al., Phys. Rev. Lett. 42 (1979) 951.
10. M. J. Corden et al., Phys. Lett. 68B (1977) 96; 76B (1978) 226.
11. J. D. Dowell; these proceedings.
12. Y. M. Antipov et al., Phys. Lett. 60B (1976) 309; Y. B. Bushnin et al., Phys. Lett. 72B (1977) 269.
13. A. J. Buras and K. J. F. Gaemers, Nucl. Phys. B132 (1978) 249.
14. J. D. Bjorken and H. Weissberg, Phys. Rev. D13 (1976) 1405.
15. D. Schrempp and B. Schrempp; these proceedings.
16. E. V. Shuryak, Phys. Lett. 78B (1978) 150.
17. G. Domokos and J. I. Goldman "Quark Matter Diagnostics" Johns Hopkins University preprint HET-8004.
18. G. Altarelli and G. Parisi, Nucl. Phys. B126 (1977) 298.
19. J. F. Owens and E. Reya, Phys. Rev. D17 (1978) 3003.
20. G. Altarelli, G. Parisi and R. Petronzio, Phys. Lett. 76B (1978) 356.
21. J. Badier; these proceedings.

PRODUCTION OF μ-PAIRS IN THE FORWARD DIRECTION: FERMILAB EXPERIMENT 615

A.J.S. Smith
Princeton University Physics Department
Princeton, N.J., U.S.A. 08540

ABSTRACT: A brief description is given of a new experiment at Fermilab, the goal of which is a sensitive measurement of the pion structure function, including the spin dependence of the coupling of hadrons to virtual photons. Particularly interesting is the region $x_1 \to 1$, in which a single quark contains most of the beam momentum.

The purpose of this brief contribution is to report on the goals and status of Fermilab experiment 615, an upcoming study of μ-pair production in the forward direction. Approved in June 1979, this experiment is a collaborative effort among groups from the University of Chicago, Fermilab, the Iowa State University and Princeton University. The experiment was motivated by results[1,2] of our previous Chicago-Princeton experiments using the Cyclotron spectrometer at Fermilab (E 331/444), which completed their data-taking in early 1978. The exposure of E-331/444 is summarized in fig. 1, where the μ-pair production cross-section for $X_F \gtrsim 0.1$ in the reaction $\pi^- P \to \mu^+\mu^- + X$ is plotted as a function of the pair mass M. It is seen that the Drell-Yan mechanism (DY) accounts for the yield in the 4-8 GeV mass region, between the J/ψ and Υ resonances. This experiment was also the first to confront and verify the other unique predictions of DY, such as the charge ratios at high mass $\sigma(\pi^-$ Carbon $\to \mu\mu + X) \tilde{\gtrsim} 4\sigma(\pi^+$ Carbon $\to \mu\mu + X)$ and $\sigma(\pi^-$ Carbon $\to \mu\mu + X) >> \sigma(P$ Carbon $\to \mu\mu X)$.

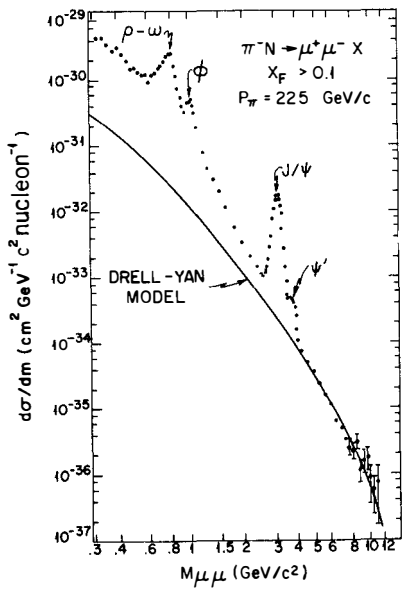

Fig. 1. Mass spectrum of μ-pairs measured by Chicago-Princeton group in π^--Nucleon collisions at 225 GeV/c. The solid line is the Drell-Yan cross-section based on Chicago Princeton structure functions.

Particularly interesting is the angular distribution in the polar angle θ^* of the decay muons in the rest frame of the virtual photon. The polar axis is chosen as described by Collins and Soper.[3] Our results[2] are shown in Fig. 2 as a function of $\cos\theta^*$ for various intervals of x_1, the fractional momentum of the annihilating quark of the beam particle (π^-). For the J/ψ, an isotropic distribution is seen for all x_1 intervals. For the DY region (M > 4 GeV), however, the distribution changes from $\sim 1 + \cos^2\theta^*$ at low x_1 (the DY prediction), to isotropic at high x_1 ($0.8 < x_1 < 1.0$). This striking effect is shown again in fig. 3, where the distribution has been fitted to the form $1 + \alpha\cos^2\theta^*$. The quantity α is shown as a function of x_1. The deviation of α from one at large x_1 is a signal of a production mechanism more complicated than simple annihilation of on-shell massless fermions. Brodsky and Berger have

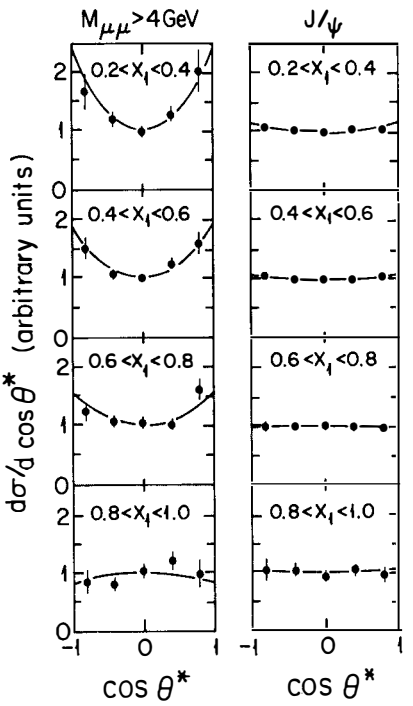

Fig. 2. Relative cross-section as functions of polar angle θ^*, for various regions of x_1.

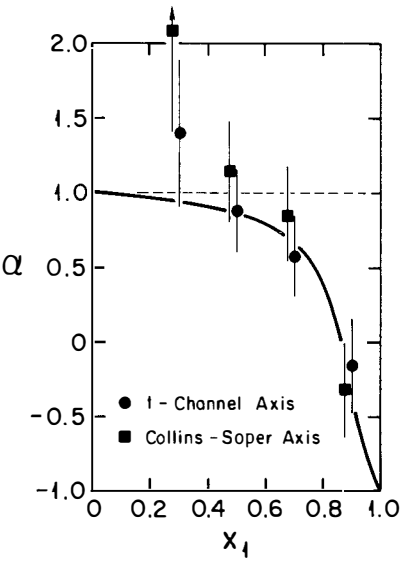

Fig. 3. Dependence of α on x_1 for pair masses M > 4 GeV. The solid line is the prediction of Reference 4.

proposed[4] a mechanism to account for this behavior, shown in fig. 4, in which a single hard gluon is exchanged between the two beam valence quarks to enable one quark to attain virtually the entire π^- momentum. They argue that this process becomes much more likely than simple $q\bar{q}$ annihilation as $x_1 \to 1$, and hence modifies the angular distribution. Their prediction is shown as the solid line in fig. 3. Not only does the Brodsky-Berger process affect $d\sigma/d(\cos\theta^*)$ but its prediction for the pion structure function integrated over angles, namely

$$x_1\, \bar{u}(x_1) \sim (1 - x_1)^2 + \frac{2}{9}\,\frac{\langle K_T^2\rangle}{M^2}\text{, where}$$

$\langle K_T^2\rangle \sim 1\,(\text{GeV/c})^2$, is explicitly scale breaking. To summarize, our results have indicated that there is much exciting μ-pair physics to be studied at high x_1.

We thus have designed an experiment to run in the high-intensity π^- beam, in the proton-west area of Fermilab. A major goal is to measure the pion

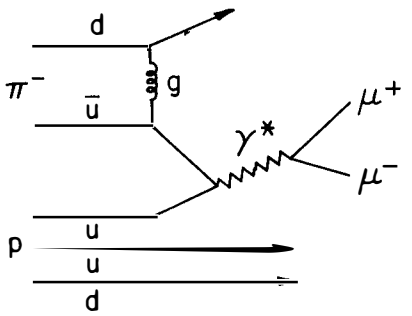

Fig. 4. Mechanism for high-x_1 μ-pair production proposed by Berger and Brodsky.

structure function and μ-pair angular distribution at high x_1 with more than 100 times the sensitivity of previous experiments.[5] By measuring at two different beam energies, we can search for effects dependent upon pair mass M, as opposed to those depending only upon the scaling parameter $\tau = M^2/S$.

The apparatus is shown in fig. 5. Separate configurations are used at 225 and 75 GeV/c to optimize the acceptance in polar angle θ^*. Of particular importance is sensitivity close to the beam direction, because in asymmetric events at high x, one of the two muons is always near the beam momentum. Typical beam intensities should be 10^9/pulse. Particles produced in the target are bent as they pass through the selection magnet in such a way that only high mass pairs, mainly inbending, are directed into the downstream spectrometer. Most low P_T, low - x muons are swept out. Hadrons are absorbed by a filter in the magnet gap; the filter materials are chosen to minimize multiple scattering and keep a reasonable acceptance.

Tracking is accomplished with multiwire proportional chambers upstream of the analysis magnet and by drift chambers downstream. Mass resolution is better than 1.5 per cent. Accidental coincidences between a halo muon and a muon from uninteresting events should be the major trigger background. To suppress this background, we first

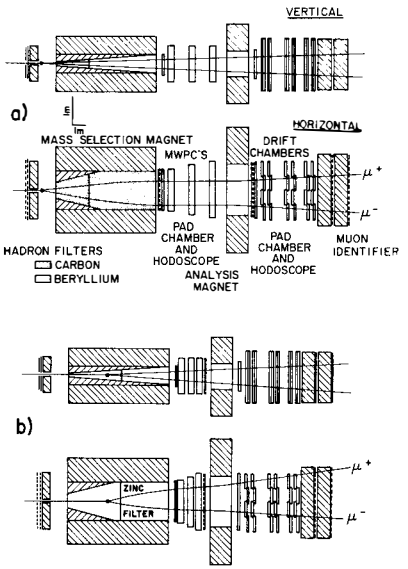

Fig. 5. Detector for experiment 615. The 250 GeV/c configuration is shown in a), the 75 GeV/c configuration in b).

use a scintillator hodoscope upstream of the target to veto halo muons. Also, a trigger processor uses information from the cathode-readout pads of two mini-drift "Pad Chambers" to decide in about a microsecond whether a trigger is worth recording. Basically a crude estimate of pair mass is made assuming the event originated in the target. Studies show that the processor should reduce the trigger rate to less than a few hundred per 10^9 beam particles.

The acceptance of the apparatus, including effects of the trigger processor, is shown as a function of cos θ^* in fig. 6, for two situations each with $M^2/S = 0.14$ and Feynman-x $x_F = 0.9$. Reasonable acceptance is maintained out to $|\cos\theta| \sim 0.8$. Typical acceptances in x_1, P_T, and M are shown in fig. 7.

The experiment will run beginning in January 1982. To demonstrate its expected sensitivity, we show in the next two figures some Monte-Carlo simulations of what we would measure if the Brodsky-Berger model were correct. First, the scale-breaking would be clearly evident, as seen in fig. 8 where the π^- structure function is shown for two values of M at the same τ. The exposures needed for this measurement are also indicated.

The angular distributions are also very sensitively measured as is seen in fig. 9, where the parameter α defined above is given as a function of x_1.

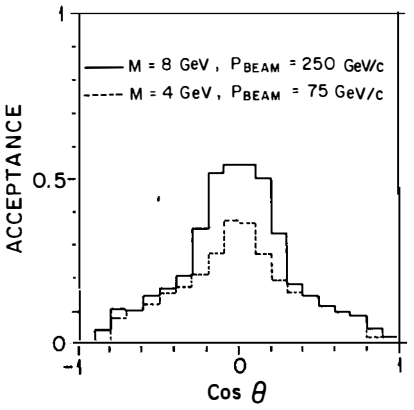

Fig. 6. Acceptance vs. cos θ^*

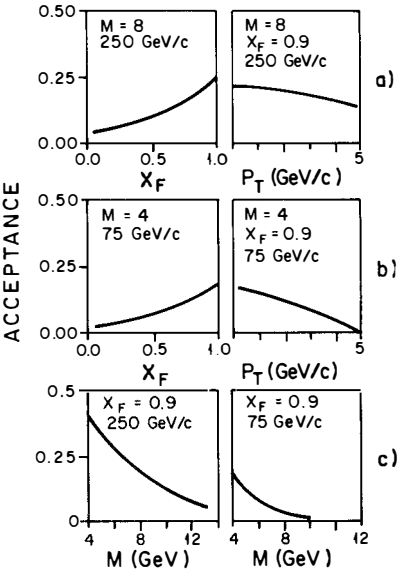

Fig. 7. Acceptance vs x_1, P_T, and M.

Naturally, the experiment is not merely a test of the Brodsky-Berger effect. By designing as complete an angular acceptance as possible we hope to explore in an entirely general way the spin structure of the photon-hadron coupling. This has been expressed[6] as

$$d\sigma/d^4Qd\Omega^* = W_T(1 + \cos^2\theta^*) + W_L \sin^2\theta^* + W_\Delta \sin 2\theta^* \cos\phi^* + W_{\Delta\Delta} \sin^2\theta^* \cos 2\phi^*$$

where the 4 structure functions W depend on x, P_T, and M. To separate the W's, one must have good coverage both in θ^* and ϕ^* to prevent unpleasant correlations. So far, E-615 is the only experiment presently planned with adequate capability.

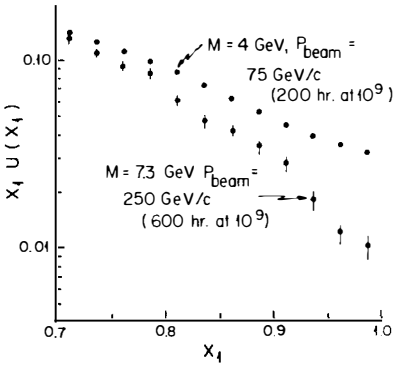

Fig. 8. Simulation of structure function results from E-615 if Berger-Brodsky prediction holds.

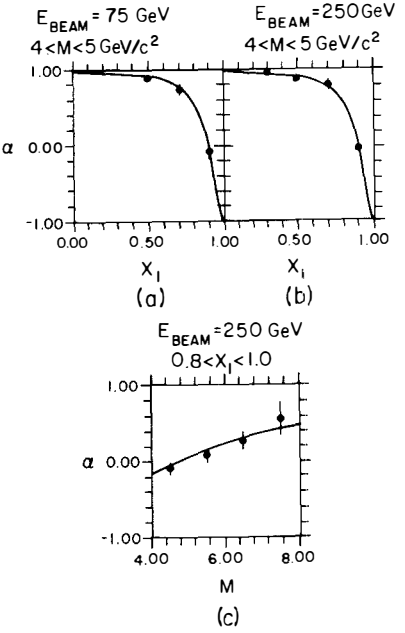

Fig. 9. Simulated measurements of α if Berger-Brodsky prediction holds.

References

1. K.J. Anderson et. al, Phys. Rev. Lett. 42, 944 (1979), G.E. Hogan et al, ibid, p 948, C.B. Newman et al, ibid, p 951, and earlier references cited therein.

2. K.J. Anderson et al, Phys. Rev. Lett. 43, 1219 (1979).

3. J.C. Collins and D.E. Soper, Phys. Rev. D 16, 2219 (1979).

4. E.L. Berger and S.D. Brodsky, Phys. Rev. Lett. 42, 940 (1979).

5. The π^- structure function was first measured by Newman et al (Reference 1) and with more precision, by the NA-3 group, as reported by J. Badier and O. Callot at this workshop.

6. C.S. Lam and Wu-Ki Tung, Phys. Rev D 18, 2447 (1978).

"Systematic approach to inclusive lepton pair production in Parton Model"

PROPERTIES OF HADRONS ASSOCIATED WITH LEPTON-PAIR PRODUCTION

B. Pietrzyk
CERN, Geneva, Switzerland

ABSTRACT

According to the Drell-Yan mechanism a lepton pair is produced in π^-N interaction through $u\bar{u}$ quark fusion. The spectator d quark from the pion then fragments into hadrons. What are the properties of these hadrons? Do they form a jet? Do they remember the quantum numbers of the d quark? Are they similar to the hadrons associated with the J/ψ production, and to those produced in the normal hadronic interactions?

Properties of hadrons associated with the Drell-Yan pairs and with the J/ψ production were studied in the WA11 (Goliath) experiment at CERN.

1. INTRODUCTION

Most of the experimentalists skiing at Les Arcs do not like the physics presented in this article. They not only do not like it, but they even hate it! They hate it so much that they use very brutal methods in order to kill it by putting a very hard material just after the production target, and the hardness of the material used depends on the brutality factor of a particular experiment.

This article describes properties of hadrons associated with lepton pairs. The first-order analysis presented here deals with all the hadrons, that means with the low-p_T hadrons. This should be interesting also for the quantum chromodynamics (QCD) fans since in their future analysis of high-p_T hadrons they should be able to understand how much of the effects observed by them is just a tail of the physics described here.

What is interesting in the physics of hadrons associated with lepton pairs? Figure 1 presents a graph of the dimuon pair production through the Drell-Yan mechanism in π^-N interactions. Since the negative pion is composed of the down (d) and the anti-up ($\bar{u}$) quarks and since the latter annihilates in the production of a lepton pair, the d quark continues its trajectory in the forward direction and fragments into hadrons. In a similar way a diquark from the nucleon fragments into hadrons in the backward direction, but this is less interesting in this analysis for reasons which will become clear later. It is important to realize that knowing the x and the mass of the lepton pair one knows the fraction of the momentum carried by the forward d quark x_d for every event (as $1 - x_{\bar{u}}$)[1].

For the J/ψ production we expect a different situation (Fig. 1). Since the J/ψ is produced mostly through the gluon-gluon fusion (at the energies of this experiment), both the d and $\bar{u}$ quarks are fragmenting in the forward direction. Again, here one knows the momentum of the fragmenting system event by event.

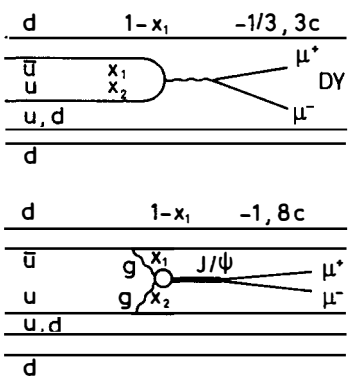

Fig. 1
Graphs describing the parameters of a hadronic system accompanying the Drell-Yan and J/ψ productions

Therefore there are basic differences for these two cases. First of all, in the case of the Drell-Yan production, it is a system with a charge of $^1/_3$ which is fragmenting, while in the case of the J/ψ production it is the whole -1 charge. Do we see this difference experimentally? Secondly, for the Drell-Yan production (quark fusion) the fragmenting system is in the three-colour state, while for the J/ψ production (gluon fusion) the fragmenting system is in the eight-colour state. According to the QCD predictions one could expect a higher multiplicity by a factor of 9/4 for the fragmentation of the eight-colour state[2]. Finally, what are the fragmentation functions? Particularly, is the d quark (accompanying Drell-Yan production) fragmenting as a "well-established jet" (WEJ).

In order to investigate these questions, properties of hadrons associated with the Drell-Yan and the J/ψ production were investigated and compared with the properties of hadrons produced in the normal hadronic interactions as measured in the same experiment. All these were compared with the properties of WEJ. Since the best examples of WEJ are those seen in the e^+e^- annihilation and since the Field-Feynman fragmentation is describing them very well, for obvious technical reasons the Field-Feynman Monte Carlo (MC) simulation is taken as a model for WEJ[3].

2. EXPERIMENTAL SET-UP AND PROCEDURE

The experiment was performed by the Saclay-Imperial College-Southampton-Indiana-CERN Collaboration (WA11-Goliath)[4] in the CERN SPS West Hall. The experimental set-up is presented in Fig. 2. Negative pions with energy between 175 and 197.5 GeV/c were interacting in three beryllium targets with a length of 3, 4.2, and 3 cm. Coordinates of outgoing particles were measured by 13 chambers placed in the magnetic field of the Goliath magnet and three outside. Muons were identified as particles passing through 4 m of iron and leaving information in a few additional hodoscopes. A Čerenkov counter, which could identify charged kaons, was not used in the analysis presented here. Every chamber had a small insensitive region with a radius of 2.5 cm, where the incoming beam passed. This "beam

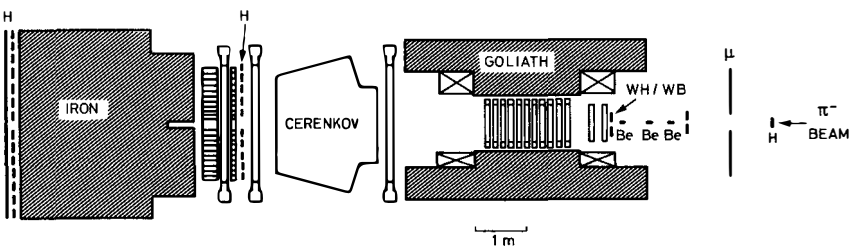

Fig. 2 The WA11-Goliath experimental set-up

killer" was slightly displaced for every chamber in order to follow the beam curvature. In this way an asymmetry in the acceptance for positive and negative particles was built into the apparatus. Despite its geometrical smallness the "beam killer" was quite important for the acceptance owing to the strong Lorentz boost of the outgoing particles at these high energies. In addition, it increased difficulties of the pattern recognition program in the region of high-particle density.

In order to investigate the experimental acceptance a sophisticated Monte Carlo program was developed. In this program a uniform distribution in rapidity and p_T was generated for both positive and negative particles. Each particle was traced through the set-up and the response of every detector was generated. This information, after taking into account inefficiency of chambers, was then mixed with a real event as measured during a standard data-taking period. Afterwards, such a set of events was processed through the standard pattern-recognition program. Finally, the ratio of the number of tracks surviving this procedure to the number of generated events determined the efficiency for every bin in a table of rapidity

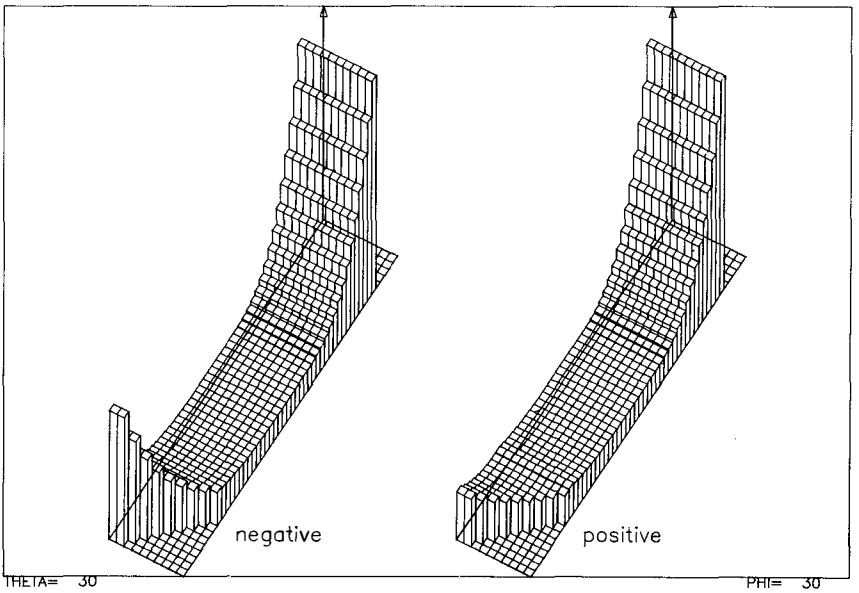

Fig. 3 Distribution of weight used in the evaluation of this experiment. The scale in p_T is between 0 and 2 GeV/c from left to right. The scale in rapidity is between -2 and 2.9 from up to down. Regions where the weight was set at zero are clearly seen.

versus p_T. This procedure consumed a large amount of computer time, but it was the only method of obtaining efficiency in a model-independent way. However, owing to this fact the results were subject to large statistical fluctuations. Therefore a smooth surface was fitted to the MC results.

During the data analysis every particle with a given rapidity and p_T obtained a weight defined as an inverse of efficiency. A two-dimensional plot of the weight distribution is presented in Fig. 3. One can see that at large rapidities (above two) there is a difference in acceptance between positive and negative particles. In addition, for rapidities where the acceptance was very small, the weight was set at zero. *Therefore in all results of the jet MC calculation all particles with a rapidity and p_T for which the weight was set at zero (in Fig. 3) were ignored.*

3. EVENT SELECTION

Figure 4 shows the $\mu^+\mu^-$ invariant mass spectrum. It is worth noting an excellent mass resolution for the J/ψ (σ = 31 MeV). A total of 42,456 events with the lepton-pair mass between 2.95 and 3.25 were defined as those accompanying J/ψ production. As can be seen in Fig. 4, the background contamination below the J/ψ

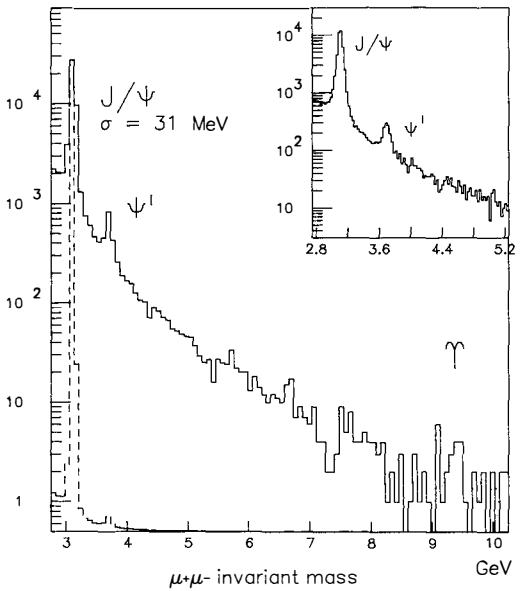

Fig. 4 $\mu^+\mu^-$ invariant mass spectrum measured in this experiment. Dashed line shows the same spectrum in a linear scale.

peak is very small. On the other hand, the 2126 events with the $\mu^+\mu^-$ mass between 3.85 and 9.3 were selected to represent the Drell-Yan production. Finally, these two sets of data were compared with those from normal π^-N interactions at 192.5 GeV/c in a beryllium target measured in the same experiment.

It is convenient to define the energy of the forward hadronic system as $x_{tot} = 1 - x_1$ (Fig. 1). In this way the longitudinal momentum of the hadronic system is described in the units $\sqrt{s}/2$. Owing to the different mass of the lepton-pair system the distribution of x_{tot} is different for the hadrons accompanying J/ψ and Drell-Yan production (Fig. 5), being slightly higher for the former.

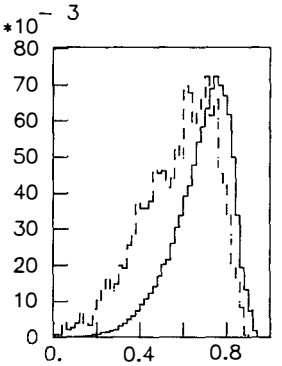

Fig. 5
Distribution of the total longitudinal momentum x_{tot} of the forward hadronic system accompanying the J/ψ (solid line) and the Drell-Yan (dashed line) production.

One of the major problems of the analysis of the properties of hadrons in this experiment was the fact that the interactions took place not with the proton but with the beryllium. The unpublished results of the Heidelberg-Lund[5] experiment at CERN show that the ratio of the number of fast particles produced in the hadron-nucleus interaction to the number of fast particles produced in the hadron-nucleon interaction is close to one in the forward direction, while it is strongly rising in the backward direction in the hadron-hadron c.m.s., which may be interpreted as indicating that the forward-going particles do not reinteract in the nucleus. Noting in addition that beryllium is a very small nucleus one can conclude that while in the backward direction one is studying basically nuclear effects, in the forward direction one can measure properties of hadrons produced in the elementary interaction. However, one should not forget that even there the small (< 15%) nuclear effects are not excluded.

Bearing in mind all these considerations, we will investigate properties of hadrons in terms of the following variables: charge flow, multiplicity, and fragmentation functions. *It is essential to note that all the experimental and MC curves and numbers presented in this paper are normalized to one (experimental or MC) event.*

Naively, the integration of these histograms over rapidity in the forward direction gives a very interesting number, the charge of a fragmenting system, e.g. $-\frac{1}{3}$ for the fragmentation of the d quark accompanying the Drell-Yan production, or -1 for the π^-N interactions or J/ψ production through the gluon-gluon fusion. Unfortunately, the reality is much more complicated; for example, the fragmentations in the forward and backward directions may overlap, the reinteractions in the beryllium target may add some positive charge also in the forward direction; finally, even in the fragmentation of the ideal d quark jet one does not expect to find a charge of $-\frac{1}{3}$. One should realize that for the balance of charge only the first (d) quark and the last antiquark in the fragmentation chain are important (the others cancel). If the last one is the $\bar{d}$, the $\bar{u}$, or the $\bar{s}$ with equal probability, then the net charge is really $-\frac{1}{3}$. On the other hand, if only the first two are produced, then the integrated charge is -0.5, while in the case of their production with the probability of 0.4, 0.4 and 0.2 (as in the case of Field-Feynmann fragmentation) one can expect to observe a net charge of 0.4.

Experimental results are presented in Table 1. Both the measured and corrected-for acceptance numbers are presented there. In addition four other entries in this table give the integrated charge for the d and $\bar{u}$ jet MC calculation both without any cuts and after rejection of particles for which the weight was set at zero (Section 2). Since for the experimental data the correction in the region of the "beam killer" was not made, an extrapolated number is also given. For this extrapolation an assumption was made that the distributions in y and p_T for the jet MC calculation and data had the same shape, so the extrapolation was done for the percentage of the charge loss in the MC calculation in the "beam killer" region.

Table 1

Integrated charge in the forward direction

	Drell-Yan	J/ψ	π^-N
Observed	-0.20	-0.29	-0.33
Corrected	-0.32	-0.45	-0.61
Corrected + extrapolated	-0.35	-0.52	-0.75
d corrected	-0.29	-0.30	-0.28
d total	-0.33	-0.35	-0.35
$\bar{u}$ corrected	-0-45	-0.45	-0.43
$\bar{u}$ total	-0.49	-0.51	-0.52
π^-N normalized to -1	-0.46	-0.70	-1.0

4. CHARGE FLOW

The upper left corner of Fig. 6 shows the distribution of charge in the function rapidity in the π^-N c.m.s. for the J/ψ production (dashed line). Every particle entered this distribution with the weight of charge times the weight as defined in Section 2. The solid line represents the same distribution without the weight correction. It is clearly seen that the corrected distribution is dominated by the positive particles in the backward direction, while in the forward direction the distribution is dominated by the negative charge with the crossover at the rapidity zero. Since the positive charge is strongly rising in the backward direction, clearly showing nuclear effects, only the physics in the forward direction is analysed in what follows. In addition, Fig. 6 shows the charge-flow distribution of the forward hadronic system accompanying the J/ψ, the Drell-Yan production, and in the normal hadronic interactions, compared with the same distribution of the jet MC calculation generated for the $\bar{u}$ or d quarks.

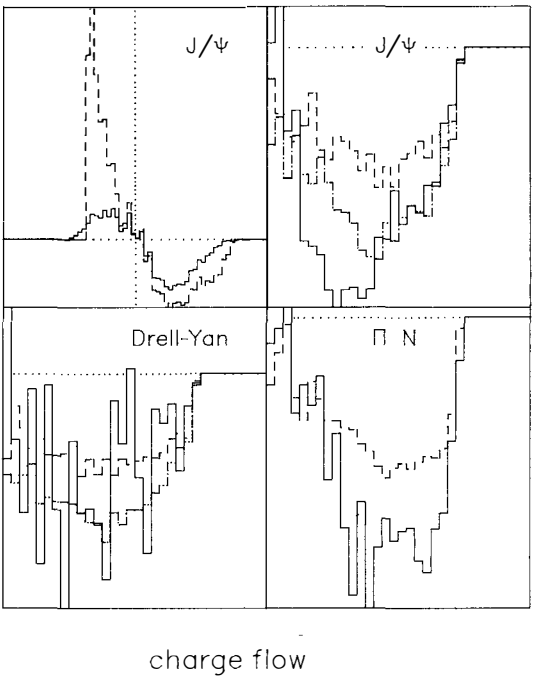

Fig. 6 Distribution of charge versus rapidity. Upper left corner: distribution corrected for acceptance (dashed line) and not corrected for acceptance (solid line), scale from -4 to 4. The other pictures are in rapidity scale from 0 to 4 and show data (solid line), d quark MC (dashed line), and $\bar{u}$ quark MC (dash-dotted line).

It is interesting to note that the forward charge for the π^-N interactions is not -1 as one could naively expect, but is about -0.75. Results of the measurements in the bubble chamber[6] show that this value is changing with energy (having the above value at the energy of this experiment).

Therefore one should not be extremely happy to see the forward charge of $-1/3$ accompanying the Drell-Yan production since this number is probably also varying with energy. Therefore more interesting numbers are ratios of charges after normalizing the charge in π^-N interactions to -1. This approach is justified since whatever is the reason for the charge "leak" through the region of rapidity zero it should be proportional to the charge in the elementary πN interaction. However, admixture of positive charge of nuclear origin is not, but is considered to be unimportant since the result for the π^-N obtained here is, within 10% (compatible with experimental errors), the same as that of the bubble chamber experiment on a hydrogen target.

For the Drell-Yan production we obtain in this way a number of -0.46, in agreement with the number 0.4 predicted above for the fragmentation of the d quark. In a similar way, for the J/ψ production one gets the value of -0.7. Assuming that the J/ψ is produced partly through the gluon-gluon fusion -- giving the charge seen in the π^-N interactions -- and partly through the quark-quark fusion -- giving the charge accompanying the Drell-Yan production -- one finds that the fraction of the J/ψ produced through the quark-quark fusion is 57% at the energy of this experiment.

This number may be in disagreement with the evidence from the fit to other variables of the J/ψ production presented at this Workshop[7] (25% of quark-quark fusion) and with the results of Goliath (only a small contribution of quark-quark fusion possible). However a careful study of errors in all experiments is needed before the conclusion can be drawn on the importance of this discrepancy. Also other effects may be non-negligible, as, for example, the influence of pion and nucleon seas.

The errors are still to be determined, but they should not be bigger than 15% for the absolute values and, of course, smaller for the ratios.

5. FRAGMENTATION FUNCTION

The simplest variable describing the fragmentation process is the z distribution, where z is the ratio of the x of every hadron to the x_{tot} of the hadronic system, as defined in Section 3. In this way fragmentation in the longitudinal momentum is investigated. The z distribution both in the linear and logarithmic scale for the hadrons accompanying J/ψ and Drell-Yan production and for the normal hadronic interactions in the forward direction is presented in Fig. 7 and compared with the jet MC distribution. For the normal hadronic interactions there seems

to be no difference in the fragmentation above z = 0.1, and an increase of particles is observed below. This increase at small z is also observed for the hadrons produced together with the J/ψ and Drell-Yan productions, but there it is accompanied by a little decrease in the number of particles at moderate z for the J/ψ production and with much smaller statistical significance for the Drell-Yan production. The present knowledge of the experimental efficiency does not allow us to say how much this difference is significant (this problem is now under investigation).

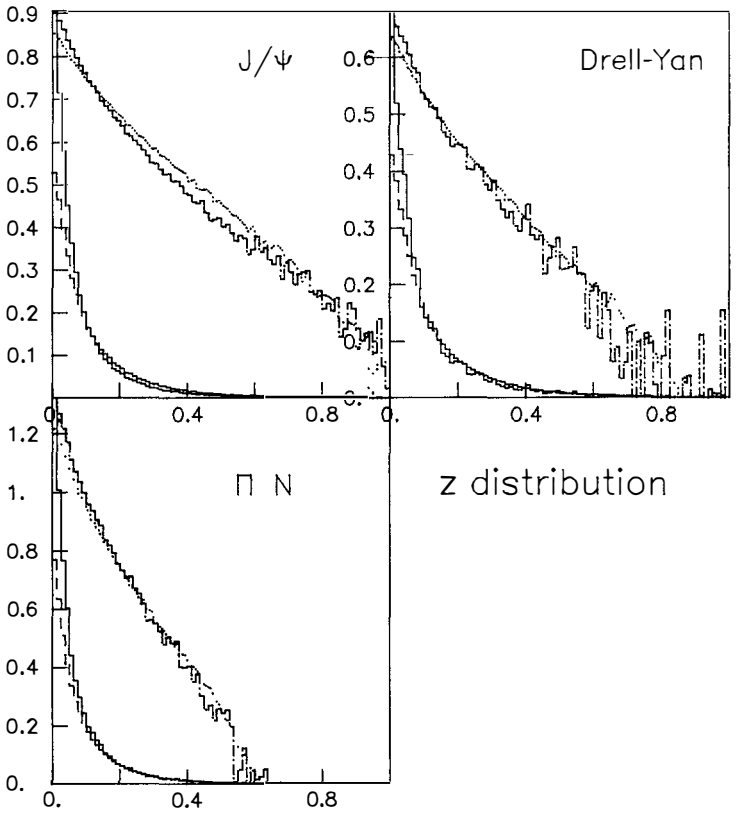

Fig. 7 z distribution describing the fragmentation both in linear and logarithmic scale. Linear scale: data (solid line), q MC (dashed line). Logarithmic scale: data (dash-dotted line), q MC (dotted line). All curves have absolute normalization to one experimental (or MC) event.

However, one should be very surprised that these different fragmentations are so similar and so close to the jet MC calculation. There are plenty of reasons why they could be different:

a) The quark contents of the hadronic systems are different. In the case of the Drell-Yan production it is the d quark which is fragmenting, while in the case of the J/ψ or normal hadronic interactions, both of them are fragmenting.

b) Colour charges are different. The forward hadronic system is in the three-colour state in the case of Drell-Yan production, mostly in the eight-colour state for the J/ψ production, and in a mixture of different colour states in the case of normal hadronic interactions.

c) Valence quarks are not the only partons in the hadrons. There are plenty of gluons and sea partons in the hadrons fragmenting together with the valence quarks. In the case of e^+e^- annihilation we start with the point-like quarks, while in the soft fragmentation described here we have a system of fragmenting partons (or quarks with a form factor). This is a difference between current and constituent quarks.

d) Finally, nuclear (beryllium) effects may be important. The forward-going partons may reinteract in the nucleus, scatter, or lose a little bit of energy; small effects of this kind are not excluded by the present data on hadron-nucleus scattering.

6. MULTIPLICITY

The measured multiplicity of the forward hadronic system is presented in Table 2. It is lowest for the Drell-Yan production, higher for the J/ψ production, and highest for the normal hadronic interactions.

Table 2

Multiplicity

	Drell-Yan	J/ψ	π^-N
Measured	3.4	3.9	4.8
Jet corrected	4.2	4.7	5.4
Ratio	1.24	1.21	1.13

One should, however, remember that the energy of the forward hadronic system is lowest for the Drell-Yan, higher for the J/ψ production, and finally highest for the normal hadronic interactions. Therefore it is natural to ask if this difference is just a trivial energy dependence.

The same table shows the values of multiplicity obtained for the jet MC calculation generated according to the energy distribution of the hadronic systems. It is difficult to compare both sets of data since the measured multiplicities were not corrected for acceptance, but one can ask if the ratios of calculated-to-measured multiplicities are the same. It turns out that within 10% they are. Therefore one can conclude that the difference in the observed multiplicity comes mainly from the energy dependence, and the colour effects discussed in Section 1 are not observed (of course in the energy region of this experiment).

7. CONCLUSIONS

The hadronic system may be described by many variables: its flavour (and correlated electric charge), its colour charge, its geometrical size, the description of its "construction" (set of structure functions).

In this work different hadronic systems have been investigated: three- and eight-colour objects, fragmentation starting from a point-like object (e^+e^- annihilation seen through the jet MC calculation) and from a large system (all the data presented here), fragmenting systems of a unit or fractional charge.

Any colour effects in the multiplicity were not observed. Fragmentation of the point-like system or large system, current quarks or constituent quarks, three- or eight-colour system is surprisingly the same in the first approximation. Further research will soon show if the small differences between data and MC calculation observed in this experiment are effects of acceptance or contain an interesting physical message.

However, one major difference is observed in the charge flow. The presence of the d quark in the fragmentation of the forward hadronic system accompanying the Drell-Yan production is clearly seen. The balance of charge is different there from that of normal hadronic interactions and from that accompanying the J/ψ production.

The investigation of the properties of hadrons accompanying the production of lepton pairs may help in the understanding of their production mechanism. In addition, investigation of high-p_T hadrons accompanying the production of high-p_T lepton pairs (not covered in this article) will give new information about higher-order QCD effects. Finally, this research gives a perfect tool for the investigation of general properties of hadron-hadron interactions. Usually, it is very difficult to investigate them since the outgoing hadrons originate from a mixture of many different parton-parton interactions. Here, with the lepton-pair trigger we know which elementary parton-parton interaction took place in the initial state event by event.

This article is a sort of a status report on the evaluation of a pioneering experiment in this field. The evaluation continues and as usual the first results trigger new interesting questions.

A careful observer may notice some differences between the curves presented at the meeting and those presented here. This comes from the fact that great progress has been made in the meantime in the understanding of efficiency. While the data presented in Les Arcs were evaluated only with the correction for the geometrical efficiency, for the curves presented here also losses by the pattern recognition program are included (Section 2).

The Workshop at Les Arcs was organized in order to have fruitful informal contacts between experimentalists and theorists. I profited from excellent contacts with many physicists present at this Workshop. Particularly meaningful were discussions I had with B. Andersson from Lund, whose influence on this work was important.

REFERENCES AND FOOTNOTES

1) According to formulae $x_{\mu\mu} = x_1 - x_2$; $x_1 x_2 = \text{Mass}^2_{\mu\mu}/s$; (where $x_1 = x + \bar{u}$).

2) S.J. Brodsky and J.F. Gunion, Phys. Rev. Lett. 37, 402 (1976).

3) The so-called Lund Monte Carlo program was used for the jet MC calculation: T. Slöstrand and B. Söderberg, Lund preprint LU TP 78-18 (1978). It is equivalent to the Field-Feynman Monte Carlo calculation.

4) The members of the collaboration are : R. Barate, P. Bareyre, P. Bonamy, P. Borgeaud, M. David, F.X. Gentit, G. Laurens, Y. Lemoine, G. Villet and S. Zaninotti (CEN-Saclay, Gif-sur-Yvette, France); P. Astbury, A. Duane, G.J. King, R. Namjoshi, B.C. Nandi, D. Pittuck, D.M. Websdale and J. Wiejak (Imperial College, London, England); J.G. McEwen (Southampton University, England); B. Brabson, R. Crittenden, R. Heinz, J. Krider and T. Marshall (Indiana University, Bloomington, Indiana, USA); B. Pietrzyk and R. Tripp (CERN, Geneva, Switzerland).

5) K. Braune et al., to be published.
M. Faessler, New experimental results for particle production from nuclei, to be published in Annals of Physics (1981).

6) R. Göttgens, preprint CERN-EP/80-110 Rev. (1980), submitted to Phys. Lett. B.

7) J. Dowell, report at this Workshop; for Goliath results see Proc. 20th Int. Conf. on High-Energy Physics, Madison, USA, 17-23 July 1980.

CHARACTERISTICS OF HADRONS ASSOCIATED WITH $\mu^+\mu^-$ AT $\sqrt{s}$ = 62 GeV

V. Cavasinni*)
Scuola Normale Superiore, INFN Pisa, Italy
CERN, Geneva, Switzerland

ABSTRACT

Charged hadrons associated with μ pairs at $\sqrt{s}$ = 62 GeV were measured in Experiment R209 at the CERN ISR[1]). The number of produced particles was found to depend basically on two variables: the hadronic missing mass and the dimuon transverse momentum p_T. A search for jets was made using a thrust-like analysis of our data, comparing our results with a simple Monte Carlo calculation. This analysis shows that the data can be explained by the production of weakly collimated jets of low multiplicity emitted back-to-back in azimuth and positively correlated with the dimuon rapidity.

*) Present address: Istituto di Fisica dell'Università, Bologna, Italy.

1. INTRODUCTION

The virtual time-like photon giving rise to $\mu^+\mu^-$ is a good probe for investigating the intimate structure of hadronic matter. In particular, the characteristics of the hadrons produced in association with dimuons should be strongly affected by the presence of this hard process and a comparison between such events and minimum-bias (inclusive) events could give significant information about the interaction mechanism.

General crossing arguments suggest similarities between hadrons produced in μ-pair events and hadrons generated in e^+e^- annihilation via a time-like photon. In particular, a comparison can be made between the charged-particle multiplicities measured in dimuon events and the values obtained in e^+e^- at PETRA[2].

The original Drell-Yan model of quark-antiquark annihilation into lepton pairs via a time-like photon makes specific predictions on the dilepton cross-section. In this model, no correlation is expected between the dimuon and the associated hadrons because the incident quarks not participating in the annihilation fragment independently of the annihilating quarks. However, we know that the Drell-Yan model is not adequate to account for the measured, wide p_T distribution of the pair and quantum chromodynamics (QCD) corrections[3] are necessary to explain the experimental results. Quantum chromodynamics diagrams like gluon bremsstrahlung and gluon-quark scattering, which are first order in α_s, could be the source of the large p_T of the lepton pair. In pp interactions the Compton diagram is expected to dominate at large transverse momenta and a quark jet should recoil against the lepton pair. This jet would be superimposed on a large uncorrelated background which, therefore, makes its identification considerably more difficult in pp interactions than in the cleaner e^+e^- channel.

Any recoiling jet would have low multiplicity (typically 2, 3 particles) and large opening angles ($\sim 20°$), as found at SPEAR/DORIS. Such an angular cluster would be emitted opposite in azimuth to the μ pair and, if the production mechanism involves a valence quark hitting a gluon or a sea antiquark, the jet would be produced nearby in rapidity to the μ pair (positive correlation)[4]. We shall see that there are indications of such effects in our data.

2. THE EXPERIMENT

The muon detector[5] was composed of seven magnetized iron toroids providing an 18-kG field for the momentum analysis of the muons. Drift chambers, covering the angular region $80° < \theta < 165°$, were used to determine the muon trajectories in these toroids.

The intersection region was surrounded by another set of smaller drift chambers[6] (see Fig. 1). These chambers determined 3-5 points for each charged

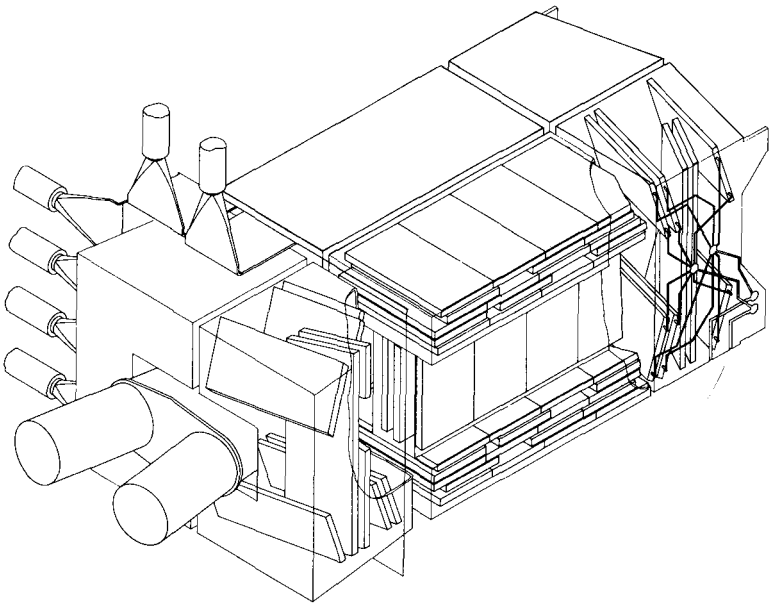

Fig. 1 Sketch of the hadron detector in the central region

particle emitted within $9^\circ < \theta < 171^\circ$ over the whole azimuth. In the arm away from the toroidal magnets, a third set of drift chambers[7] extended the coverage of the central-chamber system to polar angles of $\sim 1^\circ$.

Muon trajectories were determined using the first set of chambers and were then extrapolated backwards to provide an approximate event vertex. The information provided by the central vertex detector was then used to reconstruct an accurate event vertex using clear tracks in these chambers. The momenta of the dimuons were finally calculated making use of the vertex seen by the central chambers as well as the tracks in the outer chambers.

In the study of hadron correlations, a minimum $\int B \cdot dl$ cut was imposed on the dimuons. This cut, which was restrictive only for dimuon masses below 5 GeV, reduced the data sample to 2208 events but minimized background contamination. The surviving events were analysed by a refined reconstruction program to find all tracks, rescuing as far as possible all hits in the hadron chambers. Those tracks fitting with the muon trajectories were excluded and the remaining tracks were examined for correlations.

3. DETECTOR PERFORMANCE

The efficiency of the hadron detector at large angles was found to be $\gtrsim 90\%$; the number of tracks coming from secondary vertices was $\lesssim 10\%$. This efficiency falls to zero in the forward direction at a pseudorapidity ~ 2. The uncertainty in the absolute efficiency does not, however, influence the arguments made in this paper.

Figure 2 shows the raw multiplicity distribution of events at $\sqrt{s}$ = 62 GeV collected with an inclusive trigger (solid line). This distribution can be compared with that found by Thomé et al.[8] (broken line in Fig. 2): we find that the average multiplicity and its dispersion are both $\sim 20\%$ less than the measurement of Ref. 8. This indicates that $\sim 20\%$ of tracks produced in each event were not measured by our apparatus, mainly because of the incomplete angular coverage. (In some of the data presented, we have corrected for this loss.) Figure 2 shows also the raw multiplicity distribution for μ-pair events (dot-dash line). We note that ⟨n⟩ in dimuon events is about 3.5 units higher than it is in inclusive events.

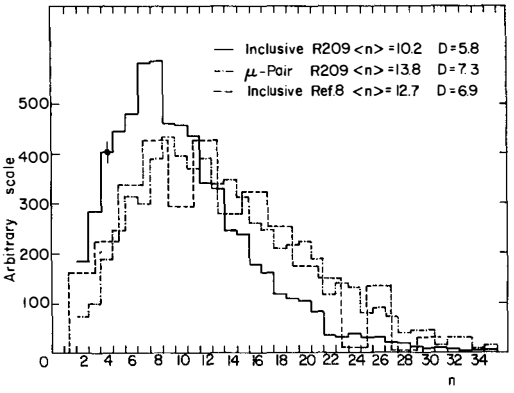

Fig. 2 Raw multiplicity distributions in inclusive events (solid line) and in dimuon events (dot-dash line). The broken line is the distribution measured by Thomé et al.[8]. All distributions are normalized to the same area.

4. HADRON TOPOLOGIES IN DIMUON EVENTS

Since an appreciable fraction of the energy available for hadronization can be removed by the dimuon, one might expect that dynamical effects should be studied as a function of the hadronic missing mass, $M_h = (s + m_{\mu\mu}^2 - 2\sqrt{s}\, E_{\mu\mu})^{\frac{1}{2}}$, where $m_{\mu\mu}$ and $E_{\mu\mu}$ are the invariant mass and the energy of the μ pair. We have made an extensive study of hadronic effects as a function of a variety of dynamical

variables at fixed M_h. Our conclusion is that no feature of the associated hadron system depends explicitly on $m_{\mu\mu}$; the appropriate parameter is M_h. (There is, however, an exception to this rule for a particular category of J/ψ events, which will be discussed later.)

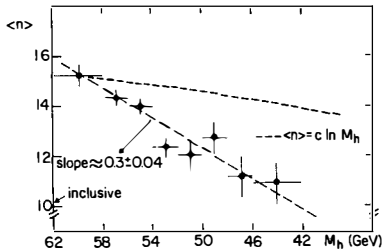

Fig. 3
Average multiplicity as a function of the hadronic missing mass, M_h. The broken line represents a logarithmic dependence.

Figure 3 shows the total ⟨n⟩ as a function of M_h. When minimal energy is taken away by the μ pair ($M_h \approx 60$ GeV), the average multiplicity is larger by about five than in inclusive events. This shows that μ-pair events are central, highly inelastic collisions. The decrease of ⟨n⟩ with decreasing M_h is much faster than the logarithmic behaviour (broken curve in Fig. 3) expected from the dependence of ⟨n⟩ on $\sqrt{s}$ in normal, inelastic pp collisions. The slope of the data (approximately 6 particles for 20 GeV of M_h) extrapolates to zero ⟨n⟩ for $M_h \approx 0$. This is evidence of a minimal leading-particle effect in dimuon events.

Figure 4 is a comparison between our data and average multiplicities measured in e^+e^- annihilation into hadrons[2]. (The data here were corrected for the ∿ 20%

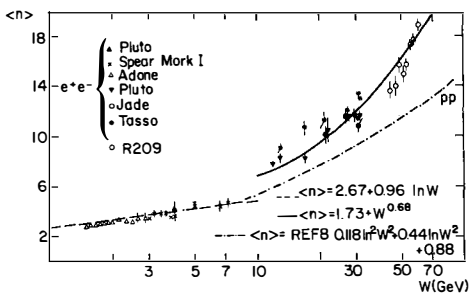

Fig. 4 Comparison of the average multiplicity measured in e^+e^- annihilations into hadrons with the multiplicity measured in this experiment in μ-pair events. Our data are plotted versus the hadronic missing mass. The dash-dot line is the fit of Thomé et al.[8] for pp inclusive multiplicities.

loss mentioned previously.) The ISR dimuon data in Fig. 4 are plotted as a function of M_h, whereas the ISR inclusive data and the e^+e^- data are plotted as a function of $\sqrt{s}$. Our measurement ($\sqrt{s} > 40$ GeV) appears to be in agreement with e^+e^- data at $10 < \sqrt{s} < 30$ GeV. It appears that high-energy e^+e^- and pp dimuon data have similar hadronic features, which contrast with what is found at low energy in e^+e^- or in pp inclusive interactions: the energy dependence of $\langle n \rangle$ in the former channels differs in both scale and shape from that found in the latter channel.

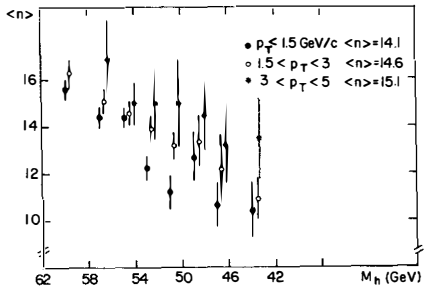

Fig. 5 Average multiplicity as a function of the hadronic missing mass for three intervals of the dimuon transverse momentum, p_T

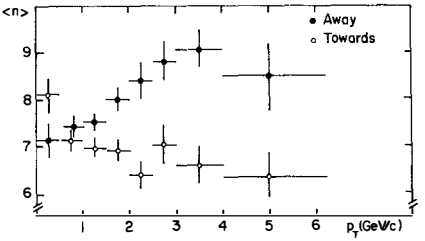

Fig. 6 Average multiplicity in the hemispheres towards and away from the transverse-momentum vector as a function of p_T

The other appropriate variable for the study of the hadronic system is the dimuon transverse momentum, p_T. Figure 5 shows the dependence of $\langle n \rangle$ on M_h for three p_T intervals: the three curves are parallel (within errors) with a difference in $\langle n \rangle$ of ~ 0.5 particles: $\langle n \rangle = 14.1$, 14.6, and 15.1 for $p_T < 1.5$, $1.5 < p_T < 3$, and $3 < p_T < 5$ GeV/c. Thus, one may summarize our results in the following way: ~ 0.3 particles are produced per GeV of M_h and an additional ~ 0.4 particles are produced per GeV/c of p_T. Dividing the solid angle into a towards and an away hemisphere with respect to the p_T vector of the dimuon, we find (Fig. 6) that the increase of multiplicity with p_T occurs in the hemisphere away from the dimuon. In Fig. 7 $\langle n_{away} \rangle$ is plotted versus p_T for three intervals of M_h. We note that these distributions depend on M_h only for scale: the multiplicity distributions factorize in their dependence on M_h and p_T.

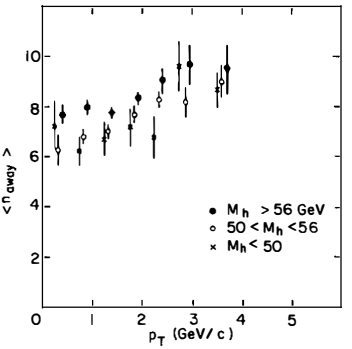

Fig. 7
Average away multiplicity as a function of p_T for three intervals of the hadronic missing mass

Figure 8 shows the azimuthal distribution of secondaries from 0° to 180° (relative to $\vec{p}_T$) for M_h > 56 GeV and M_h < 56 GeV in three p_T bins. For lower M_h, a broad bump develops opposite to $\vec{p}_T$ with increasing p_T. This bump is not seen in the large-M_h, large-p_T bin. The lack of this excess may be dynamical in origin: in selecting large-M_h, large-p_T events, one selects low dimuon masses with low

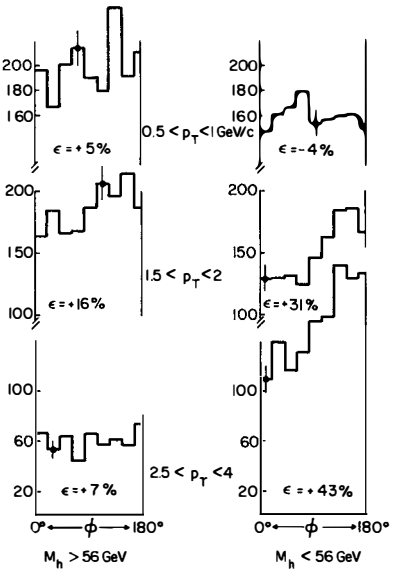

Fig. 8 Azimuthal distribution of individual tracks relative to $\vec{p}_T$ for two bins of M_h and three intervals of p_T. ε is the excess in the away hemisphere relative to that in the towards hemisphere.

longitudinal momentum (because of phase-space constraints), in practice, $m_{\mu\mu} < 4$ GeV and $y_{\mu\mu} < 1$. If this were true, the excess in the away multiplicity should be accompanied by an excess in the towards multiplicity.

Let us examine this low-mass region. Figure 9 shows the azimuthal distribution in this region for two rapidity intervals: as expected, the sample of J/ψ events with $y_{\mu\mu} < 1$ exhibits a flat distribution in p_T. We are at present studying a much larger sample of J/ψ events to understand better the role of the J/ψ in high-p_T dimuon physics.

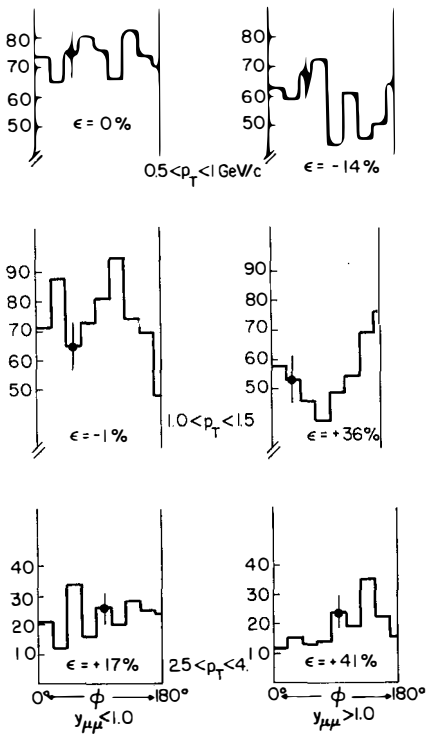

Fig. 9 Azimuthal distribution of individual tracks relative to $\vec{p}_T$ for dimuon masses below 4 GeV in two dimuon-rapidity intervals and in three p_T bins

5. JET SEARCH

The general features of associated production that we have discussed so far have shown that the dependence on the p_T of the dimuon is similar to what has been

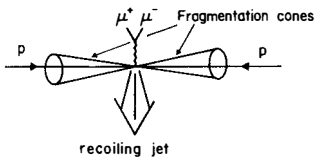

observed[9] in large-p_T π^0 production. From QCD ideas, one might imagine that in each event a subset of the hadronic system -- a small jet, say, or a cluster of hadrons -- is more strictly correlated both in p_T and in rapidity with the μ pair, as illustrated in the above sketch.

The method adopted to search for a recoiling jet is similar to the "thrust" method used in e^+e^- physics. First, all particles emitted with $\theta < 39°$ relative to each incident beam (the fragmentation cones) were disregarded. Then, for each group of 2 or 3 tracks, each track being identified by its direction cosines $\vec{C}_i$, a vector $\vec{T} = \Sigma_i \vec{C}_i$ was constructed. The vector $\vec{T}$ with the largest modulus determined the thrust axis (T axis), and the thrust, T, of the event is then the average cosine (of the 2 or 3 tracks) relative to this axis.

This procedure gives values of T that, for statistical reasons, grow smoothly with the event multiplicity, as shown in Fig. 10 for both μ-pair and inclusive events. This search for the narrowest angular cluster was performed including tracks in both hemispheres (Fig. 10a) and including tracks in the away hemisphere only (Fig. 10b), this being where the jet is expected. We observe a similar picture in the two cases and also a similarity of clustering in μ-pair events and in inclusive ones.

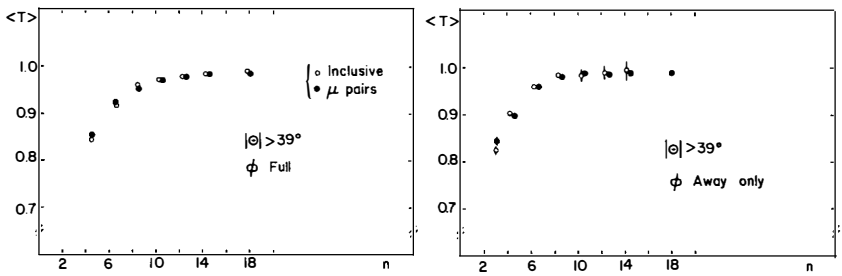

Fig. 10 Average value of the thrust determined: (a) in the full azimuth (see text) as a function of the event multiplicity in inclusive events and in dimuon events; (b) only by tracks in the away hemisphere. In the inclusive sample the away hemisphere was defined relative to the azimuthal angle of one of the reconstructed tracks randomly selected.

The possible correlation of the jet, i.e. of the T axis with the μ-pair momentum, was studied further. Figure 11 shows the azimuthal distribution of the T axis in two intervals of M_h and three intervals of p_T. At low M_h, the relative away-towards excess, ε, grows as p_T increases; however, this peaking is not stronger than that observed in the azimuthal distribution of individual tracks (Fig. 8). Even if one selects large-T, large-p_T events (bottom distributions in Fig. 11), the effect does not differ very much. Again, for large M_+, any away peaking is hardly noticeable.

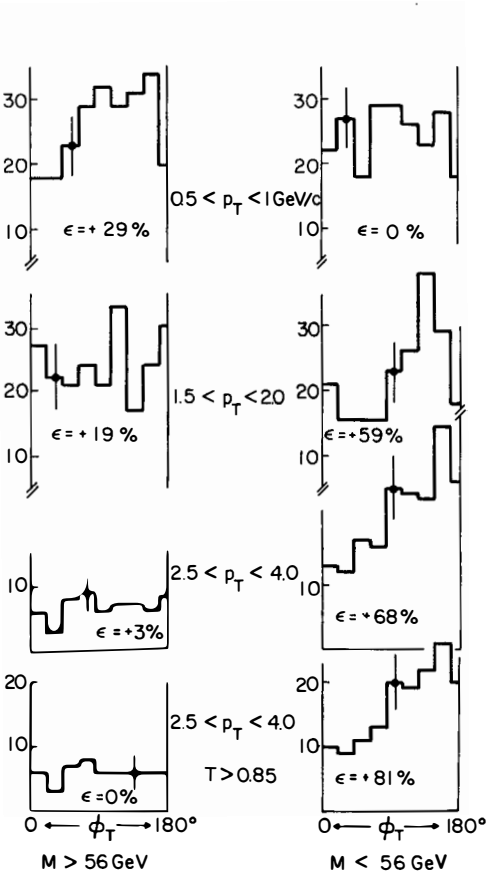

Fig. 11 Azimuthal distribution of the T axis relative to $\vec{p}_T$ in two M_h intervals for three p_T bins. In the bottom distributions a large value of T is also required.

Figure 12a shows the longitudinal correlation of the average T-axis pseudorapidity, $\langle\eta_T\rangle$, with the dimuon rapidity, $y_{\mu\mu}$, for $m_{\mu\mu} < 4$ GeV and $m_{\mu\mu} > 4$ GeV. For $m_{\mu\mu} > 4$ GeV, there is a modest ($\sim$ 15%) correlation between $\langle\eta_T\rangle$ and $y_{\mu\mu}$. This positive correlation disappears for $y_{\mu\mu} > 1$. This is because of the angular cut that we have applied at $\theta = 39°$ ($\eta \approx 1$). Correlations for $m_{\mu\mu} < 4$ GeV are smaller and hardly significant. Figure 12b is the equivalent of Fig. 12a, where tracks in the away hemisphere only contribute.

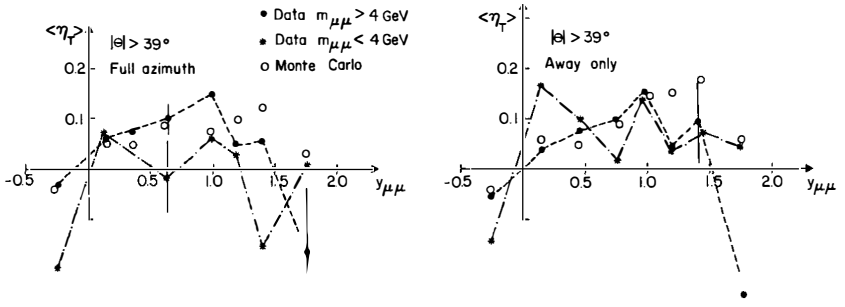

Fig. 12 a) Average value of the T-axis pseudorapidity determined in the full azimuth as a function of dimuon rapidity for two $m_{\mu\mu}$ intervals. b) Same as (a), but the thrust is determined from away-hemisphere tracks only. (The broken and dash-dotted lines are drawn to guide the eye.) The predictions of a Monte Carlo calculation are also shown (open points).

These data are compared with the predictions of a Monte Carlo calculation incorporating three sources of secondaries:

a) two fragmentation beam-jets,

b) a flat rapidity plateau at large angles, and

c) a small jet of average multiplicity 2.5 emitted at the same rapidity as the μ pair and back-to-back in azimuth (with widths of ± 1 and $\pm\pi/4$ in rapidity and azimuth).

The parameters of the calculation were adjusted to fit the measured longitudinal distribution. The results of the Monte Carlo calculation are also shown in Fig. 12 (open circles). One sees that they agree qualitatively with the data for large $m_{\mu\mu}$. From this we conclude that, as far as our thrust method is effective, the existence of a weakly collimated jet of a few hadrons local in rapidity and opposite in azimuth to the dimuon is consistent with our measurements.

6. CONCLUSIONS

Hadrons produced in association with μ pairs are much more abundant than in inclusive events, indicating a very inelastic collisions. This hypothesis is supported by the large variation of the multiplicity with the hadronic missing mass and by the agreement with the multiplicities measured in high-energy $e^+ e^-$ annihilation.

The dependence of the associated hadrons on the transverse momentum of the μ pair is similar to that measured in other large-p_T interactions. Small clusters appear to be emitted at large angles in μ-pair events as well as in inclusive ones. The correlation, both in azimuth and in rapidity, of the narrowest of the clusters with the μ pairs is stronger for large-mass pairs than for J/ψ events. The large-$m_{\mu\mu}$ data can be qualitatively reproduced in a Monte Carlo calculation when a cluster of $\langle n \rangle = 2.5$ is produced locally in rapidity and back-to-back in azimuth with respect to the μ pair and is superimposed on a "normal" event.

The apparently different mechanism observed for the associated production of the J/ψ is still being studied.

Acknowledgement

I am indebted to D. Lloyd Owen for his careful reading of the manuscript.

REFERENCES AND FOOTNOTES

1) The members of the collaboration of Experiment R209 are : K. Antreasyan, W. Atwood, U. Becker, G. Bellettini, P.L. Braccini, J.G. Branson, J.D. Burger, F. Carbonara, R. Carrara, R. Castaldi, V. Cavasinni, F. Cervelli, M. Chen, G. Chiefari, T. Del Prete, E. Drago, M. Fujisaki, M.F. Hodous, T. Lagerlund, P. Laurelli, O. Leistam, D. Luckey, M.M. Massai, T. Matsuda, L. Merola, M. Morganti, M. Napolitano, H.Newman, D. Novikoff, J.A. Paradiso, L. Perasso, R. Rinzivillo, G. Sanguinetti, I. Shulz, G. Sciacca, P. Spillantini, M. Steuer, K. Strauch, S. Sugimoto, Samuel C.C. Ting, W. Toki, M. Valdata Nappi, C. Vannini, F. Vannucci, F. Visco and S.L. Wu.

2) PLUTO Collaboration, Ch. Berger et al., Phys. Lett. 95B, 313 (1980), and references therein.

3) For a discussion of possible mechanisms leading to large p_T of lepton pairs see, for instance, E.L. Berger, Hadroproduction of massive lepton pair and QCD, SLAC-PUB-2234 (1979).

4) K. Kajantie, J. Lindfors and Risto Raitio, Nucl. Phys. B144, 422 (1978). Kisei Kinoshita and Yukiko Kinoshita, Prog. Theor. Phys. 61, 526 (1979).

5) D. Antreasyan et al., Phys. Rev. Lett. 45, 863 (1980).

6) A. Bechini et al., Nucl. Instrum. Methods 156, 181 (1978).

7) F. Carbonara et al., Nucl. Instrum. Methods 171, 479 (1980).

8) W. Thomé et al., Nucl. Phys. B129, 365 (1977).

9) R. Kephart et al., Phys. Rev. D 14, 2909 (1976).

SINGLE PHOTON PRODUCTION AT THE CERN ISR

James T. Linnemann
The Rockefeller University
New York, N.Y., U.S.A.

ABSTRACT

A measurement of single photon production from p-p collisions at ISR energies is presented.

A signal comparable to single π^0 production is found at large p_T. A study of associated particles favors production dominated by the first-order QCD process of gluon-valence quark production $q\ g \rightarrow q\ \gamma$.

Today I'll be talking about an experiment measuring single photon production in proton-proton collisions at the CERN ISR. I should first mention that most of this work was actually done by Mike Tannenbaum, Leslie Camilleri and John Yelton. The single photon measurement is a by-product in this experiment, since it was designed to study high p_T π^0 production, jets, and e^+e^- pairs.

The apparatus is shown in Fig. 1. A superconducting solenoid [1] provides the magnetic field for momentum measurement. Its coil is 1 radiation length thick. The cylindrical drift chambers [2] give a momentum resolution of $\Delta p/p = .07\ p/GeV/c$ and 80% reconstruction efficiency (per track). They cover 2π in ϕ, and $90^o \pm 40^o$ in θ.

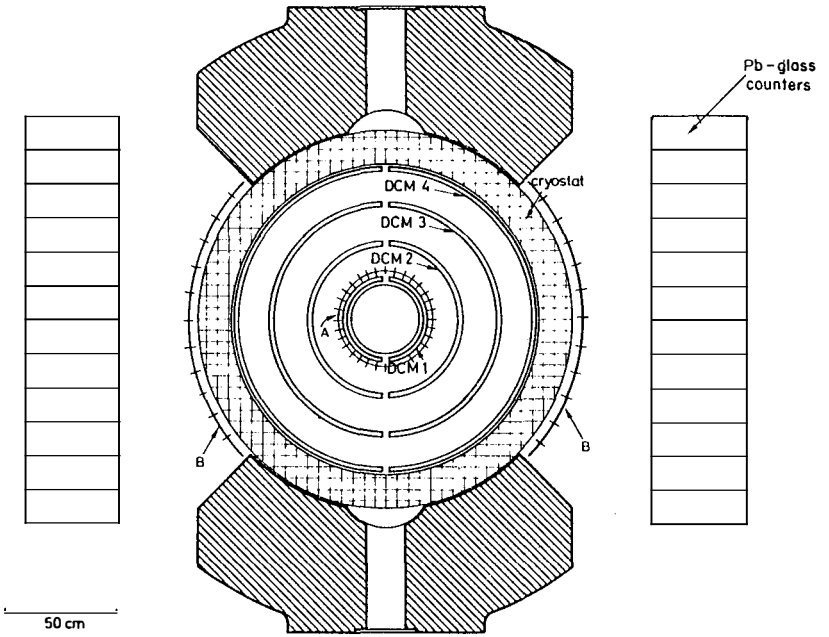

Fig. 1

"Inside Array" "Outside Array"

Center of mass motion towards the outside array

The scintillators A give the event time. The B hodoscope, located just outside the magnet coil, is used in this analysis to look for conversions of

photons in the coil. Each of the counters had a solid angle of .09 sr in the "inside" array or .14 sr for the "outside" array, the difference being due to the motion of the center of mass at the ISR.

The lead glass arrays detected electromagnetic showers. Each had 168 blocks, 15 x 15 cm x 17 radiation lengths, with solid angles for the whole array of .87 and 1.42 sr for the "inside" and "outside" arrays. The energy resolution was $\Delta E/E = .06/\sqrt{E/GeV}$, with < 5% overall systematic scale error and 5% r.m.s. block scale variation.

Given this apparatus, which cannot spatially resolve the two photons of π^0 decay at high p_T, one needs motivation to look for single photon events. QCD provides such motivation, since it claims single photons, that is, events with a high energy photon with few or no other particles nearly in phase space, are not only interesting but relatively frequent. In particular, there are first order diagrams representing fundamental hard scattering of partons, which produce single photons (Fig. 2a).

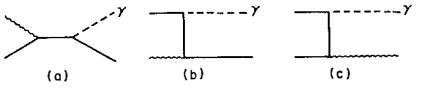

Fig. 2a

They allow the possibility of studying the gluon distribution function of the proton. However, besides these simple $q\,g \to q\,\gamma$ and $q\,\bar{q} \to g\,\gamma$ processes, there are more complex contributions from quark bremsstrahlung (Fig. 2b), $g\,q \to g\,(q\,\gamma)$ and the infamous higher twist effects (including the constituent interchange contributions). Thus we must see to what extent the data support which mechanisms.

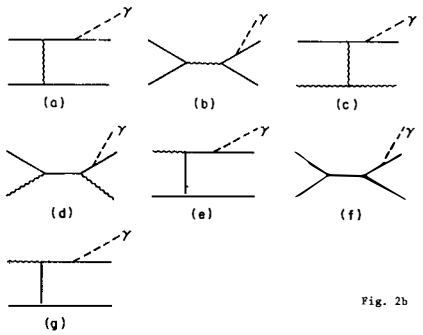

Fig. 2b

Amply motivated, we proceed to the data. The trigger was simply deposition of energy greater than a threshold in either of the lead glass arrays. This was refined off line to require that the energy form a cluster of 3 x 3 blocks (or smaller). To ensure the events were real, it was required that 4 of the A counters fired, and that two or more charged tracks were found which made a vertex in the beam intersection region.

The next step in the analysis was to locate the 2 B counters closest to a straight line between the event vertex and the glass energy cluster center.

Events with any charged or neutral particles other than the triggering particle were rejected. Thus the B counter information referred to the trigger cluster alone. The effect of this cut is shown in Fig. 3. It is seen to induce no p_T (center of mass momentum of the trigger particle transverse to the beam axis) dependence. The fraction of events passing the cut for "inside" and "outside" array triggers is due to the different solid angles. Note that charged tracks which kill the event must have ϕ track $\neq \phi$ cluster at the vertex, because of the magnetic field. Thus any bias included by this cut is not straightforward geometrically. After this cut , if there is a pulse height in the 2 B counters corresponding to the cluster of 1.5 single ionization, the particle is defined as having converted in the coil, and the cluster energy is corrected (between 3 and 4%, depending on p_T).

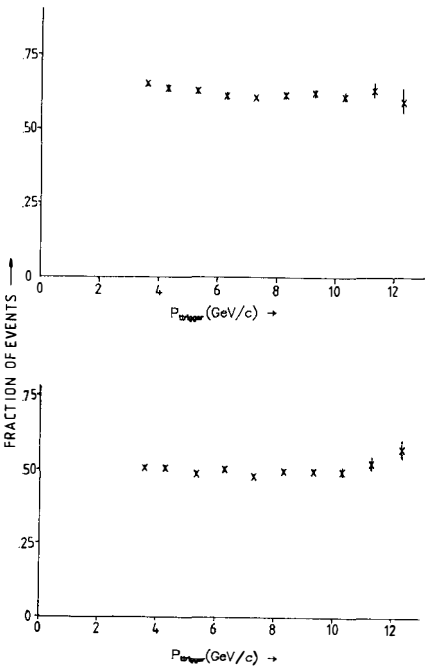

Fig. 3

B counter cut efficiency for the inside (upper plot) and outside arrays.

This is the working event sample. To deduce the fraction of single photon events, we must use a statistical technique, since our spatial resolution is too poor to see π^0's as two distinct photons. There is a compensating advantage to the statistical technique, however : we are limited in p_T only by event rate, not by π^0 merging, and thus have measured γ/π^0 to higher p_T than anyone.

In the magnet coil, the probability of a photon not converting is

$$\nu_1 (E) = \exp (- 7/9 (1 - \xi (E)) t)$$

where t is measured in radiation lengths and contains the weak energy dependence (ν_1 (3 GeV) = .468; γ_1 (13 GeV) = .459). We measure ν_{obs} = the fraction of clusters in the lead glass which have less than 1.5 single ionizing pulse height in the B counter (that is, the non-conversion fraction).

This fraction is much less for π^0 (2 photons) than for single photons so we can use ν_{obs} to deduce the single γ fraction. The effect of neutral decays of the measu red[3] production of, K_s^0, ω^0, η, η' combines with π^0 to give $\nu_E(E)$, an effective non-conversion fraction in the absence of single photons. This, according to a Monte Carlo calculation incorporating production and branching ratios, and using our cluster size cuts, varies with energy from ν_E (3 GeV) = = .237 to ν_E (13 GeV) = .195. The single fraction is then derived using

$$f_\gamma = \frac{\gamma}{all} = \frac{\nu_{obs} - \nu_E}{\nu_1 - \nu_E}$$

The measured ν_{obs} for the inside and outside arrays at two beam energies are shown in Fig. 4. The lower curve is the calculated ν_E, while the upper curve is ν_1. Unfortunately, the data are seen to sometimes lie below ν_{obs}, indicating a negative single γ contribution. The problem is that only neutral meson decays are taken into account by the Monte Carlo. The effect of unreconstructed particles on the observed B counter pulse height, with different solid angles for the inside and outside B counters, is ignored.

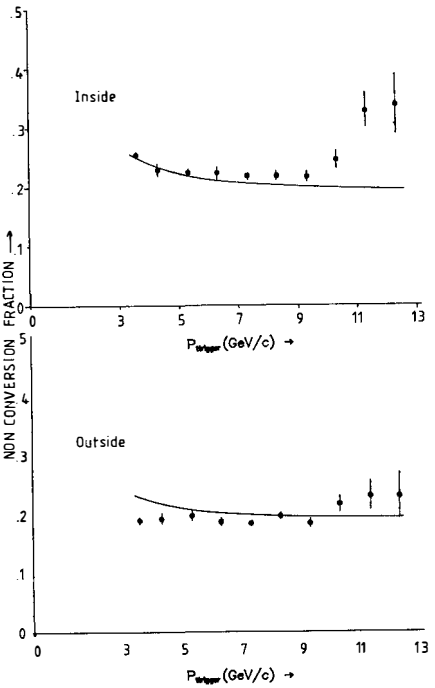

Fig. 4

Rather than attempting a detailed (and model-dependent) Monte Carlo of the associated particles, we have chosen to renormalize ν_E, and ν_1 seperately on the inside and outside for the bin (3.5 - 5 GeV/c) so as to agree with the earlier ISR data on γ/π^0 of Amaldi et al [4]. In this region f_γ is only $\sim$ 2%. We include only a p_T-independent shift (recall the B counter cut was independent of p_T). This renormalisation has the advantages that 1) the two arrays now give consistent f_γ at all p_T 2) we are rendered less sensitive to details of cuts (e.g. 1.5 single ionization in the conversion definition) 3) exact knowledge of the coil thickness is

no longer needed and 4) the average value (though not the dependence) of the coil energy loss correction drops out.

The final results for f_γ are shown in Fig. 5. We estimate that the physics bias introduced by the B counter cut means that f_γ inclusive = (f_γ plotted) x (.8 to 1.0). Combining in quadrature our estimated systematic error from the normalization to the Amaldi data and the energy dependence of ν_E and the coil energy loss correction, we get an estimated systematic error of .05 in f_γ.

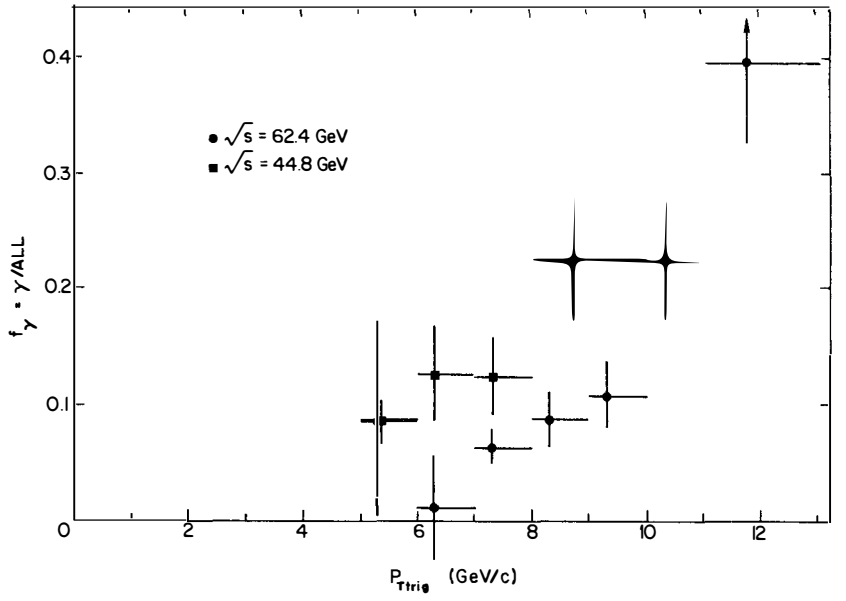

Fig. 5

In addition, there may be a 3% normalization error between the $\sqrt{s}$ = 62.4 and $\sqrt{s}$ = 44.8 data. The single photon invariant cross section obtained at $\sqrt{s}$ = 62.4 is shown in Fig. 6, together with curves showing the effect of the ± .05 systematic error in f_γ.

Signal in hand we now turn to the question of prediction mechanism. To increase statistics for this study, we combine the samples of $\sqrt{s}$ = 44.8 and 62.4 GeV. Note that the first order QCD, mechanisms $g\,q \to g$ and $q\,\bar{q} \to \gamma\,g$ both give a photon unaccompanied by other particles in the same hemisphere, while quark brehmsstrahlung, $q\,g \to g + q\,\gamma$ gives a γ accompanied by a q jet, much like a π^0-led fragmentation of a quark jet. About half of all events which pass the

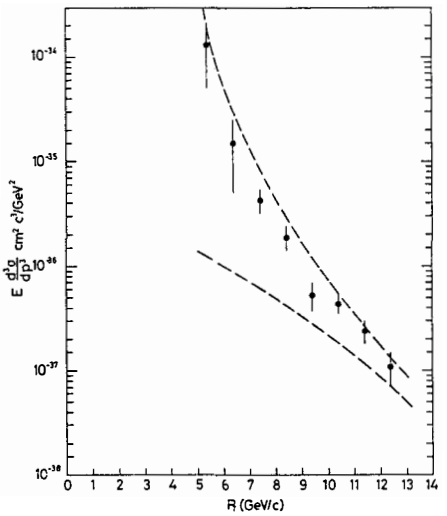

Fig. 6

clean B counter cut have the trigger particle accompanied by at least one particle on the trigger side ($|\eta| < .7$, $|\phi$ trigger $- \phi$ track $| < 90^{o}$, η = pseudo rapidity). Calculating f_γ separately for the accompanied and unaccompanied events (Fig. 7) we find most γ's are unaccompanied, consistent with first order QCD diagrams dominating over quark bremsstrahlung.

If one assumes $q\, g \to \gamma\, q$ and $q\, \bar{q} \to \gamma\, g$ dominate, one might ask which is more important. To distinguish between them, we look at charged particles recoiling from the trigger side. The leading particles should remember the parton charge, if any. To define leading particles, we measure $x_E = - p_{T\text{track}}\ p_{T\text{trig}} / p^2_{T\text{trig}}$. We will plot the charge ratio $R_\pm (x_E) = N_+ (x_E) / N_- (x_E)$. We expect the uncharged gluon jet of the annihilation graph to give $R_\pm (1) \to 1$, while the quark jet would have $R_\pm (1) \to 8$ (because of the charge-squared quark-photon coupling and the relative valence abundances of u and d quarks).

In Fig. 8, the charge ratio $R_\pm$ is shown for two sub-samples of the data : the accompanied converting ($f_\gamma \sim .04$ for $p_T > 7$ GeV/c, i.e. γ suppressed), and unaccompanied nonconverting ($f_\gamma \sim .40$ GeV/c for $p_T > 7$ GeV/c , i.e. γ enhanced). $R_\pm$ (γ enhanced) > $R_\pm$ (γ suppressed) at large x_E and large p_T, as would be expected if the gluon jet process (valence-sea annihilation) is suppressed with respect to the valence-gluon process leading to quark jets recoiling from the single γ.

If one pushes our data to the limit and does a global fit [5] for $R_\pm$ γ, $R_\pm$ meson to all four sub-samples (converting + non-converting) x (accomanied + unaccompanied), one obtains Fig. 9. The fit is based on the expression

$$R_{\pm \text{observed}} = \frac{\alpha R_\gamma (1 + R_m) + R_m (1 + R_\gamma)(1 - \alpha)}{\alpha (1 + R_m) + (1 + R_\gamma)(1 - \alpha)}$$

where $\alpha = f_\gamma$ for the bin, and $R_{\gamma,m}$ are $R_\pm$ γ and $R_\pm$ meson. The error bars here are those derived from the statistics of the fit only ($\pm$ 1.0 σ gives $\Delta \chi^2 = 1.0$). The trend of $R_\gamma > R_{meson}$ is made explicit, but the exact values of R_γ extracted are subject to systematic errors, for example the inequality of the number of tracks recoiling from accompanied and unaccompanied trigger particles.

Thus we conclude that we have seen single photons with a cross section of greater than 10% of that for π^0 production at p_T beyond 9 GeV/c, that most of these are unaccompanied on the trigger side and that there is a larger ratio of positive to negative particles recoiling from single photons than from neutral mesons at high x_E. In a QCD picture these results favor dominance of 1st order processes over quark bremsstrahlung, and dominance of valence quark-gluon over valence quark-sea quark production.

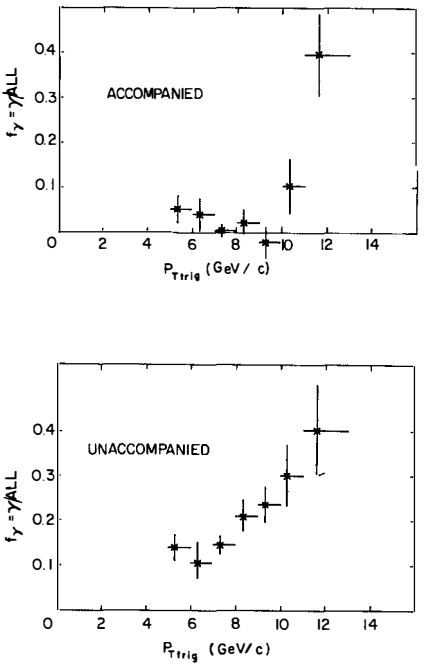

Fig. 7

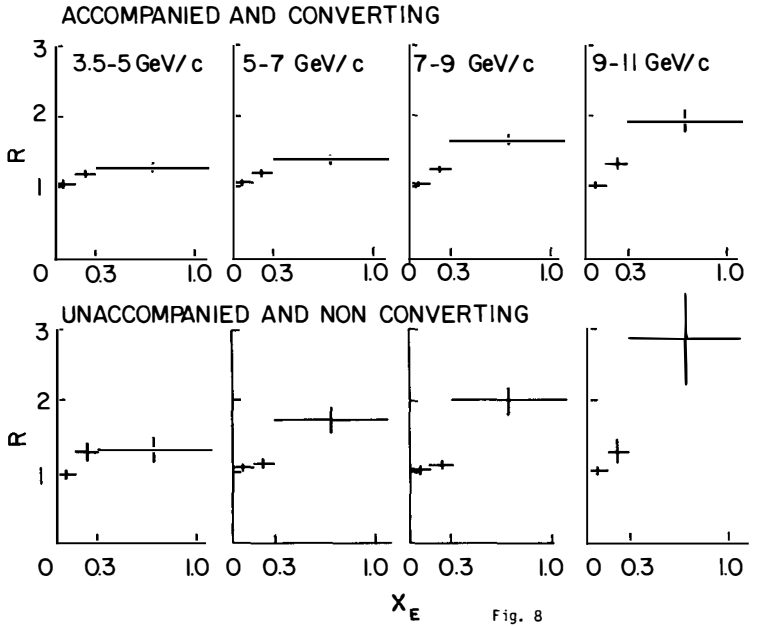

Fig. 8

$R_{\pm}$ for various bins of p_{Ttrig} and x_E

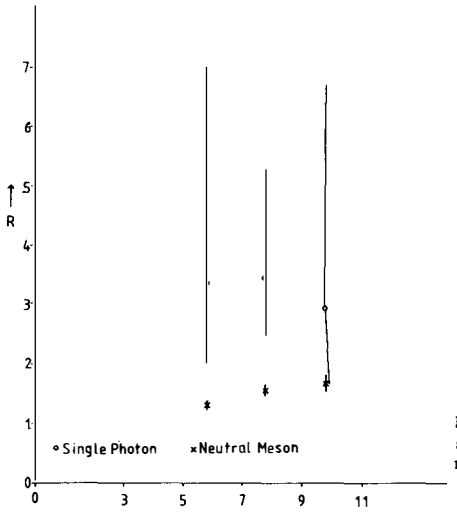

$R_{\pm}$ extracted from all data for single photons and neutral mesons

Fig. 9

REFERENCES

1) M. Morpurgo, Cryogenics 17, (1977) 89.

2) L. Camilleri et al., Nucl. Instrum. Methods 156, (1978) 275.

3) F.W. Büsser et al., Phys. Letters 55B, (1975) 232;
F.W. Büsser et al., Phys. Letters 61B, (1976) 309;
B. Alper et al., Nucl.Phys. B87, (1975) 19;
D. Antreasyan et al., Phys. Rev. Lett. 38, (1977) 112;
M. Diakonou et al., Phys. Letters 89B, (1980) 432;
A.L.S. Angelis et al., Phys. Letters 94B, (1980) 106.

4) E. Amaldi et al., Phys. Letters 77B, (1978) 240;
Nucl. Phys. B150, (1979) 326;
Phys. Letters 84B, (1979) 360.

5) J.M. Yelton, Ph. D. Thesis, Oxford University 1981, unpublished;
A.L.S. Angelis et al., Phys. Letters 98B, (1981) 115.

A MEASUREMENT OF THE SINGLE-PHOTON PRODUCTION AT THE CERN ISR

C. Kourkoumelis
Physics Laboratory, University of Athens, Greece

ABSTRACT

The production of single photons at large transverse momenta was measured at the CERN ISR for c.m. energies $31 \leq \sqrt{s} \leq 63$ GeV using lead/liquid-argon calorimeters. The ratio of single-photon to π^0 production is significantly larger than zero, starting at $p_T \simeq 4$ GeV/c and increasing to a value of 0.4 at 9 GeV/c, the largest p_T measured. Finally, using our experimental results on both the real and virtual photons we attempt to connect the single-photon production with the dielectrons of high p_T.

The observation of large p_T single photons is very topical since the present theories predict that the single photons are produced directly in hard-scattering processes between quarks and gluons. More precisely they predict that in proton-proton interactions the single photons are produced mainly via the "Compton" scattering of a quark and a gluon, $gq \rightarrow \gamma q$. Furthermore, since the photons couple point-like to the quarks, they can be used to probe the constituent structure of hadrons.

The apparatus used for the single-photon production measurements consisted mainly of lead/liquid-argon calorimeters subdivided both longitudinally and laterally for effective hadron rejection. The calorimeters were used in a retracted geometrical configuration, allowing thus the separation of the two photons from the π^0 decay up to the maximum p_T of 10 GeV/c. This permitted us to separate π^0 from single-photon events on an event-by-event basis, i.e. a single photon was defined as a single electromagnetic (e.m.) shower in a calorimeter, while a π^0 was taken as two e.m. showers reconstructing the π^0 mass. Additional requirements to allow the identification of single photons were imposed on the shower radius, namely a single photon was required to have a radius of less than 13.5 mm. Finally a requirement on the "cleanness" of the event was imposed: the event should have no additional shower in the calorimeter and all the energy in the calorimeter has to be assigned to the triggering particle. More details about the apparatus, triggers, and analysis methods can be found elsewhere[2].

Figure 1 shows the apparent γ/π^0 ratio as a function of p_T together with the background contribution calculated from the known meson decays as π^0's and η's. The main fraction of this background is due to decays where one photon falls in the calorimeter and the other outside. Besides the known meson decays a number of effects which could contribute to the apparent γ/π^0 ratio, such as cosmic rays, beam-gas interactions, hadrons simulating e.m. showers, and the non-linear response of the calorimeter were studied and included in the background calculation.

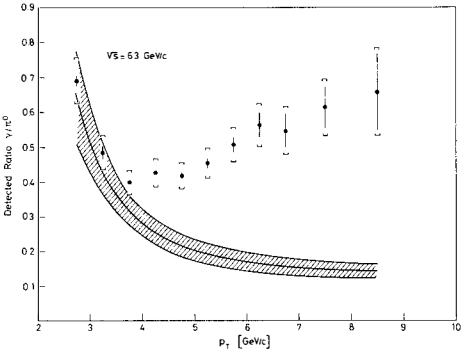

Fig. 1
Observed ratio of γ/π^0 at $\sqrt{s}$ = 63 GeV. Inner error bars are statistical errors and outer error bars include possible systematic effects due to calorimeter non-linearity.

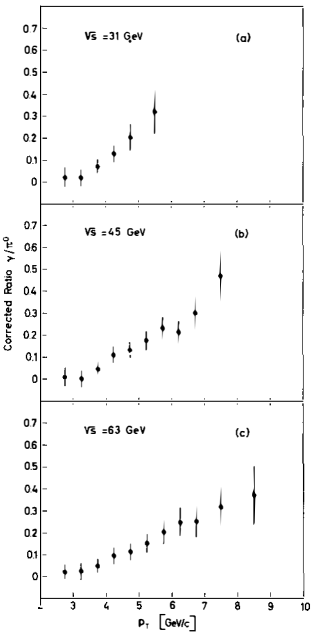

Fig. 2 Corrected γ/π^0 ratio after background subtraction at a) $\sqrt{s}$ = 31 GeV, b) $\sqrt{s}$ = 45 GeV, and c) $\sqrt{s}$ = 63 GeV.

Figure 2 shows the corrected γ/π^0 ratio after the subtraction of the above backgrounds. An excess of single photons is seen in all three values of the c.m. energies used in data taking. The γ/π^0 ratio rises with the p_T, from a value of 5% at 3.5 GeV/c to a value of about 35% at 9 GeV/c of p_T and exhibits no significant $\sqrt{s}$ dependence. The "cleanness" requirement discussed above introduces a physics bias on the γ/π^0 ratio and its effect is estimated to be 0.85 ± 0.15 on the fully inclusive γ/π^0.

We proceed further, seeking for a connection between our single-photon results and our high-p_T dielectron results reported in a preceding talk. QCD theories[3] predict that both the real photons and the virtual photons -- which decay into lepton pairs -- are produced via the same basic mechanisms, i.e. the "Compton" scattering and the quark-antiquark annihilation. Since our experiment has measured both the real and the virtual photon production by two independent methods, we should be able to compare them with each other and decide about the predicted similarity of the two production mechanisms.

We carried out the following analysis: we used the measured γ/π^0 ratio to calculate the expected high p_T e^+e^- yield and then compared it with the measured one.

The theoretical cross-section for real photon production via the Compton scattering gq is given by the formula:

$$\frac{d^2\sigma^{theor}}{dydp_T^2} = \int_0^1\int_0^1 dx_1\, dx_2 \sum_i f_i^A(x_1) g_i^B(x_2) \hat{s}\delta(\hat{s}+\hat{t}+\hat{u}) \frac{d\sigma}{d\hat{t}}(\hat{s},\hat{t},\hat{u}) + A \leftrightarrow B \ , \quad (1)$$

where $d\sigma/d\hat{t}$ is the subprocess cross-section and f_i and g_i are the quark and gluon structure functions, respectively. The theoretical calculations based on the above formula depend, of course, on the choice of f(x), g(x), and k_T, but in general fail to reproduce the absolute value of the measured single-photon cross-section as shown in Fig. 3. Figure 3 shows that the theoretical calculations are

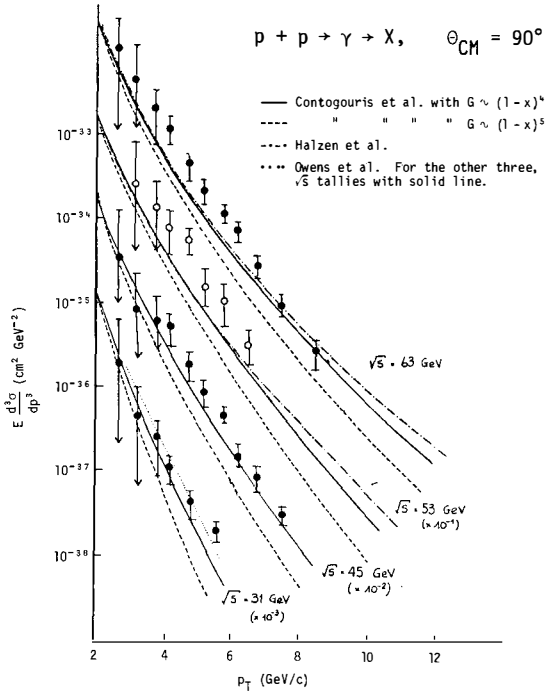

Fig. 3 The measured single-photon invariant cross-section compared with a few recent theoretical calculations

a factor of about 2.4 below the data but, with the appropriate choice of f(x) and g(x), reproduce well the shape of the experimental data. We attribute the extra normalization factor of 2.0 (2.4 × 0.85) to other mechanisms which are not yet included in the theoretical calculations. We then take the f(x) and g(x) which fit the shape of our single-photon spectrum[4] and use them to calculate the expected yield of high p_T dielectrons via the Compton scattering, which is the main production mechanism at high p_T's:

$$\frac{d^3\sigma^{theor}}{dm^2 dy dp_T^2} = \int_0^1 \int_0^1 dx_1\, dx_2 \sum_i f_i^A(x_1) g_i^B(x_2) \hat{s}\delta(x_1 p_A + x_2 p_B - p^2) \frac{d^2\sigma}{dm^2 d\hat{t}}(\hat{s},\hat{t},\hat{u}) + A \leftrightarrow B \,. \tag{2}$$

The above-mentioned additional mechanisms which produce extra single photons should also produce virtual photons of high p_T, and assuming that the production mechanisms are not strongly dependent on the mass of the pairs, then a similar extra factor of two should be present here as well; namely the following should hold:

$$\frac{d^3\sigma^{pred}}{dm^2 dy dp_T^2} \simeq 2.0 \frac{d^3\sigma^{theor}}{dm^2 dy dp_T^2} \,. \tag{3}$$

The above predicted cross-section for the production of high p_T dielectrons via the Compton scattering -- obtained after the integrations of formula (2) combined with the extra factor of formula (3) -- is then compared with the experimentally measured one.

The experimentally measured cross-section[5] has the form:

$$\left.\frac{d^3\sigma^{exp}}{dm^2 dy dp_T^2}\right|_{y=0} = A(m)\, e^{-b(m)p_T} \quad \text{with} \quad A(m) = \left.\frac{b^2}{4m}\frac{d^2\sigma^{exp}}{dm dy}\right|_{y=0}$$

Comparing the predicted cross-section with the measured one we find for the ratio R:

$$R = \left.\frac{d^3\sigma^{exp}}{dm^2 dy dp_T^2}\right|_{y=0} \Big/ \left.\frac{d^3\sigma^{pred}}{dm^2 dy dp_T^2}\right|_{y=0} \simeq 2.0 \quad \text{for} \quad 2 < p_T < 4 \text{ GeV/c} \,.$$

The above factor of 2.0 probably means that there are still more sources of dielectron production to be considered, but in general the above analysis and result show the following:

a) the two different and independent measurements (real and virtual photons) are consistent with each other within a factor of two,

b) the production mechanisms of real and virtual photons are similar and in support of the QCD predictions,

c) most of the high p_T lepton pairs are produced via the Compton scattering $gq \to \gamma q$, which gives a recoiling quark.

REFERENCES AND FOOTNOTES

1) Work done by the Athens[2]-Brookhaven-CERN Collaboration (M. Diakonou, C. Kourkoumelis, L.K. Resvanis, T.A. Filippas, E. Fokitis, C. Trakkas, A.M. Cnops, E.C. Fowler, D.M. Hood, R.B. Palmer, D.C. Rahm, P. Rehak, I. Stumer, C.W. Fabjan, T. Fields, D. Lissauer, I. Mannelli, W. Molzon, P. Mouzourakis and W.J. Willis).

2) M. Diakonou et al., Phys. Lett. 87B, 292 (1979) and 91B, 296 (1980).

3) See, for example: J. Lefrançois, Rapporteur's talk at the 20th Int. Conf. on High-Energy Physics, Madison, Wisconsin, July 1980.

4) R. Hagelberg et al., Direct photon production in hadron-hadron collisions at the SPS, CERN/SPSC/80-106, SPSC/P 153 (1980).

5) C. Kourkoumelis et al., Phys. Lett. 91B, 475 (1980).

WHAT CAN WE LEARN ABOUT PARTONS FROM LEPTON PAIR EXPERIMENTS?

Louis Lyons
Nuclear Physics Laboratory, Oxford, UK.

ABSTRACT

The information on quark, antiquark and gluon structure functions derived from continuum and from resonance lepton pair production is reviewed, and compared with similar information from other sources.

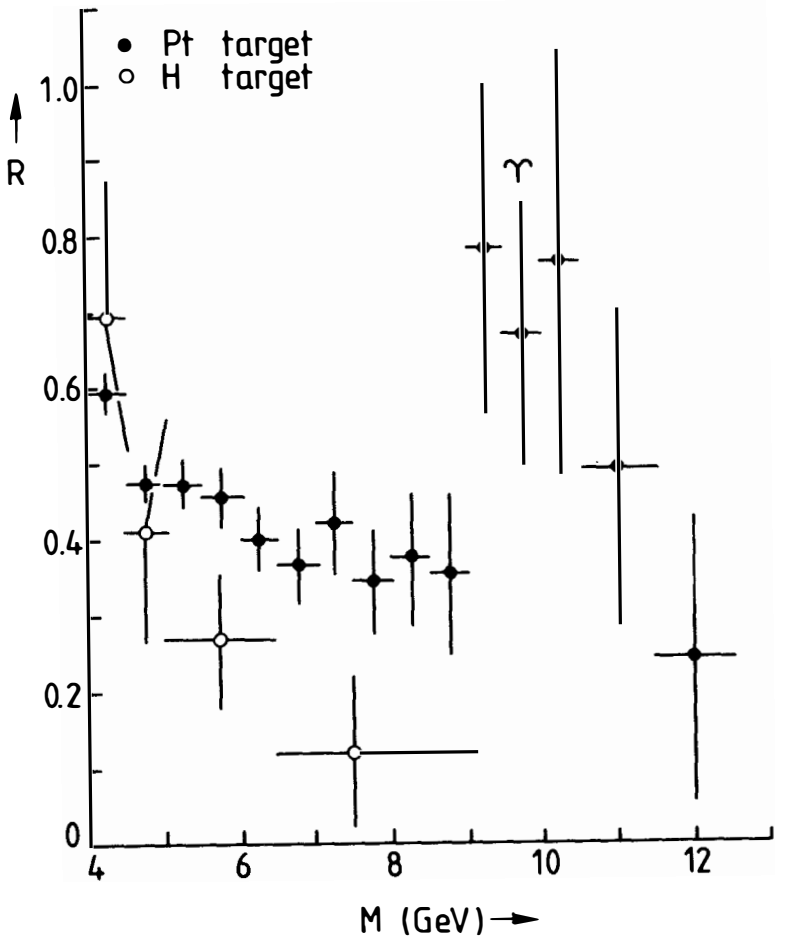

Fig.1 Ratio R of lepton pair production for π^+/π^- beams on a platinum target (solid circles) and on a hydrogen target (open circles), for a beam momentum of 200 GeV/c. If $u(x) = 2\bar{d}(x)$, R for hydrogen tends to 1/8 at large τ. The resonances are not produced by the Drell-Yan mechanism; R for the T is larger than for the continuum, and for the Ψ is $1.003 \pm .004$ (for a platinum target).

1. Introduction

In this talk, I will review the information that we can obtain from experiments involving the hadronic production of lepton pairs (both resonance and continuum) concerning the partons within the initial state hadrons.

This will not include a discussion of the evidence that quarks are coloured. For several years the experimental Drell-Yan cross-section exceeded the calculated value for coloured quarks[1]. Then for a short period, they agreed and lepton pair production was included in the list of reasons for believing quarks are coloured[2]. Now we are back in the situation where the experimental values are a factor of ~2-3 larger than the naive Drell-Yan prediction[3]. We currently believe (or at least want to believe) that this is due to the effect of higher order QCD correction effects[4], rather than explaining the discrepancy in terms of colourless quarks. But in view of the uncertainties concerning the calculations of higher order QCD effects, it would at present be foolhardy to invoke lepton pair cross-sections as giving any evidence in favour of colour.

Another topic worthy of further investigation but not dealt with here is whether lepton pair data provide evidence that quarks and gluons interact as expected in terms of QCD. Again it would be desirable to have more specific theoretical predictions before attempting a comparison.

Thus I shall confine my attention to parton structure functions in hadrons. The hadrons investigated include protons, pions and kaons. I consider separately the structure functions for valence quarks, for sea quarks and for gluons. Where possible the lepton pair information is compared with that available from other sources.

2. Valence quark distributions

In order to provide an easily assimilatable picture of the structure functions, they are presented in Table 1 in terms of parametrisations as

$$\text{Structure function} \sim x^{\alpha} (1-x)^{\beta}$$

A more detailed point-by-point comparison can be made if required from the original references. The normalisation constant is not given, as this in general has been determined (from α and β) to give the correct number of valence quarks in the hadron.

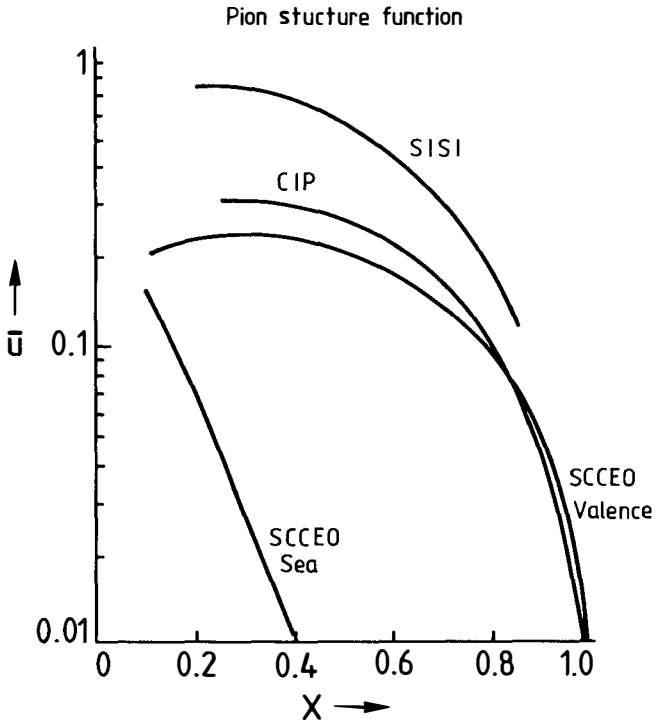

Fig.2 The pion structure function, as determined from dilepton production data. The SCCEO Collaboration's valence structure function has been normalised to one $\bar{u}$ quark in the π^-; they also allow for a contribution from the π^- sea, and obtain its structure function. The CIP and SISI structure functions are normalised by comparing the Drell-Yan calculation with the experimental cross-section and ignoring the sea. The CIP values should be renormalised upwards by a factor of about 2, to allow for their assumed dependence on A. The BCE structure functions for valence and sea (not shown) agree well with those of the SCCEO collaboration. The SISI and corrected CIP structure functions would be embarrasingly large - too much momentum carried by the quarks, and too many valence quarks. This effect can be explained by the enhancement of the cross section produced by QCD corrections to the naive Drell-Yan prediction. If this correction factor is approximately independent of the kinematic variables, then the shape of the structure function may be reliable.

2.1 Nucleons

The proton valence structure function is determined from the difference in $\bar{p}N$ and pN lepton pair production[5]; the numbers of events used are 275 and 35 for the two reactions. The statistical accuracy is far inferior to that of the neutrino experiments[6].

We may hope in the future to obtain information on $u(x)/d(x)$ in the proton. The ratio R of lepton pair production in π^+p and π^-p experiments is expected to tend to 1/8 for large τ ($=M^2/s$), provided that $u(x)=2d(x)$. There is evidence[16] and prejudice[17] that the distribution of d quarks falls off faster than that of u quarks, in which case the R limit is below 1/8. The current data (see fig.1) are suggestive, but higher statistics in a region away from the T would be useful.

2.2 Pions

The situation for mesons differs from that concerning hadrons, since lepton pair data currently provide the best information on meson structure functions. Four experiments [7-10] have analysed their $\pi p \to \mu^+\mu^-$ data to extract pion structure functions. These are listed in Table 1, and are shown in Fig.2; a more detailed discussion and comparison can be found in ref.(18).

The exponents β are in the range 1-1.5. These compare (favourably?) with predictions[19] based on counting rules of 0, 1 or 2. In view of this spectrum of predicted values, the question of at what value of Q^2 they should be compared with the data becomes irrelevant.

Pion structure functions have also been determined [12,13] by analysing forward particle production (in reactions in which at least one of the incident and outgoing particle is a pion) at small transverse momentum in terms of the recombination model[20]. Another method involves comparing the production of large transverse momentum jets in πN and in pN reactions[11]; their ratio is related to the structure function ratio of pions and of protons, with the latter taken from neutrino experiments. These alternative methods yield structure functions or parametrisations consistent with those from the lepton pair experiment, but they involve more assumptions concerning the reaction dynamics.

2.3 K^-

The ratio $\bar{u}(K^-)/\bar{u}(\pi^-)$ has been obtained[14] by comparing lepton pair production by negative pions and kaons in the same apparatus and in the same beam. The ratio, shown in fig.3, is consistent with unity at small x, but falls at $x \gtrsim 0.6$. This is in agreement with expectations[21], based on the larger mass of the remaining s quark in the kaon, compared with the d quark in the pion.

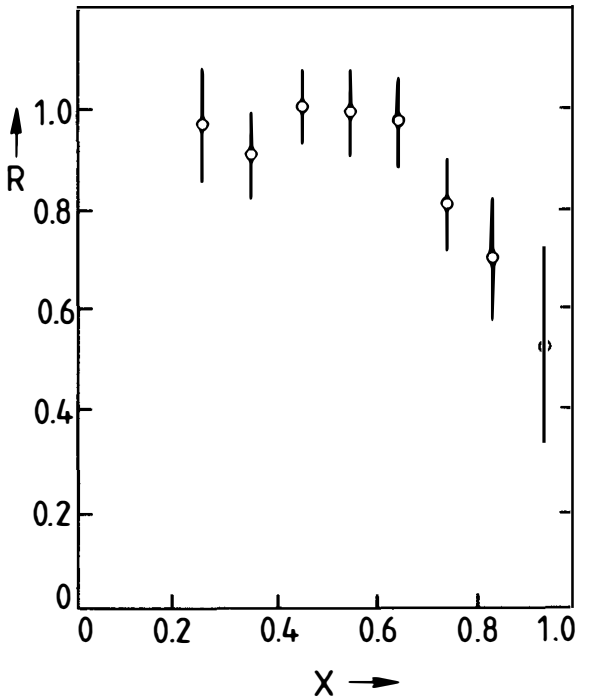

Fig.3 The ratio $R=\bar{u}_{K^-}(x)/\bar{u}_{\pi^-}(x)$ of the $\bar{u}$ quark distribution in a K^- as compared with that in a π^-. The fact that R falls below unity for x>0.7 can be understood in terms of the kaon's s quark being heavier than the pion's d quark.

3. Sea Quark Distributions

In pN experiments, the nucleon sea can be extracted by fitting the observed $\mu^+\mu^-$ mass spectrum, using valence quark distributions as determined from deep inelastic experiments[22]; or by subtracting nucleon total[23] and valence structure functions as determined by a comparison of pN and $\bar{p}$N data. The exponent s (see Table 2) is much larger than β for the nucleon's valence distributions, and is in tolerable agreement with that determined by the CDHS group[16] from νN data.

A comparison of the sea structure functions as obtained from the lepton pair and deep inelastic scattering experiments is shown in fig.4. It is apparent that the lepton pair data tends to be at larger values of x than most of those from the neutrino experiments, but appear to be somewhat larger, perhaps by a factor of 1.5-2. This is the well-known enhancement of the cross-section above the simple Drell-Yan prediction.

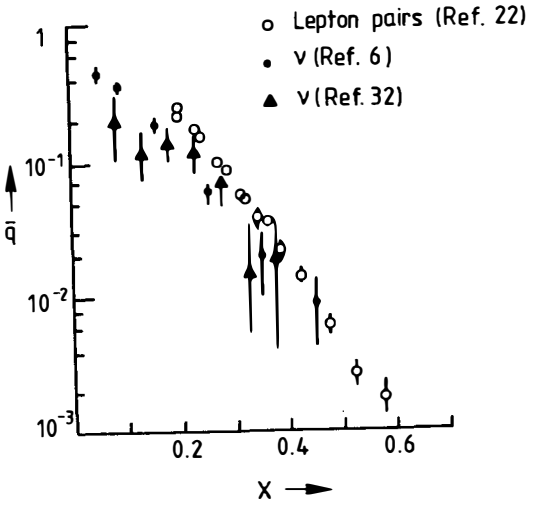

Fig.4 The nucleon sea as determined from lepton pair production data[22] (open circles) and from neutrino experiments[6,32] (solid circles and triangles respectively). The quantity $\bar{q}$ plotted as a function of x is $\bar{u}+\bar{d}+2\bar{s}$; this combination arises naturally in the neutrino experiments, and is deduced in the lepton pair experiment from the parametrisations $\bar{u}=\bar{d}(1-x)^{3.5}$ and $\bar{s}=(\bar{u}+\bar{d})/4$. The larger value of the sea at x~0.2 for the lepton pair data as compared with the neutrino experiments is the same phenomenon as the enhancement of the observed lepton-pair cross-section above the Drell-Yan prediction.

The CFS collaboration[22] have also investigated whether the $\bar{u}$ and $\bar{d}$ distributions are the same. They find that they obtain a better fit to their $\mu^+\mu^-$ mass spectrum with $\bar{u}(x)/\bar{d}(x) = (1-x)^{s'}$, with $s' = 3.5 \pm 1.5$. An independent confirmation is provided by the rapidity distributions of their lepton pairs (See fig.5). Since the collisions involve a beam proton and a target nucleon, the angular distribution is not required to be symmetric about 90° in the centre of mass system, and indeed we expect an enhancement in the forward hemisphere. The observed magnitude of this effect is consistent with a value of $s' \sim 2.5$. Because the proton contains two valence u quarks and one valence d, the $u\bar{u}$ sea pairs could be suppressed at larger x with respect to $d\bar{d}$ pairs because of the influence of the Pauli principle[24]; a QCD calculation[25] also predicts $\bar{d} > \bar{u}$.

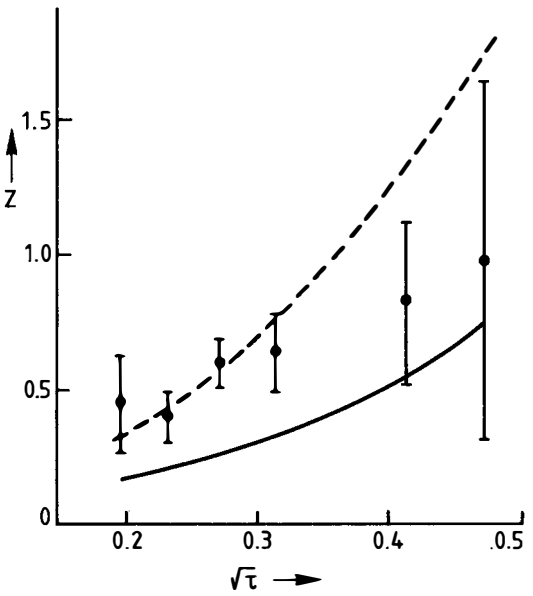

Fig.5 The CFS data[22] on 400 GeV/c pN collisions, showing that the dilepton pair is produced preferentially forwards. The quantity Z is $\frac{d}{dy}\left[\ln\left(\frac{d^2\sigma}{dy d\sqrt{\tau}}\right)\right]_{y=0}$ i.e. it is the fractional rate of change (with respect to rapidity) of the cross-section, evaluated at 90° in the centre of mass system. Symmetry of the cross-section about 90° would imply Z=0, while positive Z corresponds to an enhancement in the forward hemisphere. The two curves are predictions for Z as a function of $\sqrt{\tau}$, obtained from a Drell-Yan calculation, using structure functions for q obtained from deep inelastic scattering experiments and for $\bar{q}$ obtained by the CFS group from their dilepton mass spectrum. The solid curve corresponds to $\bar{u}=\bar{d}$, while the dashed curve is for $\bar{u}/\bar{d}=(1-x)3.5$.

The pion sea can be determined from a comparison of π^-N and π^+N lepton pair experiments. The exponent of the sea has been measured as 6.9 ± 2.9 by the SCCEO collaboration[7] and ~5 by the BCE group[10]. The sea has also been determined[12] from forward meson production experiments via the recombination model, with the result $s = 3.5\pm0.2$. The magnitude of this sea contribution, however, is such that the entire momentum of the pion is carried by the valence and sea quarks, leaving none to be ascribed to gluons (in contrast to the ~50% gluon contribution as determined in neutrino experiments on nucleons). This "enhanced" sea is said to be due to the production of extra $q\bar{q}$ pairs during the long time scale of the low p_T reaction. Thus the sea as determined by the recombination model may have little in common with that seen in hard scattering experiments.

4. Gluons

In neutrino interactions, the existence of gluons is inferred from the fact that they do not interact with the weak current; their structure function is deduced from those of the quarks via the QCD evolution equations. In hadronic scattering processes, however, gluons can themselves interact, and hence their properties can be deduced more directly. Lepton pair experiments are relevant in two different ways:

(a) The contribution $gq \to q"\gamma"$ to large p_T continuum lepton pairs.*
(b) Resonance production via a gluon from each of the initial state hadrons.†

The CFS group[22] have used method (a) to deduce the exponent of the gluon's structure function. It is to be noted that their data extends only to p_T~4 GeV/c. Their fit to the data includes a prescription for the effects of confinement at low p_T. Their value of g presumably depends on the input assumptions and parametrisations used in their overall fit.

---

* The major QCD correction to the Drell-Yan process, especially in NN reactions, is from the $q\bar{q}\to g\gamma$ mechanism. However, this has a steeper dependence on the lepton pair transverse momentum than the $qg\to q\gamma$ mechanism, which should thus dominate at large enough p_T. It is this which in principle allows the high p_T data to determine the gluon structure function.

† Vector mesons do not couple to 2 gluons. It is thus necessary to assume that a soft gluon is radiated in the process, and that this does not affect the determination of the structure functions.

Barger et al[26] have used the second method for Ψ production in pN interactions, after allowing for a small $q\bar{q}\to\Psi$ contribution. Similarly McEwen[27] has used the SISI collaboration data on $\pi^- p\to\Psi$ to determine both the pion and the nucleon gluon structure function. These values are all presented in Table 3.

They are to be compared with exponents of 5 from the counting rules[28]; 5.3 from the CDHS neutrino data[6]; ~5 from Barger's fit[29] to Ψ photoproduction data; and the Feynman-Field parametrisation[24]

$$(1 - x)^4 (1 + 9x)$$

In the future we may hope that similar fits to data on $pN\to\Upsilon$ may give information on the gluon structure function at a Q^2 of 100 GeV^2. This could then provide evidence for or against the scaling violation effects expected on the basis of QCD.

Similar analyses with meson beams give information on the gluon structure functions of mesons. Thus McEwen[27] finds that $g=2.3\pm0.3$ for pions, while Barger obtains a value of ~3 for both pions and kaons. The counting rule prediction for gluons in mesons is $g=3$.

5. Conclusions

It is clear that we are emerging from the time when the predominant question was:

"Are lepton pair experiments consistent
with parton model calculations?"

into the era of using such data to provide new information on parton properties. We can hope for this to be a fruitful field for many years.

Table 1 Valence Structure Functions

The structure functions have been parametrised as $x^{\alpha}(1-x)^{\beta}$

Quark	Particle	Method	Reference	α	β	$\lvert Q2\rvert$ (GeV^2)	Comment
u	p	pN and $\bar{p}N \to \mu^+\mu^-$	SCCBO[5]	0.8 ± 0.3	3.3 ± 0.5	~20	a) b)
		νN and $\bar{\nu} N$	CDHS[6]	$0.51 \pm .02$	$3.03 \pm .09$	20	
		Counting Rules			3		
$\bar{u}$	π^-	$\pi^- N \to \mu^+\mu^-$	SCCBO[7]	$0.4 \pm .15$	$1.07 \pm .12$	~25	
			CIP[8]	0.5	$1.27 \pm .06$	~25	c) d)
			SISI[9]	0.5	$1.57 \pm .18$	~25	c) d)
			BCE[10]	$0.44 \pm .12$	$0.98 \pm .15$	~6	
		High p_T jets	Dris[11]		~CIP		
		Recombination model	Aitkenhead[12]		$1.0 \pm .1$		
		Recombination model	Hwa[13]		$0.8 \pm .2$		
		Counting rules			0,1 or 2		
$\bar{u}$	K^-	$K^- N \to \mu^+\mu^-$	SCCBO[14]	See fig 2		~25	d)
			BCE[15]	Like SCCBO		~6	d)
		Recombination model	Aitkenhead[12]		2.5 ± 0.6		
		Counting rules			Same as π		

Comments:

(a) p structure function from $\pi^- N$ is similar[7].
(b) If α is fixed at 0.5, $\beta = 3.0 \pm .3$
(c) Value of α is fixed at 0.5.
(d) Valence and sea contributions to $\bar{u}$ in meson are not separated.

Table 2 Sea Quark Structure Functions

The sea quark structure functions have been parametrised as $A_s(1-x)^s$

Hadron	Quark	Method	Reference	A_s	s	Q^2 (GeV^2)	Comments
p	$\bar{d}$	$M_{\mu^+\mu^-}$	CFS[22]	0.55±.17	7.6±0.4	~30	
		Total-valence st. fn.	SCCBO[5,23]		7.1±0.5	~20	(a)
		$\nu N, \bar{\nu} N$	CDHS[6]	0.25±.02	8.1±0.7	20	(b)
	$\bar{s}$	$\nu N, \bar{\nu} N$	CDHS[6]		$10^{+1.8}_{-1.4}$	20	
	$\bar{u}/\bar{d}$	$M_{\mu^+\mu^-}$ spectrum	CFS[22]	1	3.5±1.5	~30	
		Rapidity distribution	CFS[22]	1	~2.5	~30	
		Pauli Principle	Feynman[24]		>0		
		QCD	Ross[25]		>0		
π	Non-strange	$\pi^- N$ and $\pi^+ N \to \mu^+\mu^-$	SCCBO[7]	0.25±0.15	5.4±2.0	~25	
		$\pi^- N$ and $\pi^+ N \to \mu^+\mu^-$	BCE[10]		~5		
		Recombination model	Aitkenhead[12]	0.82±.08	3.5±0.2	~6	(c)

Comments:

(a) For $\bar{u}(x)=\bar{d}(x)$, $s=8.5\pm0.5$.

(b) A_s and s for the neutrino data are for $(\bar{u}+\bar{d})/2$.

(c) Enhanced sea.

Table 3 Gluon Structure Functions

The gluon structure functions are parametrised as $(1-x)^g$. The normalisation of these structure functions in general has been chosen as $2/(g+1)$ to ensure that 50% of the hadron momentum is carried by the gluons.

Hadron	Method	Reference	g	Q^2 (GeV^2)
Nucleon	Overall fit	CFS[22]	4.1±0.2	~36
	$pN \to \Psi$	Barger[26]	~4.6	10
	$\pi N \to \Psi$	McEwen[27]	>5.1±0.6	10
	Counting rules		5	
	Neutrino data + QCD	CDHS[6]	5.3±1.5	20
	$\gamma N \to \Psi$	Barger[29]	~5	10
	High p_T	Feynman[24]	4	4
Mesons	$\pi N \to \Psi$	McEwen[27]	2.3±0.3	10
	$\pi N \to \Psi$	Barger[26]	~3	10
	$KN \to \Psi$	Barger[26]	~3	10
	Counting rules		3	

References

1) J.H. Christenson et al. Phys.Rev. D8(1973)2016;
P.A. Piroue, Proceedings of the XVIII International Conference on High Energy Physics (London, 1974) pV-47;
P.V. Landshoff, Ibid pV-76;
G.R. Farrar, Nucl.Phys. B77(1974)429;
W. Lee, Proceedings of SLAC Summer Institute on Particle Physics (1975)p285;
etc.

2) S.P. Denisov, International Conference on High Energy Physics (Tbilisi, 1976) pN-31;
D.C. Horn et al. Phys.Rev.Lett. 36(1976)1236;
K. Kajantie, Proceedings of the 1977 European Conference on Particle Physics (Budapest, 1977) p 467;
etc.

3) See, for example, Table 3 of ref.(18).

4) For example G. Altarelli, R.K. Ellis and G. Martinelli, Nucl.Phys. B157(1979)461.

5) J. Badier et al. Phys.Lett. 96B(1980)422

6) J.G.H. de Groot et al. Z.Phys. C1(1979)143 and Phys.Lett. 82B(1979)456.

7) J. Badier et al. Preprints CERN/EP 79-67 and 80-148.

8) K.J. Anderson et al. Phys.Rev.Lett. 42(1979)951.

9) R. Barate et al. Phys.Rev.Lett. 43(1979)1541.

10) M. Corden et al. Phys.Lett. 96B(1980)417.

11) M. Dris et al. Phys.Rev. D19(1979)1361 and Phys.Rev.Lett. 44(1980)514.

12) W. Aitkenhead et al. Phys.Rev.Lett. 45(1980)157.

13) R.C. Hwa and R.G. Roberts, Z.Phys. C1(1979)81.

14) J. Badier et al. Phys.Lett. 93B(1980)354.

15) Data presented at this meeting by J. Dowell.

16) A. Bodek, Phys.Lett. 51B(1974)417;
G.R. Farrar, P. Schreiner and W.G. Scott, Phys.Lett. 69B(1977)112;
P. Allen et al. Aachen-Bonn-CERN-Munich-Oxford preprint (1980).

17) G.R. Farrar and D.R. Jackson, Phys.Rev.Lett. 35(1975)1416;
R.P. Feynman, "Photon Hadron Interactions" (W.A. Benjamin Inc., 1972) p150

18) L. Lyons, "Massive Lepton Pair Production in Hadronic Interactions, and the Quark Model" (To appear in Progress in Particle and Nuclear Physics, 1981).

19) Z.F. Ezawa, Nuovo Cimento 23A(1974)271;
G.R. Farrar and D.R. Jackson (Ref.17);
E.L. Berger and S.J.Brodsky, Phys.Rev.Lett. 42(1979)940;
R.P. Feynman and R.D. Field (Ref.24).

20) K.P. Das and R.C. Hwa, Phys.Rev. 68B(1977)459.

21) F. Martin, A. de Rujula and P. Sorba, CERN Preprint TH 2845.

22) A.S. Ito et al. Phys.Rev. D28(1981)604.

23) J. Badier et al. Phys.Lett. 89B(1979)145.

24) R.P. Feynman and R.D. Field, Phys.Rev. D15(1977)2590; and R.P. Feynman, R.D. Field and G.C. Fox, Phys.Rev. D18(1978)3320.

25) D.A. Ross and C.T.Sachrajda, Nucl.Phys. B149(1979)497.

26) V. Barger, W.Y. Keung and R.J.N. Phillips, Z.Phys. C6(1980)169.

27) J.G. McEwen, "J/ψ production by π^- at momenta from 150-193 GeV/c", XX International Conference on High Energy Physics (Madison, 1980).

28) G.R. Farrar, Nucl.Phys. B77(1974)429.

29) V. Barger, W.Y. Keung and R.J.N. Phillips, Phys.Lett. 91B(1980)253.

30) R.J.N. Phillips, "Phenomenology of New Particle Production", XX International Conference on High Energy Physics, (Madison 1980).

31) J. Badier et al. Preprint CERN/EP 79-137.

32) A. Benvenuti et al. Phys.Rev.Lett. 42(1979)1317.

BRIEF DESCRIPTION OF THE NA 10 EXPERIMENT

K. Freudenreich
CERN, Geneva, Switzerland

ABSTRACT

The most recent dimuon experiment, NA 10, at CERN is briefly described. It studies inclusive dimuon production at high incident flux and high mass resolution. NA 10 is a collaboration of CERN, ECOLE POLYTECHNIQUE PALAISEAU, CRN and University Louis PASTEUR STRASBOURG and ETH ZURICH.

The NA 10 experiment is installed in the North Area High Intensity Facility (NAHIF) of the CERN SPS.

The NAHIF H10 beam line can transport primary protons (later antiprotons) and negative secondary particles with momenta up to 450 GeV/c and positive secondary particles with momenta up to 300 GeV/c. The secondary beam has a large acceptance (±10% momentum bite) and a small spot size at the focus (r.m.s. radius = 2.5 mm). An intensity of 5×10^{12} protons/burst on the production target yields 4×10^{8} π^-/burst at 280 GeV/c and 2.5×10^{9} π^-/burst at 200 GeV/c. The beam line is rather short (190 m) and is equipped with magnetic spoilers to fight the important muon halo.

Figure 1 shows the layout of the NA 10 spectrometer. At a distance of 0.4 m downstream of the target a 4.8 m long hadron absorber is installed. In the centre it consists of a W/U core which begins 1.2 m downstream of the centre of the target. This core is surrounded by high-density graphite (ρ = 1.9 g/cm^3, i.e. 8 absorption lengths) in a cone defined by the acceptance of the magnet, and embedded in iron and concrete blocks.

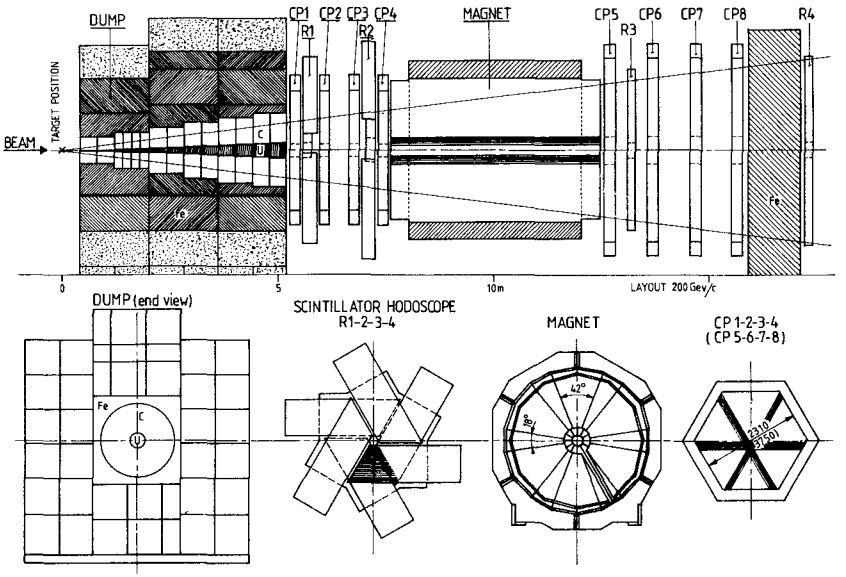

Fig. 1 NA 10 experimental set-up

The magnet of the spectrometer is a toroid. It has six 42° air gaps which are defined by wedge-shaped iron pole pieces. In pulsed operation the field integral is 3 T•m at the mean radius of 0.75 m.

Upstream and downstream of the magnet there are two scintillator hodoscopes R_i and four multiwire proportional chambers PC_K. The last hodoscope R_4 is placed behind a 1.2 m long iron filter. All detectors have the same sextant structure as the magnet. The whole apparatus can be expanded longitudinally in order to preserve scaling (and resolution) when changing the incident energy.

Figure 2 shows diagrammatically the trigger principle. Elements of the front hodoscopes R_1 and R_2 select trajectories which come from the target and reject those originating in the W/U core of the absorber. To suppress accidental triggers from high-multiplicity hadronic showers only events with less than 6 counter hits per sextant are accepted. A fast matrix logic selects for each $R_1 \cdot R_2$ coincidence elements in the allowed range of the back hodoscopes R_3 and R_4 corresponding to a given $p_\perp$ range. A two-particle trigger is obtained by forming the coincidence of two such single-particle triggers in non-adjacent sextants. Adding the two $p_\perp$'s permits a rough on-line dimuon mass selection ($m_{\mu\mu} \simeq p_{\perp 1} + p_{\perp 2}$). Events in the J/ψ region are prescaled.

The installation of the experiment was finished by April 1980. After a short period of running-in we took some data with 280 GeV/c π^- at 4×10^8 π^-/burst before the $p\bar{p}$ shutdown in June 1980. We used four different targets: 12 cm W, 6 cm W, 9.1 cm Cu, and 30 cm C, the last three targets having approximately the same ratio of target length/absorption length. Targets were interchanged on a regular basis and the magnet polarity was periodically reversed.

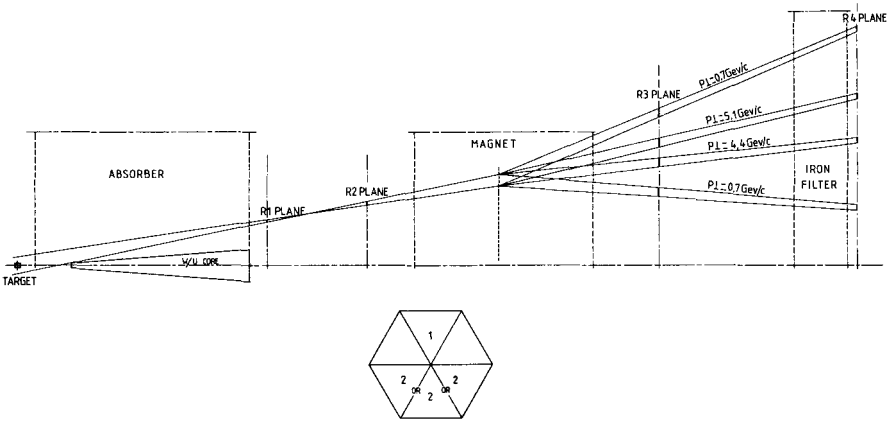

Fig. 2 Trigger principle. Single-particle trajectories for four $p_\perp$ values are shown (at p_{π^-} = 280 GeV/c).

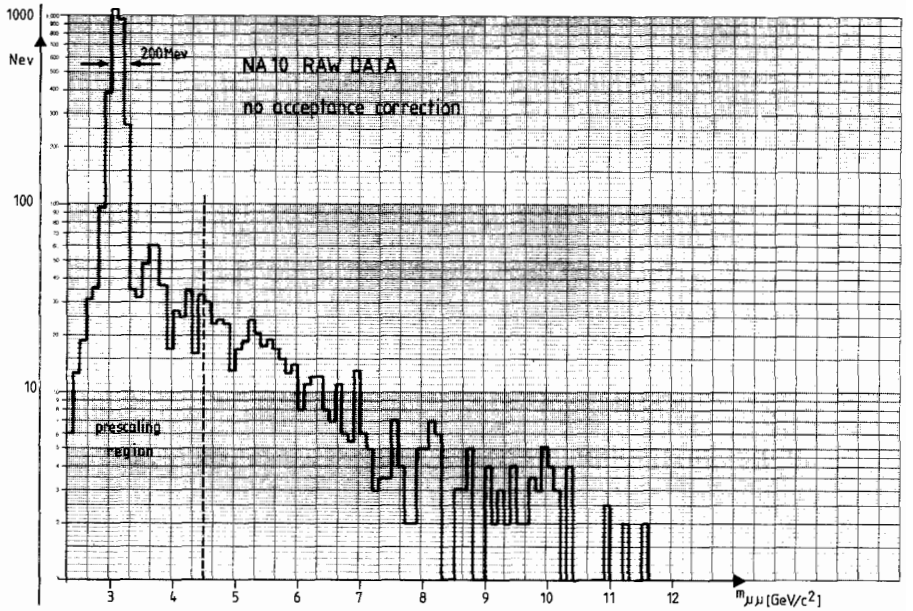

Fig. 3 Raw $\mu^+\mu^-$ mass spectrum for π^-Cu interactions at 280 GeV/c

Figure 3 shows the raw dimuon mass spectrum from the Cu target for events having both tracks going through air sectors of the magnet. The resolution at the J/ψ peak is 3%. This agrees with the predicted resolution and extrapolates to 2% at the upsilon. The data are not corrected for acceptance and for the trigger prescaling in the J/ψ mass region. One sixth of the events in Fig. 3 come from a run without prescaling.

Such data will allow the determination of the A dependence of dimuon production as a function of mass, $p_\perp$, etc.

THE EXPERIMENT UA1 AT THE $p\bar{p}$ COLLIDER

J. Strauss

CERN, Geneva, Switzerland

and

Institut für Hochenergiephysik der
Österreichischen Akademie der Wissenschaften, Vienna, Austria

ABSTRACT

The $p\bar{p}$ collider project at the CERN SPS will provide the opportunity for experimentation at c.m. energies ten times higher than ever reached before with accelerators. The associated physics programme is described. Some features of the UA1 detector are listed, and its lepton-detection capabilities are discussed.

1. INTRODUCTION

The $p\bar{p}$ collider[1] at the CERN SPS will be operational in a few months from now. Antiprotons are produced by the CERN PS, and then precooled, cooled, and accumulated in the Antiproton Accumulator ring. Bunches of antiprotons are then injected into the PS, accelerated, transferred into the SPS and further accelerated (together with proton bunches circulating in the opposite direction) to an energy of 270 GeV [2-3]. The c.m. energy of the collision will hence be 2×270 GeV. The design luminosity is 10^{30} cm^{-2} s^{-1}, i.e. about 50,000 hadronic events per second.

The rate of production of antiprotons together with their acceptance in the accumulator is one order of magnitude below design at the moment. It may turn out to be impossible to produce and accumulate 10^{12} antiprotons per day. In such a case the luminosity at a given intersection region could be increased by a good order of magnitude by minimizing the β value during special high-luminosity runs. Superconducting quadrupole magnets would have to be installed on either side of the intersection region, about 6 m away from the intersection point. We are confident that a reasonable luminosity will be reached soon after switching on and running in of the SPS in the collider mode.

2. PHYSICS PROGRAMME

Two underground areas are available for experimentation, and will be shared by five experiments[4]. The physics programme is concentrated on the following subjects:

a) Search for the weak bosons $W^{\pm}$ and Z^0 [5].
b) Production of new flavours[6].
c) Study of the Drell-Yan continuum[7].
d) Physics at large p_T [8] and low p_T [9].
e) Measurement of the total and elastic cross-sections[10].
f) Search for magnetic monopoles[11].
g) Surprising hadronic events[12].

The possible detection of the weak bosons is clearly the primary motivation behind the collider project, as was already pointed out in the original proposal[1].

Production of weak bosons, Drell-Yan pairs and large-p_T hadrons is supposed to proceed via hard scattering between point-like constituents of the colliding protons and antiprotons at effective c.m. energies of up to 150 GeV and higher. The well-defined theory describing these high-Q^2 (or small-distance) interactions is perturbative quantum chromodynamics (QCD)[13] with its characteristic scale-breaking pattern: the Z^0-production cross-section rises by an order of magnitude between $\sqrt{s}$ = 300 GeV and $\sqrt{s}$ = 600 GeV in the case of QCD, compared to a factor of

two in the scaling parton model[5d,e]. We will however not be able to study this effect at the beginning of collider operation as the Z^0 rate is marginal even at design luminosity and $\sqrt{s}$ = 540 GeV. Cross-sections for Z^0 production at varying $\sqrt{s}$ would be better accessible at Isabelle and the Tevatron.

Analogous QCD effects for production of Drell-Yan pairs at lower Q^2 do exist but are less dramatic in our energy range [see Fig. 1, compare $Q^2 = (88.66)^2$ GeV^2 and Q^2 = 100 GeV^2]. At Q^2 values above 400 GeV^2 there is no counting rate for Drell-Yan pairs even at design luminosity. Despite some reservations, Z^0 and Drell-Yan production will probably become a powerful laboratory tool for checking and upgrading our present views on strong interaction theory during extensive second-generation experimentation after the weak bosons are found.

Special interest will be devoted to large-p_T hadronic events which will probably strike the eye when looking at their jet-like structure. We will have the unique chance to follow in detail how large-p_T phenomena evolve from the low-p_T régime. Better understanding of the transition region between soft scattering at small transverse momenta and hard scattering is one of the central issues in strong interaction theory.

Finally, surprises are always possible when one enters a new and unexplored land. Quarks may become free, and magnetic monopoles may be produced. The usual hadronic event may differ drastically from what we are used to. Centauro events contain about 100 charged particles and no neutrals. They may start to show up at our energies.

3. THE UA1 FACILITY

UA1 is a collaboration between the following institutions: Aachen, Annecy, Birmingham, CERN, Collège de France, Queen Mary College, Riverside, Rome, Rutherford, Saclay, and Vienna. Let me comment briefly on the principles behind the design of the detector. The central detector[14] should provide enough information to resolve difficult high-multiplicity events. Many space points per track are therefore measured, and the obtained high degree of redundancy is further used for particle identification by dE/dx. The momentum resolution $\Delta p/p$ is better than $0.001 \times p$ (p in GeV/c) over most of the detector volume when using the vertex in the fit. Special care has been devoted to the problem of keeping the central detector shells as thin as possible, so that conversion of photons from π^0 decays is not more copious than internal conversion (i.e. Dalitz decays). Electromagnetic calorimeters[15] surround the central detector to measure with high precision the energies of electrons and photons. The cell-size of the electromagnetic (e.m.) calorimeters is large, with the advantage of keeping the number of photomultipliers (PMs) small. Large position corrections have, however, to be applied, and a careful mapping of the calorimeters is compulsory. Proper adding of the PM

signals will provide us with a 20% resolution for the trigger threshold. The e.m. calorimeters are surrounded by hadronic ones[16] to trigger on hadron jets, to serve as the return yoke for the magnet, and as the filter for muons[17]. Two forward arms with momentum measurement, and e.m. and hadron calorimetry down to 2 mrad complete the 4π feature of the experiment. More details are given in Tables 1 to 4, and the general layout is presented in Figs. 2 to 4.

Installation of the various parts advances quickly. Our aim is to have a checked and calibrated detector when the first collisions will take place in late summer or autumn 1981.

4. LEPTON-DETECTION CAPABILITIES OF UA1

Momenta of electrons and muons are measured in the central detector. Then the energy of the electron is measured with high precision in the e.m. shower counters, and the muon has to pass through about 1 m of iron before identification in the muon chambers. Neutrinos can be detected and measured by missing transverse energy.

The electron to charged hadron rejection ratio has been investigated in a test beam. It is found to be better than 1:200 at 10 GeV and 1:500 at 40 GeV. The contribution of π^0 Dalitz decays and conversions of photons from π^0's depends on the shape of the π^0 spectrum, and is expected to be less than one part in 10^3. The contamination of the muon signal is dominated by decays of charged pions and kaons, or non-interacting pions punching through 7-8 absorption lengths.

The fact that electrons and muons are both measured in the same experiment may turn out to be very valuable not only from the point of view of doubling the rates for the weak bosons, but also because the same physics can be studied in two independent channels, which are subjected to different systematic biases.

5. CONCLUSIONS

(The items are ordered according to increasing demands for luminosity.)

a) The first 1000 events will suffice to measure Centauro-type events and other exotic effects (if present) in the first week of collider operation.

b) Large-p_T physics will start to become accessible already at moderate luminosity. Based on a simple calculation, we expect to collect about 250 jets with p_T (jet) > 20 GeV/c per hour at $L = 10^{28}$ cm^{-2} s^{-1}, most of them due to gluon-gluon scattering.

c) At a luminosity of 10^{29} cm^{-2} s^{-1} (the most probable figure during the first year of collider operation) we expect a total of 5-10 $W^{\pm}$ bosons per day which decay into $e^{\pm}\nu$ or $\mu^{\pm}\nu$. The rejection against hadrons will be about 1:200 or better (for electrons) and 1:1000 or better (for muons). Neutrino detection will provide another rejection factor of about 10. The characteristic asymmetry behaviour (see Fig. 5) will tell us that the leptons come from the weak bosons.

d) At the design luminosity of 10^{30} cm^{-2} s^{-1} we expect a total of 5-10 Z^0 bosons per day which decay into e^+e^- or $\mu^+\mu^-$. The rejection ratio against hadron pairs will be $1:(500)^2$ or better.

e) An extensive second generation program to check and upgrade strong-interaction theory will be possible by using weak-boson and Drell-Yan signatures.

I would like to express my thanks to C. Rubbia, P. Aurenche, K. Eggert, B. Humpert, J. Saas and M. Spiro for numerous comments and discussions.

REFERENCES

1) C. Rubbia, P. McIntyre and D. Cline, Proc. Int. Neutrino Conf., Aachen, 1976 (eds. H. Faissner, H. Reithler and P. Zerwas) (Vieweg, Braunschweig, 1977), p. 683.

2) S. van der Meer, Proton-antiproton colliding beam facility, report CERN/SPC/423 (1978).

3) Design study of a $\bar{p}p$ colliding beam facility, report CERN/PS/AA 78-3 (1978).

4) UA1: A. Astbury et al., proposal CERN/SPSC/78-06 (1978);
UA2: M. Banner et al., proposals CERN/SPSC/78-08 (1978), and CERN/SPSC/78-54 (1978); V. Hungerbuhler, these proceedings.
UA3: B. Aubert et al., proposal CERN/SPSC/78-15 (1978);
UA4: G. Matthiae et al., proposal CERN/SPSC/78-11 (1978); R. Battiston et al., proposal CERN/SPSC/79-10 (1979);
UA5: M.G. Albrow et al., proposal CERN/SPSC/78-70 (1978).

5) a) R.B. Palmer et al., Phys. Rev. D 14, 118 (1977);
L.B. Okun and M.B. Voloshin, Nucl. Phys. B120, 459 (1977);
b) C. Quigg, Rev. Mod. Phys. 49, 297 (1977);
c) R.F. Peierls et al., Phys. Rev. D 16, 1397 (1977);
d) F.E. Paige, *in* Proc. Topical Workshop on the Production of New Particles in Super High Energy Collisions, Madison, Wisconsin, October, 1979 (ed. V. Barger and F. Halzen), and BNL-27066 (1979);
e) B. Humpert and W.L. van Neerven, Phys. Lett. 93B, 456 (1980);
P. Aurenche and J. Lindfors, Phys. Lett. 96B, 171 (1980); preprint CERN TH.3016 (1981);
R. Kinnunen and C. Rubbia, CERN/UA1/$p\bar{p}$ Note 67 (1981).

6) D.M. Scott, *in* Proc. Topical Workshop on the Production of New Particles in Super High Energy Collisions, Madison, Wisconsin, October 1979 (ed. V. Barger and F. Halzen);
S. Wojcicki, Rapporteur's talk, to be published in Proc. Int. Conf. on High Energy Physics, Madison, Wisconsin, 1980.

7) F. Vannucci, Acta Phys. Polon. B12, 21 (1981).

8) P. Darriulat, Ann. Rev. Nucl. Sci. 30, 159 (1980).

9) H. Boggild and T. Ferbel, Ann. Rev. Nucl. Sci. 24, 451 (1974).

10) U. Amaldi and K.R. Schubert, Nucl. Phys. B166, 301 (1980).

11) L.W. Jones, Rev. Mod. Phys. 49, 717 (1977).

12) R.W. Ellsworth et al., Phys. Rev. D 23, 771 (1981), and references therein.

13) J. Ellis and C.T. Sachrajda, preprint CERN TH.2782 (1979);
Yu.L. Dokshitzer et al., Phys. Rep. 58, 269 (1980).

14) M. Calvetti et al., Nucl. Instrum. Methods 174, 285 (1980), and 176, 255 (1980);
M. Barranco Luque et al., Nucl. Instrum. Methods 176, 175 (1980);
B. Hallgren and H. Verweij, preprint CERN-EP/79-133 (1979).

15) L. Allemand et al., Nucl. Instrum. Methods 164, 93 (1979);
E. Locci and M. Spiro, Nucl. Instrum. Methods 164, 97 (1979);
J.C. Thevenin et al., Nucl. Instrum. Methods 169, 53 (1980);
J. Colas and J.C. Lacotte, Nucl. Instrum. Methods 176, 283 (1980);
B. Aubert et al., Nucl. Instrum. Methods 176, 195 (1980);
M. Della Negra, Preprint LAPP-EXP/80-07 (1980);
J.P. Lees, Thesis, LAPP-EXP/81-01 (1981).

16) M.J. Corden et al., *in* Proc. Int. Conf. on Experimentation at LEP, Uppsala, 1980, to be published in Physica Scripta;
R.K. Bock et al., preprint CERN-EP/80-206 (1980).

17) K. Eggert et al., Nucl. Instrum. Methods 176, 217 (1980), and 176, 223 (1980).

Table 1

Central detector

Detector type	Drift chambers with drift space of 20 cm
Read-out	Three-dimensional read-out by continuous digitization in drift direction, and charge division along the wires
Number of space points per track	110 (on an average)
Tilt of drift angle	about 25° (at nominal magnetic field)
Resolutions	σ = 250 μm (in drift direction) σ = 1% of wire length (along wire) σ = 6% for dE/dx
Mass resolution for Z^0 (FWHM)	Γ = 8 GeV/c^2 (at 79% efficiency) Γ = 7 GeV/c^2 (at 65% efficiency)
Calibration and alignment	Straight tracks are generated by X-rays

Table 2

Electromagnetic calorimeters

Detector type	Lead-scintillator sandwich (25 rad lengths) with BBQ read-out; drift tubes for better space resolution in forward direction
Read-out	Amplifiers attached to low-gain PMs; 2 ADCs per PM separated by a factor of 30 in sensitivity
Resolutions a) Angular region $25° < \theta < 155°$ ("gondolas")	$\sigma(E) \simeq 0.15/\sqrt{E} + 0.01$ $\sigma(x) = 4$ cm$/\sqrt{E}$ (space resolution along θ) $\sigma(y) = 16$ cm$/\sqrt{E}$ (space resolution along ϕ) $\sigma(E_t) = 0.12/\sqrt{E}_t$
b) Angular regions $5°, \theta < 25°$ and $155° < \theta < 175°$ ("bouchons")	
c) Mass resolution for Z^0 (FWHM)	Γ = 3.5 GeV
Calibrations a) Mapping of calorimeters	1) ^{60}Co source 2) Betatron
b) Long-term stability of PMs	Laser calibration system. Monitors: ^{241}Am (imbedded in NaI) and vacuum diode; light distribution by optical fibres

Table 3

Hadron calorimeters

Detector type	Iron scintillator sandwich with BBQ read-out
Resolution	$\sigma \simeq 0.8/\sqrt{E}$
Calibration	(Long-term stability of scintillators and PMs.) Laser calibration system with source monitors.

Table 4

Muon detector

Detector type	Large-area drift-tube chambers
Angular resolution	σ = 1 mrad
Trigger	a) Fast trigger to reduce rate at L = $= 10^{30}$ cm^{-2} s^{-1} to less than 1 kHz b) Microprocessor trigger (to select stiff tracks aiming at vertex)

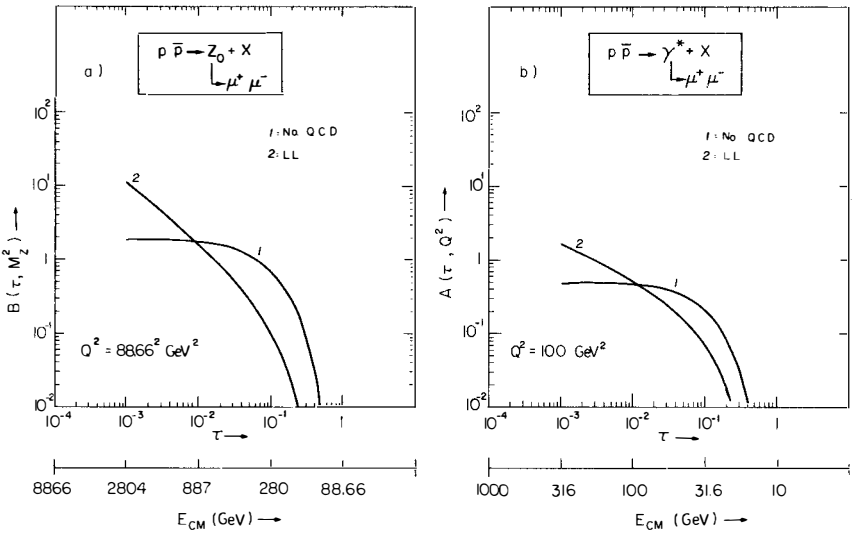

Fig. 1 Z^0 and Drell-Yan cross-section, with A and B defined in Ref. 5e as

$$\left(\frac{d\sigma}{dQ^2}\right)_\gamma = \frac{4\pi\alpha^2}{9}\,\frac{A(\tau,Q^2)}{Q^4}$$

$$\left(\frac{d\sigma}{dQ^2}\right)_{Z^0} = \frac{G^2 M_{Z^0}^2}{288\pi}\left[(4\sin^2\theta_w - 1)^2 + 1\right]\frac{B(\tau,Q^2)}{(Q^2 - M_{Z^0}^2)^2 + \Gamma_{Z^0}^2 M_{Z^0}^2}$$

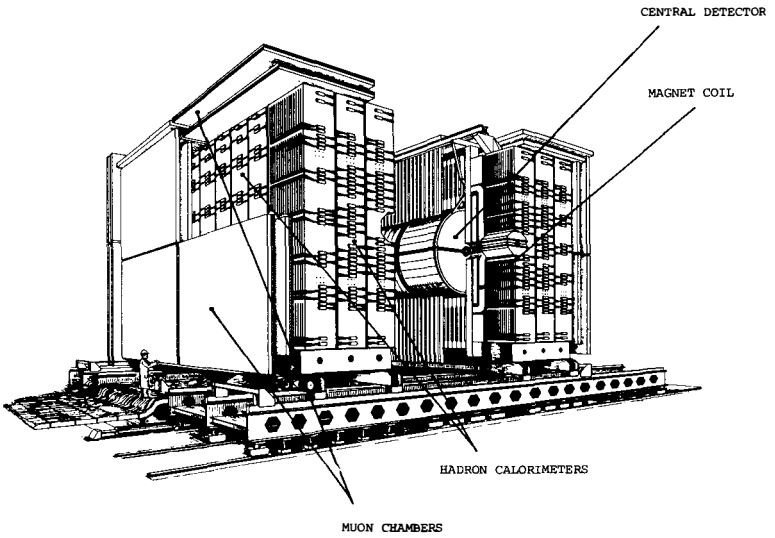

Fig. 2 The UA1 detector

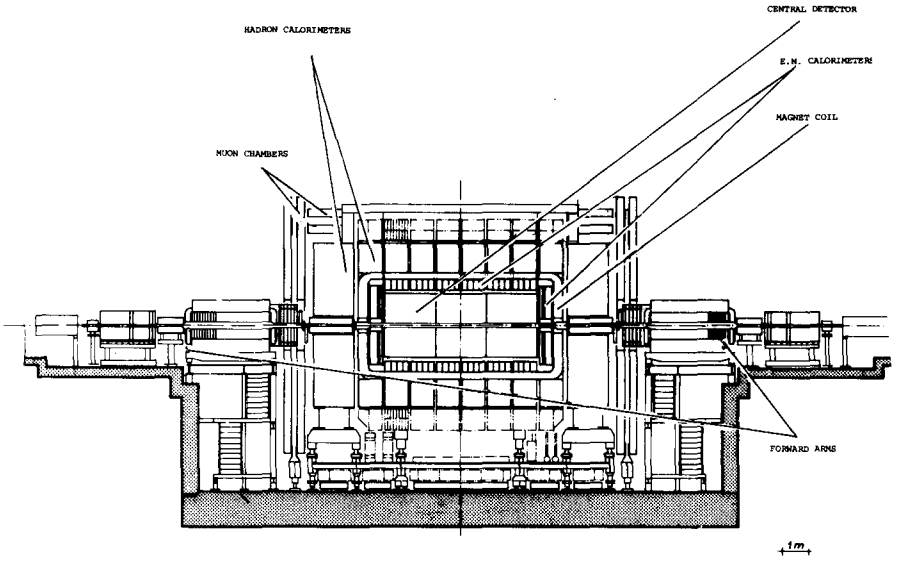

Fig. 3 Cross-section through the UA1 detector (along the beams)

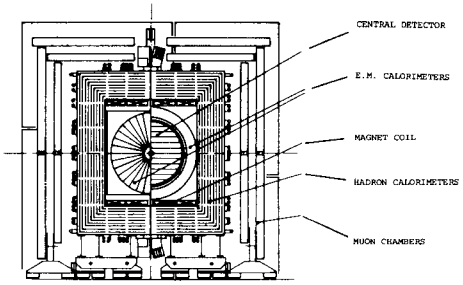

Fig. 4 Cross-section through the UA1 detector (perpendicular to the beams)

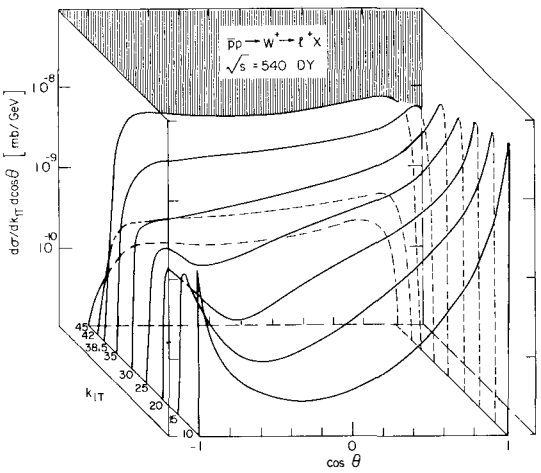

Fig. 5 Three-dimensional plot of the single lepton spectrum in $p\bar{p}$ collisions at $\sqrt{s}$ = 540 GeV (from Ref. 5e)

UA2, A DETECTOR TO STUDY $p\bar{p}$ INTERACTIONS AT THE SPS-COLLIDER

V. Hungerbühler
CERN, Geneva, Switzerland

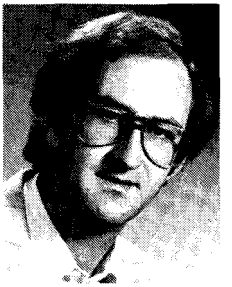

ABSTRACT

The principal aim of the UA2 detector is to detect the production and decay of $W^{\pm}$ and Z° bosons. The design combines large solid angle coverage with compactness and simplicity of operation. It includes electromagnetic and hadronic calorimetry in the central region and magnetic spectrometers in the forward and backward cones equipped for electron detection. A high resolution vertex detector provides an accurate measurement of the event topology. In addition a small azimuthal wedge in the central region is instrumented to explore new aspects of $p\bar{p}$ interactions at very high energies.

1 - Physics Interest

The injection of cooled antiprotons into the SPS [1] and their acceleration to 300 GeV opens up the possibility of studying $p\bar{p}$ collisions at a centre-of-mass energy $\sqrt{s}$ = 600 GeV where many new phenomena are expected to occur.

In particular with a luminosity $L \cong 10^{30}$ cm^{-2}s^{-1} it becomes possible to produce a significant number of $W^{\pm}$ and Z°, the weak intermediate bosons of unified gauge theories, if their production cross section is of the order of a few 10^{-33} cm^2 as predicted by current QCD calculations.

In the Weinberg Salam model, with $\sin^2\Theta_W$ = . 23 the masses of the gauge bosons are m_{Z° = 89 GeV/c^2 and m_W = 78 GeV/c^2 and their branching fractions into the electron channels $Z^\circ \to e^+e^-$ and $W^\pm \to e^\pm \upsilon$ are 3% and 8% respectively.

The V-A coupling of the W's to quark and lepton doublets is expected to result in a strong forward-backward decay asymmetry.

2 - The Experimental Apparatus

The detector [2] is largely dedicated to the observation of the hadronic and leptonic decay modes of the weak vector bosons ($W^{\pm}$, Z°). Nevertheless, the resulting apparatus is very suitable for the detection of other expected -or unexpected- phenomena.

A constant and major concern has been to maintain simplicity and compactness in the design, as imposed by the constraint of operating the detector in the difficult environment of the SPS tunnel.

For this reason, and because of the good energy resolution obtainable in lead-scintillator sandwich counters, we have concentrated on the electron rather than the muon decay modes of the $W^{\pm}$ and Z°. Electron identification is therefore instrumented over nearly 4π sr by lead-scintillator sandwich counters.

A drawing of the entire detector is presented in Fig. 1. At the centre of the apparatus is the vertex detector, a system of cylindrical proportional and drift chambers, that will measure particle trajectories in a region free of magnetic fields. This detector is under construction at LAL, Orsay (Table 1). In the central region, covering ±1 rapidity unit about 0, the vertex detector is surrounded by lead-scintillator sandwich counters followed by hadron calorimeters. The calorimeter assembly consists of 240 independent cells, each cell covering 15° in azimuthal and 10° in polar angle. This is a compromise between minimizing dead space and providing sufficient space resolution. Light is collected with BBQ-doped wavelenght shifting light guides. Each compartment is viewed with 2 light guides and 2 photomultipliers to provide information on the position of the shower so that light collection efficiency corrections can be made (Table 2).

The extension of hadron identification to forward angles was not considered, because it would need the addition of very voluminous and expensive calorimeter elements.

As noted above, an electron-positron asymmetry in the W-decay is expected in some models, with the most significant signal between 20° and 30°. Our apparatus measures this asymmetry. The angular range to cover, and the angular dependence of the electron energy (harder electrons at smaller angles) indicate a toroidal field as a suitable configuration to perform the charge measurement. The polar angular regions of 20° to 37.5°and 142.5°to 160° are each instrumented with a toroidal magnet consisting of 12 coils. The average field integral along particle trajectories is .38 Tm. Each region between two adjacent toroid coils is followed by a set of 9 drift chamber planes with an average lever arm of 80 cm. Together with the vertex detector, these forward/backward (F/B) chambers allow reliable charge measurements on electrons up to 60 GeV/c transverse momentum. The F/B drift chambers are being built at NBI, Copenhagen, and at the Istituto di Fisica Nucleare in Pavia. Each drift chamber set is followed by a converter of 6mm Pb and proportional tubes for an accurate measurement of the position of electromagnetic showers. This allows an improved rejection of the overlap background (a low momentum hadron track near a π^0, simulating an electron in the calorimeter that follows) and a better hadron rejection. The tubes are constructed at the University of Bern. The proportional tubes are followed by the F/B calorimeters, consisting of lead scintillator sandwiches and covering the same solid angle as the toroid magnets. The F/B calorimeters are built at CEN, Saclay (Table 3).

The detector is blind below 20° causing the loss of some $W^{\pm}$ and Z^0 decays. However the identification of electrons in this region would in any case have been made more difficult by higher particle densities, higher average particle energies, and beam-halo background.

The momentum measurement of charged secondaries in the central region would permit the measurement of charged particle inclusive production, and greatly benefit the study of jet strucutre at large transverse momentum, free quark production, etc... To this end a 30° azimuthal window will be opened in the calorimeter in the first phase of operation of the detector and equipped as a magnetic spectrometer. The use of the calorimeter iron as the return yoke of the magnetic spectrometer allows a very compact geometry. Electron identification remains possible in this azimuthal wedge because of the presence of a large lead-glass wall behind the magnetic spectrometer. The field integral is of the order of 1 Tm and charged particle trajectories are measured in a set of 12 large drift chamber planes. This "wedge detector" is composed of elements left over from a previous CERN-Saclay experiment at the ISR (Table 4).

In the symmetric configuration the total acceptance is ≅ 63% for $Z^\circ \to e^+e^-$ and ≅ 75% for $W^\pm \to e^\pm \nu$; it is independent of the p_T-distribution of the produced boson, up to at least $\langle p_T \rangle$ = 10 GeV/c. Thus, with a Z° production cross section of 2 x 10^{-33} cm^2 and the leptonic branching ratio mentioned above, .14 detected $Z^\circ \to e^+e^-$ per operating hour are expected. The mass resolution at the Z° peak is expected to be ≅ 1.5%.

3 - Trigger and Data Acquisition

To trigger on the electronic decays of the intermediate vector bosons, only the electromagnetic calorimeters are used. The pulse-heights of 4 adjacent calorimeter elements are linearly added and integrated. The trigger then consists of requiring two such energy clusters above some minimum p_T-threshold or one above a higher threshold. The background comes mainly from the neutral component of jets, whose p_T spectrum drops sharply. Thus, we expect to be able to keep the trigger rate near 1/sec without any significant loss of W or Z events by setting the thresholds in the 10 GeV/c p_T-range. Other triggers are being designed, such as very large amounts of electromagnetic or hadronic energy deposited in the entire calorimeter, large particle multiplicity etc...

The data acquisition will be done through a VAX 11/780 computer. Four other minicomputers will be available for parallel detector testing before runs and for in-depth monitoring during data-taking.

I would like to acknowledge numerous useful discussions with P. Darriulat and L. Di Lella.

REFERENCES

1) C. Rubbia, P. McIntyre and D. Cline, in Proceedings of the International Neutrino Conference Aachen 1976, ed. Faissner, H. Reithler, P. Zerwas (Vieweg, Braunschweig, 1977) ;
S. Van der Meer, CERN/SPC/423 (1978) ;
Design Study of a $p\bar{p}$ Colliding Beam Facility, CERN/PS/AA 78-3 (1978) ;
J. Strauss, these Proceedings.

2) M. Banner et al., CERN/SPSC/78-08 (1978) and CERN/SPSC/78-54 (1978).

TABLE 1

VERTEX DETECTOR

Cylindrical chambers in magnetic field free region, consisting of :

- 4 multiwire proportional chambers (MWPC) with cathode strip readout
- 2 Jade type drift chambers (JC) with charge division and multihit readout ; 6 sense wires per JC
- 1 cylindrical scintillator hodoscope
- 1.5 radiation length of tungsten followed by a MWPC

Angular coverage : 2π in ϕ, 20° to 160° in θ

Resolution : 200 μm in all 3 projections

Number of points per track : 16 in each projection

TABLE 2

CENTRAL CALORIMETER

Lead-scintillator and iron-scintillator sandwiches consisting of :

- electromagnetic compartment of 26 lead-plates of 3.5 mm and 27 NE 104 scintillator plates of 4 mm (total : 17 radiation lengths)
- two hadron compartments of 18 and 22 x (15 mm iron plate + 5 mm scintillator) respectively (total : 4.5 nuclear absorption lengths)

Angular coverage : 2π in ϕ, and 40° to 140°in θ

Readout : 2 BBQ doped light guides and 2 photomultipliers per compartment

Energy resolution : $\frac{\sigma}{E} = \frac{15\%}{\sqrt{E}}$ for electrons $= \frac{60\%}{\sqrt{E}}$ for hadrons

TABLE 3

THE FORWARD/BACKWARD DETECTORS

24 magnetic spectrometers, each consisting of :

- (toroidal) magnetic field of .38 Tm
- 9 drift planes with 5 cm drift space
- 6 mm lead converter followed by 2 planes of proportional tubes
- 24 radiation lengths of lead-scintillator sandwich calorimeter, followed by a 6 radiation length hadron veto.

Angular coverage : 80% of 2π in ϕ, 20° to 37.5° and 142.5° to 160° in θ

Spatial resolution : 200 μm in bending direction (drift chambers)
1 mm in non-bending direction (drift chambers)
1 cm (proportional tubes)

Energy resolution : $\frac{\sigma}{E} \simeq \frac{15\%}{\sqrt{E}}$ for electrons

TABLE 4

WEDGE DETECTOR

Large angle magnetic spectrometer, consisting of :

- Magnetic field of 1 Tm
- 12 planes of drift chambers (2.5 cm drift space, resolution of left-right ambiguity)
- 28 counter scintillator hodoscope for time-of-flight
- 2 cm of iron, followed by a scintillator hodoscope, acting as a shower counter.
- 280 blocks of lead glass, 14 radiation lengths deep

Angular coverage : 30° in ϕ, 55° to 125° in θ

Momentum resolution : $\frac{\Delta p}{p} = 2\%\ p$ (magnetic field) ; $\frac{\sigma}{E} = \frac{12\%}{\sqrt{E}}$ (lead glass array)

Spatial resolution : 200 μm /charged particles)

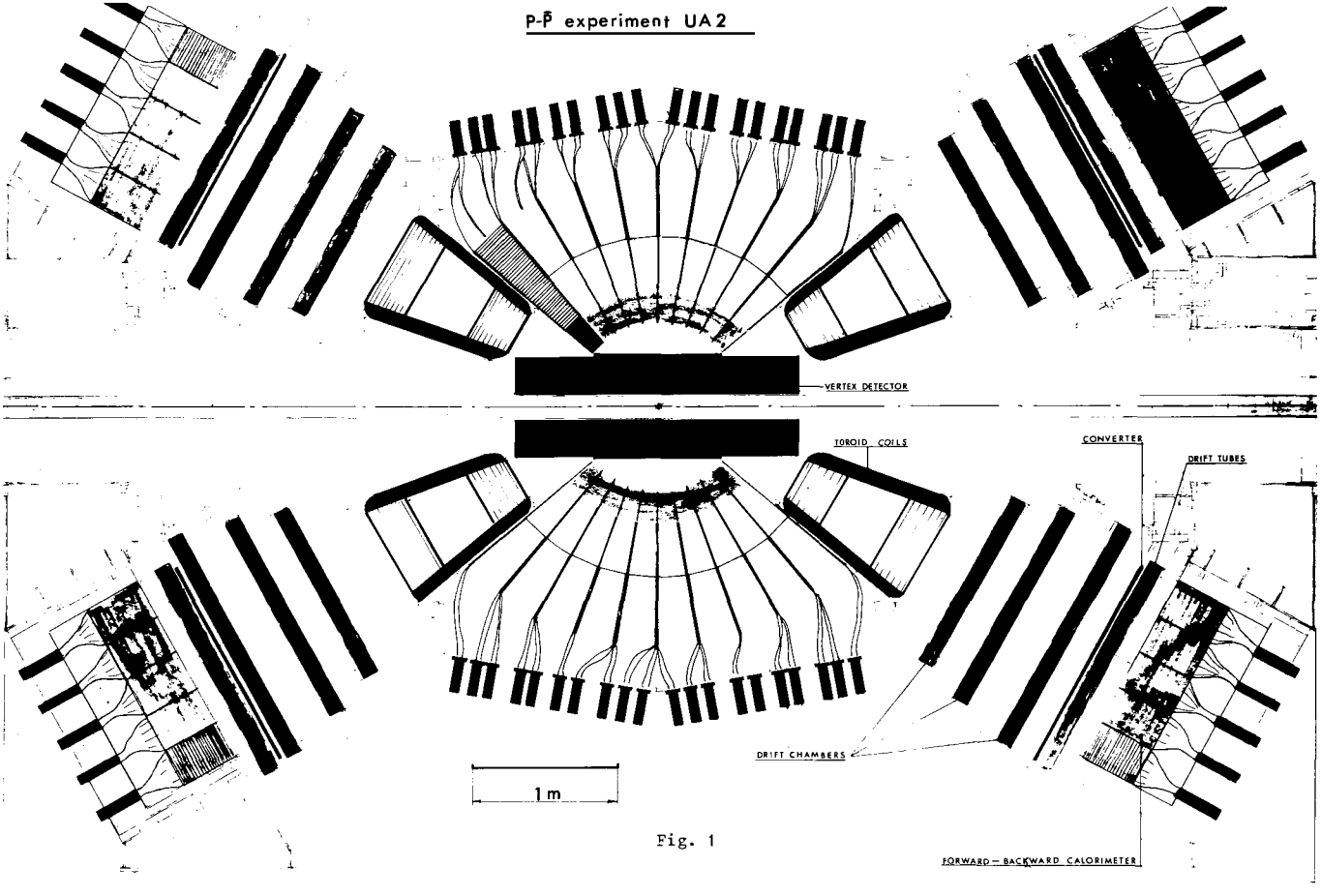
P-P̄ experiment UA2
VERTEX DETECTOR
TOROID COILS
CONVERTER
DRIFT TUBES
DRIFT CHAMBERS
1 m
FORWARD – BACKWARD CALORIMETER

Fig. 1

THE K FACTOR IN LOWEST ORDER PERTURBATION THEORY AND BEYOND

R.K. Ellis
Theoretical Physics Division
CERN
1211 Geneva 23
Switzerland

ABSTRACT

The calculation of the perturbative corrections to the Drell-Yan mechanism due to gluon radiation is illustrated. The results for the total cross-section and the cross-section differential in the rapidity calculated in order (α_s) are presented. Conjectured forms which resum the higher-order terms are reviewed.

The hadronic production of muon pairs occupies an almost unique place among the set of hard scattering processes described by the parton model for which the corrections due to gluon radiation have been calculated [1),2)]. It owes this privileged position to the fact that the calculated cross-section is predicted to be roughly twice as big as one would expect from the naive parton model - in substantial agreement with the experimental data [3)]. Moreover the reason for the size of the correction term which comes from the diagrams involving quark-antiquark annihilation can be simply understood. The only embarassment which mars this scenario is that the first order correction is so large that it casts doubt on the validity of the perturbative approximation. Nevertheless the simple explanation of the size of the correction terms encourages the belief that, because of their connection to the cancelled soft singularity, the large terms in the correction may be singled out and resummed leaving a small residual correction amenable to perturbative treatment. The muon pair production cross-section is thus on a par with the cross-section for electron-positron annihilation in providing strong evidence (albeit indirect) for the existence of gluon degrees of freedom.

As indicated elsewhere in this volume, the strength of the basic Drell-Yan formula lies in the definite prediction which it makes for muon pair production using as input parton distribution functions from deep inelastic scattering. Thus we will be able to make a firm prediction in QCD only by calculating the radiative corrections both to deeply inelastic electron nucleon scattering and muon pair production. It turns out when we perform these calculations that both these quantities separately contain infinities because of the energy degeneracy between an incoming massless quark state and the state containing an incoming quark together with parallel gluons (and in higher orders quarks and antiquarks). However, these infinities are independent of the particular process and hence can be factored out in a universal way in both processes and absorbed in an infra-red "renormalized" parton distribution function. To control these infinities in the intermediate stages of the calculation we choose to continue the dimensionality of space-time to n dimensions $(n = 4-2\varepsilon)$.

From the diagrams of Figs. 1 and 2, we obtain, for the deep inelastic scattering (DIS) structure function F_2

$$\frac{F_2(x,t)}{x} = \int_x^1 \frac{dy}{y} \left\{ \Sigma_f e_f^2 \left[\delta(1-\frac{x}{y}) + \frac{\alpha_s}{2\pi}\left(t - \frac{1}{\bar{\varepsilon}}\right) P_{qq}\left(\frac{x}{y}\right) + \alpha_s f_{q,2}\left(\frac{x}{y}\right) \right] q_o f(y) \right.$$

$$\left. + \Sigma_s e_f^2 \left[\frac{\alpha_s}{2\pi}\left(t - \frac{1}{\bar{\varepsilon}}\right) P_{qG}\left(\frac{x}{y}\right) + \alpha_s f_{G,2}\left(\frac{x}{y}\right) G_o(y) \right\} \right. \qquad (1)$$

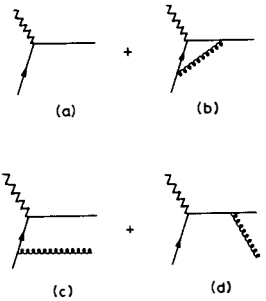

Fig. 1 - *Diagrams contributing to the process* $\gamma^* + q \to q + X$ *through to order* α_s.

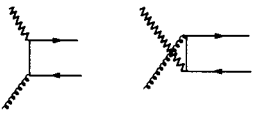

Fig. 2 - *Diagrams contributing to the process* $\gamma^* + G \to q + X$ *in order* α_s.

where $t = \ell n(Q^2/\mu^2)$, $1/\hat{\epsilon} = 1/\epsilon + \ell n 4\pi - \gamma_\epsilon$ and μ is an arbitrary mass-scale and $q_o(y)$ and $G_o(y)$ indicate bare parton distribution functions.

$$P_{qq}(z) = \frac{4}{3}\left[\frac{1+z^2}{(1-z)_+} + \frac{3}{2}\delta(z-1)\right] \quad , \quad P_{qG} = \frac{1}{2}\left[z^2 + (1-z)^2\right] \tag{2}$$

and

$$\alpha_s f_{q,2}(z) = \frac{\alpha_s}{2\pi}\frac{4}{3}\left\{(1+z^2)\left(\frac{\ell n(1-z)}{1-z}\right)_+ - \frac{3}{2}\frac{1}{(1-z)_+} - \frac{1+z^2}{1-z}\ell n\, z + 3 + 2z - \left(\frac{9}{2} + \frac{\pi^2}{3}\right)\delta(z-1)\right\} \tag{3}$$

$$\alpha_s f_{G,2}(z) = \frac{\alpha_s}{2\pi}\frac{1}{2}\left\{(z^2 + (1-z)^2)\,\ell n\left[\frac{(1-z)}{z}\right] + 6z(1-z)\right\} \tag{4}$$

The coefficients of the singularities in Eq. (1) are the normal Altarelli-Parisi functions [4]. In accordance with the philosophy outlined above we define the "renormalized" quark distribution functions beyond the leading order by [1]

$$q(x,t) \equiv \frac{F_2(x,t)}{x} \tag{5}$$

We now proceed to the corresponding calculation for the Drell-Yan process. The corresponding diagrams are shown in Figs. 3 and 4. The contribution to the total cross-section is given by (dropping obvious over-all factors) :

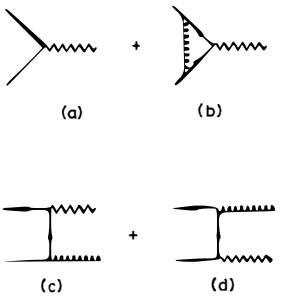

Fig. 3 - Diagrams contributing to the process $q+\bar{q}\to\gamma^*+X$ *through to order* α_s.

Fig. 4 - Diagrams contributing to the process $q+G\to\gamma^*+X$ *in order* α_s.

$$\frac{d\sigma^{DY}}{dQ^2} \sim \int_o^1 \frac{dx_1}{x_1} \int_o^1 \frac{dx_2}{x_2} \left\{ \left[q_o^{[1]}(x_1)\, \bar{q}^{[2]}(x_2) + (1 \leftrightarrow 2) \right] \cdot \left[\delta(z-1) + \theta(1-z) \left(\frac{\alpha_s}{2\pi} 2\, P_{qq}(z) \left(t - \frac{1}{\hat{\epsilon}} \right) + \alpha_s\, f_{q,DY}(z) \right) \right] + \left[\left(q_o^{[1]}(x_1) + \bar{q}_o^{[1]}(x_1) \right) G_o^{[2]}(x_2) + (1 \leftrightarrow 2) \right] \cdot \left[\theta(1-z) \frac{\alpha_s}{2\pi} \left(t - \frac{1}{\hat{\epsilon}} \right) P_{qG}(z) + \alpha_s\, f_{G,DY}(z) \right] \right\} \tag{6}$$

where $z = Q^2/Sx_1x_2$ and the finite parts are :

$$\alpha_s\, f_{q,DY}(z) = \frac{\alpha_s}{2\pi} \frac{4}{3} \left\{ 4 (1+z^2) \left(\frac{\ell n(1-z)}{1-z} \right)_+ - 2 \frac{1+z^2}{1-z} \ell n\, z + \left(\frac{2\pi^2}{3} - 8 \right) \delta(z-1) \right\} \tag{7}$$

$$\alpha_s f_{G,DY}(z) = \frac{\alpha_s}{2\pi}\ \frac{1}{2}\left\{\left(z^2+(1-z)^2\right)\ \ell n\ \frac{(1-z)^2}{z}\ -\ \frac{3}{2}\ \ z^2 + z + \frac{3}{2}\right\} \tag{8}$$

Using these relations we find for the total Drell-Yan cross-section the formula

$$\frac{d\sigma}{dQ^2} \sim \int \frac{dx_1}{x_1}\ \frac{dx_2}{x_2}\ \left\{\left[q^{[1]}(x_1,t)\ \bar{q}^{[2]}(x_2,t) + (1 \leftrightarrow 2)\right]\cdot\right.$$
$$\cdot\left[\delta(1-z) + \alpha_s(t)\ \Theta\ (1-z)\ \left[f_{q,DY}(z) - 2f_{q,2}(z)\right]\right]$$
$$+\ \left[\left(q^{[1]}(x_1,t) + \bar{q}^{[1]}(x_1,t)\right)\ G^{[2]}(x_2,t) + (1 \leftrightarrow 2)\right]\cdot$$
$$\left.\cdot\left[\alpha_s(t)\ \Theta\ (1-z)\ \left(f_{G,DY}(z) - f_{G,2}(z)\right)\right]\right. \tag{9}$$

where [1), 2)]

$$\alpha_s\left(f_{q,\ DY}(z) - 2f_{q,2}(z)\right) = \frac{\alpha_s}{2\pi}\ \left\{\frac{4}{3}\left[\frac{3}{(1-z)_+}\ - 6 - 4z + 2(1+z^2)\left(\frac{\ell n(1-z)}{1-z}\right)_+\right.\right.$$
$$\left.\left. + \left(1 + \frac{4}{3}\pi^2\right)\ \delta(z-1)\right]\right\} \tag{10}$$

$$\alpha_s\left(f_{G,DY}(z) - f_{G,2}(z)\right) = \frac{\alpha_s}{2\pi}\ \left\{\frac{1}{2}\ \left[\left(z^2+(1-z)^2\right)\ell n(1-z)\right.\right.$$
$$\left.\left. + \frac{9}{2}\ z^2 - 5z + \frac{3}{2}\right]\right\} \tag{11}$$

Although the individual terms Eqs. (3), (4) and (7), (8) are dependent on the particular method chosen to regularize the infra-red divergences any such dependence cancels out in the differences Eqs. (10), (11).

In order to make a preliminary estimate of the size of these terms we define moments as

$$f^{(n)} = \int_0^1 \frac{dz}{z} \; z^n \; f(z) \tag{12}$$

In Fig. 5 we have plotted the quantities in curly brackets in Eqs. (10) and (11), so that in the case of the $q\bar{q}$ terms the scale of the corrections is given by multiplying the quantity plotted by $\alpha_s/2\pi$. Taking a notational value of $\alpha_s/2\pi \sim (1/20)$ appropriate for $Q^2 \sim 100$ GeV^2 we see that for this value of α_s the $q\bar{q}$ corrections are by no means small compared to 1. The gluon corrections (expanded scale) are negative and small. Whilst it is true that in the evaluation of the cross-section the gluon corrections will be convoluted with a substantial gluon distribution tending to increase their effect, for reasonable parametrizations of the gluon distribution they will remain small. We therefore concentrate our attention on the quark-antiquark terms.

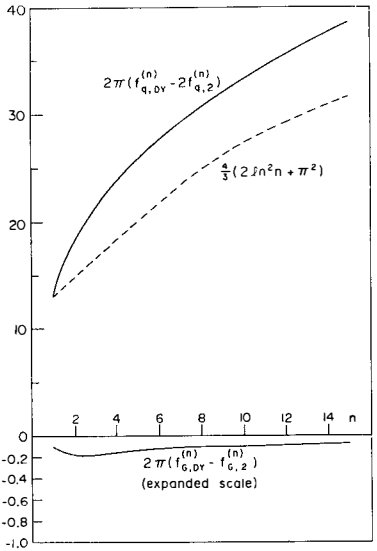

Fig. 5 - Plot of the moments of the Drell-Yan correction terms as a function of n.

The terms in Eq. (10) which are giving large corrections are the last two. Would it have been possible to predict the form of these terms before doing the calculation ? The answer is that in large measure we could have. Consider first of all the logarithmic distribution $2(1+z^2)(\ell n(1-z)/(1-z))_+$. The calculation of the logarithmic terms in the real-gluon emission graphs for the leptoproduction and the Drell-Yan process can be represented, in a slightly schematic notation, as

$$\frac{F_2}{z} \sim \delta(z-1) + \frac{\alpha_s}{2\pi} \; \frac{4}{3} \; \frac{1+z^2}{1-z} \int_{t_{min}}^{t_{max}} \frac{dt}{t} \tag{13}$$

$$\frac{d\sigma^{DY}_{q\bar{q}}}{dQ^2} \sim \delta(z-1) + \frac{\alpha_s}{2\pi} \; \frac{4}{3} \; 2 \; \frac{1+z^2}{1-z} \int_{t_{min}}^{t_{max}} \frac{dt}{t} \tag{14}$$

where the integration over the final two-particle phase space is represented as an integral over the four-momentum transfer squared. The value of t_{min} in Eqs. (13) and (14) is common to both integrals and depends on the particular method chosen to regulate the collinear divergences. The values of t_{max} on the other hand depend on the particular process and are, for leptoproduction

$$t_{max} = \frac{-Q^2}{z} \quad , \quad z = \frac{Q^2}{2p.q} \tag{15}$$

whereas for the Drell-Yan process we have

$$t_{max} = \frac{-Q^2(1-z)}{z} \quad , \quad z = \frac{Q^2}{s} \tag{16}$$

Performing the integration we obtain, in this extended leading logarithmic approximation

$$\alpha_s \left(f_{q,DY} - 2f_{q,2}\right) \sim \frac{\alpha_s}{2\pi} \frac{4}{3} \frac{1+z^2}{(1-z)} \ell n(1-z) \tag{17}$$

The above derivation is valid for values of $z < 1$. In order to see how the expression in Eq. (17) becomes the distribution $(\ell n(1-z)/(1-z))_+$ (a result connected with the cancellation of the soft singularities) we have to consider the also virtual graphs.

The other large term in Eq. (10) is the delta function at $z = 1$ with coefficient $(1+\frac{4}{3}\pi^2)$. A term of size π^2 in this result is associated with the virtual graphs. In DIS we find for the virtual graph, Fig. 1b

$$\Gamma^{\mu}(q^2) = \gamma^{\mu} \left\{ 1 + \frac{\alpha_s}{4\pi} \frac{4}{3} \left(\frac{4\pi\mu^2}{-q^2} \right)^{\varepsilon} \frac{\Gamma(1+\varepsilon)\Gamma^2(1-\varepsilon)}{\Gamma(1-2\varepsilon)} \left[\frac{-2}{\varepsilon^2} - \frac{3}{\varepsilon} - 8 \right] \right\} \tag{18}$$

For DIS, $q^2 = -Q^2 < 0$ whereas for the Drell-Yan process $q^2 = Q^2 > 0$. For the latter process we therefore obtain (Fig. 3b),

$$\text{Re } \Gamma^{\mu}(Q^2) = \gamma^{\mu} \left\{ 1 + \frac{\alpha_s}{4\pi} \frac{4}{3} \left(\frac{4\pi\mu^2}{Q^2} \right)^{\varepsilon} \frac{\Gamma(1+\varepsilon)\Gamma^2(1-\varepsilon)}{\Gamma(1-2\varepsilon)} \left[\frac{2}{\varepsilon^2} - \frac{3}{\varepsilon} - 8 + \pi^2 \right] \right\} \tag{19}$$

The extra π^2 term comes from the mismatch between spacelike and timelike between the two processes. It is important to note that this explains some <u>but not all</u> of the terms proportional to π^2.

More precise estimates of the size of the correction terms are shown in Fig. 6a,b where the quantity

$$K = \frac{\text{Drell-Yan cross-section in } O(\alpha_s)}{\text{Drell-Yan cross-section from naive parton model}} \qquad (20)$$

is plotted for pN and $\pi^- N$ collisions using reasonable parametrizations for the parton densities.

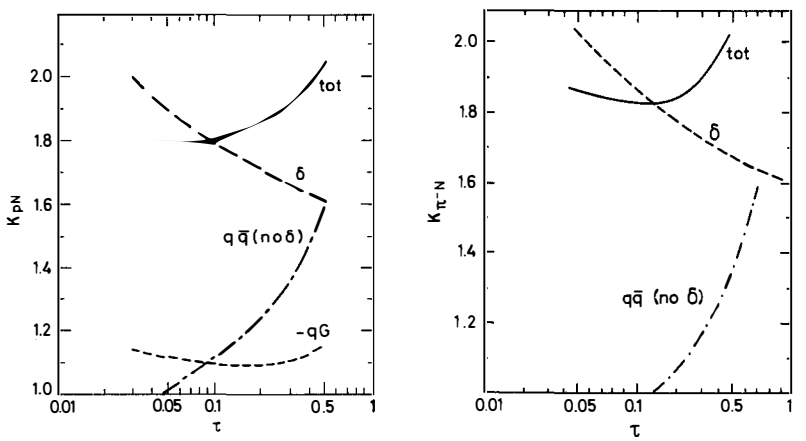

Fig. 6 - Plot of relative contributions to K factor of various pieces of the cross-section for pN scattering (left-hand figure) and $\pi^- N$. scattering (right-hand figure).

For both cases, the total $q\bar{q}$ correction has two components. The correction labelled δ is the piece having the same kinematic structure as the lowest order coming from the delta function in Eq. (10). This term is a decreasing function of τ because as we go out to larger values of τ the running coupling constant $\alpha_s(Q^2)$ decreases. The rest of the correction (as one might expect from the growth with n illustrated in Fig. 5) increases as one goes out to larger values of τ. The end result is that for both cases the total correction is approximately constant at presently accessible values of τ because of these two compensating effects.

The first order corrections to the differential cross-section in the rapditiy or in Feynman x_F have also been calculated. There are no problems in principle in the extraction of the rapidity differential cross-section from the corresponding parton differential cross-section - but the algebra is complicated by the need to make the poles in the differential cross-section manifest so that they may cancel from the final result.

In practice this requires the definition of plus distributions

$$\int_o^1 dx \frac{f(x)}{(1-x)_+} \equiv \int_o^1 dx \frac{f(x) - f(1)}{(1-x)} \tag{21}$$

which are normally defined to span the range from zero to one. Using this definition the plus distribution integrated over a restricted range becomes

$$\int_o^1 dx \frac{f(x)}{(1-x)_+} \equiv \int_o^1 \frac{f(x) - f(1)}{(1-x)} + f(1) \ln (1-a) \tag{22}$$

In the naive parton model the rapidity differential cross-section is given by

$$\frac{Q^2 d^2\sigma}{dQ^2 dx_F} = \frac{A}{(x_1^o + x_2^o)} H_o(x_1^o, x_2^o) \tag{23}$$

where

$$A = \frac{4\pi\alpha^2}{9S}, \quad H_o(x_1,x_2) = \sum_f e_f^2 \left[q_{of}^{[1]}(x_1) \bar{q}_{of}^{[2]}(x_2) + (1 \leftrightarrow 2) \right] \tag{24}$$

and

$$x_1^o = \frac{1}{2}\left(x_F + \sqrt{(x_F^2 + 4\tau)}\right), \quad x_2^o = \tau/x_1^o \tag{25}$$

The full $O(\alpha_s)$ formula takes into account the cascade of partons from values x_1 (x_2) greater than x_1^o (x_2^o) due to the emission of gluons and is given by [1),5)] :

$$\begin{aligned}\frac{Q^2 d^2\sigma}{dQ^2 dx_F} = A \Bigg\{ & \frac{1}{(x_F^2+4\tau)^{1/2}} (H(x_1^o, x_2^o, t) \left[1 + \frac{\alpha_s(t)}{2\pi} \frac{4}{3}\left(\frac{4}{3}\pi^2+1\right)\right] \\ & + \alpha_s(t) \int_{x_1^o}^1 \frac{dx_1}{x_1} H(x_1, x_2^o, t)\, g\left(\frac{x_1^o}{x_1}\right) + \alpha_s(t) \int_{x_2^o}^1 \frac{dx_2}{x_2} H(x_1^o, x_2, t)\, g\left(\frac{x_2^o}{x_2}\right) \Bigg) \\ & + \frac{\alpha_s(t)}{2\pi} \frac{4}{3} \int_{x_1^o}^1 \frac{dx_1}{x_1} \int_{x_2^o}^1 \frac{dx_2}{x_2} \frac{H(x_1, x_2, t)}{(1-z)(x_1+x_2)} \Bigg[-2(1-z) \\ & + \frac{1+z^2}{(1-z)_+} \left(\frac{1}{(1-y^*)_+} + \frac{1}{(y^*)_+} \right) \Bigg] \Bigg\}\end{aligned} \tag{26}$$

where

$$\alpha_s\, g(z) = \frac{\alpha_s}{2\pi}\,\frac{4}{3}\left[-2 - 3z + (1+z^2)\left(\frac{\ln(1-z)}{1-z}\right)_+ + \frac{3}{2}\,\frac{1}{(1-z)_+}\right] \tag{27}$$

and $H(x_1,x_2,t)$ is the analogous function to that defined in Eq. (24) for parton densities defined in terms of Eq. (5) and

$$y^* = \frac{(x_2 - x_2^0)(x_2 + x_1^0)}{x_2(1-z)(x_1+x_2)} \tag{28}$$

The last term in Eq. (26) contains a product of two distributions and must be handled with care. A different treatment of the doubly singular terms and plus distributions is given in Ref. 5) but the formula agrees when account is taken of these differing definitions. For further details and the formula for quark gluon scattering the reader is referred to Refs. 1), 5).

It turns out, as illustrated in Fig. 7, that the enhancement of the cross-section above its naive parton model value is substantially independent of y. This result is not unexpected in view of the connection of the large terms with soft radiation.

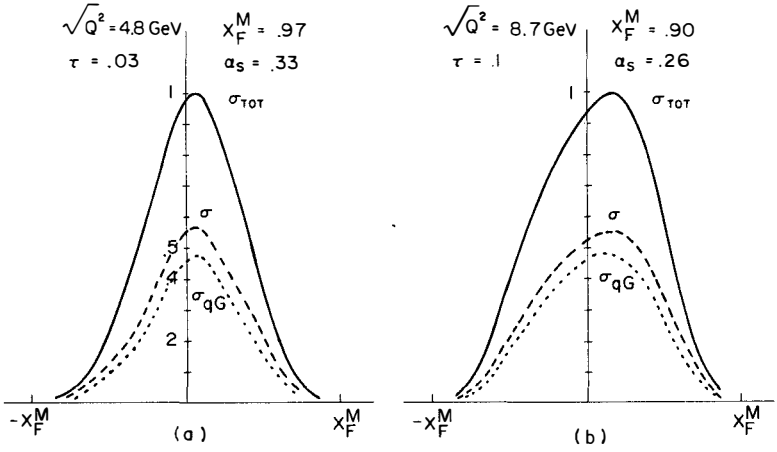

Fig. 7 - Corrected x_F differential cross-section (solid line), lowest order differential cross-section (dashed line) and quark gluon contribution (dotted line) plotted vs. x_F. Only relative normalization of the curves is important. Curves are for pN scattering at $\sqrt{s}$ = 27 GeV.

The conjectured form of the resummed Drell-Yan cross-section [6] is based on simple arguments coming from QED. The quark form factor is believed to have an asymptotic form

$$F(q^2) \to \exp -\frac{4}{3}\int^{Q^2} dq_T^2 \; \frac{\alpha_s(q_T^2)}{2\pi} \; \frac{\ell n(q_T^2)}{q_T^2} \tag{29}$$

which leads to a form for the squares of the form factor

$$\lim_{Q^2\to\infty} \left|\frac{F(Q^2)}{F(-Q^2)}\right|^2 = \exp\left[\frac{4}{3} \; \frac{\alpha_s(Q^2)}{2\pi} \; \pi^2\right] \tag{30}$$

In a similar vein the $\ell n^2 n$ pieces illustrated in Fig. 5 can be treated

$$F_2^{(n)} \sim 1 + \frac{\alpha_s(Q^2)}{2\pi} \; \frac{4}{3} \; \ell n^2 \, n \to \exp \frac{\alpha_s(Q^2)}{2\pi} \; \frac{4}{3} \; \ell n^2 \, n \tag{31}$$

$$\frac{d\sigma^{(n)}}{dQ^2} \sim 1 + \frac{\alpha_s(Q^2)}{2\pi} \; \frac{16}{3} \; \ell n^2 \, n \to \exp \frac{\alpha_s(Q^2)}{2\pi} \; \frac{16}{3} \; \ell n^2 \, n \tag{32}$$

We therefore find a form for the dominant terms in the moments of the K factor given by

$$K^{(n)} = \left|\frac{F(Q^2)}{F(-Q^2)}\right|^2 \; \frac{\exp\left[\frac{\alpha_s(Q^2)}{2\pi} \; \frac{16}{3} \; \ell n^2 \, n\right]}{\exp\left[\frac{\alpha_s(Q^2)}{2\pi} \; \frac{8}{3} \; \ell n^2 \, n\right]} \tag{33}$$

In view of the experimental importance of the K factor it is clearly of great importance to try and put formulae such as Eq. (33) on a firmer theoretical basis. At a simpler level there is still much work to be done checking which other hadronic processes undergo similar enhancements.

REFERENCES

1) G. Altarelli, R.K. Ellis and G. Martinelli - Nuclear Phys. B143 (1978) 521 (E:B146(1978)544), Nuclear Phys. B157 (1979) 461.

2) J. Kubar-André and F.E. Paige - Phys.Rev. D19 (1979) 221.

3) J. Lefrançois - Rapporteur's talk at the Madison Conference.

4) G. Parisi - Proc. 11th Rencontre de Moriond (1976), Ed. J. Tran Thanh Van. G. Altarelli and G. Parisi - Nuclear Phys. B126 (1977) 298.

5) J. Kubar-André et al. - Nuclear Phys. B175 (1980) 251. G. Plaut - These proceedings.

6) G. Parisi - Phys.Letters 90B (1980) 295 ; M. Greco and G. Pancheri - These proceedings.

FIRST ORDER CORRECTIONS TO LEPTON PAIR PRODUCTION IN PERTURBATIVE QCD

G. PLAUT

Physique Théorique, Université de Nice

ABSTRACT : We have recently computed the differential cross section $\frac{d\sigma}{dQ^2\, dy}$ for lepton pair production, and the decay angular distribution of the pair up to first order in the strong coupling constant α_s. In this contribution we insist on the present status of such calculations as a first step beyond the LLA. Then attention is forcussed on the way we handle infrared and colineard sigularities. We show some numerical results and briefly comment about the suprisingly good phenomenology one gets with first order corrections to the Drell-Yan model in perturbative QCD. In particular the "K-factor" is found to be approximately constant in πp and pp collisions, in good agreement with the CERN-NA3 experiment, so that in the framework of this first order calculation the shape of the pion structure function extracted from dilepton production in πp collisions is approximately correct.

I. INTRODUCTION

Lepton pair production is now a classical topic in perturbative QCD. The zeroth order is just the so-called "naive" Drell-Yan model [1]. First order corrections include both initial and final single gluon graphs, and virtual gluon corrections (fig.1).

The "naive" model alone yields a cross-section which has quite a right shape but is too small by a factor of 2. Moreover it cannot account for the observed transverse momenta of the lepton pairs. First order (FO) corrections go in the right direction for both diseases (size of the cross-section, transverse momenta), but they suffer from infrared and colinear divergences and have to be regularized. Infrared divergences cancel when one adds real and virtual gluon contributions; to get rid of colinear singularities, one uses Politzer's observation that they are universal so that they can be consistently absorbed into the unknown, uncalculable bare structure functions [2]. One thus gets universal "effective Q^2-dependent structure functions", in terms of which corrections to the naive Drell-Yan model are finite.

Indeed, when these singularities have been removed, there remain to all order large logarithms (typically $\ln Q^2/Q_0^2$) which are in a manner their remembrance, and have to be summed in some way if one wants a perturbative expansion to make sense; the summation is achieved in the so-called leading log approximation (LLA) where it amounts to perform the evolution of the structure functions with Q^2 [2,3,4].

In this contribution I will present the main points of our recent calculation [5,6] of FO corrections to the Drell-Yan model. These calculations can be viewed as a first step beyond the LLA and as an illustration of universality up to first order in α_s. I will insist on both points of view as well as on the way we handle the singularities of the partonic cross-section and on the numerical results. So, in part II, I will try to situate our calculation within the framework of the LLA. Then I will present in part III our explicit calculation of the singular part of annihilation graphs to FO in α_s. Part IV will be devoted to some comparison with experiment whereas, in part V, I will deal with FO corrections to decay angular distributions.

II. THE LEADING LOG APPROXIMATION AND THE FIRST ORDER CORRECTIONS

In this part, we want to situate briefly our FO calculation as a first step beyond the LLA. We first recall the regularization algorithm initiated by Politzer [2]; for simplicity, we limit ourselves to FO in α_s; to this order the deep inelastic scattering (DIS) structure function F_2 is given by formula (10) of the compendium by K.Ellis [7]. We use his formulae and notations, to define an

effective Q^2-dependent structure function (SF) $q_f(x,Q^2)$ in terms of the bare SF $q_{0f}(x,Q^2)$:

$$F_2(x,Q^2)/x = \sum_f e_f^2 \, q_f(x,Q^2) = \sum_f e_f^2 \left[q_{0f}(x) + \Delta q_f(x,Q^2) \right] \qquad (1)$$

One can see in ref.4) that Δq_f so defined includes both constant corrections and large logs. Keeping only the logs, one can evaluate the moments of q_f with respect to x and find [2,3] :

$$q_f^{(n)}(Q^2) = q_{0f}^{(n)} \, (1 + \alpha_s \, a_n \, \ell n \, Q^2/\mu^2) \qquad (2)$$

where a_n is the moment of some function. The bracket in the RHS of (2) diverges when $\mu \to 0$. However, following Politzer, we do not bother about this divergence since it has to cancel with some corresponding infinity in $q_{0f}^{(n)}$, in order for the physically significant quantity $q_f^{(n)}(Q^2)$ to be finite.

If one now defines effective SF in the Drell-Yan process and compute them up to the same FO in α_s, one finds the same FO correction $\alpha_s \, a_n \, \ell n \, Q^2/\mu^2$ to the moments of the bare SF. This is the famous miracle of universality, not fully a miracle however since the same Feynman graphs occur in both reactions; the definition of the effective SF is thus the same in the DY process and in DIS. Universality may be proved (in a highly non trivial way) to hold to all orders in the LLA, and, as a consequence, the DY model is exact in the LLA provided one uses Q^2-dependent SF extracted from DIS.

A possible first step beyond the LLA consists in keeping, in addition to the leading logs to all orders, constant terms up to order α_s [5,8]. This we have done in ref.5) where we compute (keeping both logarithmic and constant terms) the lepton pair production cross-section up to FO in α_s, in terms of the DIS structure functions. The leading logs are then incorporated to all orders through the use of Q^2-dependent SF à la Altarelli-Parisi [4]. As an illustration of universality, we observe that all infrared and colinear divergences as well as log Q^2 terms cancel in the final results which amount to finite corrections to the DY term.

III. ANNIHILATION CORRECTIONS TO FIRST ORDER IN α_s

We have computed in ref.5) all logarithmic and constant FO corrections to the Drell-Yan model according to the scheme discussed in part II. Here I will focus my attention on the singular terms coming from annihilation graphs. My notations are those of ref.5); when I consider partonic subprocesses, I call t_1 and t_2 the fractions of incident hadron momenta taken by initial partons. We thus have for the hadronic cs :

$$d\sigma/dQ^2\, dy = \sum_i \int_{x_1}^1 dt_1 \int_{x_2}^1 dt_2\, Q_i(t_1, t_2)\, d\hat{\sigma}^i/dQ^2\, dy \qquad (3)$$

where $x_1 = \sqrt{\tau}\exp(y)$, $x_2 = \sqrt{\tau}\exp(-y)$ as in ref.7). $Q_i(t_1, t_2)$ is a suitable product of SF depending on the subprocess, and $d\hat{\sigma}^i/dQ^2\, dy$ is the corresponding partonic cs. To regularize, we chose to take massless quarks, but massive gluons with a mass $\mu \to 0$ [5]. Thus the singular terms which have to disappear in the final results are of the form $\ell n\, Q^2/\mu^2$ or $\ell n^2\, Q^2/\mu^2$.

We compute the partonic annihilation cs in three steps :

i) First step. We consider the subgraphs of fig. 1b. Defining the Mandlestam variables in the usual way, we find :

$$\frac{d\hat{\sigma}^A}{dQ^2\, dy} = A\, \frac{\tau(\tau + t_1 t_2)}{t_1 t_2\, (t_1 x_2 + t_2 x_1)^2} \left\{ \frac{\hat{s}^2 + Q^4}{\hat{t}\,\hat{u}} - 2 - \mu^2 Q^2 \left(\frac{1}{\hat{t}^2} + \frac{1}{\hat{u}^2} \right) \right\} \qquad (4)$$

where $A = 16\,\alpha^2\,\alpha_s/27\,SQ^2$. Henceforth, we focus on the first term in (4) which may be seen to be the only singular one on the frontier of the phase space when $\mu \to 0$. Indeed $\hat{t}\,\hat{u} \simeq \hat{s}\, q_\perp^2 + \mu^2 Q^2$ and this term may be written :

$$d\hat{\sigma}_1^A/dQ^2\, dy = A\, R(t_1, t_2, x_1, x_2)/D(t_1, t_2, x_1, x_2) \qquad (5)$$

where R is a regular function and :

$$D(t_1, t_2, x_1, x_2) = (t_1 - x_1)(t_2 - x_2) + (\mu^2/2S)(\tau - t_1 t_2)/(t_1 t_2) \qquad (6)$$

It is convenient to divide the domain of integration in the (t_1, t_2) plane into four parts; for this purpose we introduce an auxiliary small number ε which has to verify $1 >> \varepsilon >> \mu^2/S$. The function D^{-1} gets singular in regions I, II, III when $\mu \to 0$ (see fig. 2). To get tractable expressions, we replace the singular contributions by distributions with accurate weights before going to the limit $\mu \to 0$:

$$D^{-1} \xrightarrow[\mu \to 0]{} \delta(t_1 - x_1)\, \delta(t_2 - x_2) \int_{(I)} D^{-1} dt_1 dt_2 + \delta(t_2 - x_2)\, \theta_\varepsilon(t_1) \int_{(II)} D^{-1} dt_2$$
$$+ \delta(t_1 - x_1)\, \theta_\varepsilon(t_2) \int_{(III)} D^{-1} dt_1 + \theta_\varepsilon(t_1)\, \theta_\varepsilon(t_2)\, D^{-1} \qquad (7)$$

where $\theta_\varepsilon(t) = \theta(t - (1 + \varepsilon)\, x)$. One has to compute the weights assigned to the singular distributions in (7) before taking the limit $\varepsilon, \mu \to 0$. Region (I) gives the so-called infrared singularity. One has indeed :

$$\int_{(I)} D^{-1} dt_1 dt_2 \xrightarrow[\substack{\mu\to 0\\ \varepsilon\gg\mu}]{} \int_{(I)} \frac{dt_1\, dt_2}{(t_1-x_1)(t_2-x_2)} = \frac{1}{2}\ \ell n^2\ \frac{Q^2\,\varepsilon^2}{\mu^2} \qquad (8)$$

(note that $\ell n\varepsilon$ are artifical singularities which disappear in the final result). Dealing in the same way with regions II and III, we finally get for D^{-1} the following sum of distributions :

$$D^{-1} \xrightarrow[\mu\to 0]{} \delta(t_1 - x_1)\ \delta(t_2 - x_2)\ \frac{1}{2}\ \ell n^2\ \frac{Q^2\,\varepsilon^2}{\mu^2} \qquad (9)$$
$$+\ \theta_\varepsilon(t_1)\ \frac{\delta(t_2 - x_2)}{t_1 - x_1}\ \ell n\ \frac{2Q^2\ (t_1 - x_1)\ t_1\varepsilon}{\mu^2 x_1 (t_1 + x_1)} + (1\leftrightarrow 2) + \theta_\varepsilon(t_1)\ \theta_\varepsilon(t_2)\ D^{-1}$$

In the next two steps, we will see that the large logs in $d\hat{\sigma}_1^A$ (coming from (9)) cancel with those coming from the contributions we now take into account.

ii) Second step. We add the virtual corrections of order α_s which give the following contribution : (10)

$$d\hat{\sigma}^V/dQ^2\ dy = 1/2\ A\ \delta(t_1 - x_1)\ \delta(t_2 - x_2)\ \left[-\ \ell n^2 Q^2/\mu^2 + 3\ell n Q^2/\mu^2 - 7/2 + \pi^2/3\right]$$

When $d\hat{\sigma}^V$ is added to $d\hat{\sigma}_1^A$, the $\ell n^2 Q^2/\mu^2$ are seen to cancel according to the Block-Nordsiek theorem.

iii) Third step. To benefit from universality, we make the substitution :

$$q_0(x) \to q_0(x) + \Delta q^{DIS}(x,Q^2) - \Delta q^{DIS}(x,Q^2) = q(x,Q^2) - \Delta q^{DIS}(x,Q^2) \qquad (11)$$

in the DY term. $q(x,Q^2) = q_0 + \Delta q$ is the effective DIS structure function computed up to the same order α_s within the same regularization scheme. Remark we need here only the quarkonic part of Δq^{DIS}; the gluonic part has to be added to the Compton FO correction. We find the following FO correction to the DY cross-section [9] :

$$\frac{d\,\hat{\sigma}^{DIS(1)}}{dQ^2 dy} = -\ \frac{1}{2}\ A \left\{\delta(t_1-x_1)\ \delta(t_2-x_2)\left[\frac{3}{2}\ \ell n^2\ \frac{Q^2}{\mu^2} - 2\frac{\pi^2}{3} - \frac{9}{4} + 2\ell n\varepsilon\ \ell n\ \frac{Q^2}{\mu^2}\right.\right.$$
$$\left. + \ell n^2\varepsilon - \frac{3}{2}\ \ell n\varepsilon\right] + \theta_\varepsilon(t_1)\ \delta(t_2-x_2)\left[\left(1 + \frac{x_1^2}{t_1^2}\right)\frac{1}{t_1-x_1}\ \ell n\ \frac{Q^2 t_1 (t_1-x_1)}{\mu^2\, x_1^2}\right.$$
$$\left.\left. - \frac{3}{2(t_1-x_1)} + \frac{1}{t_1} + \frac{4x_1}{t_1^2}\right]\right\} \quad ; \qquad (12)$$

the superscript (1) indicates that we have listed the contribution coming from $\Delta q(x_1,Q^2)$; the similar contribution from $\Delta q(x_2,Q^2)$ has to be added. Adding $d\hat{\sigma}^A_1$, $d\hat{\sigma}^V$ and $d\hat{\sigma}^{DIS}$, one can verify that all infrared and colinear divergences cancel so that the final result is free from $\ell n \frac{Q^2}{\mu^2}$ and $\ell n^2 \frac{Q^2}{\mu^2}$ terms. It is composed of finite terms; however the expression is very long and we refer the interested reader to ref. 5) since our goal in this contribution is not to show all calculations but to illustrate how things work.

IV. PHENOMENOLOGICAL CALCULATIONS AND DISCUSSION

The annihilation and Compton FO corrections of ref. 5) have been folded by products of SF and integrated over t_1 and t_2. To be consistent with our previous discussion about the necessity to sum large logs to all orders, we used Q^2-dependent SF such as those of Owens and Reya [10]. Notice however that in ref. 5) we also tried scaling SF in order to check the dependence of FO corrections on the choice of SF. Before going into some details, we want to point a remarkable feature of FO corrections : at given (y, Q^2) or, equivalently (x_1, x_2)*, the annihilation correction is usually large ($\sim \sigma^{DY}$) and positive, whereas the Compton correction is usually small ($\sim 10\%$ of σ^{DY}) and negative. So, the addition of FO corrections roughly amounts to multiply the naive σ_{DY} by a factor of 2. To be more precise, we define as usually a K-factor by :

$$K(y,Q^2) = (\sigma^{DY} + \sigma^A + \sigma^C)/\sigma^{DY} = \sigma^{(1)}(y,Q^2)/\sigma^{(0)}(y,Q^2) \qquad (13)$$

1) Proton-proton scattering. We note on fig.2 the very weak dependence of K on y (at least for Q^2-dependent SF). To illustrate in an other way this constancy, we computed in ref.5) $K(x_1,x_2)$ for (x_1,x_2) in the range $10\ GeV^2 < Q^2 < 100\ GeV^2$; we found an average $\bar{K} = 1.95$ with a very small standard deviation $\sigma = 0.04$. These results compare quite well with the experimental value [11] $K = 2.2 \pm .4$. Such an agreement has even something intriguing since one has not genuine arguments that things will not considerably change to next order in α_s !

2) Pion-proton scattering. In the same range of Q^2-values, we find $\bar{K} = 1.78$ and $\sigma = 0.14$ with the SF of Owens and Reya**. The constancy of K (within 10% error

---

* Let us recall that the results we show are integrated over the full range of $q_\perp$ since to integrate over (t_1,t_2) at given (y,Q^2) is identical to integrate over $\vec{q}_\perp$.

** In facts, we took $Q_0^2 = 25\ GeV^2$ for pion SF, not $3\ GeV^2$ like in ref 10), since experiment [11] suggests the counting rules to be approximately valid at this value of Q^2.

bars) has the important phenomenological consequence that lepton pair production from pions on protons can be used to measure the pion SF with a rather good accuracy. Indeed, in πp collisions, the DY cross-section is dominated by the annihilation of the valence antiquark from the pion with the corresponding valence quark from the proton, so that the full cross-section

$$\sigma^{(1)}(x_1,x_2) \approx \overline{K}\,\sigma^{DY}(x_1,x_2) \simeq \overline{K}\,\bar{q}_\pi(x_1)\,q_p(x_2) \qquad (14)$$

almost factorizes.

In ref. 6), we also computed the average QCD-transverse momentum of the pair. In view of the large values of K, we thought it would be better (although quite questionable) to normalize with $\sigma^{(1)} = \sigma^{DY} + \sigma^{A} + \sigma^{C}$. Our results agree with those of ref. 12), except of course for the normalization. Let us notice that we predict a slow decrease of $\langle q_\perp^2 \rangle$ with $\tau = Q^2/S$, whereas data shown by Badier at this meeting seem to indicate some (slight) increase.

To conclude part IV, QCD-FO corrections to the Drell-Yan model generally work surprisingly well from a phenomenological point-of-view; in particular the K-factor is predicted to be practically constant, so that the factorization of the zeroth order cross-section almost extends to the FO (see formula (14)). The calculated value of $K \simeq 2$ is in good agreement with experiment. However, there are some discrepancies between the calculated and measured $q_\perp$'s; we think other mechanisms may be important for $q_\perp$'s, like gluon emission to all orders [13].

V.ANGULAR DECAY DISTRIBUTION

In view of the agreement between FO phenomenology and experiment for cross-sections, it was natural to consider also FO corrections to the angular decay distribution of the pair in its rest-frame. Remember the "naive" Drell-Yan model predicts the decay distribution to be $1 + \cos^2\theta$ in the Gottfried-Jackson frame of the pair. So the question we now turn to is the following : how do FO corrections change this prediction ? Several calculations of FO ocrrections to the lepton pair decay angular distribution exist in the litterature [14], but the authors used unregularized cross-sections, so they could not approach $q_\perp = 0$. To our knowledge, our calculation [6] is the first one which allows one to integrate over the full range of $q_\perp$*. For a given set of partonic variables (x_1,

---

* However, earlier calculations of coefficients like $\hat{K}$, $\hat{G}$, and $\hat{H}$ in formula (15) below, allowed us to partially check our formulae (see ref. 6)).

x_2, t_1, t_2), we got a cross-section of the form :

$$d\hat{\sigma}^{(A,C)}/dQ^2\ dy\ d\Omega = 3/16\pi \times d\hat{\sigma}^{(A,C)}/dQ^2\ dy \times (1 + \cos^2\theta) \qquad (15)$$
$$+ \hat{K}^{(A,C)}(1 - 3\cos^2\theta)/2 + \hat{G}^{(A,C)} \sin 2\theta \cos\phi + \hat{H}^{(A,C)} \sin^2\theta \cos 2\phi/2$$

where we have no more integrated over the solid angle $\Omega(\theta,\phi)$ of the pair. $\hat{K}$, $\hat{G}$ and $\hat{H}$ are rather complicated functions of t_1, t_2, x_1, and x_2, and are listed in ref. 6). They receive contributions from both annihilation (A) and Compton (C) graphs. Since we have the regularized cross-section formulae of part III and ref. 5) at our disposal, we may integrate (15) over the partonic variables t_1 and t_2, after suitably folding it by products of SF. The result can be put in the form :

$$d\sigma/dQ^2\ dy\ d\Omega = C(y,Q^2)\ \{1 + \lambda\cos^2\theta + \mu \sin 2\theta\ \cos\phi + \frac{\nu}{2} \sin^2\theta \cos 2\phi\} \qquad (16)$$

where $C(y,Q^2) = d\sigma/dQ^2\ dy/4\pi\ (1 + \lambda/3)$, and λ, μ, and ν are trivially related to the normalized (i.e. divided by $d\sigma/dQ^2 dy$) integrals of $\hat{K}$, $\hat{G}$ and $\hat{H}$ folded by SF. Note that we have $\lambda = 1 - 2\nu$.

The numerical results look very similar for πp and pp collisions, so we only show on fig.4 λ, μ and ν as functions of y at given Q^2 (in the Gottfried-Jackson frame) for pp collisions. It is straightforward to realize that FO corrections very weakly affect the predictions of the naive DY model. These predictions are actually rather well verified; for instance [15] :

i) pp ISR data integrated over **x** and $q_\perp$ give $1 + (1.15 \pm .34)\cos^2\theta$

ii) the πN CIP collaboration found $1 + \cos^2\theta$ except at large **x** values

where the departure of λ from 1 may well be accounted for by higher twist effects [16] which we neglected; anyway, the lepto-production cross-section is very small at such values of **x**.

VI. CONCLUDING REMARKS

Our conclusion is that the situation looks truely perturbative for decay angular distributions, in contrast with that for cross-sections. But the intriguing point is that in both cases the phenomenology one gets with FO corrections is surprisingly good : quantities which do not need to change (because they roughly agree with experiment) don't : shape of cross-sections, angular distributions; quantities which should change (because they do not agree with experiment) do : K-factors !

1. S.D. DRELL and T.M. YAN, Phys. Rev. Lett. 25 (1970) 316; Ann. Phys. (N.Y.) 66

2. H.D. POLITZER, Nucl. Phys. B129 (1977) 301.

3. See, e.g. E. REYA, Perturbative Quantum Chromodynamics, DESY 79-88, DO.TH 79-20 preprint, and references quoted therein.

4. G. ALTARELLI and G. PARISI, Nucl. Phys. B126 (1977) 298.

5. J. KUBAR, M. LE BELLAC, J.L. MEUNIER and G. PLAUT, Nucl. Phys. B175 (1980) 251.

6. T. GRANDOU, J.L. MEUNIER and G.PLAUT, to be published in Phys. Lett.

7. R.K. ELLIS, A compendium of formulae for lepton pair production, these Proceedings.

8. G. ALTARELLI, R.K. ELLIS and G. MARTINELLI, Nucl. Phys. B143 (1978) 521 (E : B146 (1978) 544) ;
K. HARADA, T. KANEKO and N.SAKAI, Nucl. Phys. B155 (1979) 169.

9. Y. GABELLINI, Thèse de 3è cycle, Université de Nice, (1980), unpublished.

10. J. OWENS and E. REYA, Phys. Rev. D17 (1978) 3003.

11. J. BADIER et al., Phys. Lett. 89B (1979) 145.

12. M. GLUCK and E. REYA, Nucl. Phys. B145 (1978) 24.

13. See contributions by G. PANCHERI-SRIVASTAVA, and D.M. SCOTT at this meeting.

14. K. KAJANTIE, J. LINDFORS and R.RAITIO, Nucl. Phys. B144 (1978) 422 ;
J. CLEYMANS and M.KURODA, Phys. Lett. 80B (1979) 385 ;
R.L. THEWS, Phys. Rev. Lett. 43 (1979) 987.

15. J. LEFRANCOIS, Proceedings of Madison Conference (1980).
E.L. BERGER and S.J. BRODSKY, Phys. Rev. Lett. 42 (1977) 940.

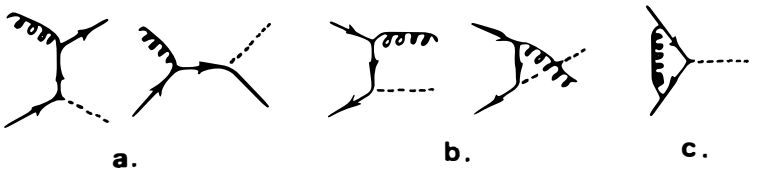

Fig.1. a) Compton graphs. b) Annihilation graphs : gluon production.
c) Virtual gluon correction.

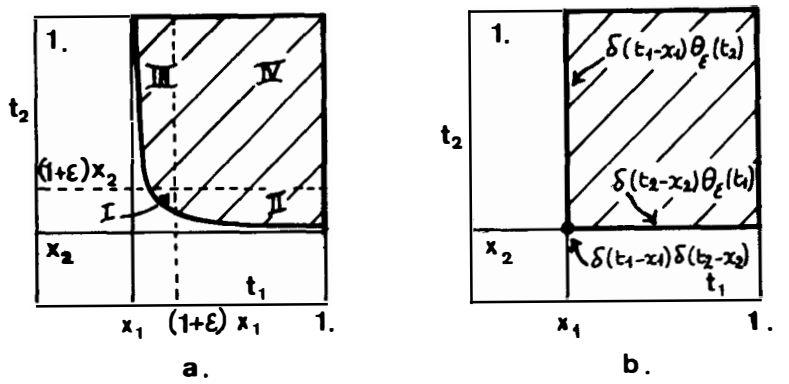

Fig.2. The domain of integration in the (t_1,t_2) plane.
a) $1 >> \varepsilon >> \mu^2/S$ but ε, $\mu \neq 0$. The hyperbola $(t_1-x_1)(t_2-x_2) = \mu^2/S$ which limits this domain is shown.
b) The limit ε, $\mu \simeq 0$, and the singular distributions appearing.

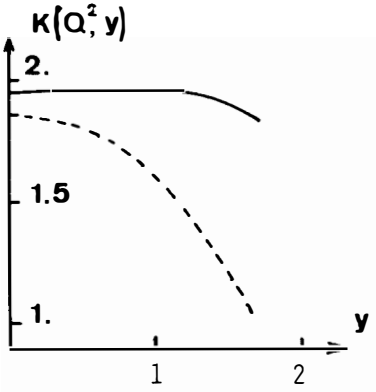

F.3. The factor $K(Q^2, y)$ as a function fo y for pp collisions at $S = 729$ $(GeV)^2$ and $Q^2 = 25$ $(GeV)^2$. Full line : Q^2 dependent SF. Sashed line : scaling SF.

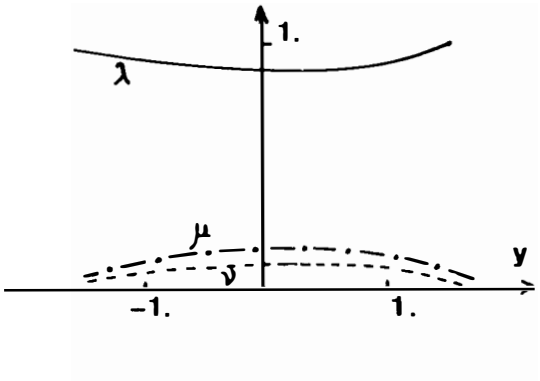

Fig.4. λ, μ, and ν decay coefficients at $Q^2 = 20$ $(GeV)^2$ and $S = 729$ $(GeV)^2$ as functions of y in pp collisions.

SUMMING QCD SOFT CORRECTIONS

M. Greco
INFN, Laboratori Nazionali di Frascati, Italy

ABSTRACT

In this review the effect of soft gluon emission in hard process is discussed to all orders in QCD. A general formalism for resumming these large corrections is presented and detailed implications are considered for deep inelastic leptoproduction, Drell-Yan processes and e^+e^- annihilation. A short discussion of $k_\perp$ effects in Drell-Yan and e^+e^- jets is also presented.

Leading logarithmic analyses (LLA) i.e. a summation of all terms of the type $(\alpha_s(Q^2)\ln Q^2)^n$, have been very useful in understanding the corrections to the Born terms in the perturbative Quantum Chromo-Dynamics (QCD) treatments of hard processes[1]. More recently, accurate computations of non leading corrections have been performed in various processes and often found[1, 2] numerically large, particularly near the boundary of the phase space. These results cast doubt on the validity of the perturbative series at present energies, unless these large non leading terms can be summed up to all orders. However the effect of higher order corrections can be possibly minimized by a judicious choice of the renormalization prescription, in other words by a better definition of the expansion parameter. Much work has been done along this line[3]. Furthermore it has been also realized the important role played by soft gluon effects and simple resummation techniques have been proposed[4, 5, 6] which take into account a large part of higher order corrections.

In this talk I will briefly review this latter subject, discussing in detail various hard processes where the emission of soft QCD radiation is quantitatively relevant. After recalling the main results from first order calculations and a discussion of their physical origin, I will present a general formalism for resumming these large soft corrections based on the scheme of coherent states. Next, detailed implications for deep inelastic scattering, Drell-Yan process and e^+e^- annihilation will be given. To conclude, a short discussion of $k_\perp$ effects in Drell-Yan processes as well as in e^+e^- jets will be presented. Higher twist contributions and more general mass effects will be neglected in our discussion. Further details on the topics studied here can be also found in various and more extensive reviews which are listed in ref. [1].

Let us start with deep inelastic leptoproduction. The quark densities $q_k(x,t)$, defined for example in terms of the structure function $\mathcal{F}_2(x,t)$ as

$$\mathcal{F}_2(x,t) = \sum_k e_k^2 q_k(x,t) , \tag{1}$$

to first order in α_s satisfy the following equation[7]

$$q_k(x,t) = \int_x^1 \frac{dy}{y}\left[\delta(1-\frac{x}{y}) + \frac{\alpha_s}{2\pi} t P_{qq}(\frac{x}{y}) + \alpha_s f_q^{DI}(\frac{x}{y})\right] q_{ok}(y) + \tag{2}$$

$$+ \text{(gluon contributions)} ,$$

where $t = \ln Q^2/\mu^2$, $q_{ok}(x)$ are the bare densities, $P_{qq}(z)$ has its usual meaning[8] and $f_q^{DI}(z)$ gives the correction to the leading order result. In terms of n-moments eq. (2) can be rewritten as

$$q_k^{(n)} = 1 + \frac{\alpha_s}{2\pi} t\, c_F\, \gamma_{qq}^{(n)} + \alpha_s f_q^{DI(n)} \tag{3}$$

with $c_F = 4/3$,

$$\gamma_{qq}^{(n)} = -2 \sum_{j=1}^{n} \frac{1}{j} + \frac{3}{2} + \frac{1}{n(n+1)} = -2\ln(\gamma n) + \frac{3}{2} + O\left(\frac{1}{n}\right), \tag{4}$$

and $\ln\gamma \equiv \gamma_E = 0.5772$ is the Euler's constant. Then for $z \lesssim 1$ one finds, forthe most singular terms,

$$f_q^{DI}(z) = \frac{c_F}{2\pi}(1+z^2)\left[\frac{\ln(1-z)}{1-z}\right]_+ + \cdots\cdots \tag{5}$$

or

$$f_q^{DI(n)} = \frac{c_F}{\pi} \sum_{k=1}^{n} \frac{1}{k} \sum_{j=1}^{k} \frac{1}{j} + \cdots\cdots = \frac{c_F}{2\pi}(\ln\gamma n)^2 + \cdots\cdots \tag{6}$$

The physical origin of this large correction term can be simply traced back to the appropriate use of the exact kinematics in the calculation of the emission of a real gluon. In fact the leading and next-to-leading logarithmic terms in the square bracket of eq. (2) come from the bremsstrahlung contribution to $\mathcal{F}_2$ as

$$\mathcal{F}_2 \sim \delta(1-z) + \frac{c_F}{2\pi}\left(\frac{1+z^2}{1-z}\right) \int_{\mu^2}^{k_{\perp max}^2 \sim Q^2(1-z)} \frac{dk_\perp^2}{k_\perp^2}\, \alpha_s(k_\perp) \tag{7}$$

Then if $\alpha_s \ln(1-z) \sim O(1)$, and this happens near the boundary of the phase space, a large correction is obtained to the leading order result, which simply comes approximating $k_{\perp max}^2 \sim Q^2$.

A similar result is found in the Drell-Yan process[9]. With the usual notations, the corrections to order α_s to the Born term are obtained from[7]

$$\frac{d\sigma^{ll}}{dQ^2} = \frac{4\pi\alpha^2}{9SQ^2} \int \frac{dx_1}{x_1}\frac{dx_2}{x_2}\left[\sum_k e_k^2 q_k(x_1,Q^2)\,\bar{q}_k(x_2,Q^2) + (1 \rightarrow 2)\right] \cdot$$
$$\cdot \left\{\delta(1-z) + \alpha_s\, \theta(1-z)\left[f_q^{DY}(z) - 2 f_q^{DI}(z)\right]\right\} + (\text{gluon contributions}), \tag{8}$$

where $z = \tau/x_1x_2 \equiv Q^2/Sx_1x_2$ and we have explicitly introduced the Q^2 depen-

dence in the parton densities in deep inelastic scattering (see eq. (2)). Then the correction $\tilde{f}_q(z) \equiv \left[f_q^{DY}(z) - 2 f_q^{DI}(z)\right]$ gets two important contributions

$$\tilde{f}_q(z) = \frac{c_F}{2\pi}\left\{2(1+z^2)\left[\frac{\ln(1-z)}{1-z}\right]_+ + \pi^2\,\delta(1-z) + \cdots\cdots\right\}. \tag{9}$$

The first one, which is just twice that of eq. (5), has the same dynamical origin. Namely, as in eq. (7), one has

$$\frac{d\sigma^{l\bar{l}}}{dQ^2} \sim \delta(1-z) + \frac{2c_F}{2\pi}\left(\frac{1+z^2}{1-z}\right)\int_{k^2_{min}\sim Q^2(1-z)}^{k^2_{max}\sim Q^2(1-z)^2} \frac{dk_\perp^2}{k_\perp^2}\,\alpha_s(k_\perp). \tag{10}$$

Here the factor $(2c_F)$ is simply related to the emission of a gluon from two legs, the upper limit $k^2_{\perp max}$ is the appropriate kinematical bound for $z \sim 1$ for this process and $k^2_{\perp min}$ is the effective lower limit obtained subtracting the effect of gluon emission in deep inelastic scattering, which is already included in the definition of $q_k(x_i, Q^2)$ and $\bar{q}_k(x_i, Q^2)$ in eq. (8).

The second contribution in eq. (9), i.e. the π^2 term, has also a simple explanation. In Drell-Yan the vertex correction is proportional to $\mathrm{Re}\ln^2(-q^2) = \ln^2|q^2| - \pi^2\,(q^2 > 0)$. The $\ln^2|q^2|$ term cancels with the analogous contribution from real emission, exactly as it does in deep inelastic scattering where, however, being $q^2 < 0$ no such π^2 term is present. Working to all orders, the expected exponential form of the quark form factor[10], leads to exponentiate[4,5] this term, namely $\sim \exp\left\{c_F \pi \alpha(Q^2)/2\right\}$.

As next example of occurrence of large corrections to the usual LLA let us consider the thrust (T) distribution in the process $e^+e^- \to q\bar{q}g$. The lowest order result is[11]

$$\frac{1}{\sigma_o}\left(\frac{d\sigma}{dT}\right)_o \simeq \frac{c_F \alpha_s}{\pi}\left\{\frac{3T^2 - 3T + 2}{T(1-T)}\ln\left(\frac{2T-1}{1-T}\right) - \frac{3(3T-2)(2-T)}{2(1-T)}\right\} \tag{11a}$$

which for $T \sim 1$ becomes

$$\frac{1}{\sigma_o}\left(\frac{d\sigma}{dT}\right)_o \underset{T\sim 1}{\sim} \frac{2c_F \alpha_s}{\pi}\left(\frac{1}{1-T}\right)\left(\ln\frac{1}{1-T} - \frac{3}{4}\right). \tag{11b}$$

Now it is easy to see that the effect of the emission of soft radiation gives corrections $\propto \alpha_s^n \ln^{2n}(1-T)$ which invalidate the lowest order result (11b).

The above examples show that the soft behaviour of the theory plays an im

portant role in the evaluation of the corrections to the leading order results. If one is able to sum them up, then one can hope to have a better control on the residual series.

The formalism of coherent states, developed in ref. [12] is indeed a rather powerful resumming technique. It provides one with matrix elements which are free from infrared singularities at all orders in the leading log approximation. This has been obtained by extending from QED to QCD the concept of classical currents associated with the external particles to incorporate the new properties of colour and the appearance of the effective coupling constant. Furthermore the question of mass singularities can also be incorporated[13] in the formalism by including the emission of collinear radiation. Various applications can be found in the literature[5, 14].

To our purposes let us first consider, in this formalism, the valence quark densities in the region $x \lesssim 1$, in the usual LLA, i.e. when $\alpha(Q^2)\ln Q^2 \sim O(1)$ and $\alpha(Q^2)\ln(1/(1-x)) << 1$. Then one finds[5, 15]

$$q(x, Q^2) = \frac{1}{2\pi}\int_{-\infty}^{+\infty} db\, e^{ib(1-x)} \exp\left\{\int_0^1 dz\, P(z)\, \xi(Q^2)\left[e^{-ib(1-z)} - 1\right]\right\} \quad (12)$$

where $P(z) = \frac{c_F}{2}\frac{1+z^2}{1-z}$ and

$$\xi(k^2_{max} \sim Q^2) = \int_{\mu^2}^{k^2_{\perp max}} \frac{dk^2_\perp}{k^2_\perp}\, \alpha(k_\perp)\,. \quad (13)$$

In eq. (12) the exponentiated factor $\left\{\int dz\, P(z)\, \xi(Q^2)\, e^{-ib(1-z)}\right\}$ corresponds the multiple real gluon emission constrained by the condition that the total energy carried out by the radiation does not exceed (1-x). Then the factor (-1), coming from virtual emissions, cancels the infrared singularities at $z \to 1$. The connection with the more conventional approach becomes clearer by rewriting eq. (12) as

$$q(x, Q^2) \simeq \frac{1}{2\pi i}\int_{-i\infty}^{i\infty} dn\, x^{-n} \exp\left[\frac{c_F}{2}\int_0^1 dz \left(\frac{1+z^2}{1-z}\right)\xi(Q^2)(z^n - 1)\right], \quad (14)$$

having approximated, for $x \to 1$, $\ln x \sim (x-1)$.

This result explicitly shows that the moments of the distribution (12) coinci de with the usual moments of the parton densities in the large n limit. The eq. (14) becomes

$$q(x,Q^2) \simeq \frac{1}{2\pi i}\int_{-i\infty}^{i\infty} dn\, x^{-n} \exp\left\{-c_F\,\xi(Q^2)\left[\ln\gamma n - \frac{3}{4} + o\left(\frac{1}{n}\right)\right]\right\}, \qquad (15)$$

and, by saddle point techniques

$$q(x,Q^2) \simeq \frac{e^{(\frac{3}{4}-\gamma_E)c_F\xi}}{\Gamma(c_F\xi)}(1-x)^{c_F\xi-1}. \qquad (16)$$

This result coincide with that obtained in refs.[16] by conventional diagrammatic analyses and explicitly shows the simplicity of this approach.

When the condition $\alpha(Q^2)\ln(1/(1-x)) \ll 1$ is released, the corrections to the above LLA result have been shown in ref.[5] to arise simply by taking into account the correct kinematics in eq. (12), namely $\xi(Q^2) \to \xi\left[Q^2(1-z)\right]$. Then in analogy to eq. (14), one obtains for the n-th moment of the valence densities

$$q^{(n)}(Q^2) \sim \exp\left\{\frac{c_F}{2\pi}\int_0^1 dz\left(\frac{1+z^2}{1-z}\right)\int_{\mu^2}^{Q^2(1-z)}\frac{dk_\perp^2}{k_\perp^2}\,\alpha(k_\perp^2)\left[z^n-1\right]\right\}. \qquad (17)$$

For $\alpha(k_\perp) = \text{const} = \alpha_s$ this corresponds to the simple exponentiation of the first order result (eq. (6))

$$q^{(n)}(Q^2) \sim \exp\left\{\frac{\alpha_s c_F}{\pi}\left[\left(\frac{1}{2}(\ln\gamma n)^2 + \frac{\pi^2}{6}\right) + \ln\frac{Q^2}{\mu^2}\left(-\ln\gamma n + \frac{3}{4}\right) - \frac{7}{8} + o\left(\frac{1}{n}\right)\right]\right\}. \qquad (18)$$

Transforming back eq. (18) by the saddle point method one finally obtains, in place of eq. (16),

$$q(x,Q^2) \simeq e^{\beta\left[\frac{3}{4}\ln\frac{Q^2}{\mu^2} + \frac{\pi^2}{12} - \frac{7}{8} + \frac{\gamma_E^2}{2}\right]}\frac{e^{-\gamma_E\beta\ln\frac{Q^2}{\mu^2 n_o}}}{\Gamma(\beta')} \cdot (1-x)^{\beta'-1}\, e^{-\frac{\beta}{2}\ln^2 n_o}, \qquad (19)$$

where $\beta = c_F\alpha_s/\pi$, and n_o is the saddle point value defined by the equation

$$n_o = \frac{1}{1-x}\ \beta \ln\left(\frac{Q^2}{\mu^2 \gamma n_o}\right) \equiv \frac{1}{1-x}\ \beta' \ . \tag{20}$$

The effect of the running coupling constant in eq. (17) can also be included. An explicit expression for $q(x, Q^2)$ in this limit is obtained in ref. [17] by using the same techniques.

An important consequence of eq. (17) is that the Altarelli-Parisi evolution equation for the non-singlet quark density is modified[5, 6], for $x \sim 1$, as

$$\frac{dq(x, Q^2/Q_o^2)}{d\ln(Q^2/Q_o^2)} = \frac{1}{\pi}\int_x^1 \frac{dy}{y}\left\{P\left(\frac{x}{y}\right) \bar{\alpha}\left[\frac{Q^2}{Q_o^2}\left(1-\frac{x}{y}\right)\right]\right\}_+ q\left(y, \frac{Q^2}{Q_o^2}\right) \ , \tag{21}$$

where $P(z)$ is defined in eq. (12). In other words, the simple rescaling of the argument of the running coupling constant from Q^2 to $Q^2(1-z)$ takes into account the most important higher order corrections. Expanding

$$\alpha\left[(Q^2(1-z)\right] = \frac{1}{\ln\left[Q^2(1-z)\right]} = \frac{1}{\ln Q^2}\left[1 - \frac{\ln(1-z)}{\ln Q^2} + O\left(\frac{1}{\ln Q^2}\right)^2\right] = \tag{22}$$

$$= \alpha(Q^2)\left[1 + \ln(1-z)\,\alpha(Q^2) + O(\alpha^2(Q^2))\right] \ ,$$

one obtains the leading log term, the next-to-leading term, and so on.

Of course eq. (17) is valid for $n \gg 1$ but limited by $n < Q^2/\mu^2$ or roughly $1-x > \mu^2/Q^2$. In this very tiny region of the phase space one finds a strong damping of the form of a Sudakov form factor, which makes the leading twist contribution discussed here probably negligible with respect to higher twist effects. More details about this point can be found in ref. [6].

Phenomenological implications of the threshold behaviour of the structure functions for deep inelastic scattering, namely the question of the parametrizations to be used in analysing the experimental data which are compatible with the above dicussion, are considered in ref. [18].

Similar modifications of the leading order result in the case of the photon structure functions which, in the near future, can be measured for x enough close to one, have been recently studied in ref. [19].

We now discuss the implications of the above results in the Drell-Yan process. By taking into account the soft gluon emission at all orders, and omitting

for simplicity the contribution of gluons in the initial state, eq.(8) is replaced by[5,20]

$$\frac{d\sigma^{l\vec{l}}}{dQ^2 dx_F} = \frac{4\pi\alpha^2}{9SQ^2}\int \frac{dx_1}{x_1}\frac{dx_2}{x_2}\,\delta(x_1 - x_2 - x_F)\Big[\sum_k e_k^2 q_k(x_1, Q_o^2)\cdot \\ \cdot \bar{q}_k(x_2, Q_o^2) + (1 \to 2)\Big]\tilde{f}(z, Q^2, Q_o^2)\exp\left\{\frac{\alpha(Q^2)}{2\pi} c_F \pi^2\right\}, \tag{23}$$

with

$$\tilde{f}(z, Q^2, Q_o^2) = \frac{1}{2\pi}\int_{-\infty}^{\infty} db\, e^{ib(1-z)} \exp\left\{\frac{c_F}{\pi}\int_0^1 dy\left(\frac{1+y^2}{1-y}\right)\cdot\right. \\ \left.\cdot \int_{Q_o^2(1-y)}^{Q^2(1-y)^2} \frac{dk_\perp^2}{k_\perp^2}\,\alpha(k_\perp)\left[e^{-ib(1-y)} - 1\right]\right\}. \tag{24}$$

In eq.(23) we have more generally introduced the parton densities at a mass scale Q_o^2, which leads to the lower bound $k_{\perp min}^2 = Q_o^2(1-y)$ in the $k_\perp^2$ integral in eq. (24). Furthermore the π^2 term coming from the mismatch in the quark form factor from space like to time like regions is exponentiated, as discussed earlier.

The easiest way to solve eq.(23) is to consider its τ^n moments. Then the r.h.s. reduces to the product of the n-th moments of the q, $\bar{q}$ and $\tilde{f}$ distributions, which can be easier transformed back. Without going into details which can be found in ref.[20], one obtains the soft correction factor K to the naive model ($\tau \lesssim 1$)

$$K = e^{\frac{\alpha(Q^2)}{2} c_F \pi}\,\frac{\Gamma(1+\xi)}{\Gamma\left[1 + \xi + \beta\ln\left(\frac{Q^2}{Q_o^2 n_o}\right)\right]}\, e^{\beta\left(\frac{3}{4} - \gamma_E\right)\ln\frac{Q^2}{Q_o^2}}\cdot \\ \cdot e^{\gamma_E \beta \ln n_o}\,(1-\tau)^{\beta\ln\frac{Q^2}{Q_o^2 n_o}}\, e^{-\frac{1}{2}\beta\ln^2 n_o\left(1 - \frac{3}{4}\beta\ln n_o\right)}, \tag{25}$$

where $\beta = 2\alpha_s c_F/\pi$, n_o is the saddle point value defined by

$$n_o = \frac{1}{1-\tau}\left[1 + \xi + \beta \ln\left(\frac{Q^2}{Q_o^2 \gamma n_o}\right)\right], \qquad (26)$$

and $\xi = \xi_1 + \xi_2$, having parametrized, at $q^2 = -Q_o^2$, and for $x \sim 1$, $q(x)$ and $\bar{q}(x)$ as $(1-x)^{\xi_1}$ and $(1-x)^{\xi_2}$ respectively. In deriving this result we have kept all leading logarithmic terms in $(1-\tau)$ and ξ. Furthermore eq. (25) has been explicitly checked to first order in α_s. The phenomenological implications of eq. (25) are shown[20] in Figs. 1 and 2 for p-p and π-p collisions respectively, for

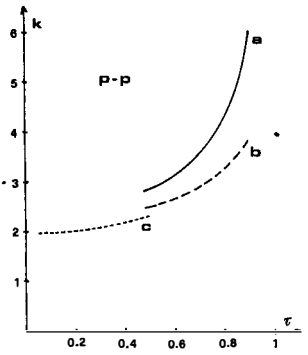

FIG. 1

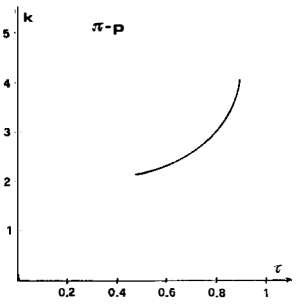

FIG. 2

for $\sqrt{s} = 30$ GeV, $\alpha_s \simeq 0.2$ and $Q^2 = Q_o^2$. In Fig. 1 the full curve (a) represents eq. (25), the dashed line (b) represents the leading log approximation of (25) (e. g. first order in α_s) and for comparison the full first order calculation of ref.[7] is also shown (dotted line (c)). As it is clear from this figure, the inclusion of soft contributions to all orders do not change significantly the first order result up to $\tau \sim 0.6$-0.7. On the other hand for larger values of τ the absolute cross section falls down so rapidly that the increasing behaviour of K will not be observable. In the case of pion-proton collisions (Fig. 2) smaller corrections are found. An improvement of the actual experimental accuracy could, for this case, reveal the τ dependence of K.

As a last example we will consider how the lowest order result (eq. (11b)) for the T-distribution in the process $e\bar{e} \rightarrow q\bar{q}g$ is modified for $T \lesssim 1$ by soft radiation. The analysis proceeds quite similarly to the previous cases. The physical idea is that the quark, antiquark and the gluon as well will develop into

jets of invariant mass $\sim Q^2(1-T)$. The corresponding T distribution is found[21]

$$\frac{dP}{dT} \simeq \left(\frac{dP}{dT}\right)_0 \frac{e^{\left[\left(\frac{3}{4} - \gamma_E\right)\beta_q + \left(\frac{11}{12} - \frac{N_f}{18} - \gamma_E\right)\beta_g\right] \ln\left(\frac{1}{1-T}\right)}}{\Gamma\left[1 + (\beta_q + \beta_g)\ln\left(\frac{1}{1-T}\right)\right]} \cdot \tag{27}$$

$$\cdot\ e^{-\frac{1}{2}(\beta_q + \beta_g)\ln^2\left(\frac{1}{1-T}\right)} ,$$

where $\left(\frac{dP}{dT}\right)_0$ is given by eq. (11a), $\beta_q = \left(\frac{8\alpha_s}{3\pi}\right)$ and $\beta_g = \left(\frac{3\alpha_s}{\pi}\right)$. This result goes beyond the usual LLA, where only the term $\exp\left[-\beta_q \ln^2(1-T)/2\right]$ is found[22] to multiply the Born term. In Fig. 3 we plot the Born distribution $\left(\frac{dP}{dT}\right)_0$ given by eq. (11a) (full line) and compare it with $\left(\frac{dP}{dT}\right)$ of eq. (27) (broken line). For completeness the first order expansion in $(\beta_q + \beta_g)$ of eq. (27) is also shown. This figure shows clearly that for large T the higher order corrections are quite important, and in qualitative agreement with the experimental results. Of course a complete comparison with data must await suitable addition of finite α_s^2 corrections, which have been shown to be sizeable[23].

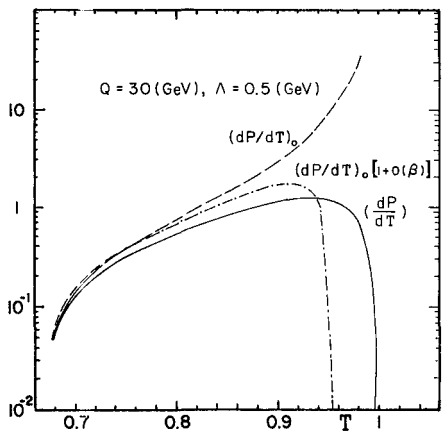

FIG. 3

We conclude this short review by discussing $k_\perp$ effects which have been most extensively studied in Drell-Yan and e^+e^- annihilation[24]. As well known, gluon bremsstrahlung provides a non-zero transverse momentum $k_\perp$ for the lepton or the quark pair in the two processes. However, whereas for $k_\perp^2 \sim O(Q^2)$ the transverse momentum distribution is expected to be fully described by first order QCD diagrams, for $\Lambda^2 \ll k_\perp^2 \ll Q^2$ the perturbation theory breaks down due to the appearance of large $\alpha_s^n \ln^{2n}(Q^2/k_\perp^2)$ terms arising from the emission of n gluons, both soft and collinear, which have to be summed to all orders of perturbation theory.

In Drell-Yan this task has been essentially accomplished by Dokshitzer, Dyakonov and Troyan[25], who gave an expression valid in the leading double logarithmic approximation. An improvement of this result has been suggested by Parisi and Petronzio[26], by transforming to the impact parameter space, where transverse momentum conservation can be taken into account exactly. This is particularly relevant when $k_\perp \to 0$, which can be reached by emission of atleast two gluons whose transverse momenta are not small and add to essentially zero momentum. They proposed

$$\left.\frac{d\sigma}{dQ\, dk_\perp^2\, dy}\right|_{y=0} = \frac{1}{2}\int_0^\infty b\, db\, J_o(b k_\perp)\, \tilde{\sigma}(b, Q, S)\ , \tag{28}$$

where

$$\tilde{\sigma}(b,Q,S) = \frac{8\pi\alpha^2}{9QS}\sum_i e_i^2\left[q_i^{(1)}(\sqrt{\tau}, \frac{1}{b^2})\, q_i^{(2)}(\sqrt{\tau}, \frac{1}{b^2}) + \right.$$
$$\left. + (1 \to 2)\right]\exp\left[\Delta(Q^2, b)\right] \tag{29}$$

and

$$\Delta(Q^2, b) = \frac{16}{3\pi}\int \frac{dq_\perp}{q_\perp}\ln\left(\frac{Q}{q_\perp}\right)\, \alpha_s(q_\perp)\left[J_o(bq_\perp) - 1\right]\ . \tag{30}$$

In e^+e^- annihilation the same result has been independently obtained by Curci, Greco and Srivastava[27] for the transverse momentum distribution of a $q\bar{q}$ jet, namely

$$\frac{dP}{dk_\perp^2} = \frac{1}{2}\int_0^\infty b\, db\, J_o(bk_\perp)\, \exp\left\{\Delta(Q^2, b)\right\} \tag{31}$$

with $\Delta(Q^2, b)$ given by eq. (30).

More recent analyses[28] have confirmed in Drell-Yan the general structure of eq. (28). So far there is no detailed phenomenological analysis of recent $k_\perp$ data in Drell-Yan based on eq. (28). On the other hand a very recent analysis[29] of the total transverse momentum distribution of e^+e^- jets at various energies from the PLUTO Group strongly supports the QCD prediction (31). Deviations from this formula at the highest energies and large $k_\perp$ have been found in agreement with first order results. This is explicitly shown in Fig. 4. Thus the

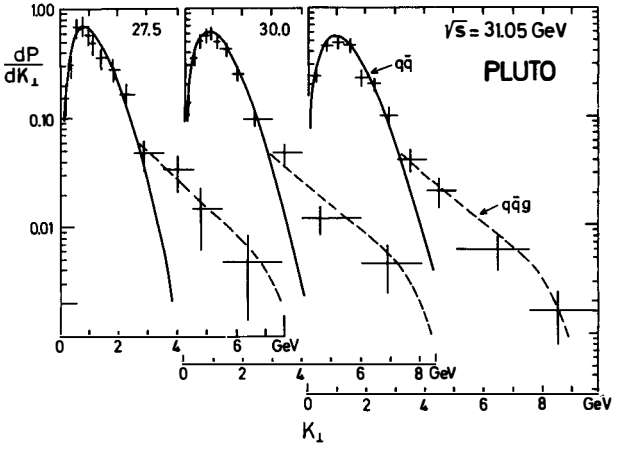

FIG. 4

resummation in $k_\perp$ of these soft effects in the double leading log approximation and using explicit momentum conservation seems in excellent agreement with experimental observations.

To conclude, we have discussed the problem of large higher order corrections which are related to the soft behaviour of the theory. The resummation of these effects have been explicitly studied in various processes. It is plausible that the residual series is then under much better control. As stated at the beginning the optimization of the convergence of this residual expansion can be further improved by an accurate choice of the renormalization prescriptions which reduce the effect of genuine higher order corrections.

REFERENCES.

1) For reviews and more complete bibliography see Yu. L. Dokshitser, D. I. Dyakonov and S. Y. Troian, Phys. Rep. 58, 269 (1980); A. J. Buras, Rev. Mod. Phys. 52, 199 (1980) and Fermilab preprint 80/79 (1980); C. H. Llewellyn-Smith, Talk given at the XX Intern. Conf. on High Energy Physics, Madison 1980, Oxford preprint 68/80 (1980); A. H. Mueller, Columbia Univ. preprint CU-TP-192 (1980).

2) For illustration only a few references are given: G. Altarelli, R. K. Ellis and G. Martinelli, Nuclear Phys. B157, 461 (1979); R. Barbieri, E. D'Emilio, G. Curci and E. Remiddi, Nuclear Phys. B154, 535 (1979); W. A. Bardeen and A. J. Buras, Phys. Rev. D20, 166 (1979); W. Celmaster and R. J. Gonsalves,

Phys. Rev. Letters 44, 560 (1980) and Phys. Rev. D21, 3112 (1980); R. K. Ellis, D. A. Ross and A. E. Terrano, Phys. Rev. Letters 45, 1226 (1980).
3) See for example W. Celmaster and D. Sivers, Phys. Rev. D23, 227 (1981) and references therein.
4) G. Parisi, Phys. Letters 90B, 295 (1980).
5) G. Curci and M. Greco, Phys. Letters 92B, 175 (1980).
6) D. Amati, A. Bassetto, M. Ciafaloni, G. Marchesini and G. Veneziano, Nuclear Phys. B173, 429 (1980).
7) G. Altarelli, R. K. Ellis and G. Martinelli, ref. 2); see also R. K. Ellis, "A compendium of formulae for lepton pair production", these proceedings.
8) G. Altarelli and G. Parisi, Nuclear Phys. B126, 298 (1977).
9) S. D. Drell and T. M. Yan, Phys. Rev. Letters 25, 316 (1970).
10) J. M. Cornwall and G. Tiktopoulos, Phys. Rev. D13, 3370 (1975); R. Coqueraux and E. de Rafael, Phys. Letters 69B, 181 (1978).
11) A. De Rujula, J. Ellis, E. G. Floratos and M. K. Gaillard, Nuclear Phys. B138, 387 (1978).
12) M. Greco, F. Palumbo, G. Pancheri-Srivastava and Y. Srivastava, Phys. Letters 77B, 282 (1978); See also D. R. Butler and C. A. Nelson, Phys. Rev. D18, 1196 (1978).
13) G. Curci and M. Greco, Phys. Letters 79B, 406 (1978).
14) G. Curci, M. Greco and Y. Srivastava, Phys. Rev. Letters 43, 834 (1979) and Nuclear Phys. B159, 451 (1979); H. D. Dahmen and F. Steiner, DESY preprint 80/37 (1980); C. A. Nelson, Fermilab preprint 80/82-THY (1980).
15) M. Ramon-Medrano, G. Pancheri-Srivastava and Y. Srivastava, Nuclear Phys. B176, 198 (1980).
16) V. N. Gribov and L. N. Lipatov, Sov. J. Nuclear Phys. 15, 458, 675 (1972); Yu. L. Dokshitser, Sov. J. Nuclear Phys. 46, 641 (1977); K. Konishi, A. Ukawa and G. Veneziano, Nuclear Phys. B157, 45 (1979).
17) Yu. L. Dokshitser, ref. 16).
18) C. Lopez and F. J. Yudurain, CERN preprint TH-2930 (1980).
19) M. K. Chase, Univ. of Oxford preprint 97/80 (1980).
20) G. Curci and M. Greco, Frascati preprint LNF-81/7 (1981).
21) M. Greco and Y. Srivastava, Northeastern Univ. preprint NUB-2482 (1981).
22) P. Binetruy, Phys. Letters 91B, 245 (1980); G. Schierholz, SLAC Summer Inst. in Part. Phys. (July 1979), Ed. A. Mosher.
23) R. K. Ellis, D. A. Ross and A. E. Terrano, ref. 2).
24) See also J. Cleymans, J. C. Collins, G. Pancheri-Srivastava, D. Scott and D. Soper, these proceedings.
25) Yu. L. Dokshitser, D. I. Dyakonov and S. I. Troyan, Phys. Letters 78B, 290 (1978) and 79B, 269 (1978).
26) G. Parisi and R. Petronzio, Nuclear Phys. B154, 427 (1979).
27) G. Curci, M. Greco and Y. Srivastava, ref. 14).
28) C. Y. Lo and J. D. Sullivan, Phys. Letters 86B, 327 (1979); S. D. Ellis and W. J. Stirling, Phys. Rev. D23, 214 (1981); J. C. Collins and D. E. Soper, Oregon Univ. preprint OITS-155 (1981), and these proceedings.
29) Ch. Berger et al., PLUTO Collaboration, DESY preprint 80/111 (1980).

ENERGY MOMENTUM DISTRIBUTION OF LEPTON PAIR PRODUCTION THROUGH SOFT QCD RADIATION

G. Pancheri
Physics Department, Northeastern University
Boston, Massachusetts 02115

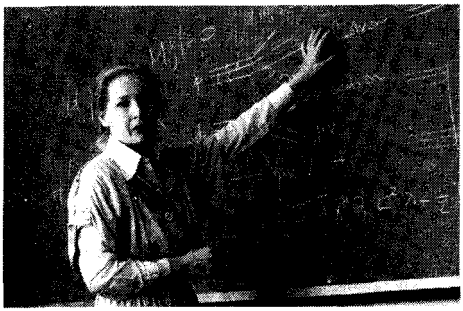

ABSTRACT

The soft gluon contribution to hadronic lepton pair production is described using a four-momentum probability function supported by the coherent state approach to QCD. Factorization into light cone variables produces Q^2-dependent parton densities in agreement with the evolution equations and a transverse momentum distribution which fits small and medium energy data. A sum rule is presented for the S-dependence of the mean square value $\langle q_\perp^2 \rangle$. For πN, one obtains $\langle q_\perp^2 \rangle \simeq 0.003$ S, in good agreement with the experimental value.

In this paper, I present a modification of the basic Drell-Yan (DY) cross-section which incorporates soft and collinear hard gluon corrections.

The role of soft gluon contribution to basic QCD processes is slowly being recognized as very important in order to explain the low energy or small transverse momentum behavior of processes like hadronic μ-pair production and deep inelastic scattering (DIS). Indeed it will be shown in the following that soft gluon corrections lead phenomenologically to:

i) Q^2-dependent quark densities in both DY and DIS,
ii) small and medium transverse momentum distribution of μ-pairs,
iii) normalization of the Drell-Yan cross-section.

A unified formalism which deals with the above effects is provided by the Bloch Nordsieck method [1]. In the impulse approximation, the "naive" hadronic cross-section for lepton pair production is factorized into the (inclusive) probability of producing a $q\bar{q}$ pair times the (exclusive) cross-section for the scattering $q\bar{q} \to \mu^+\mu^-$. This picture is usually modified by QCD through first [2] and, now, second order [3] corrections to the Born term, and through Q^2-dependent parton densities obeying the evolution equations [4].

As a step toward a unified treatment of QCD corrections, we propose to directly calculate the inclusive cross-section for

$$q\bar{q} \to \mu^+\mu^- + G(K) \tag{1}$$

where G(K) arises from hard, wide angle bremsstrahlung and from soft and hard collinear gluon emission. The cross section for process (1) can then be written as

$$\frac{d^4\sigma}{d^4q} = \int d^4\mathcal{P}(K)\ \hat{\sigma}(P' - K)\ \delta^4(P' - K - q)$$

where $d^4\mathcal{P}(K)$ gives the probability for emitting soft and collinear hard gluons of total momentum K and $\hat{\sigma}(P' - K)$ is the DY cross-section modified by the remaining hard QCD corrections. The integration is over the unobserved momentum K, P' is the momentum of the incoming $q\bar{q}$ pair.

Turning to the hadronic cross-section and ignoring, for simplicity, higher order terms in $\hat{\sigma}$, one has

$$(d^4\sigma/d^4q)^{had} = (4\pi\alpha^2/9Q^2)\sum e_f^2 \int \left[q_{of}^{[1]}(y_1)\bar{q}_{of}^{[2]}(y_2) + 1 \leftrightarrow 2\right] dy_2 dy_1$$
$$\times \int d^4\mathcal{P}(K)\delta^4(P' - K - q) \quad . \tag{2}$$

In Eq. (2), the "bare" parton densities refer to the $q\bar{q}$ pair before soft gluon emission takes place. As shown elsewhere [5] for the specific Bloch-Nordsieck mechanism the distribution $d^4\mathcal{P}(K)$ exhibits, asymptotically, the separability

$$d^4\mathcal{P}(K) \simeq d\mathcal{P}(K_+)d\mathcal{P}(K_-)d^2\mathcal{P}(K_\perp) \quad , \tag{3}$$

where $K_\pm = K_o \pm K_3$. In Eq. (2) the $q_\perp$ dependence can then be factorized out and one obtains

$$(d^4\sigma/d^4q)^{had} = (4\pi\alpha^2/9Q^2)\sum e_f^2 \left[I_f^{[1]}(x_1,Q^2)\,\bar{I}_f^{[2]}(x_2,Q^2) + 1 \Leftrightarrow 2\right](d^2\mathcal{P}(q_\perp)/d^2q_\perp)$$

with $I_f(x_{1,2},Q^2) = \int d\mathcal{P}(K_\pm)q_{of}(y)$ and it is understood that $K = P' - q$. Notice that, because of Eq. (3), the soft gluon emission mechanism maintains the basic factorization into x_1 and x_2 variables. That the densities $I_f(x,Q^2)$ are exactly the same as those encountered in DIS, can be seen when one considers soft gluon emission in deep inelastic scattering. For this case, the above mechanism induces a Q^2-dependence such that the moments factorize into a "running" part and a constant part [6]. It can be shown that the "running" moments obey a differential equation which coincides, to first order in α_s, $\ell n Q^2$, with the corresponding evolution equations.

We shall now discuss in some detail the distribution $d^4\mathcal{P}(K)$. In a number of papers [7], it has been proposed that the leading soft and collinear hard gluon spectra exponentiate. By imposing energy-momentum conservation [1,8], one obtains

$$d^4\mathcal{P}(K) = (2\pi)^{-4}\, d^4K \int d^4x\, e^{iK\cdot x} \exp\left\{-\int d^3\bar{n}_k(1 - e^{-ik\cdot x})\right\} \quad . \tag{4}$$

Restricting for simplicity to soft gluons alone (see ref. 5 for the complete treatment), one gets for the single gluon distribution

$$d^3\bar{n}_k = \frac{32}{\pi(33 - 2N_f)\ell n(Q^2/\Lambda^2)}\left(\frac{d^3k}{2k\,k_\perp^2}\right) \quad . \tag{5}$$

Equation (4) reduces to $\delta^4(K)$ when $\alpha_s \to 0$, thus restoring the naive Drell-Yan cross-section in Eq. (2). Upon inspection, $d^4\mathcal{P}(K)$ exhibits a mass singularity which can be dealt with introducing a small regulator mass $\mu \sim m_q^2$. The factorizability of $d^4\mathcal{P}(K)$ in the light-cone variables, Eq. (3), is a consequence of taking the $\mu \to 0$ limit in Eqs. (4) and (5). Using the soft gluon spectrum given by Eq. (5), one gets

$$d\mathcal{P}(K_\pm) = (2\pi)^{-1} dK_\pm \int dt\, e^{iK_\pm t} \exp\left\{-\frac{4}{3\pi}\int_\mu^{\varepsilon^2}\frac{dk_\perp^2}{k_\perp^2}\,\alpha_s(k_\perp^2)\int_0^{2\varepsilon}\frac{dk}{k}(1 - e^{ikt})\right\} \quad ,$$

where ε is the c.m. energy of each emitting quark, and

$$d^2\mathcal{P}(K_\perp) = (2\pi)^{-2} d^2K_\perp \int d^2x_\perp \, e^{iK_\perp \cdot x_\perp} \exp\left\{\frac{-4}{3\pi}\int \frac{dk_\perp^2}{k_\perp^2}\,\alpha_s(k_\perp^2)[1-J_o(k_\perp x_\perp)]\int \frac{dk_3}{\sqrt{k_3^2+k_\perp^2}}\right\}$$

For $K_\pm < 2\varepsilon$, one can easily obtain a closed form for $d\mathcal{P}(K_\pm)$, i.e.,

$$d\mathcal{P}(K_\pm) = (dK_\pm/2\varepsilon)[\gamma^{+\beta_\ell}\,\Gamma(\beta_\ell)]^{-1}(K_\pm/2\varepsilon)^{\beta_\ell - 1}$$

with $\beta_\ell = \frac{4}{3\pi}\int_\mu^{E^2} \frac{dk_\perp^2}{k_\perp^2}\,\alpha_s(k_\perp^2) \sim \frac{16}{25}\,\ell n\left(\ell n \frac{Q^2}{\Lambda^2}\right)$. This in turn gives the following Q^2-dependent parton densities:

$$I_f(x,Q^2) = \frac{1}{\gamma^{\beta_\ell}\Gamma(\beta_\ell)}\int_x^1 \frac{dy}{y}\, q_{of}(y)\left(1-\frac{x}{y}\right)^{\beta_\ell - 1} .$$

Integrating on the transverse momentum, one obtains for the double differential cross section:

$$S\,\frac{d^2\sigma}{dx_1dx_2} = \frac{4\pi\alpha^2}{9x_1x_2}\exp\left\{\frac{2\pi}{3}\,\alpha_s(Q^2)\right\}\sum e_f^2\left\{I_f^{[1]}(x_1,Q^2)\,\bar{I}_f^{[2]}(x_2,Q^2) + 1 \Leftrightarrow 2\right\} .$$

The normalization factor $K = \exp\left\{\frac{2\pi}{3}\,\alpha_s(Q^2)\right\}$, as first suggested by G. Paris [9], derives from analytically continuing the quark form factor from space to time-like Q^2. An interesting application of this formalism is the calculation of the S-dependence of the mean squared transverse momentum $\langle q_\perp^2\rangle$. The analyticity properties of $d^4\mathcal{P}(K)$ lead to the general formula

$$\langle q_\perp^2\rangle = \frac{4}{3\pi}\,\bar{\alpha}_s(Q^2)\; S\; \frac{\sum e_f^2\left\{\int_{x_1}^1 \frac{dy_1}{y_1}\, I_f^{[1]}(y_1,Q^2)\int_{x_2}^1 \frac{dy_2}{y_2}\,\bar{I}_f^{[2]}(y_2,Q^2) + 1 \Leftrightarrow 2\right\}}{\sum e_f^2\left\{\frac{I_f^{[1]}(x_1,Q^2)}{x_1}\,\frac{\bar{I}_f^{[2]}(x_2,Q^2)}{x_2} + 1 \Leftrightarrow 2\right\}} .$$

This equation has been obtained assuming no intrinsic transverse momentum for the quarks. As such it can be used to calculate the slope of $\langle q_\perp^2\rangle$ vs. S. Saturating the integrals with valence quarks alone and using NA_3 parametrization [10] for pion and nucleon densities, for $x_1 = x_2 = 0.275 = \sqrt{\tau}$ one gets

$$(\partial\langle q_\perp^2\rangle/\partial S) \sim 0.003 \qquad \text{for } \bar{\alpha}_s = 0.38 .$$

This result is of the right [10] order of magnitude for the slope in πN scattering. For lower energies, more precise kinematic limits have to be imposed.

Having exploited the energy and longitudinal distribution properties of the soft QCD radiation, one can inquire about the predictions for the transverse momentum distribution itself. In reference (8), the following expression was first proposed for the transverse momentum distribution of soft QCD radiations emitted in parton-parton collisions:

$$d^2\mathcal{P}(K_\perp) = (2\pi)^{-1} dK_\perp \int d^2x_\perp \, e^{-iK_\perp \cdot x_\perp} \exp\left\{ - \int d^3\bar{n}_k (1 - e^{+ik_\perp \cdot x_\perp}) \right\} \quad . \qquad (6)$$

For the DY process, this function represents the transverse momentum distribution of the μ-pairs, as the previous discussion shows. It enjoys the following two important properties:

i) the distribution is a function of $K_\perp / \langle K_\perp \rangle$, apart from logarithmic corrections,

ii) it can be used to describe the transverse momentum distribution of many inclusive hadronic and semihadronic processes.

The second property follows directly from the factorization of the leading soft gluon corrections and the separability property Eq. (3). It is indeed confirmed by various phenomenological analyses [11] based on an approximated expression for $d^2\mathcal{P}(K)$. Property (i) appears to be a consequence of exponentiating the soft gluon spectrum. Equation (6) in general depends from two scale parameters, Q^2 and Λ, the renormalization mass. To determine the scaling variable for $K_\perp$, one can study the behavior of the exponential in Eq. (6) for small and large values of $x_\perp$. The leading logarithmic approximation alone cannot determine the scale uniquely since any (roughly) constant term can always be neglected in the large Q^2-limit.- On the other hand, as $x_\perp \to 0$ one has

$$\int d^3\bar{n}_k (1 - e^{-ik_\perp \cdot x_\perp}) \underset{x_\perp \to 0}{\sim} (\tfrac{1}{4}) x_\perp^2 \int k_\perp^2 d^3\bar{n}_k = (\tfrac{1}{4}) x_\perp^2 \langle K_\perp^2 \rangle \quad ,$$

where the last equality follows directly from Eq. (6)

Property (i) is encountered in almost all inclusive hadronic distributions where it is known as scaling-in-the-mean [12] or mean scaling. Our formula predicts mean scaling also for current induced processes like DY, DIS and e^+e^- annihilation [11].

To conclude, a condensed account of soft gluon corrections to the DY process has been presented. The formalism is borrowed, with adequate modifications, from the Bloch-Nordsieck method in QED. This approach is direct, intuitive and physically appealing. Based as it is in terms of probability distributions, it meshes nicely with the underlying probabilistic parton picture of the DY process.

Most of the work presented here has been done in collaboration with Y. Srivastava. Different parts are the result of collaborations with M. H. Friedman and M. Ramon-Medrano.

References

1. E. Etim, G. Pancheri and B. Toushek, Nuovo Cimento 51B, 276 (1967); M. Greco, F. Palumbo, G. Pancheri-Srivastava and Y. Srivastava, Phys. Lett. 77B, 282 (1978).

2. G. Altarelli, R. K. Ellis and G. Martinelli, Nucl. Phys. B157, 461 (1979).

3. R. K. Ellis and G. Martinelli, these proceedings.

4. G. Altarelli and G. Parisi, Nucl. Phys. B126, 298 (1977).

5. M. H. Friedman, G. Pancheri and Y. Srivastava, Northeastern University preprint NUB #2486, Jan. 1981. Submitted to Phys. Review.

6. G. Pancheri, Y. Srivastava and M. Ramón-Medrano, Frascati Preprint LNF-80/49 (P), Sept. 1980. To be published in Phys. Review.

7. J. M. Cornwall and G. Tiktopoulos, Phys. Rev. D13, 3370 (1976); ib. D15, 2937 (1977); K. Konishi, A. Ukawa and G. Veneziano, Nucl. Phys. B157, 45 (1979).

8. G. Pancheri and Y. Srivastava, Phys. Rev. Lett. 43, 11 (1979).

9. G. Parisi, Phys. Lett. 90B, 295 (1980); G. Curci and M. Greco, Phys. Lett. 92B, 175 (1980).

10. J. Badier, these proceedings. For the latest review, see also G. Matthiae, CERN Preprint EP/80-183, Oct. 1980 (to appear in Rivista del Nuovo Cimento).

11. G. Parisi and R. Petronzio, Nucl. Phys. B154, 427 (1979); G. Pancheri and Y. Srivastava, Phys. Rev. D21, 95 (1980); J. C. Collins and D. Soper, these proceedings.

12. F. T. Dao, et al., Phys. Rev. Lett. 33, 389 (1974).

PARTON TRANSVERSE MOMENTUM AND QCD

John C. Collins
Physics Department
Illinois Institute of Technology
Chicago, IL 60616, USA

Davison E. Soper
Institute of Theoretical Science
University of Oregon
Eugene, OR 97403, USA

ABSTRACT

We give an expansion for the Drell-Yan cross-section that is applicable at all values of transverse momentum, including all logarithmic corrections. At low transverse momentum, the cross-section has power-law dependence on energy and on the QCD scale. We discuss a difficulty in the proof (to all orders of logarithmic corrections) as compared with the corresponding completely solved case in e^+e^- annihilation.

I. Introduction

Most of the cross-section for dilepton production in hadron collisions is at low transverse momentum, q_T, precisely where perturbative QCD is most difficult to apply. We propose for the cross-section an expansion that is applicable at all values of q_T. It embodies (with corrections) the idea that q_T is the sum of the intrinsic transverse momenta of the annihilating quark-antiquark pair in the Drell-Yan model[1]. The most important feature is that the intrinsic transverse-momentum distributions are strongly energy-dependent, but in a calculable way.

Previous work[2-4] has concentrated on the leading or next-to-leading[4] (doubly) logarithmic approximation. However, non-leading logarithms can overwhelm leading logarithms[5]. Our proposed expansion, eq.(6.1) below, includes all logarithmic terms, and it displays a leading term together with systematically smaller corrections.

We have a complete proof[6-7] in QCD perturbation theory of the corresponding expansion for two particle production in e^+e^- annihilation. However, there are still some unresolved difficulties in the proof for the Drell-Yan case. Similar difficulties appear in trying[8] to prove factorization of the Drell-Yan cross-section integrated over q_T.

In Sections II to V, we sketch the derivation of our expansion. Section VI gives the expansion and includes all formulae necessary to calculate the cross-section up to a factor $1+O(\alpha_s)$. A two-dimensional Fourier transformation is needed, and we explain how to compute it by saddle point methods[9] in Section VII. We explain in Section VIII the unresolved difficulties mentioned above, and we state our conclusions in Section IX.

II. Statement of Problem

The parton model[1] for dilepton production is illustrated in Fig.1. We use light-cone coordinates, defined by $v^\mu = (v^+, v^-, v^T)$ with $v^\pm = (v^0 \pm v^3)/\sqrt{2}$ in a frame where the hadron collision is along the z-axis. Then we define $x_A = q^+/P_A^+$, $x_B = q^-/P_B^-$, so that the dilepton mass is $Q = \sqrt{q^2} = \sqrt{x_A x_B s - q_T^2}$. In the

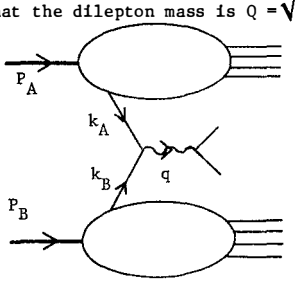

Fig.1 Drell-Yan process

Drell-Yan limit, $s\to\infty$ with x_A and x_B fixed, the parton model gives

$$\frac{s d\sigma}{dx_A dx_B d^2q_T} = N\Sigma e_q^2 \int d^2k_A^T \; d^2k_B^T \; P_{q/A}(x_A,k_A) \; P_{\bar{q}/B}(x_B,k_B^T) \; \delta(q^T-k_A^T-k_B^T). \tag{2.1}$$

Here, $P_{q/H}(x,k_T)$ is the number density in hadron H of partons of flavor q with fractional longitudinal momentum x and transverse momentum k_T. The sum is over flavors of quark and antiquark, and the normalization factor is

$$N = \frac{4}{9}\pi\alpha^2 s/Q^2. \tag{2.2}$$

Our expansion (eq.(6.1) below) for the cross-section in QCD amounts to the following:

1. The parton model is essentially correct, with (perturbatively) calculable effects from soft gluon exchange, vertex corrections, etc.
2. The k_T-dependence of $P(x,k_T)$ is (perturbatively calculable for all k_T, even $k_T=0$, if Q^2 is large enough. Unlike the situation in the parton model, the simplest definition[6] of P makes it a function also of Q^2, but with computable Q^2 dependence.

The existence of a result such as ours raises some obvious questions:

1. How can there be a QCD prediction for $k_T<\Lambda$?

   Answer (Parisi and Petronzio[3])

   a) Physically, if a particle is observed at $k_T=0$, it got that way as the result of several large P_T transfers which have $\Lambda<<P_T<<Q$ and which just happen to cancel. See Fig.2.

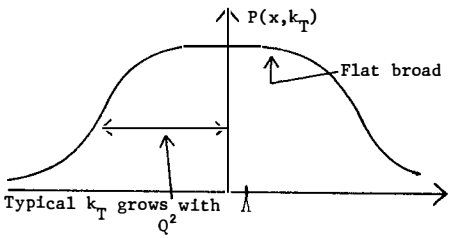

Fig.2 Parton transverse momentum distribution

   b) Technically, one Fourier transforms into the space of transverse position, b (i.e., impact parameter). Large values of b will turn out to be strongly cutoff.

2. How does $P(x,k_T)$ know about Q^2?

   Answer We work in a physical gauge (e.g. $n^\mu A_\mu=0$) with a gauge fixing vector n^μ. Then P depends on

$$\zeta \equiv (2P\cdot n)^2/|n^2|\,. \tag{2.3}$$

In applications $\zeta \sim s$.

3. What has happened to the usual perturbative expansion of the cross-section?

Answer Our generalization of (2.1) applies if $q_T \ll Q$. To it is added a correction term[10] which, although negligible at small q_T, is needed to reproduce the usual result when q_T is of order Q.

There is also a set of theoretical problems we have had to overcome:

1. The presence of two large momentum scales 1/b and Q with $\Lambda \ll 1/b \ll Q$. One can usefully apply renormalization group methods to a function f(Q) or F(1/b) that depends on one momentum scale. Thus

$$\begin{aligned} f(Q,\mu,\alpha_S(\mu)) &= e^{\int\gamma} f(Q,\mu',\alpha_S(\mu')) \\ &= e^{\int\gamma}[C_0+C_1\alpha_S(\mu'^2)\ln(Q^2/\mu'^2)+\ldots], \end{aligned} \tag{2.4}$$

where γ is an anomalous dimension. We can set $\mu'=Q$ to eliminate large logarithms. Simlarly for F(1/b) one sets $\mu'=1/b$. But such a procedure does not help for a function h(Q,1/b) of both varibles.

Solution Manipulate h into a factorized form

$$h(Q,1/b) \sim f(Q)\ F(1/b). \tag{2.5}$$

2. There are double logarithms in $P(x,k_T;\zeta)$ and its Fourier transform $P(x,b;\zeta)$. Thus we have terms of the form

$$\alpha_S(\zeta)^N[C_{N,0}\ln^{2N}(\zeta b^2) + C_{N,1}\ln^{2N-1} +\ldots]. \tag{2.6}$$

Factorization as in eq.(2.5) only generates a single logarithm per loop.

Solution $\tilde{P}$ and P are not simple, but we derive an equation

$$\frac{\partial}{\partial \ln\zeta}\tilde{P} = T\tilde{P} \tag{2.7}$$

in which T is simple. Since a change in ζ is achieved by a change in the gauge fixing vector, use of gauge invariance helps in the analysis of T.

3. Exchange of soft gluons upsets the factorized form shown in Fig.1.

Solution Use a non-abelian generalization[7-8] of the Grammer-Yennie

method[11].

III. Soft Gluon Approximation

The dominant regions of integration in graphs for the cross-section when $q_T \ll Q$ have the form[7,10] of Fig.3. There the lines in J_A and J_B are collinear

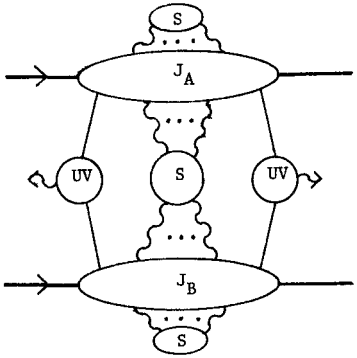

Fig.3 Dominant graphs at low q_T

to the incoming hadron momenta P_A and P_B, respectively, while the lines in UV are ultraviolet and the lines in S are soft. That a momentum k^μ is soft means that in the overall center-of-mass frame all its components are much less than $\sqrt{s}$. All external lines of S are gluons.

In order to reduce Fig.3 to a useful form, we apply a non-abelian version[7-8] of the soft approximation of Grammer and Yennie[11]. This is obtained by noting that, for the coupling of a soft gluon of momentum k^μ to a current J^μ collinear to P_A^μ, we have

$$J^\mu A_\mu \sim J^+ A_+ \sim J^\mu k_\mu A^-/k^- , \tag{3.1}$$

where corrections are smaller by a power of s. This results in Fig.4 where

$$U(x) = T\exp[ig\int_0^\infty d\lambda v_\alpha A_a^\alpha(x+\lambda v)t_a] , \tag{3.2}$$

and v^μ is a lightlike vector collinear to P_A^μ. An example of its perturbation expansion is given in Fig.5. A similar result holds for soft gluons coupling to a line collinear to P_B^μ.

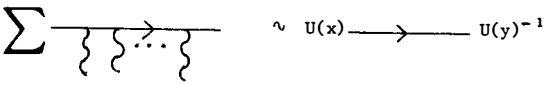

Fig.4 Soft approximation

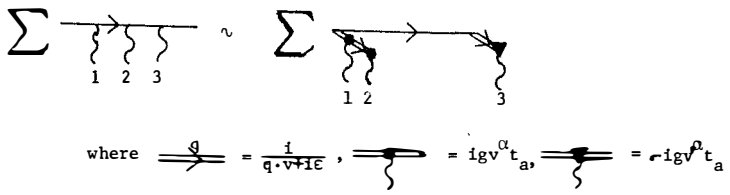

Fig.5 Example of perturbation expansion of Fig.4

After we sum over all attachments of the soft gluons in Fig.3 to the jets, we find that the U factors in Fig.4 cancel at all internal vertices of the jets. This gives Fig.6. Since it involves the convolution in transverse momentum

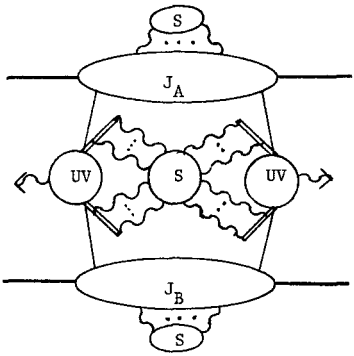

Fig.6 Factorization of cross-section

space of three objects, it is convenient to Fourier transform, so as to obtain

$$\frac{sd\sigma}{dx_A dx_B d^2q_T} \sim N\sum_q e_q^2 \left|H(x_A x_B s/\mu^2, g(\mu))\right|^2$$

$$(2\pi)^2 \int d^2b\ e^{-iq_T b}\ \tilde{P}_{q/A}(x_A,b;\zeta_A)\ \tilde{P}_{\bar{q}/B}(x_B,b;\zeta_B)\tilde{U}(b\mu,g(\mu)). \qquad (3.3)$$

The factor $\tilde{U}$ represents the effect of the bubble S in Fig.6, and UV vertices give the factor $|H|^2$. Both are defined by certain subtraction procedures and have perturbation expansions $1+O(g^2)$. The parton distribution $P_{q/A}(s,k_T;\zeta)$ was defined in Ref.6, and in eq.(3.3) we use its Fourier transform

$$\tilde{P}(x,b;\zeta) = (2\pi)^{-2}\int d^2k_T\ e^{ik_T b}\ P(x,k_T;\zeta). \qquad (3.4)$$

We have set $\zeta_A = sx_B/x_A, \zeta_B = sx_A/x_B$.

IV. Gardens and tulips

In defining the UV and soft factors $|H|^2$ and $\tilde{U}$ in eq.(3.3), we must avoid double counting. Our procedure[7] is like that of Zimmermann[12], who gives a procedure for renormalizing the UV divergences of Feynman graphs. To subtract subdivergences non-recursively, he defines objects called trees and forests. Our analogs of these, for subtracting the soft regions, we call tulips and gardens.

The basic idea is elementary and is illustrated by the example of Fig.7. It consists of two quarks which are in opposite jets and which exchange interacting gluons. Three momentum regions contribute to the leading power of s:

A) The bottom two gluons are soft and the top three are collinear.

B) The top two are soft and the bottom three are collinear.

C) All the gluons are soft.

Now the original graph G in region A is correctly given by the soft approximation applied to the bottom two gluons, as in graph (a). Similarly region B is given by graph (b). Then these are included in the sum over all exchanges of two soft gluons, which gives a term in S in Fig.6.

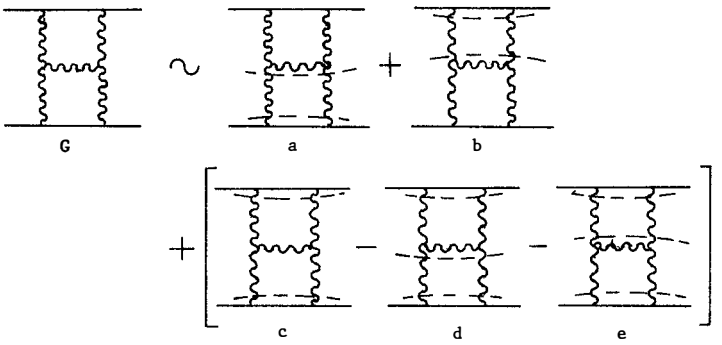

Fig.7 Subtraction procedure for soft exchanges

Now region C is correctly approximated by graph (c). However, graphs (a) and (b) are non-zero in this region and were already included in S in Fig.6. Thus we must make internal subtractions inside graph (c) as shown in graphs (d) and (e).

We can now check that the sum of (a) to (e) is a good approximation to G in any of the regions A, B, or C (so that errors are $O(1/s)$). In region A, graph (a) is a good approximation to G, while (e) cancels (b) and (d) cancels (c). In region B, graph (b) is a good approximation to G, while (d) cancels

(a) and (e) cancels (c). Finally, in region C, graph (c) is a good approximation to G, while (d) cancels (a) and (e) cancels (b).

V. ξ and b dependence of $\hat{P}$

When ζ is large and $1/b \ll \sqrt{\zeta}$, the methods of Ref.7 show that

$$\frac{\partial}{\partial \ln\sqrt{\zeta}} \hat{P}(x,b;\zeta) = [G(x\sqrt{\zeta},g(\mu),\mu)+\hat{K}(b,g(\mu),\mu)]\hat{P}(x,b;\zeta)+O(\tfrac{1}{\zeta})$$

$$= [G(x\sqrt{\zeta},g(x\sqrt{\zeta}),x\sqrt{\zeta})+\hat{K}(b,g(\tfrac{1}{b}),\tfrac{1}{b}) -$$

$$- \int_{1/b}^{x\sqrt{\zeta}} \frac{d\mu'}{\mu'}\gamma_k(g(\mu'))]\ \hat{P}(x,b;\zeta)+O(1/\zeta). \quad (5.1)$$

Here μ is a renormalization mass, and $\hat{K}$,G and γ have perturbation series starting at order g^2. The second equality follows from the renormalization group. Eq.(5.1) can be solved (with the $O(1/\zeta)$ term ignored):

$$\hat{P}_{q/H}(x,b;\zeta) = e^{-S_1(x\sqrt{\zeta},b)}\hat{P}_{q/H}(x,b), \quad (5.2)$$

where

$$S_1 = -\int_{1/b}^{x\sqrt{\zeta}} \frac{d\mu}{\mu}\ [\ln(\tfrac{x\sqrt{\zeta}}{\mu})\gamma_k(g(\mu)) - G(\mu,g(\mu),\mu) - \hat{K}(b,g(\tfrac{1}{b}),\tfrac{1}{b})], \quad (5.3)$$

and $\hat{P}$ is independent of ζ.

For small b (i.e., sufficiently smaller than $1/\Lambda$, where $\Lambda \lesssim 500$MeV is the usual scale parameter of QCD) $\hat{P}$ has a light-cone expansion[6-7] in terms of ordinary parton distributions:

$$\hat{P}_{q/H}(x,b) \sim (2\pi)^{-2}\sum_a \int_x^{1+} \frac{d\xi}{\xi}\ T_{qa}(\tfrac{\xi}{x},b\mu,g(\mu))\ f_{a/H}(\xi,\mu). \quad (5.4)$$

The sum is over parton types (gluon and flavors of quark and antiquark), and

$$T_{qa} = \delta_{qa}\delta(\xi/x-1) + O(g^2). \quad (5.5)$$

VI. The expansion

Combining the results of the previous sections gives

$$\frac{s d\sigma}{dx_A dx_B d^2q_T} \sim N\sum_q e_q^2\, |H(1,g(\sqrt{x_A x_B s}))|^2\ (2\pi)^2 \times$$

$$\times \int d^2b\, e^{iq_T\cdot b}\, \hat{P}_{q/A}(x_A,b,\mu=\tfrac{1}{b})\, \hat{P}_{\bar{q}/B}(x_B,b,\mu=\tfrac{1}{b})\, \tilde{U}(1,g(\tfrac{1}{b}))\, e^{-S}$$

$$+ \frac{N}{s}\sum_{ac}\int \frac{d\xi_A d\xi_B}{\xi_A\xi_B}\, f_{a/A}(\xi_A;\mu) f_{c/B}(\xi_B;\mu)\, \frac{1}{\xi_A\xi_B} D_{ac}(\tfrac{\xi_A}{x_A},\tfrac{\xi_B}{x_B},\tfrac{q_T}{Q};\tfrac{Q}{\mu},g(\mu))$$

$$= \Sigma + Y. \tag{6.1}$$

Here, the first term Σ dominates if $q_T \ll Q$, but the "correction term" Y is equally important if q_T is of order Q. Errors are a power of Q smaller than the terms retained. We have used the renormalization group to avoid large logarithms; thus we set $\mu^2 = x_A x_B s = Q^2+q_T{}^2$ in V and we set $\mu = 1/b$ in $\tilde{U}$ and in $\hat{P}$. This has the result that S is $2S_1$ plus an anomalous dimension term. From the definition (5.3) of S_1, we find that

$$S = 2\int_{1/b}^{\sqrt{x_A x_B s}} \frac{d\mu}{\mu}\left[\frac{1}{2}\ln(\frac{x_A x_B s}{\mu^2})\gamma_k(g(\mu)) - \tilde{K}(b;g(\tfrac{1}{b}),\tfrac{1}{b}) - G(\mu;g(\mu),\mu) + \gamma_c(g(\mu))\right], \tag{6.2}$$

where $\gamma_c(g)$ is the anomalous dimension just noted. The factor N in eq.(6.1) was defined in eq.(2.2). In the second term Y, the renormalization point μ should be chosen of order Q.

There is a certain amount of prescription dependence[13] in the precise definitions of the various factors in Σ. This arbitrariness does not affect the cross-section, but it is convenient to use it to simplify the expression for the low transverse momentum term Σ. We rewrite it as

$$\Sigma = N\sum_q e_q^2\, (2\pi)^2 \int d^2b\, e^{-iq_T\cdot b}\, F_{q/A}(x_A,b)\, F_{\bar{q}/B}(x_B,b)\, e^{-\hat{S}}, \tag{6.3}$$

where

$$\hat{S} = \int_{1/b}^{\sqrt{x_A x_B s}} \frac{d\mu}{\mu}\left[\ln\frac{x_A x_B s}{\mu^2}\,\bar{\gamma}_k(g(\mu)) - 2\bar{K}(b,g(\tfrac{1}{b}),\tfrac{1}{b})\right], \tag{6.4}$$

with $\bar{\gamma}_k$, $\bar{K}$ and F computable in terms of $\beta(g)$ and the quantities appearing in Σ in eq.(6.1). Also F has a light-cone expansion just like (5.4).

To compute the cross-section correct to leading order, so that corrections give a factor $1+O(g^2)$, it is necessary to know the following perturbation expansions to the order given:

$$\bar{\gamma}_k(g) = \frac{8}{3}\frac{\alpha_s}{\pi} + \bar{\gamma}_k^{(2)}\left(\frac{\alpha_s}{\pi}\right)^2 + \ldots, \tag{6.5a}$$

$$\bar{K} = \left[2 + \frac{8}{3}(\ln 2 - \gamma_E)\right]\frac{\alpha_s(1/b)}{\pi} + \ldots, \tag{6.5b}$$

$$\tilde{U} = 1 + \ldots, \tag{6.5c}$$

$$F_{q/H}(x,b,\mu = 1/b) = (2\pi)^2 f_{q/H}(x,\mu = 1/b) + \ldots, \tag{6.5d}$$

$$D_{gq} = D_{g\bar{q}} = \frac{\alpha_s}{4\pi^2} e_q^2 \xi_A \xi_B \left\{ \delta\left((\xi_A - x_A)(\xi_B - x_B) - \frac{q_T^2}{s}\right)\left[\frac{(\hat{s}+\hat{u})^2 + (\hat{t}+\hat{u})^2}{-\hat{s}\hat{t}}\right] - \frac{s}{q_T^2}\left[\frac{x_A^2 + (\xi_A - x_A)^2}{\xi_A^2}\right]\delta\left(\frac{\xi_B}{x_B} - 1\right)\right\} + \ldots, \tag{6.5e}$$

$$D_{qg} = D_{\bar{q}g} = D_{gq}(A \leftrightarrow B), \tag{6.5f}$$

$$D_{q\bar{q}} = D_{\bar{q}g} = \frac{2\alpha_s}{3\pi} e_q^2 \frac{s}{q_T}(x_A^2 \xi_B^2 + \xi_A^2 x_B^2) \times \left\{ \delta((\xi_A - x_A)(\xi_B - x_B) - \frac{q_T^2}{s}) - \delta(\xi_A - x_A)\delta(\xi_B - x_B)\ln\frac{(1-x_A)(1-x_B)}{q_T^2/s} - \delta(\xi_A - x_A)\left(\frac{1}{\xi_B - x_B}\right)_+ - \delta(\xi_B - x_B)\left(\frac{1}{\xi_A - x_A}\right)_+ \right\} + \ldots . \tag{6.5g}$$

Here $\hat{s} = \xi_A \xi_B s, \hat{t} = Q^2 - x_A \xi_B s$, and $\hat{u} = Q^2 - x_B \xi_A s$. As usual $\alpha_s = g^2/(4\pi)$, $g(\mu)$ is the effective coupling, γ_E is Euler's constant (0.577...), e_q is the charge of quark q in units of the positron change, and

$$\int_x^1 d\xi h(\xi)\left(\frac{1}{\xi - x}\right)_+ = \int_x^1 d\xi \frac{h(\xi) - h(x)}{\xi - x} . \tag{6.6}$$

The parton distribution $f_{q/A}(x,\mu)$ is measured in deep inelastic scattering with $Q^2 = \mu^2$.

The only one of the above coefficients that we have not yet calculated is for the two loop term in $\bar{\gamma}_k$. It has an important effect on the cross-section, as can be seen from the leading order form:

$$\frac{s d\sigma}{dx_A dx_B d^2 q_T} \sim N \sum_q e_q^2 (2\pi)^2 \int d^2 b\, e^{i q_T \cdot b} f_{q/A}(x_A; \frac{1}{b})\, f_{\bar{q}b}(x_B; \frac{1}{b})$$

$$\exp\left\{ -\int_{1/b}^{\sqrt{x_A x_B s}} \frac{d\mu}{\mu} \ln\left(\frac{x_A x_B s}{\mu^2}\right)\left[\frac{8}{3}\frac{\alpha_s(\mu)}{\pi} + \bar{\gamma}_k^{(2)}\left(\frac{\alpha_s(\mu)}{\pi}\right)^2\right] + \frac{8}{3}\left(\frac{3}{4}+\ln 2-\gamma_E\right)\frac{\alpha_s(1/b)}{\pi}\ln(x_A x_B s b^2)\right\} + Y. \qquad (6.7)$$

Here we assume that small values of b dominate in the Fourier transform, as we will prove in the next section.

Parisi and Petronzio[3] suggested this formula, but without the second term in the exponent, without $\bar{\gamma}_k^{(2)}$, and without the correction term Y. All these three quantities are necessary to obtain correctly the normalization and shape of the cross-section with fractional errors of order g^2. Nevertheless, their result is qualitatively correct, and in particular, gives the correct leading form for the s-dependence of the cross-section at small transverse momentum.

We expect there to be a "K-factor", as usual[2].

VII. Fourier transform

Qualitative properties of the transverse momentum distribution are easily derived from eq.(6.3). The factor e^{-S} provides a cut off at large b. This cut off gets stronger as s increases with x_A and x_B fixed. This behavior is illustrated in Fig.8, where $sd\tilde{\sigma}/(dx_A dx_B)$ is the Fourier transform of $sd\sigma/(dx_A dx_B d^2q_T)$.

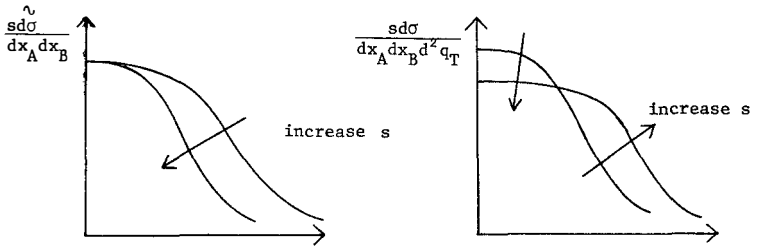

Fig.8 Effect of increasing s with x_A and x_B fixed

This behavior is seen in the CFS data[14] with about the predicted magnitude. (We have not made detailed numerical fits.) Since large values of b are cut off, the whole of the cross-section is dominated by short distance effects.

To get quantitative results, we can perform the Fourier transform numerically (which we are in the process of doing) or we can use the following analytic method[5,9,15]:

1. Mellin transform the integrand in Σ, to give $\Sigma_M(r)$.
2. Write $\Sigma(q_T)$ in terms of $\Sigma_M(r)$.
3. Compute $\Sigma_M(r)$ by expanding about a saddle point.
4. Compute $\Sigma(q_T)$ by expanding about a saddle point.

The analytic method works as follows. Define new variables by:

$$\begin{aligned} \omega &= \ln(x_A x_B s/\Lambda^2), \\ \omega z &= \ln(1/(b^2\Lambda^2)), \\ t &= \ln(\mu^2/\Lambda^2), \\ \tau &= t/\omega \\ u &= \ln(q_T^{\,2}/(4\Lambda^2))/\omega, \end{aligned} \tag{7.1}$$

so that we have

$$\frac{\alpha_s(\mu)}{\pi} = \frac{12}{33-2N}\frac{1}{t} - \frac{72(153-19N)}{(33-2N)^3}\frac{\ln t}{t^2} + O\left(\frac{\ln^2 t}{t^3}\right), \tag{7.2}$$

with N flavors of massless quark. Then we rewrite Σ in eq.(6.1) as:

$$\Sigma = \int d^2b\, e^{iq_T\cdot b}\, e^{-\omega I(z)} R(z,\omega). \tag{7.3}$$

Here

$$\begin{aligned} \omega I(z) &= A \int_{1/b^2}^{x_A x_B s} \frac{d\mu^2}{\mu^2} \ln\frac{x_A x_B s}{\mu^2} \frac{1}{\ln\mu^2/\Lambda^2} \\ &= A\omega \int_z^1 d\tau(1-\tau)/\tau, \end{aligned} \tag{7.4}$$

where $A = 16/(33-2N)$, is the leading logarithm contribution to S. The factor $R(z,\omega)$ varies less rapidly with ω.

The Mellin transform is defined to be:

$$\begin{aligned} \Sigma_M(r) &= \int_0^\infty \frac{db^2}{b^2} (\Lambda^2 b^2)^r\, e^{-\omega I(z)} R(z,\omega) \\ &= \omega \int_{-\infty}^{\infty} dz\, e^{-\omega[rz - I(z)]} R(z,\omega). \end{aligned} \tag{7.5}$$

Then we have

$$\Sigma(q_T) = \frac{2}{iq_T^{\,2}} \int_\Gamma dr \frac{\Gamma(1-r)}{\Gamma(r)} \left(\frac{q_T^{\,2}}{4\Lambda^2}\right)^r \Sigma_M(r), \tag{7.6}$$

where Γ is the contour in Fig.9.

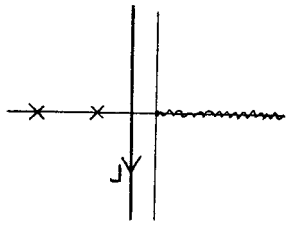

Fig.9 The contour Γ

The integral in eq.(7.5) is dominated by the saddle point at $z = z_o(r) = A/(A+r)$, so

$$\Sigma_M(r) \sim \frac{(2\pi A\omega)^{\frac{1}{2}}}{A+r} e^{-\omega[z_o r+I(z_o)]} R(z_o,\omega). \tag{7.7}$$

Thus

$$\Sigma(q_T) = \frac{(8\pi A\omega)^{\frac{1}{2}}}{iq_T^2} \int_\Gamma dr \frac{\Gamma(1-r)}{\Gamma(r)} \frac{R(z_o(r),\omega)}{A+r} \times \exp -\left\{[(z_o(r)-u)r+I(z_o(r))]\right\} \tag{7.8}$$

There is a saddle point at $r_o = A(1-u)/u$ so that $z_o(r_o) = u$. But there is also a pole at $r = 1$, so that a simple saddle point expansion does not work. We consider separately the two cases $r_o<1$ and $r_o>1$.

If $r_o<1$, then $q_T>q_{Tc}$ where

$$q_{Tc} = 2\Lambda^{1/(A+1)}(x_1x_2\omega)^{A/[2(A+1)]}. \tag{7.9}$$

We treat the pole of $\Gamma(1-r)$ exactly and the rest of the integrand in the saddle point approximation to obtain

$$\Sigma = \frac{4}{q_T^2}\left(\frac{2\pi\omega}{A}\right)^{\frac{1}{2}} \frac{\Gamma(2-r_o(u))u}{\Gamma(r_o(u))} e^{-\omega I(u)} R(u,\omega)\epsilon, \tag{7.10}$$

where

$$\epsilon = \frac{1}{2} e^{\phi^2} \operatorname{erfc}(\phi), \tag{7.11}$$

$$\phi = \frac{(A+1)}{(2A)^{\frac{1}{2}}} \omega^{\frac{1}{2}}(u-u_c), \tag{7.12}$$

$$u_c = A/(A+1).$$

If $q_T<q_{Tc}$ then $r_o>1$ and it is the pole that is most important. We find

$$\Sigma = \frac{4}{q_T^2} \frac{(2\pi A\omega)^{\frac{1}{2}}}{A+1} R(u_c,\omega)\epsilon\, e^{-\omega[u_c-u+\frac{1}{2}A(1-u/u_c)^2]}\, e^{-\omega I(u_c)}. \tag{7.13}$$

When $q_T \to 0$, we have

$$\Sigma(q_T=0) = \frac{1}{A+1}\,\pi\sqrt{2\pi A\omega}\,R(u_c,\omega)\,\frac{1}{(x_1x_2s)^{a/2(1-a)}}, \tag{7.14}$$

where

$$a = A\ln(1+1/A) \simeq 0.6, \tag{7.15}$$

The dramatically s-dependent value of $\Sigma(0)$ provides a good way of measuring Λ accurately. Note that the two loop term, which we have not yet calculated, in γ_k is necessary to normalize $R(u_c,\omega)$ correctly. Note also that the maximum relevant value of b is given by $z = z_o(1)$, i.e.

$$b_{max} = (x_1x_2s)^{-\frac{1}{2}A/(A+1)}\,\Lambda^{-1/(A+1)} \sim Q^{-A/(A+1)}\,\Lambda^{-1(A+1)}\ , \tag{7.16}$$

which illustrates the short distance nature of the problem as $Q\to\infty$.

Corrections to the saddle point expansion are computable and involve inverse powers of ω relative to the leading term (7.8) or (7.10). Some of these are order $(\ln^2\omega)/\omega$ or of order $\omega^{-\frac{1}{2}}$, and should be computed before comparison is made with data.

VIII. Problems

The result for e^+e^- → A+B + anything that corresponds to eq.(6.1) has a complete proof[6-7]. At first sight, the proof seems to apply also to the Drell-Yan case, as we have summarized in the previous sections. However[8], there is a momentum region of soft exchanges for which the soft approximation (Figs.4 and 5) is invalid. This is the region of Glauber scattering[16]. In the e^+e^- case, the momentum integrals can be deformed[8] out of this region and the $i\varepsilon$ in Fig.5 can be consistently chosen so as not to prevent the deformation. The the Glauber region is effectively absent.

We have not been able to make this procedure work for the Drell-Yan process. Thus our proof of eq.(6.1) is incomplete. Closely related phenomena are treated by Doria et al[17].

Another related problem is in the proof of factorization in the usual sense for large transverse momentum processes such as Drell-Yan with $q_T \sim Q$. It is necessary to prove cancellation of soft exchanges. The first complete proof was given in Ref.8 for the e^+e^- case, by using the soft approximation of Section III. Precisely the same obstacle described above hindered a proof for the Drell-Yan or any other process with initial state hadrons.

So factorization for dilepton production remains, on the theoretical level, a conjecture, even though strongly supported by experiment[18]. We believe that if a proof of factorization is found, then we will be able to prove eq.(6.1).

Note that no problems arise[10] in the absence of gauge fields.

IX. Conclusions

We have seen that the Drell-Yan cross-section at low transverse momentum appears to be a short distance problem. It is, therefore, perturbatively computable in terms of the parton distributions $f_{a/H}(x)$. The reason for the calculability is the copious emission of gluons. There is strong energy dependence and this will allow an accurate determination of the strong interaction scale Λ.

Two problems remain. The first is to calculate the $O(g^4)$ term in γ_k. This is needed, in particular, to relate Λ to the shape of the cross-section at low q_T. The second problem is to extend the proof of our result in e^+e^- annihilation to the Drell-Yan case.

Acknowledgements

This work was supported in part by the U.S. Department of Energy under contracts EY-76-S-06-2230 and DE-AC02-80ER10712.

References

1. S.D. Drell and T.M. Yan, Ann. Phys. (NY) 66, 578 (1971).
2. E.g.: Other talks at this meeting;
   Yu.L. Dokshitzer, D.I. Dyakonov and S.I. Troyan, Phys. Rep. 58, 269 (1980).
3. G. Parisi and R. Petronzio, Nucl. Phys. B154, 427 (1979).
4. S.D. Ellis and W.J. Stirling, Phys. Rev. D23, 214 (1981).
5. P.E.L. Rakow and B.R. Webber, Cavendish Lab. (Cambridge) preprint HEP 81/4.
6. J.C. Collins and D.E. Soper, "Parton distribution and decay functions", IIT preprint.
7. J.C. Collins and D.E. Soper, "Back-to-back jets in QCD", Oregon preprint OITS-155.
8. J.C. Collins and G. Sterman, Nucl. Phys. (to be published).
9. D.E. Soper, in L. Durand and L. Pondrom, Proc. XX International Conference on High Energy Physics, Madison, 1980; J.C. Collins and D.E. Soper, "Back-to-back jets: Fourier transform from b to Q_T", Oregon preprint OITS-153.
10. J.C. Collins, Phys. Rev. D21, 2962 (1980).
11. G. Grammer and D.R. Yennie, Phys. Rev. D8, 4332 (1973).
12. W. Zimmermann, Comm. Math. Phys. 15, 208 (1969).
13. J.C. Collins, Phys. Rev. D22, 1478 (1980).
14. A.S. Ito et al, Phys. Rev. D23, 604 (1981).
15. H.F. Jones and J. Wyndham, Imperial College preprint ICTP/79-80/48.
16. S.J. Brodsky, personal communication.
17. R. Doria, J. Frenkel and J.C. Taylor, Nucl. Phys. B168, 93 (1980).
18. E.g., experimental talks at this meeting.

LEPTON PAIR PRODUCTION AT HIGH TRANSVERSE MOMENTUM

F. Halzen
Physics Department, University of Wisconsin, Madison, WI 53706, USA

D.M. Scott
Department of Applied Mathematics and Theoretical Physics,
University of Cambridge, Silver Street, Cambridge

ABSTRACT

We give a brief account of the phenomenological status of QCD calculations for the production of lepton pairs and direct photons at high transverse momentum, and discuss some consequences for collider energies.

Introduction

Data on the production of high mass m, high transverse momentum p_T lepton pairs in proton-nucleus collisions appeared over three years ago[1], followed closely by calculations of the spectrum in lowest order perturbative QCD[2]. The similarity between calculation and data gave support to the simple interpretation in terms of $O(\alpha_s)$ QCD mechanisms, in particular, quark-gluon Compton scattering. This then led to predictions of copious direct photon production[3] at high p_T, where the same $O(\alpha_s)$ QCD mechanisms are utilised and for which there is now experimental evidence[4], and to many calculations of the high p_T cross section to leading logarithms, in a region where Q/p_T is also large.

Here we wish to give a short account of the present phenomenological status of the calculations. We review results for pN interactions, and present calculations for the p_T distributions of lepton pairs in π^-N interactions, and for the bremsstrahlung mechanism for producing high p_T direct photons. Finally we make some remarks appropriate to collider energies.

$O(\alpha_s)$ calculations

The familiar $O(\alpha_s)$ QCD subprocesses for high m, p_T virtual photon production are shown in fig. 1. Calculations are described in detail in refs 2) and here we note that:

(i) At high p_T the diagrams are appropriate for calculating[5] cross sections for lepton pairs with $0 \leq m \leq O(s^{\frac{1}{2}})$, not just high mass. We return later to the case m = 0, direct photons.

(ii) In proton-nucleon scattering, the gluon-quark Compton scattering diagram, fig. 1a, is supposed to dominate at high p_T, because of the fast fall-off with x of the antiquark density in the nucleon $\bar{q}(x)$. Consequently the high p_T cross section depends directly on the gluon density in the nucleon G(x). The similarity between data from CFS[1] and the "bare" calculation with no regularisation or smearing, for $p_T \gtrsim 1$ GeV, gives evidence for the validity of the lowest order calculation, and so for the existence of the gluon. A gluon density of the form $xG(x) = \frac{1}{2}(n+1)(1-x)^n$ with $n \simeq 5$ is consistent with this data, as demonstrated in fig. 2 (and with a lot of other data as well).

We have carried out the $O(\alpha_s)$ calculation for π^-N scattering, and compared it to data from NA3[6] in fig. 3. We used NA3 quark densities[7], and the shape of the pion's glue density was taken from an analysis of ψ production[8]. We see that the "bare" QCD calculation gives a result which is a factor $\simeq 10$ below the data for $p_T \gtrsim 1$ GeV. However if we use the methods of Altarelli, Parisi and Petronzio[2] to smear with a parton intrinsic $\langle p_T^2 \rangle = 1$ GeV^2, and multiply the result[9] by 2.4, we get much better agreement with data as shown in fig. 3. We

note that $q\bar{q}$ annihilation dominates the high p_T cross section in $\pi^- N$ scattering, while qg Compton scattering dominates in pN scattering, so there is no reason for the two processes to have the same high p_T K-factor.

As $p_T \to 0$ the cross sections diverge as

$$\frac{d\sigma^{qg}}{dp_T^2} \sim \frac{1}{p_T^2}, \qquad \frac{d\sigma^{q\bar{q}}}{dp_T^2} \sim \frac{\ell n(s/p_T^2)}{p_T^2}, \tag{1}$$

and so we may only compare the $O(\alpha_s)$ calculation to data for sufficiently high p_T. The divergences in eq.(1) are of course absorbed as scaling violations in quark and gluon densities, but the p_T moments of the cross section are finite, and dividing by the lowest order p_T-integrated (Drell-Yan) cross section, we have

$$\langle p_T^2 \rangle = \alpha_s(m^2)\, s\, F(m^2/s), \tag{2}$$

where F can be calculated from parton densities. It develops dependence on α_s in higher orders. We emphasize that QCD gives the coefficient of s in eq.(2), but that extra contributions to $\langle p_T^2 \rangle$ coming from smearing and regularisation effects must also be present — the $O(\alpha_s)$ QCD cross section does not describe the data for low p_T. It usually turns out that the contribution to $\langle p_T^2 \rangle$ from QCD is smaller than that which must be taken from intrinsic transverse momentum, and very little is known about intrinsic p_T. It may, for example be strongly x dependent[10].

In fig. 4 we show data on $\langle p_T^2 \rangle$ at fixed $\tau^{\frac{1}{2}} = m/s^{\frac{1}{2}} = 0.275$ in $\pi^- N$ scattering[11], which follows the scaling given by eq.(2). However the numerical value of the coefficient of s should be calculable in $O(\alpha_s)$ QCD. The $O(\alpha_s)$ moment divided by the theoretical Drell-Yan cross section gives an answer too small by about a factor 2. This is probably very sensitive to the argument of α_s, which we have taken to be m^2. If p_T^2 is used instead, some ad hoc cut-off to avoid the singularity at $p_T^2 = \Lambda^2$ must then be applied.

This is clearly an area warranting more investigation, both experimental and theoretical. In order to give a detailed description of the data the effects of A dependence, smearing, leading logarithms and higher orders may be needed. Finally, we should not forget the fire sausage[12], which gives an appetising description of all this data.

Direct photons

At high p_T one need not pay the extra price of high m in order to test QCD calculations. High p_T, low m lepton pair cross sections have been studied in ref. 5), and much effort has been devoted to high p_T direct photon production[3,4,13], for which m = 0. The same subprocesses as for high m lepton pairs are required,

data out to $p_T \simeq 12$ GeV from the ISR, and information about correlated hadrons exist — this makes direct photons very attractive as a probe of QCD. Present data on cross sections and correlated hadrons are consistent with QCD expectations. We show data[14] compared to an early QCD calculation[15] in fig. 5.

Another way to get a high p_T direct photon is by bremsstrahlung from a high p_T quark[16], for example as shown in fig. 6. Detailed estimates made by Contogouris, Gaskell and Marleau[17] have suggested that at very high p_T this mechanism may dominate. Simply, this may be because, as they are assumed to be controlled by a parameter like p_T^2, scaling violations make G(x) become softer relative to q(x), allowing the bremsstrahlung mechanism to appear above the previously dominant quark-gluon Compton scattering mechanism of fig. 1a. There is a discussion in ref. 18.

The experimental characteristics of the two subprocesses are that in the $2 \to 2$ scatters of fig. 1 the photon is produced unaccompanied by hadrons, whereas for the bremsstrahlung mechanism the photon is accompanied by the hadronisation products of the quark which emitted it. Experimental evidence exists for the two components[19,20], and in particular, data from CCOR[20] is plotted in fig. 7. What is plotted is

$$f_i = \gamma_i/(\gamma_i + \pi_i^o) \tag{3}$$

with i = A (accompanied), U (unaccompanied). Then

$$\frac{\gamma_A}{\gamma_U} = \frac{f_A(1-f_U)}{f_U(1-f_A)} \frac{\pi_A^o}{\pi_U^o} . \tag{4}$$

From fig. 7 we see that for $p_T \simeq 12$ GeV, $f_A \simeq f_U$ and so

$$\frac{\gamma_A}{\gamma_U} \simeq \frac{\pi_A^o}{\pi_U^o} , \quad p_T \simeq 12 \text{ GeV} . \tag{5}$$

As high p_T π^o's are fragments of high p_T quarks or gluons, we expect $\pi_A^o \gtrsim \pi_U^o$, which indicates via eq.(5), important production of accompanied photons, which we interpret as bremsstrahlung photons.

Leptons at collider energies

It is easy in principle to extrapolate the calculations to collider energies, e.g. $\sqrt{s} = 540$ GeV, but in practice it is necessary to evolve parton densities over a very large range of Q^2. This surely leads to uncertainty. However, our intention here is not to give a detailed discussion of this, and we use parton densities which scale[15] or which have simple scale violating forms[21].

As well as electro-weak production of lepton pairs, there is another important source. This is via heavy quark-antiquark production and semileptonic decay[22] :

$$\bar{p}p \to (Q \to \ell + x) + (\bar{Q} \to \bar{\ell} + x) + x \ , \qquad (6)$$

where Q = c,b,t(?). Because of weak isospin assignments, dominant production for high mass lepton pairs is from b flavour. A sample calculation of the dilepton mass spectrum in $\bar{p}p$ at $\sqrt{s}$ = 540 GeV is shown in fig. 8. The limits of the bands come from two choices of parton densities[15,21]. The p_T distribution of such pairs can also be calculated, and the result for m = 20 GeV is compared to the $0(\alpha_s)$ QCD result in fig. 9. We note that such leptons may be distinguished from electroweak pairs in that (a) they are accompanied by a hadron shower, and (b) the rates for $\mu^+\mu^-$ and μ^+e^- will be the same.

The subprocesses in fig. 1 can be used to calculate the high p_T spectra of the weak bosons, W,Z[23]. The measurement of these spectra will be useful in testing various leading logarithmic modifications of the $0(\alpha_s)$ result[24], which require Q/p_T as well as p_T to be large, and which may be appropriate for even $p_T \simeq 0$. A particularly sensitive measurement will be the p_T spectrum of the charged lepton ℓ from $W \to \ell\nu$ decay. If the W is produced with $\langle p_T \rangle \simeq 0$, then this spectrum exhibits the pronounced Jacobian peak at $p_T = \frac{1}{2}m_W$. This peak not only shows the existence of the W, but also pins down its mass — an essential quantity for testing higher order calculations[25]. The $0(\alpha_s)$ subprocesses of fig. 1 suggest that for W,Z, $\langle p_T^2 \rangle \simeq$ 100-200 GeV^2. What will happen to the Jacobian peak? In a detailed $0(\alpha_s)$ calculation, Aurenche and Lindfors show that the peak remains[26] but using a W spectrum calculated in leading logarithm may flatten it into a broad shoulder. This is under investigation[27].

Concluding remarks

(1) The high p_T spectrum of high m lepton pairs in pN collisions is understood in $0(\alpha_s)$ QCD in terms of quark-gluon Compton scattering. It seems that the spectrum in π^-N collisions may be understood in terms of $q\bar{q}$ annihilation if the factor K $\simeq$ 2.4 is applied to the p_T distribution as well as the p_T-integrated cross section. The calculation of this K factor is almost upon us[9], and more phenomenological work needs to be done.

(2) Direct photons at high p_T have provided another way of looking at the same QCD mechanisms. What they lack are the complications attendant to a two-scale process. Experimental results on cross sections and correlations are in encouraging agreement with QCD expectations, and evidence is now accumulating for the existence of the bremsstrahlung component at very high p_T.

(3) At collider energies $Q\bar{Q}$ (Q = c,b,t) production and semileptonic decay will provide an important source of lepton pairs. It should be possible to separate these from continuum pairs by examining associated hadrons, and $\mu^+\mu^-$, μ^+e^- cross sections.

(4) Because of the high energies, m's, p_T's involved, p_T spectra of the weak bosons will provide a good testing ground for leading logarithm calculations.

Acknowledgements

We thank M. Dechantsreiter, P. Landshoff, H. Lansdowne, R. Roberts, and most of all, Tran Thanh Van.

References

1. A.S. Ito et al., Phys. Rev. D23 (1981) 604.
2. G. Altarelli, G. Parisi and R. Petronzio, Phys. Lett. 76B (1978) 351, 356; K. Kajantie and R. Raitio, Nucl. Phys. B139 (1978) 72; H. Fritzsch and P. Minkowski, Phys. Lett. 73B (1978) 80; F. Halzen and D.M. Scott, Phys. Rev. Lett. 40 (1978) 1117, Phys. Rev. D18 (1978) 3378; C. Michael and T. Weiler, Proceedings of XIII Rencontre de Moriond, 1978, edited by J. Tran Thanh Van (Editions Frontieres, Gif-sur-Yvette, 1978), p.179; E. Berger, Vanderbilt Conference, 1978.
3. For a review and references see F. Halzen and D.M. Scott, Proceedings of Madison Conference, 1980.
4. M. Diakonou et al., Phys. Lett. 91B (1980) 296; A.L.S. Angelis et al., Phys. Lettt. 94B (1980) 106; E. Amaldi et al. Nucl. Phys. B150 (1979) 326.
5. J.H. Cobb et al., Phys. Lett. 78B (1978) 519; F. Halzen and D.M. Scott, Phys. Lett. 80B (1978) 410.
6. J. Badier et al., CERN/EP 80-150, submitted to Madison Conference 1980.
7. J. Badier et al., CERN/EP 80-148, submitted to Madison Conference 1980.
8. V. Barger, Y. Keung and R.J.N. Phillips, Z. Phys. C6 (1980) 169.
9. See talks by Ellis and Martinelli at this Workshop.
10. P. Landshoff, Phys. Lett. 66B (1977) 452.
11. See G. Matthiae, CERN-EP/80-183.
12. C. Bourrely, P. Chiapetta and J. Soffer, Marseille preprint 81/P.1267.
13. Direct Photon Production, ISR discussion meeting, M.G. Albrow and M. Jacob.
14. L. Cormell and J. Owens, Phys. Rev. D22 (1980) 1609.
15. Halzen and Scott, ref. 2.
16. R. Ruckl, S. Brodsky and J. Gunion, Phys. Rev. D18 (1978) 2469.
17. A.P. Contogouris, R. Gaskell and L. Marleau, Phys. Rev. D22 (1980) 1109.
18. M. Dechantsreiter, F. Halzen and D.M. Scott, UW-Madison report, 1981.
19. Talk by W. Molzon, this Workshop.
20. Talk by J. Linnemann, this Workshop; A.L.S. Angelis et al., Phys. Lett. 98B (1981) 115.
21. J. Owens and E. Reya, Phys. Rev. D17 (1978) 3003.
22. S. Pakvasa, M. Dechantsreiter, F. Halzen and D.M. Scott, Phys. Rev. D20 (1979) 2862; D.M. Scott, Proceedings of Workshop on the Production of New Particles in Super High Energy Collisions, Madison 1979; F. Halzen and D.M. Scott, Proceedings of Madison Conference, 1980.
23. F. Halzen and D.M. Scott, Phys. Lett. 78B (1978) 318.
24. Yu.L. Dokshitser, D.I. Dyakonov and S.I. Troyan, Phys. Rep. 58 (1980) 269; G. Parisi and R. Petronzio, Nucl. Phys. B154 (1979) 427; G. Curci, M. Greco and Y. Srivastava, Nucl. Phys. B159 (1979) 451; H.F. Jones and J. Wyndham,

Imperial College preprints; S. Ellis and J. Stirling, Seattle preprint; P. Rakow and B. Webber, Cavendish preprint HEP 81/4; talks by Collins, Soper, Pancheri and Cleymans at this Workshop.
25. F. Antonelli, M. Consoli and G. Corbo, Phys. Lett. 91B (1980) 90; M. Veltman, Phys. Lett. 91B (1980) 95.
26. P. Aurenche and J. Lindfors, Phys. Lett. 96B (1980) 171; TH.2992-CERN.
27. M. Dechantsreiter, F. Halzen, D.M. Scott and B. Webber, in preparation.

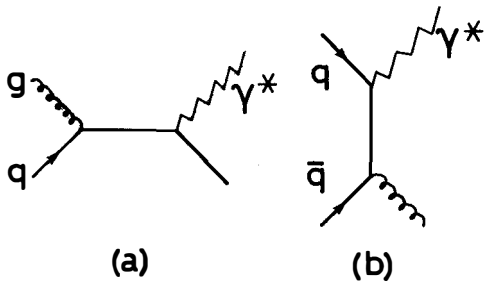

Fig. 1. $O(\alpha_s)$ QCD diagrams for producing a high p_T real or virtual proton.

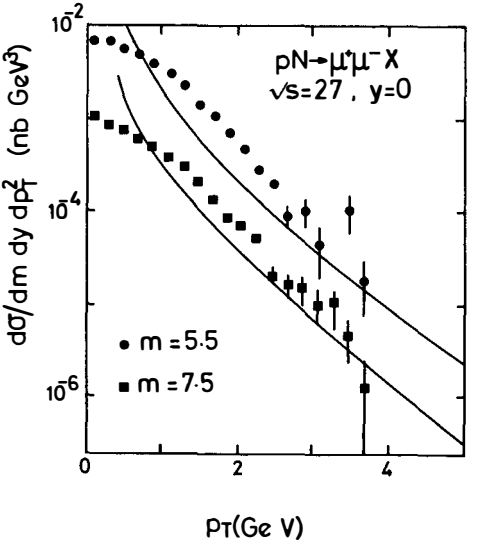

Fig. 2.

The $O(\alpha_s)$ QCD calculation is compared to data on the p_T distribution of high mass lepton pairs produced in pN collisions.

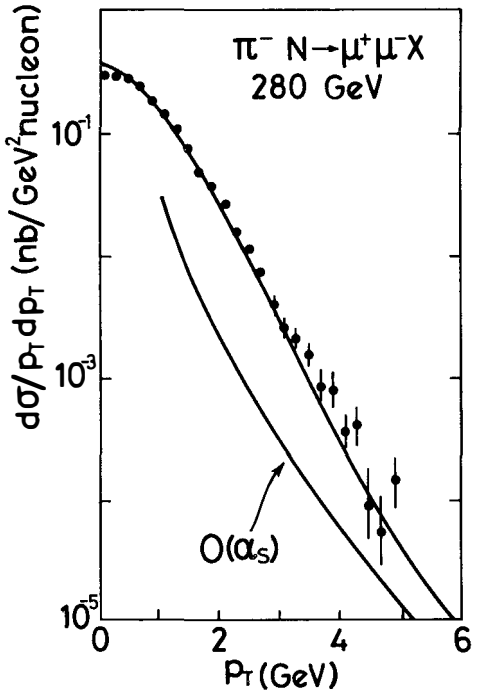

Fig. 3

The p_T distribution of lepton pairs with 4.1 GeV<m<8.5 GeV and $y \geq -0.6$ in π^--platinum collisions. Data is compared to the $O(\alpha_s)$ calculation, and to an $O(\alpha_s)$ calculation regularised with a Gaussian of $\langle p_T^2 \rangle = 1$ GeV^2 and renormalised by a constant factor 2.4.

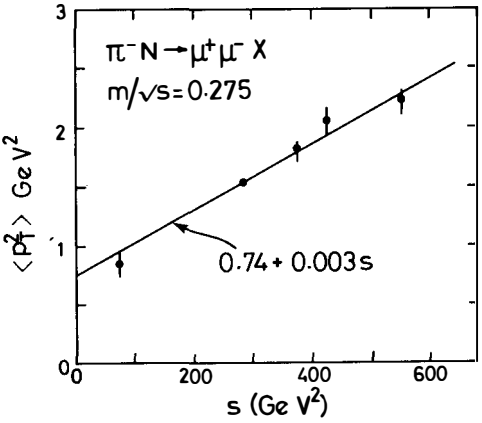

Fig. 4.

$\langle p_T^2 \rangle$ of lepton pairs in π^-N collisions at fixed $m/\sqrt{s} = 0.275$.

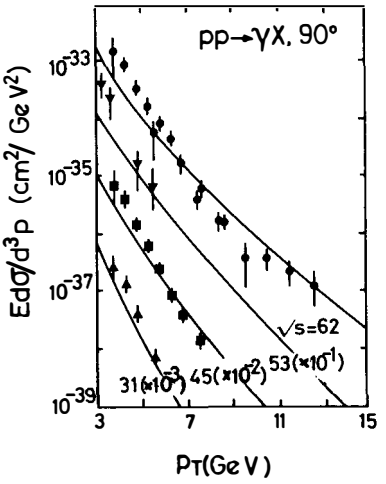

Fig. 5.

The $O(\alpha_s)$ QCD calculation is compared to data on the p_T distribution of direct photons produced in pp collisions.

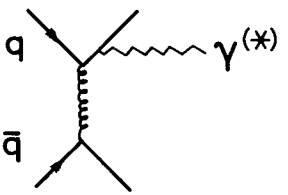

Fig. 6.

The bremsstrahlung mechanism for producing high p_T direct photons in hadron-hadron collisions.

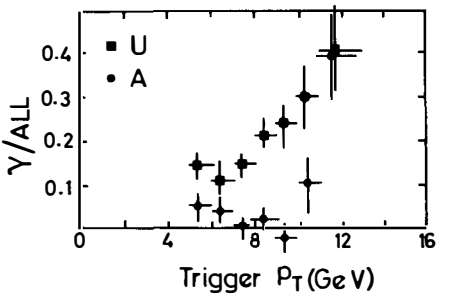

Fig. 7.

The ratios $\gamma/(\gamma+\pi^0)$ for unaccompanied (U) and accompanied (A) triggers plotted as a function of p_T. The trigger is at 90° in the centre of mass, and the data are a combination of $\sqrt{s}$ = 44 and 62 GeV.

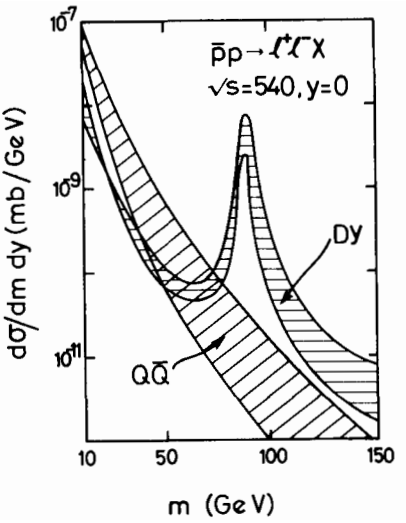

Fig. 8.

Calculation of the dilepton spectrum in $\bar{p}p$ collisions at $\sqrt{s}$ = 540 GeV, y = 0.

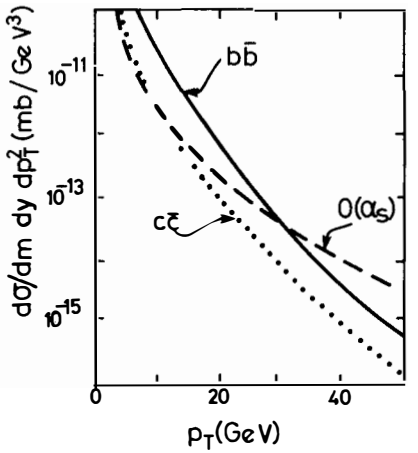

Fig. 9.

The transverse momentum distribution of lepton pairs with m = 20 GeV in $\bar{p}p$ collisions at $\sqrt{s}$ = 540 GeV, y = 0 calculated from $O(\alpha_s)$ QCD (Fig. 1) and heavy $Q\bar{Q}$ production and semileptonic decay.

$O(\alpha_S^2)$ CORRECTIONS TO HIGH TRANSVERSE MOMENTUM LEPTON PAIR PRODUCTION

G. Martinelli
CERN - Geneva

ABSTRACT

I present a calculation of the distribution of high transverse momentum lepton pairs in Drell-Yan processes up to order α_S^2.

In recent years it has been realized that QCD perturbative corrections to the naïve (renormalization group improved) parton model can give sizeable and measurable effects. In particular, we know that $O(\alpha_S)$ corrections to lepton pair production significantly modify the results given by the Drell-Yan formula [1]. Let us define the ratio :

$$K(\tau) = \frac{\frac{d\sigma}{dQ^2}\Big|_{LLA + O(\alpha_S)}}{\frac{d\sigma}{dQ^2}\Big|_{LLA}} \qquad \tau = Q^2/S \tag{1}$$

Q^2 is the mass of the virtual photon (lepton pair system) and $K(\tau)$ measures the magnitude of the first order (non-leading) corrections. $(d\sigma/dQ^2)_{LLA}$ is the Drell-Yan cross-section, improved by resumming the leading logarithms in $\alpha_S(Q^2)\,\ell n\, Q^2$ to all orders in perturbation theory [this is achieved by transforming the scaling parton densities $q(x)$ in the Drell-Yan formula into corresponding non-scaling densities $q(x,Q^2)$ obeying the Altarelli-Parisi evolution equations [2]]. $(d\sigma/dQ^2)_{LLA+O(\alpha_S)}$ is the cross-section computed by going beyond the leading logarithm approximation to include corrections $\sim\alpha_S(Q^2)$ that go to zero as $1/\ell n\, Q^2/\Lambda^2$ for $Q^2 \to \infty$. Using the parton densities measured by deep inelastic scattering, it turns out that the K factor $K(\tau)$ is significantly larger than 1 [$K(\tau)\simeq 2$] and substantially independent of τ at present accessible values of S and Q^2 [3]. The K factor is essentially (but not only) due to soft gluon emissions that, at order α_S, modify differently the electromagnetic vertex in the space-like region (deep inelastic scattering $Q^2 < 0$) and in the time-like region (Drell-Yan $Q^2 > 0$).

The scope of our research was to determine whether a similar phenomenon will happen for the transverse momentum distribution of lepton pairs.

In the limit in which all partons are collinear to the parent hadrons (i.e., neglecting terms $\sim(p_T^2)^{intrinsic}/Q^2$), virtual photons with high transverse momentum are produced via gluon bremsstrahlung or Compton scattering as shown in Fig. 1a,b,c

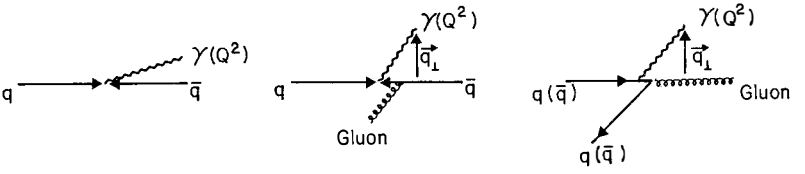

Fig. 1a - Lowest order $q\bar{q}$ annihilation. The transverse momentum of lepton pair is $\sim(p_T^2)^{intrinsic}/Q^2$.

Fig. 1b,c - $O(\alpha_S)$ high transverse momentum virtual photons are produced by gluon bremsstrahlung (1b) and Compton scattering (1c) $q_T^2 \sim Q^2$.

It is clear from Fig. 1 that, because high transverse momentum photons are produced by the interaction of quarks and gluons, the cross-section $d^2\sigma/dQ^2dq_T^2$ is at least of order α_S. Then K factor for $d\sigma/dQ^2dq_T^2$ will come out (if it is there) at $O(\alpha_S^2)$ in perturbation theory.

A second interesting (related) question is whether or not second order corrections modify the slope of the average transverse momentum plotted against S. This is defined as :

$$\frac{\langle q_T^2 \rangle}{S} = \frac{1}{S} \frac{\int dq_T^2 \, q_T^2 \frac{d\sigma}{dQ^2 dq_T^2}}{\int dq_T^2 \frac{d\sigma}{dQ^2 dq_T^2}} = \alpha_S(Q^2) \; f\left[\tau, \alpha_S(Q^2)\right] \qquad (2)$$

[the relation of Eq. (2) is true to all orders in $\alpha_S(Q^2)$ on general dimensional grounds]. If the corrections to $d\sigma/dQ^2$ were small, then formally a calculation at order α_S would only require $d\sigma/dQ^2$ at order zero in the denominator [Eq. (2)]. Because we cannot neglect the $O(\alpha_S)$ corrections of the denominator [because of the K factor in Eq. (1)], we must investigate the $O(\alpha_S^2)$ corrections of the numerator. The computation of the $O(\alpha_S^2)$ correction to $d\sigma/dq_T^2$ will also allow us to test the range of validity of various asymptotic formulae obtained by resumming to all orders leading (as well as subleading) terms in $\alpha_S \, \ell n^2 \, q_T^2/Q^2$ [4]. I briefly recall some basic formulae then I give details on the computation of $d\sigma/dQ^2dq_T^2$ at order α_S^2.

From now on, all formulae and results will refer for simplicity to the "non-singlet" lepton pair production, for example $\sigma^{\pi^+ \mathcal{N}} - \sigma^{\pi^- \mathcal{N}}$. This allows me to eliminate from the formulae the contribution coming from sea-quarks or gluons in the initial state. All formulae can be easily extended to the more general case. Moreover, I will always give the formulae for the cross-section $d\sigma/dq_T^2$ for producing a virtual photon with mass Q^2. The corresponding cross-section $d\sigma/dQ^2dq_T^2$ for lepton pair production is obtained by multiplying the cross-section by the factor $\alpha/3\pi Q^2$, α being the e.m. fine structure constant.

Let us start from the hadron invariant cross-section for producing a virtual photon of mass Q^2 and momentum $\vec{q}$ expressed in terms of the partonic cross-section :

$$Q_o \frac{d\sigma^{HADRONS}}{d^3\vec{q}} = \int dX_1 \int dX_2 \left\{ V^{H_1}(X_1) \, \bar{V}^{H_2}(X_2) \, Q_o \frac{d\sigma^{q\bar{q}}}{d^3\vec{q}} + \right.$$

$$\left. + V^{H_1}(X_1) \, V^{H_2}(X_2) \, Q_o \frac{d\sigma^{qq}}{d^3\vec{q}} \right\} \qquad (3)$$

$Q_o(d\sigma^{q\bar{q}}/d^3\vec{q})$ and $Q_o(d\sigma^{qq}/d^3\vec{q})$ are the partonic quark-antiquark and quark-quark cross-sections and $V^{H_{1,2}}(x_{1,2})$ are the probabilities of finding a valence quark (antiquark) with a fraction $x_{1,2}$ of the longitudinal momentum of the parent hadron. Equation (3) can be rewritten as :

$$\frac{d\sigma^{HADRONS}}{dq_T^2 dy} = \int_0^1 dx_1 \int_0^1 dx_2 \left\{ V^{H_1}(x_1)\, \bar{V}^{H_2}(x_2)\; S_p \frac{d\sigma^{q\bar{q}}}{dt_p du_p} + \right.$$

$$\left. + V^{H_1}(x_1)\, V^{H_2}(x_2)\; S_p \frac{d\sigma^{qq}}{dt_p du_p} \right\} \qquad (4)$$

with :

$$y = \frac{1}{2} \ln \left(\frac{Q^\circ + q_Z}{Q^\circ - q_Z} \right)$$

$$t_p = x_1(t - Q^2) + Q^2 = (p_1 - q)^2 = (x_1 P_1 - q)^2$$

$$u_p = x_2(u - Q^2) + Q^2 = (p_2 - q)^2 = (x_2 P_2 - q)^2$$

$$S_p = x_1 x_2 S = (p_1 + p_2)^2 = x_1 P_1 + x_2 P_2)^2$$

$$t = -S^{1/2}\sqrt{Q^2 + q_T^2}\, \exp(-y) + Q^2 = (P_1 - q)^2$$

$$u = -S^{1/2}\sqrt{Q^2 + q_T^2}\, \exp(+y) + Q^2 = (P_2 - q)^2$$

$p_{1,2}$ $(P_{1,2})$ are the momenta of the incoming partons (hadrons) $S_p(d\sigma^{qq}/du_p dt_p)$ is of order α_S^2. At order α_S, $S_p(d\sigma^{q\bar{q}}/du_p dt_p)$ is easily computed from diagrams shown in Fig. 2 [5].

Fig. 2

and it is given by :

$$S_p \frac{d\sigma^{q\bar{q}}}{dt_p du_p} = \frac{2\pi\alpha\alpha_S C_F}{N_c S_p} e_q^2 \left(\frac{u_p}{t_p} + \frac{t_p}{u_p} + \frac{2Q^2 S_p}{u_p t_p} \right) \cdot \delta(S_p + t_p + u_p - Q^2) \qquad (5)$$

e_{q2} = parton squared electric charge in units of α, C_F and N_c are 4/3 and 3, respectively for $SU(3)_{colour}$. We can integrate over x_2 the right-hand side of Eq. (4) using the cross-section given in Eq. (5), and we obtain :

$$\frac{d\sigma^{HADRONS}}{dq_T^2 dy} = \frac{8\pi\alpha\alpha_S}{9S} e_q^2 \int_{\frac{-u}{S+t-Q^2}}^{1} dx_1 \frac{V^{H1}(x_1)\ \bar{V}^{H2}(x_2)}{x_1 x_2 \left[x_1 S + u - Q^2\right]} \cdot \left[\frac{u_p}{t_p} + \frac{t_p}{u_p} + \frac{2Q^2 S_p}{u_p t_p}\right] \tag{6}$$

with u_p and t_p expressed in terms of u, t and Q^2 as in Eq. (4), but with x_2 given by :

$$x_2 = \frac{-Q^2 - x_1(t - Q^2)}{x_1 S + u - Q^2} \tag{7}$$

Equation (6) contains all the information we need to compute the q_T distribution and the average value $\langle q_T \rangle$ and $\langle q_T^2 \rangle$.

Note that the cross-section in Eq. (6) diverges as $\ell n\, q_T^2/q_T^2$ as $q_T^2 \to 0$.

On the other hand, when one integrates over q_T to obtain the correction to the total cross-section for lepton pair production $d\sigma/dQ^2 dy$ at fixed Q^2 and y, the logarithmic divergence at $q_T^2 = 0$ will give terms $\sim\alpha_S\, \ell n\, Q^2/\mu^2$, where μ^2 is some regularizing reference mass. These terms, resummed to all orders in $\alpha_S\, \ell n\, Q^2/\mu^2$, will precisely transform $V(x) \to V(x,Q^2)$ [2].

The numerical results, obtained by using the formula given in Eq. (6), show that, at present energies, the measured average transverse momentum is systematically higher than the $O(\alpha_S)$ predicted by QCD. This seems to indicate that an "intrinsic" non-negligible transverse momentum is needed to explain the data.

This intrinsic transverse momentum, however, will not change the slope of the distribution $d\sigma/dQ^2 dq_T^2$ versus q_T^2 for $q_T^2 \gtrsim 1 \div 2$ GeV or the slope of the average transverse momentum with S [Eq. (2)]. These quantities are uniquely predicted by QCD and can be tested by experiments.

It should be noted that Drell-Yan processes are one of the best candidates to test transverse momentum predictions of QCD because we do not need to reconstruct parton transverse momentum in the final state, unlike deep inelastic scattering, because the lepton pair defines an axis. The only unknowns in Eq. (6) are the parton densities which, at least for valence-valence annihilation, are rather well-known (even in the case of the pion [6]) from other independent experimental measurements.

In the following, I report the results of a computation made in collaboration with R.K. Ellis and R. Petronzio. In the first stage we only calculated $O(\alpha_s^2)$ corrections for $\pi^+\mathcal{N} - \pi^-\mathcal{N}$ or $\bar{p}\mathcal{N} - p\mathcal{N}$. This is a good laboratory to start with to learn how to make the computations. We also think that this first step, even if theoretically incomplete, gives us important information for Drell-Yan processes where the contribution of sea quarks and gluons in the hadrons is very small at lowest order as for $\pi^-\mathcal{N}$ or $\bar{p}\mathcal{N}$. To give an idea of the complexity of the computation, I show the relevant diagrams in Figs. 3, 4a,b.

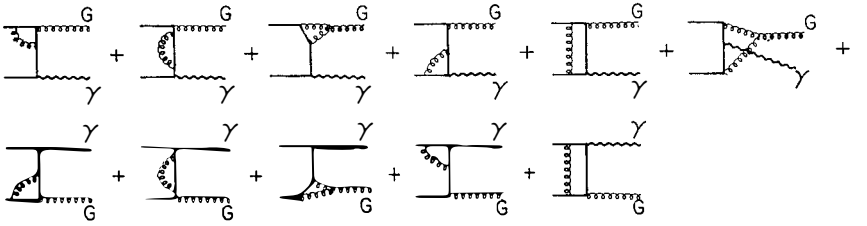

Fig. 3

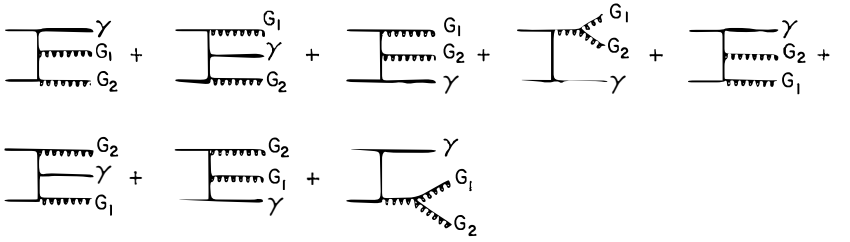

Fig. 4a

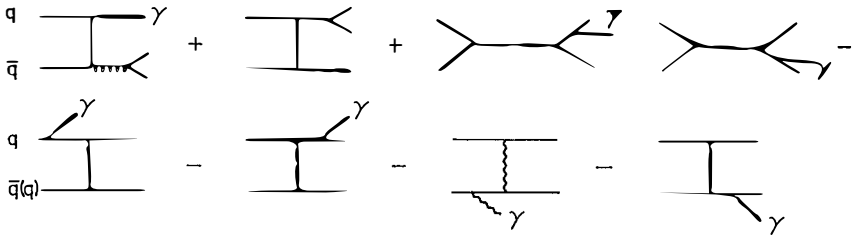

Fig. 4b

Our starting point is the computation of the partonic cross-sections $S_p(d\sigma^{q\bar{q}}/du_p dt_p)$ and $S_p(d\sigma^{qq}/du_p dt_p)$ of Eq. (4). To regularize ultra-violet, as well as infra-red, logarithmic divergences arising in the intermediate stages, we used dimensional regularization. The computation of virtual diagrams is more easily performed by first squaring the amplitudes (interference between the diagrams of Fig. 3 with those of Fig. 2) and performing the traces. Then all loop integrals can be reduced to a quite reasonable number of Lorentz scalar integrals. Our results for virtual diagrams by crossing the channels s_p, t_p, u_p, reproduces the result reported in Ref. 7) and this checks our computation for this part.

Then we consider real diagrams. We have three-body final state phase space with a massive photon of mass Q^2 and two massless quarks or gluons. For fixed u_p and t_p, the invariant mass of the system recoiling against the photon is fixed $[S_F = (p_1+p_2-Q)^2$ fixed$]$. At fixed S_F we integrate over the photon phase space and over the angles of the two quarks (gluons) system [8]. At this point we find (in dimensional regularization) terms proportional to $S_F^{-1-\varepsilon}$, with $\varepsilon = 2-D/2$, D being the dimension of the spacetime. These terms can be rewritten using the identity :

$$(S_F)^{-1-\varepsilon} = \frac{1}{(S_F)_+^{S_F^{MAX}}} - \varepsilon \left[\frac{\ell n S_F}{(S_F)_+^{S_F^{MAX}}}\right] - \frac{1}{\varepsilon}\delta(S_F) \cdot$$

$$\cdot \left\{1 - \varepsilon \ell n S_F^{MAX} + \frac{\varepsilon^2}{2} \ell n^2 S_F^{MAX}\right\} + O(\varepsilon^2) \qquad (8)$$

The distributions of Eq. (8) are defined as :

$$\int_0^{S_F^{MAX}} dS_F \frac{f(S_F)}{(S_F)_{+S_F^{MAX}}} = \int_0^{S_F^{MAX}} dS_F \frac{f(S_F) - f(0)}{S_F}$$

$$\int_0^{S_F^{MAX}} dS_F\, f(S_F) \left[\frac{\ell n S_F}{(S_F)}\right]_{+S_F^{MAX}} = \int_0^{S_F^{MAX}} dS_F \frac{\left[f(S_F) - f(0)\right] \ell n S_F}{S_F} \qquad (9)$$

for $S_F^{MAX} = 1$ we recover the usual definition of the $(S_F)_+$ distributions.

Using the identity of Eq. (8) the soft divergences that will arise at $S_F = 0$ when we integrate over x_1 and x_2 in Eq. (4) and the finite pieces at $S_F = 0$ are explicitly separated. The final result for real diagrams is then a sum of poles in ϵ, distributions in S_F and finite functions of the parton Lorentz invariants s_p, t_p, u_p and S_F.

The poles in ϵ arising when computing both virtual and real diagrams separately are related to the logarithmic singularities of the theory. They can be elimiated as follows.

a) Ultra-violet divergences associated with the renormalization of the coupling constant (see, for example, the first diagram of Fig. 3). These divergences are removed by Lagrangian counter-terms. The related Feynman diagrams transform the expansion parameter α_S into the running coupling constant.

b) Soft divergences at $S_F = 0$ for real diagrams : S_F is equal to zero when one of the two gluons (Fig. 4a) becomes soft. These divergences cancel against the corresponding soft divergences given by virtual diagrams (Kinoshita-Nauenberg theorem).

c) Collinear divergences : they are eliminated by redefining the parton densities. This can be done because collinear divergences are universal, that is, independent of the process (exactly as the parton densities are defined to be) and they depend only on the external legs (quarks or gluons).

The resulting cross-section is finite (this is a strong check of the computation). We have :

$$\frac{d\sigma^{\text{HADRONS}}}{dq_T^2 dy} = \int dx_1 dx_2 \left\{ V^{H_1}(x_1,M^2)\ \bar{V}^{H_2}(x_2,M^2) \left[S_p \left. \frac{d\sigma^{q\bar{q}}}{dt_p du_p} \right|_{0\left[\alpha_S(M^2)\right]} \right.\right.$$

$$\left.\left. + S_p \left. \frac{d\sigma}{dt_p du_p} \right|_{0\left[\alpha_S^2(M^2)\right]} \right] + V^{H_1}(x_1,M^2)\ V^{H_2}(x_2,M^2)\ S_p \left. \frac{d\sigma^{qq}}{dt_p du_p} \right|_{0\left[\alpha_S^2(M^2)\right]} \right\}$$

with

$$V^H(x,M^2) = V_o^H(x) + \alpha_S \int_x^1 \frac{dy}{y} \left\{ \ell n \frac{M^2}{\mu^2} P_{qq}\left(\frac{x}{y}\right) + f_{qq}\left(\frac{x}{y}\right) \right\} V_o^H(y) \qquad (10)$$

$P_{qq}(z)$ is the usual kernel of the Altarelli-Parisi non-singlet evolution equation and $f_{qq}(z)$ is the kernel that defines the parton densities in terms of those measured in other processes (as, for example, in deep inelastic scattering or in the q_T integrated total Drell-Yan cross-section [3]). $f_{qq}(z)$ makes $S_p(d\sigma^{q\bar{q}}/du_p dt_p)\alpha_S^2$ independent of the regularization procedure. $S_p(d\sigma^{qq}/du_p dt_p)$ (in this particular case) is by itself a finite and well-defined quantity. M^2 is the scale at which the parton densities are probed and the scale of the running coupling constant. The choice of M^2 is arbitrary in perturbation theory. Physically, the best thing to do is to choose M^2 in order to minimize the correction. We have a complete analytic answer for $S_p(d\sigma^{q\bar{q},qq}/du_p dt_p)$. The final formula is rather simple (~hundred terms) if compared to the intermediate expressions where thousands of terms are generated.

At the end of the computation, gauge invariance and crossing symmetry between u_p and t_p cancel a lot of terms. At each step of our computation we used the algebraic programme SCHOONSHIP written by Veltman. It is not very useful to present the final result here (~two pages). I want simply to make some comment on the final result :

i) the factor $(\alpha_S/2\pi)C_F\pi^2$, responsible for a large part of the correction for $d\sigma/dQ^2$, is present ;

ii) however, many other factors of the same order of magnitude are present and a detailed numerical analysis of the final formula is needed.

I can anticipate that the correction is expected to be large and positive. Some resummation theorem for large corrections coming from soft gluon emissions will probably be necessary, otherwise the result would be meaningless in perturbation theory. Our computation is easily extended to real photon production ($Q^2 = 0$).

REFERENCES

1) J. Kubar André and F.E. Paige, Phys.Rev. D19 (1979) 221 ;
G. Altarelli, R.K. Ellis and G. Martinelli, Nuclear Phys. B143 (1978) 521 [E B146 (1978) 544] ; Nuclear Phys. B157 (1979) 461.

2) H.D. Politzer, Nuclear Phys. B129 (1977) 301.

3) See, for example : R.K. Ellis, these proceedings.

4) Yu. Dokshitzer, D. Dyakonov and S. Troian, Proceedings of the 13th Winter School of the Leningrad Institute of Nuclear Physics, Leningrad (1978) ;
G. Parisi and R. Petronzio, Nuclear Phys. B154 (1979) 427.

5) H. Fritzsch and P. Minkowski, Phys.Letters 73B (1978) 80 ;
G. Altarelli, G. Parisi and R. Petronzio, Phys.Letters 76B (1978) 351, 356 ;
K. Kajantie and R. Raitio, Nuclear Phys. B139 (1978) 72.

6) J. Badier et al., Paper submitted to the International Conference on High Energy Physics, Madison, WI (1980).

7) R.K. Ellis, D.A. Ross and A.E. Terrano, CALT 68-785 (June 1980).

8) R.K. Ellis, M.A. Furman, H.E. Haber and I. Hinchliffe, Nuclear Phys. B173 (1980) 397.

MULTIPLE GLUON RADIATION IN HARD PROCESSES

J. Cleymans
University of Bielefeld
Department of Theoretical Physics
Bielefeld
Germany

Abstract: An introduction to the physics of multi-gluon radiation in hard processes is presented.

In this talk I want to present in a simple way some of the basic physics concerning gluon radiation in hard processes. At this meeting we have heard from David Scott[1] that lowest order QCD gives a diverging cross-section as the transverse momentum of the lepton-pair goes to zero:

$$\frac{d}{dQ_T^2} \sim \frac{1}{Q_T^2} \tag{1}$$

One way to avoid this singularity is to construct an ad hoc formula which reproduces the naive Drell-Yan formula at small Q_T and goes over into the QCD expression for large Q_T. This intuitive construction leads to a good description of the data as was shown by C. Brown[2] at this meeting. From a theoretical point of view this is not very satisfactory since it is an artificial construction. To discuss what really happens at small Q_T I will present the case of e^+e^- annihilation into constituents first. The corresponding treatment of lepton-pair production by the scattering of constituents differs from this only in a minor way and can best be treated starting from the formalism of G. Plaut[3] at this meeting.

To lowest order in QCD we only have the annihilation diagram for e^+e^- going into constituents:

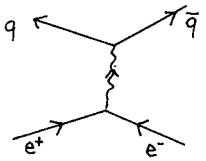

Introduce the energy fractions $x_q = \frac{E_q}{E_{beam}}$ and $x_{\bar{q}} = \frac{E_{\bar{q}}}{E_{beam}}$; the corresponding expression for the differential cross-section is then given by

$$\frac{1}{\sigma} \frac{d^2\,\sigma(e^+e^- \to q\bar{q})}{dx_q\, dx_{\bar{q}}} = \delta(1 - x_q)\, \delta(1 - x_{\bar{q}}) \tag{2}$$

since each constituent will have $x = 1$. Difficulties will show up when we look at the first order QCD-corrections; for $e^+e^- \to q\bar{q}G$ the differential cross-section is given by

$$\frac{1}{\sigma} \frac{d^2\,\sigma(e^+e^- \to q\bar{q}G)}{dx_q\, dx_{\bar{q}}} = \frac{2\alpha_s}{3\pi} \frac{x_q^2 + x_{\bar{q}}^2}{(1 - x_q)\,(1 - x_{\bar{q}})} \tag{3}$$

This expression diverges for $x_q \to 1$ and/or $x_{\bar{q}} \to 1$. These divergences are related to the behaviour in eq. (1). To clarify their origin we decompose

equation (3) according to the corresponding diagrams in the Feynman gauge

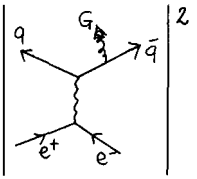

$$: \quad \frac{1 - x_{\bar{q}}}{1 - x_q} \tag{4a}$$

The divergence arises when $x_q = 1$ and $x_{\bar{q}} \neq 1$; i.e. when the final state configuration is as in the figure:

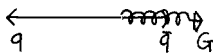

antiquark and gluon are produced parallel to each other, this is called a collinear divergence. Note that this gives rise to a simple logarithm upon integration.

Similarly when the gluon is radiated from the q we have:

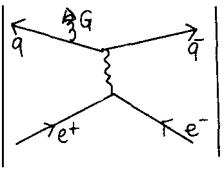

$$: \quad \frac{1 - x_q}{1 - x_{\bar{q}}} \tag{4b}$$

and the divergence arises from the configuration where quark and gluon are parallel to each other:

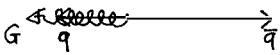

At last we have the interference term which is given by:

$$\frac{2(x_q + x_{\bar{q}} - 1)}{(1 - x_q)(1 - x_{\bar{q}})} \quad , \tag{4c}$$

it gives an extra divergence when both x_q and $x_{\bar{q}}$ are equal to 1 . This can only happen if the gluon is soft:

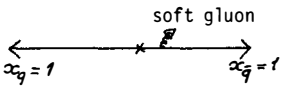

This is the only term which leads to a logarithm squared upon integration. Therefore in the Feynman gauge, the interference term (4c) is the dominant term.

When summing the contributions (4a), (4b) and (4c) we find back the differential cross-section given in (3) (up to an overall factor):

$$(4a) + (4b) + (4c) = \frac{x_q^2 + x_{\bar{q}}^2}{(1 - x_q)(1 - x_{\bar{q}})} \quad .$$

The fact that in the Feynman gauge the leading term is associated with the interference term makes it difficult to generalize this calculation to the emission of arbitrary numbers of gluons. At this point comes the crucial observation of Dokshitzer, D'Yakonov and Troyan[4] who repeated the above calculations in the axial gauge and found a different situation. In the axial gauge the summation over gluon polarizations is given by:

$$\sum_{\lambda} \varepsilon_\mu(\lambda)\, \varepsilon_\nu(\lambda) = -g_{\mu\nu} + \frac{k_\mu n_\nu + k_\nu n_\mu}{k\cdot n} - n^2 \frac{k_\mu k_\nu}{(k\cdot n)^2} \tag{5}$$

where k_μ is the 4-momentum of the gluon and n_μ is a fixed 4-vector such that $\varepsilon\cdot n = 0$. For the choice $n_\mu = \bar{q}_\mu$, the momentum of the outgoing antiquark, the factor $k\cdot n$ appearing in the denominator of (5) becomes:

$$\begin{aligned} k\cdot n &\to k\cdot\bar{q} \\ &= \tfrac{1}{2}(\bar{q} + k)^2 \\ &= \tfrac{1}{2}(Q - q)^2 \\ &= \tfrac{1}{2}Q^2(1 - x_q) \end{aligned} \tag{6}$$

Therefore, in the axial gauge, it is possible to rearrange the singularity structure corresponding to (4a), (4b) and (4c). In the case of the above example this is shown in the following table:

	Feynman gauge	Axial gauge with $n_\mu = \bar{q}_\mu$
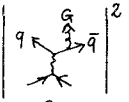	$\frac{1 - x_{\bar{q}}}{1 - x_q}$	$\frac{1 - x_{\bar{q}}}{1 - x_q}$
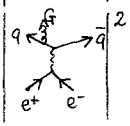	$\frac{1 - x_q}{1 - x_{\bar{q}}}$	$\frac{(1 - x_q - x_{\bar{q}})^2 + x_{\bar{q}}^2}{(1 - x_q)(1 - x_{\bar{q}})}$
Interference	$\frac{2(x_{\bar{q}} + x_q - 1)}{(1 - x_q)(1 - x_{\bar{q}})}$	$\frac{2(x_q + x_{\bar{q}} - 1)}{1 - x_q}$
Total	$\frac{x_q^2 + x_{\bar{q}}^2}{(1 - x_q)(1 - x_{\bar{q}})}$	$\frac{x_q^2 + x_{\bar{q}}^2}{(1 - x_q)(1 - x_{\bar{q}})}$

The interesting point is that in the axial gauge the dominant term is given by the diagram where the gluon is radiated from the quark line. This makes generalization to multi-gluon emission easy: in the axial gauge where n_μ is given by the antiquark momentum the dominant term in the cross-section will be given by the diagram where all gluons are coming from the quark line:

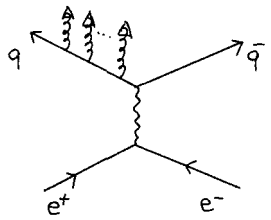

In the case of lepton-pair production one has to turn this diagram upside down and change the arrows on the fermion lines. The quark and antiquark lines will be treated in a more symmetric way if one chooses $n_\mu = q_\mu + \bar{q}_\mu$. Actually the choice most often encountered in the literature is $n_\mu = Aq_\mu + B\bar{q}_\mu$ with A and B arbitrary constants. As a check on the calculations, the final result must be independent of A and B as a consequence of gauge invariance. In the axial gauge one is finally led to the consideration of the discontinuity of ladder diagrams:

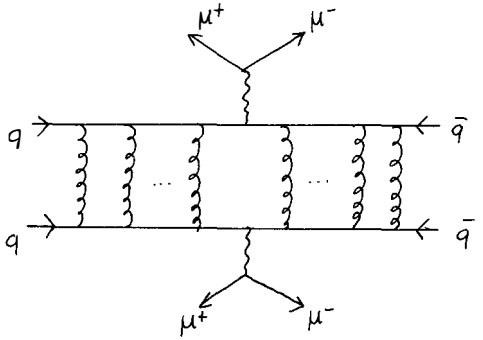

Let us proceed with the case of e^+e^- annihilation and ask what the differential cross-section is for the acollinear final state configuration:

To keep the discussion simple we consider only the nonsinglet case. Several factors appear which we discuss one by one: first of all the transverse momentum between the quark and the antiquark, P_T, is taken up by the radiated constituents, this is taken into account by a 2-dimensional delta function:

$$\delta^2(P_T - \sum_{i=1}^{n} p_{Ti}) \tag{7a}$$

where the summation runs over the n radiated constituents which we consider to be gluons for the moment; secondly the energy fraction x of the quark is given by the product of energy fractions after each radiation:

$$\delta(x - \prod_{i=1}^{n} x_i) \quad ; \tag{7b}$$

thirdly, for each gluon radiation, the leading logarithm squared term of the cross-section is given in the Weizsäcker-Williams approximation by:

$$\frac{\alpha_s(p_{Ti}^2)}{2\pi^2} \frac{4}{3} \frac{1 + x_i^2}{1 - x_i} \frac{1}{p_{Ti}^2} \tag{7c}$$

where $\alpha_s(p_{Ti}^2)$ is the running coupling constant whose argument is fixed by the scale at which the radiation occurs.

Grouping all these factors together we obtain:

$$\frac{1}{\sigma} \frac{d\sigma}{d^2 P_T\, dx} = \sum_{n=0}^{\infty} \prod_{i=1}^{n} \int_{Q_0^2}^{Q^2} \frac{d^2 p_{Ti}}{p_{Ti}^2} \frac{\alpha_s(p_{Ti}^2)}{2\pi^2} \frac{4}{3} \int_0^{1-p_{Ti}^2/Q^2} dx_i \frac{1 + x_i^2}{1 - x_i}$$

$$\delta^2(P_T - \sum_{i=1}^{n} p_{Ti})\, \delta(x - \prod_{i=1}^{n} x_i) \tag{7d}$$

The crucial difference with quantum electrodynamics lies in the appearance of the running coupling constant. The cut-off on the integral is given by Q_0^2. The dependence on this value will disappear once virtual corrections are taken into account.

At this point there are two ways of proceeding: the first one, followed by Dokshitzer, D'Yakonov and Troyan[4] and by Ellis and Stirling[5] among others, picks up at each step the dominant region of integration; the second way, proposed by Parisi and Petronzio[6] treats the p_T integration in an exact manner. I will follow this last method, a conparison between the two ways can be found in a recent paper of Rakow and Webber[7]: the two methods agree as far as leading terms are concerned.

Equation (7d) is not in a form where the summation can be performed easily.

This is because the δ-functions couple all the different terms in the product. To get rid of the energy fraction δ-function we consider energy-weighted cross-sections and integrate over x. To get rid of the transverse momentum conserving δ-function we go over to b-space:

$$\delta^2(P_T - \sum_{i=1}^{n} p_{Ti}) = \frac{1}{(2\pi)^2} \int d^2b \; e^{ib\cdot P_T - i\sum_{i=1}^{n} b\cdot p_{Ti}} \tag{8}$$

This decouples the integrations and will make the summation in (7d) easy. We now have:

$$\frac{1}{\sigma} \int_0^1 dx\, x^m \frac{d\sigma}{d^2P_T\, dx}$$

$$= \int \frac{d^2b}{(2\pi)^2} e^{ib\cdot P_T} \{ \frac{1}{n!} \sum_{n=0}^{\infty} \prod_{i=1}^{n} \int_{Q_0^2}^{Q^2} \frac{d^2p_{Ti}}{p_{Ti}^2} \frac{\alpha_s(p_{Ti}^2)}{2\pi^2}$$

$$\frac{4}{3} \int_0^{1-p_{Ti}^2/Q^2} dx_i\, x_i^m \frac{1 + x_i^2}{1 - x_i} e^{-ib\cdot p_{Ti}} \} \tag{9}$$

so that, using

$$\frac{1}{2\pi} \int_0^{2\pi} d\theta\, e^{ibp_T \cos\theta} = J_0(b\, p_T) \tag{10}$$

and performing the integration over azimuthal angle, we obtain:

$$\frac{1}{\sigma} \int_0^1 dx\, x^m \frac{d\sigma}{dP_T^2\, dx}$$

$$= \frac{1}{2} \int_0^{\infty} b\, db\, J_0(bP_T) \{ \frac{1}{n!} \sum_{n=0}^{\infty} \prod_{i=1}^{n} \int_{Q_0^2}^{Q^2} \frac{dp_{Ti}^2}{p_{Ti}^2} \frac{\alpha_s(p_{Ti}^2)}{2\pi}$$

$$\frac{4}{3} \int_0^{1-P_T^2/Q^2} dx_i \frac{1 + x_i^2}{1 - x_i} x_i^m J_0(bp_{Ti}) \} \tag{11}$$

The summation leads to the expression which has also been given by M. Greco[8] and G. Pancheri-Srivastava[9] starting from the coherent state formalism:

$$\frac{1}{\sigma}\int_0^1 dx\, x^m \frac{d\sigma}{dP_T^2\, dx}$$

$$= \frac{1}{2}\int_0^\infty bdb\, J_0(bP_T)\, \exp\left\{ \int_{Q_0^2}^{Q^2} \frac{dp_T^2}{p_T^2} \frac{\alpha_s(p_T^2)}{2\pi} \right.$$

$$\left. \frac{4}{3}\int_0^{1-p_T^2/Q^2} dx\, x^m \frac{1+x^2}{1-x} J_0(bp_T) \right\} \qquad (12)$$

This expression is well-behaved when $P_T \to 0$.

We can now return to our starting point: even though the emission of a single gluon diverges when the transverse momentum of the gluon goes to zero, as exemplified by equations (1) and (7c), summation over all possible emissions gives a finite result as shown in (12).

To make contact with phenomenology the expression (12) is convoluted with the primordial quark fragmentation (for e^+e^- annihilation) or distribution (for lepton-hadron scattering) function. Let us consider the quark distribution function since this is more relevant for the Drell-Yan process: Inside the hadron the quark will carry a fraction ξ of the hadron's momentum and have transverse momentum p_T'' :

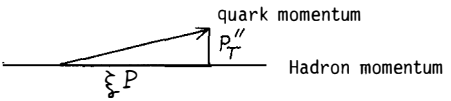

As a consequence of QCD this quark can start radiating gluons, this will bring it in a different kinematical configuration: the quark will now carry a fraction x_p of the momentum of the parent quark and have transverse momentum p_T' with respect to it:

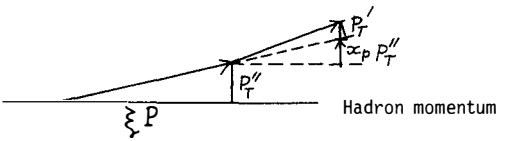

The transverse momentum with respect to the hadron is therefore approximately given by:

$$p_T = p_T' + x_p\, p_T'' \qquad . \qquad (13)$$

The convolution therefore reads:

$$q(x,Q^2,p_T) = \int_0^1 dx_p \int_0^1 d\xi \int d^2p_T' \int d^2p_T'' \, \delta(x-\xi x_p) \, \delta^2(p_T-p_T'-x_p p_T'')$$

$$\left[\frac{1}{\sigma} \frac{d\sigma}{dx_p \, d^2p_T} \right]_{QCD} \; q_0(\xi,p_T'') \tag{14}$$

It turns out that the moments in x of the b-transform of this expression are particularly well suited for theoretical consideration. Define:

$$q(b,m,Q^2) \equiv \int_0^1 dx \, x^{m-1} \int e^{ib\cdot p_T} \, q(x,Q^2,p_T) \, d^2p_T \tag{15}$$

then it is straightforward to show that this quantity satisfies an evolution equation. For the nonsinglet part of the structure function it reads[10]:

$$Q^2 \frac{\partial}{\partial Q^2} q^{NS}(b,m,Q^2)$$

$$= \frac{\alpha_s(Q^2)}{2\pi} \int_0^1 dx \, x^{m-1} \, P_{qq}(x) \, J_0(bQ\sqrt{1-x}) \, q^{NS}(bx,m,Q^2) \tag{16}$$

Equation (16) is strikingly similar to the standard Altarelli-Parisi evolution equation[11]:

$$Q^2 \frac{\partial}{\partial Q^2} q^{NS}(m,Q^2) = \frac{\alpha_s(Q^2)}{2\pi} \int_0^1 dx \, x^{m-1} \, P_{qq}(x) \, q^{NS}(m,Q^2) \quad . \tag{17}$$

In the table we list some of the correspondences:

Structure functions

x-dependence	p_T-spectrum
x-dependence cannot be calculated in perturbative QCD	p_T-spectrum cannot be calculated in perturbative QCD
evolution with Q^2 of the moments can be calculated	evolution with Q^2 of the moments in b-space can be calculated
evolution is determined by constituents having virtuality (in the ladder) $p^2 >> \Lambda^2$	evolution is determined[7] by radiation having $\Lambda^2 << p_T^2 << Q^2$

Let us now apply these considerations to the case of lepton-pair production in hadronic collisions. The naive Drell-Yan formula reads:

$$\frac{d\sigma(H_1 + H_2 \to e^+e^- + \ldots)}{d(\frac{Q^2}{s})\, d^2Q_T\, dx_p}$$

$$= \sum_i \frac{4\pi\alpha^2}{9Q^2} e_i^2 \int d^2p_{T1}\, d^2p_{T2}\, dx_1\, dx_2\, q_i(x_1, p_{T1}, Q^2)\, \bar{q}_i(x_2, p_{T2}, Q^2)$$

$$\delta^2(Q_T - p_{T1} - p_{T2})\, \delta(x_1x_2 - \frac{Q^2}{s})\, \delta(x_F - x_1 + x_2) \qquad (18)$$

The transverse momentum conserving δ-function can again be written as:

$$\delta^2(Q_T - p_{T1} - p_{T2}) = \frac{1}{(2\pi)^2} \int d^2b\, e^{ib\cdot Q_T - ib\cdot p_{T1} - ib\cdot p_{T2}} \qquad (19)$$

For theoretical convenience we take moments in τ . This gives us finally:

$$\int_0^1 (\frac{Q^2}{s})^{n-1} \frac{d\sigma(H_1 + H_2 \to e^+e^- + \ldots)}{d(\frac{Q^2}{s})\, d^2Q_T}\, d(\frac{Q^2}{s})$$

$$= \sum_i \frac{4\pi d^2}{9Q^2} e_i^2 \frac{2}{(2\pi)^2} \int d^2b\, e^{ib\cdot Q_T} \left[\int_0^1 dx_1\, x_1^{n-1} \int d^2p_T\, e^{-ib\cdot p_{T1}} q_i(x_1, p_{T1}, Q^2)\right]$$

$$\left[\int_0^1 dx_2\, x_2^{n-1} \int d^2p_T\, e^{-ib\cdot p_{T2}}\, \bar{q}_i(x_2, p_{T2}, Q^2)\right] \qquad (20)$$

In the brackets we see exactly the moments of structure functions in b-space as defined in (15). This means that for the Drell-Yan process the evolution equation (16) can be readily applied. To this end we rewrite the r.h.s. of (20), using (10) and (15), as:

$$= \sum_i \frac{4\pi d^2}{9Q^2} e_i^2 \frac{1}{2} \int_0^\infty bdb\, J_0(bQ_T)\, q_i(n, b, Q^2)\, \bar{q}_i(n, b, Q^2) \quad . \qquad (21)$$

We now have an expression for the transverse momentum dependence which is finite at $Q_T = 0$. The price to pay is that now we have to invert the moments before a realistic comparison with experiment can be made[12]. A plot of expression[13] (21) shows how QCD-effects broaden the Q_T-spectrum as the energy increases.

One case where a direct comparison with experiment is possible and has been made is for the energy-weighted acollinearity distribution in e^+e^- annihilation. Performing an analysis similar to the one described before one obtains here:

$$\frac{1}{\sigma} \sum_{a,b} \int dx_a \int dx_b\, x_a\, x_b \frac{d\sigma(e^+e^- \to a + b + \ldots)}{dx_a\, dx_b\, d(\cos\theta_{ab})}$$

$$= \sum_i e_i^2 \int d(Qb)\, Qb\, J_0(Qb\tfrac{\theta}{2}) \left[D_q^a(n=2,b,Q^2)\, D_{\bar{q}}^b(n=2,b,Q^2) + (q \to \bar{q}) \right] \qquad (22)$$

where $D_q^a(n,b,Q^2)$ is the n^{th} moment of the quark fragmentation function in

b-space

$$D_q^a(n, b, Q^2) = \int_0^1 dz\, z^{n-1} \int d^2b\, e^{i\frac{b\cdot p_T}{z}}\, D(z, p_T, Q^2) \quad . \tag{23}$$

An additional factor of $1/z$ appears in the exponential because the kinematics for the convolution is slightly different from the one described in (14) for fragmentation functions. In the analysis of Baier und Fey[14], $D(z, p_T, Q^2)$, was parametrized to fit approximately the data at[15] $Q_0^2 = (9.4\ \mathrm{GeV})^2$:

$$\sum_a D_q^a(x, p_T, Q_0^2) = 3\,\frac{(1-z)^2}{z}\,\frac{e^{-2p_T/<p_T>}}{2\pi\,\frac{<p_T>^2}{4}} \quad . \tag{24}$$

The evolution equations than lead to the full curve drawn in the figure showing the data at $Q^2 \cong (30\ \mathrm{GeV})^2$. Ignoring the Q^2 evolution leads to the dashed curve.

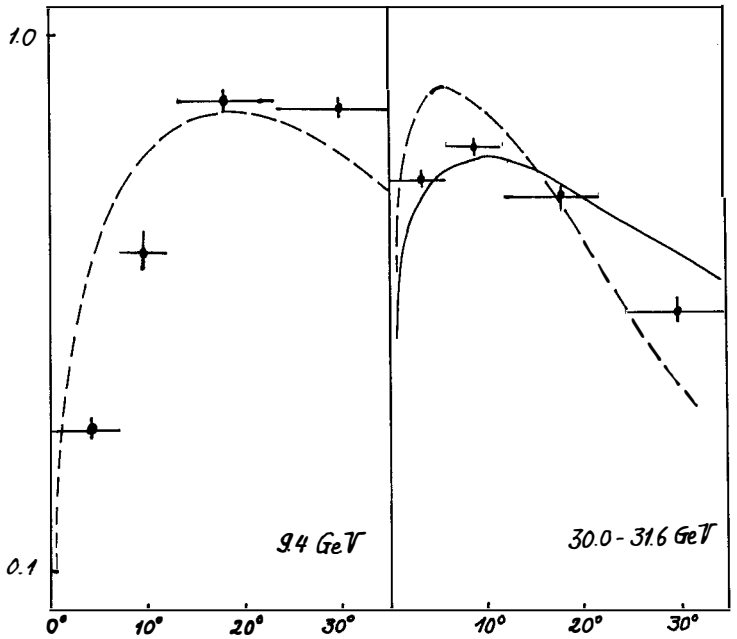

This shows that taking into account multiple gluon radiation resolves the $1/Q_T^2$ behaviour of single gluon radiation and improves the phenomenological description at higher energies.

References

1) D.M. Scott, these proceedings and references therein.

2) C.N. Brown, these proceedings and references therein.

3) G. Plaut, these proceedings and references therein.

4) Y.L. Dokshitzer, D.I. D'Yakonov and S.I. Troyan, Physics Reports 58, 269 (1980) and references therein.

5) S.D. Ellis and W.J. Stirling, University of Washington report, RLO-1388-821 (1980).

6) G. Parisi and R. Petronzio, Nucl. Phys. B154, 427 (1979).

7) P.E.L. Rakow and B.R. Webber, Cavendish Laboratory preprint, HEP 81/4.

8) M. Greco, these proceedings and references therein.

9) G. Pancheri-Srivastava, these proceedings and references therein.

10) For the fragmentation functions a similar evolution equation was first given by A. Bassetto, M. Ciafaloni and G. Marchesini, Nucl. Phys. B163, 477 (1980).

11) G. Altarelli and G. Parisi, Nucl. Phys. B126, 477 (1980).

12) J. Cleymans and M. Kuroda, in preparation.

13) J. Cleymans and M. Kuroda, University of Bielefeld preprint BI/TP 80/17.

14) R. Baier and K. Fey, Nucl. Phys. B179, 49 (1981).

15) C. Berger et al., Phys. Lett. 90B, 312 (1980).

HADRONIC PRODUCTION OF J/ψ AND T AT LARGE TRANSVERSE MOMENTUM

R. Rückl
Fakultät für Physik, Universität Bielefeld, D-4800 Bielefeld 1, FRG
and
Sektion Physik, Universität München, D-8000 München 2, FRG

ABSTRACT

This is a brief report on a QCD-calculation of large transverse momentum distributions for J/ψ and T produced in high energy pp-collisions. The picture is based on the subprocesses $gg \to {}^3S_1 g$ and $gq \to {}^3P_J q \to {}^3S_1 \gamma q$. In contrast to the duality prescription, the coupling of the S- and P-wave boundstates is computed explicitly in the framework of the quarkonium model. The agreement with the main features of the available data is satisfactory.

Most of the discussion of the present workshop is concerned with the lepton pair continuum produced in high energy hadronic collisions. In this talk I would like to focus on the heavy resonances observed above this smooth background. The most prominent of them are the $^3S_1$ groundstates of the charmonium and bottomonium system, namely the J/ψ and the Υ, respectively. Whereas the Drell-Yan process has been established as the production mechanism for the continuum, one has not yet fully explained how the resonances are produced. It seems, however, evident from the observed rates that they originate in strong interaction processes. Further, in the generally accepted parton picture, it is certainly reasonable to assume that the heavy quark constituents of the boundstates are created by the light constituents of the colliding hadrons rather than out of the small sea of heavy flavors. The crucial point is, then, the formation of a particular boundstate out of the free heavy quark pair. Here differ the existing models. Without going into details I would like to recall two proposals.

One class of models[1] is based on the assumption of semi-local duality which relates the free quark production, e.g. via the subprocesses $q\bar{q} \to Q\bar{Q}$ and $gg \to Q\bar{Q}$, to the production of $[Q\bar{Q}]$-boundstates as follows: $\sigma(ab \to [Q\bar{Q}]) = F \int_{4m_Q^2}^{4M_Q^2} dQ^2\, \sigma(ab \to Q\bar{Q})$. Here, one integrates over the invariant $Q\bar{Q}$-mass squared with the upper limit determined by the mass M_Q of the lightest meson carrying the heavy flavor Q. Spin and color singlet nature of the boundstates do not enter explicitly. For illustration, $q\bar{q} \to Q\bar{Q}$ via one gluon would need another one to carry away color such that the $Q\bar{Q}$ pair could form a color singlet. Similarly, in $gg \to Q\bar{Q}$ at least one more gluon must be involved if the $Q\bar{Q}$ pair should bind to a $^3S_1$ state since this state does not couple to two vector particles. All these effects are hidden in the duality factor F which is supposed to give the fraction of the averaged cross section due to the production a particular resonance. In practice, F is a free parameter, and, hence, these models cannot predict absolute rates. Otherwise, they provide a reasonable description[1] of the main experimentally observed features. In this picture, large transverse momenta originate in higher order QCD processes[2] like $q\bar{q} \to Q\bar{Q}g$, $gq \to Q\bar{Q}q$ and $gg \to Q\bar{Q}g$. Assuming that the duality factor is the same for all three subprocesses, the dominant mechanism in pp-collisions is the gq-subprocess as expected from what one knows about the quark and gluon structure functions. The slopes of the p_T-distributions turn out to be roughly consistent with the J/ψ-data at $\sqrt{s} = 63$ GeV and the Υ-data at $\sqrt{s} = 27.4$ GeV.

Another approach[3-7] is to evaluate the coupling of the boundstates to gluons in the framework of the quarkonium model. In a nonrelativistic approximation, the coupling of S-waves is proportional to their wavefunctions at the origin, whereas the P-waves couple proportional to the derivative of the appropriate wavefunc-

tions. Spin and color projections are considered explicitly. This allows to predict absolute normalizations in terms of resonance parameters. Further, the relative size of the contributions from the various subprocesses to a particular resonance is very different from their proportion in the duality model. Processes evaluated[3-5] by this method include $q\bar{q} \to {}^3S_1$ and $q\bar{q} \to {}^1S_0$ or ${}^3P_J$ via three and two intermediate gluons, respectively, and $gg \to {}^3P_{0,2}$. The P-waves also contribute to the production of ${}^3S_1$ states via their radiative decays ${}^3P_J \to {}^3S_1\gamma$. In pp-collision, one finds[7] that only the two gluon process is strong enough to produce rates of the observed magnitude. Further, because of the small mass differences of about 400 MeV between the ${}^3S_1$ and ${}^3P_J$ states of the charmonium and bottomonium system, all the above processes populate exclusively the small p_T region. The sources for large transverse momenta[5-7] are of next order in α_S, namely $gg \to {}^3S_1g$, $gg \to {}^3P_Jg$, $gq \to {}^3P_Jq$ and $q\bar{q} \to {}^3P_Jg$. Despite the prize one has to pay for the decay of the P-waves into S-waves, the latter cascade processes can still play a role at large p_T since, typically, $d\sigma(gq \to {}^3P_Jq) / d\sigma(gg \to {}^3S_1g) \sim \frac{p_T^2}{M^2}$ for $p_T^2 \gg M^2$. Thus, for pp-scattering in particular, the important subprocesses at large p_T are expected to be $gg \to {}^3S_1g$ and $gq \to {}^3P_Jq \to {}^3S_1\gamma q$. The reason is that the quark distribution is harder than the gluon distribution and the antiquark content in a proton is small.

In a recent preprint[7] R. Baier und myself have attempted a complete calculation of the p_T-distributions (for all p_T) and of the integrated rates for J/ψ and Υ produced in pp-collisions at FNAL and ISR energies. We also present in this paper a detailed comparison of our results with data from several experiments. In the following I am reporting on the high p_T part only.

Let me first describe briefly the calculation. The cross section for the subprocess $gg \to {}^3S_1g$ (Fig. 1a) can be obtained directly from the amplitude for the positronium decay into three photons by crossing and inserting the appropriate color factors. The normalization is determined by the wavefunction at the origin squared, $R_S^2(0)$, or, equivalently, by the leptonic width $\Gamma({}^3S_1 \to e^+e^-) = 4.8$ keV for the J/ψ and 1.3 keV for the Υ. The cross sections for $gq \to {}^3P_Jq$ and $J = 0, 1$ and 2 (Fig. 1b) have been derived from general off-shell amplitudes for ${}^3P_J \to gg$ (see ref. 7). These contributions are proportional to the derivative of the P-wavefunctions squared, $R_P'^2(0)$, which can be parametrized by $r\Gamma({}^3S_1 \to e^+e^-)$ with $r = 4R_P'^2(0) / M^2 R_S^2(0)$. Numerically, we use $r = 0.074$ for J/ψ and 0.013 for Υ, following an analysis[8] of quarkonium models. To convert the cross sections for the subprocesses into pp-cross sections one has to fold in the appropriate gluon and quark structure functions. We adopt a parametrization[7] which includes scale breaking and which is consistent with the observations in deep inelastic processes. There is a slight ambiguity which scale

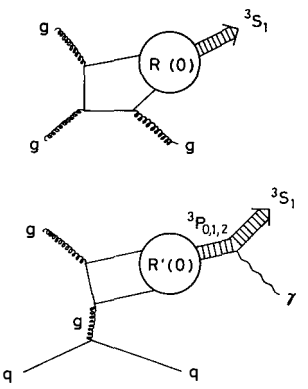

Fig. 1 : Typical diagrams which contribute to (a) $gg \to {}^3S_1 g$ and (b) $gq \to {}^3P_{0,1,2} q \to {}^3S_1 \gamma q$.

one should use to control scale breaking. Possible choices are the momentum transfer in the given subprocess, $\hat{t}$, or p_T^2 or $p_T^2 + M^2$, etc. We take the transverse mass squared, $p_T^2 + M^2$. To exhibit the effects of scale breaking we also compute the spectra in the scaling limit with $xG(x) = 3(1-x)^5$, $xQ(x) = (2.773 + 4.094x)\sqrt{x}(1-x)^3 + 1.26(1-x)^7$ and fixed $\alpha_S \sim 0.4$ for J/ψ and ~ 0.25 for Υ . Decay distributions for $^3P_J \to {}^3S_1\gamma$, finally, convert the ^3P_J yields into corresponding $^3S_1$ spectra as sketched in Fig. 1b. For the relevant masses and branching ratios of the charmonium system we use existing experimental results. For the bottomonium system, on the other hand, one must rely on the quarkonium model[8] which gives $M_P \sim 9.9$ GeV and $B(^3P_J \to \Upsilon\gamma) \sim 4\%$ for $J = 0$, $\sim 29\%$ for $J = 1$, and $\sim 10\%$ for $J = 2$. These branching ratios are not very different from the corresponding charmonium values. Further, one may try to include nonperturbative effects due to primordial transverse momenta by a simple convolution with a gaussian distribution. For its width we take $\sigma \sim 0.48$ GeV which is also used in the Drell-Yan analysis.

A parameter which deserves a special comment is the QCD scale Λ in the running coupling constant α_S . The processes under consideration are of third order in α_S and, therefore, their absolute magnitude depends rather sensitively on Λ . A priori, there exists no preferable value for Λ as long as the higher order corrections are not known. One could adopt the attitude that one should use the same value as in the description of the hadronic decay of J/ψ in terms of $J/\psi \to 3g$, namely $\Lambda \sim 100$ MeV or, equivalently, $\alpha_S(3.1\ \text{GeV}) \sim 0.2$. However, here we are dealing with hard scattering processes for which the effective Λ does not need to be the same as for decay processes, at least in leading order. The experimentally observed J/ψ yields, in fact, require $\Lambda \sim 500$ MeV , a value familiar from other hard scattering processes. In that case, $\alpha_S(3.1\ \text{GeV}) \sim 0.4$. Clearly, the Υ production is more asymptotic since $M_\Upsilon^2 \sim 100\ \text{GeV}^2$ and, hence, less affected by this uncertainty.

Fig. 2 and 3 show the resulting p_T-distributions for J/ψ and Υ together

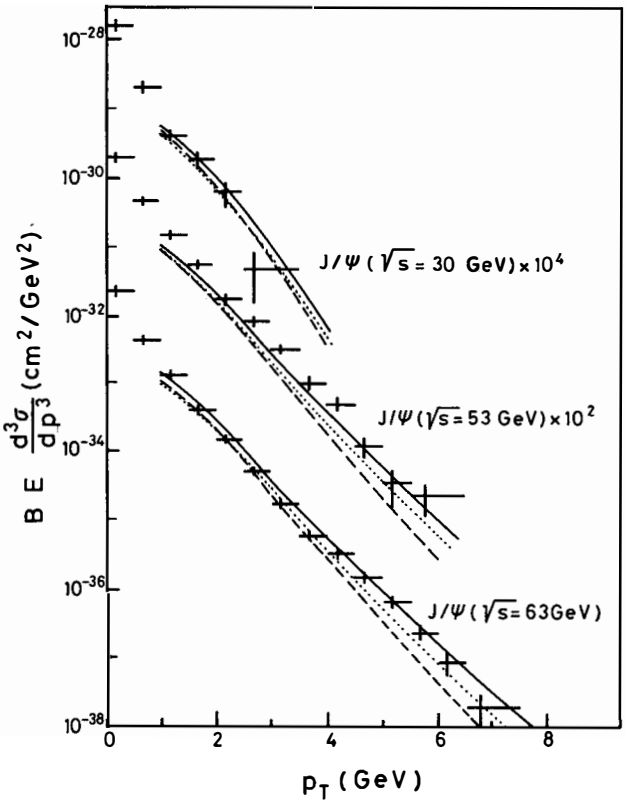

Fig. 2 : The invariant cross sections for $pp \to J/\psi\, X$ at $y = 0$ as a function of p_T at $\sqrt{s}$ = 30,53 and 63 GeV . The solid (dashed) curves show the total yields for scaling (scale breaking) structure functions. The dotted curve represents the contribution in the scaling limit from $gg \to {}^3S_1 g$ alone. The data points are reproduced from ref. 9.

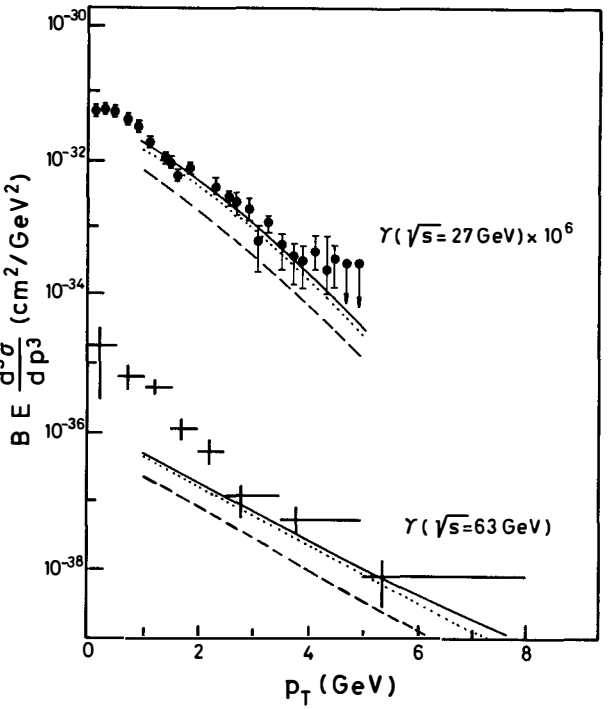

Fig. 3 : The invariant cross sections for $pp \to T\,X$ at $y = 0$ as a function of p_T at $\sqrt{s}$ = 27.4 and 63 GeV . The curves are as described in Fig. 2. The data points are taken from ref. 10) (†) and ref. 9) (+).

with data taken from ref. 9) and 10). The slopes of the invariant spectra $BE\,\frac{d^3\sigma}{dp^3}\Big|_{y=0}$ at large p_T are consistent with the experiments in all cases. The absolute normalizations are in fair agreement with the J/ψ data[9] at the three ISR energies $\sqrt{s}$ = 30,53 and 63 GeV . The predicted rate is also not much off for the T production[10] at $\sqrt{s}$ = 27.4 GeV , whereas at $\sqrt{s}$ = 63 GeV it is lower than the observed one[9] by a factor 2 to 3 at large p_T . This discrepancy, however, is small compared to the overall difference of two orders of magnitude between the J/ψ and T rates at $p_T \sim 4$ GeV and $\sqrt{s}$ = 63 GeV . In addition, the T-data reproduced in Fig. 3 contain contributions from T' and T" which have not been included in the theoretical spectra. Thus, the model provides a satisfactory description of the s-dependence of the resonance production at large

p_T and its dependence on the resonance mass at a given c.m. energy.

Further, it is clear from Fig. 2 and 3 that the distributions calculated in the scaling limit are favored by the data over the ones which include scale breaking. This could mean, in turn, that the gluon distributions are still rather hard at large Q^2 . The slopes alone do not discriminate between scaling and scale breaking structure functions. The role of the J/ψ and T production via intermediate P-waves can be inferred from the dotted curves in Fig. 2 and 3 which represent the contribution in the scaling limit from the direct process $gg \to {}^3S_1 g$ alone. Generally, the P-wave production becomes more and more important with increasing p_T for reasons mentioned in the beginning. For the J/ψ , this component contributes more than 50% to the total rates already for $p_T \sim 4$ to 5 GeV . For the T , on the other hand, it is still suppressed in this p_T range due to the large T-mass as well as due to the small value for r , $r_T/r_\psi \sim 0.2$. Consequently, the jet recoiling against the T at medium p_T is most of the time a gluon, whereas for the J/ψ it is half of the time a gluon, half of the time a quark. This can be checked, for example, by studying the positive to negative charge ratio of hadrons in the opposite side jet.

To conclude, we have achieved a detailed description of the high p_T production of heavy resonances in pp-collisions in lowest order QCD. The agreement with the available data is satisfactory. Clearly, there are uncertainties in the model which are partly familiar from QCD calculations of other hard scattering processes. More crucial, however, is the lack of knowledge of the higher order QCD corrections. A more detailed discussion together with further predictions and some subtleties concerning the comparison of our model with different experiments can be found in our preprint[7]. Several other investigations are in progress. Recently we learnt about a similar approach[11] to the inelastic photoproduction of J/ψ and T based on the subprocess $\gamma g \to {}^3S_1 g$.

I am grateful to R. Baier with whom the work reported here was done, and to C. Kourkoumelis, Z. Kunszt and D.M. Scott for discussions. In particular, I would like to thank the organizers of the workshop for a very pleasant atmosphere, indoors as well as outdoors.

REFERENCES

1) For a review and further references, see e.g. Z. Kunszt, these proceedings and E. Reya, Perturbative quantum chromodynamics, preprint DESY 79/88, DO TH 29/20 (1979).

2) Z. Kunszt, E. Pietarinen and E. Reya, Phys. Rev. D21, 733 (1980).

3) J.F. Gunion, Phys. Rev. D11, 1796 (1975); D12, 1345 (1975). M.B. Einhorn and S.D. Ellis, Phys. Rev. D12, 2007 (1975); M.B. Green, M. Jacob and P.V. Landshoff, Nuovo Cim., 29A, 123 (1975).

4) C.E. Carlson and R. Suaya, Phys. Rev. D14, 3115 (1976). S.D. Ellis, M.B. Einhorn and C. Quigg, Phys. Rev. Lett. 36, 1263 (1976).

5) J.H. Kühn, Phys. Lett. 89B, 385 (1980).

6) Chang Chao-Hsi, Nucl. Phys. B172, 425 (1980).

7) R. Baier and R. Rückl, Hadronic Production of J/ψ and T: Transverse Momentum Distributions, preprint BI-TP 81/06 (1981).

8) H. Krasemann, Z. Phys. C1, 189 (1979).

9) C. Kourkoumelis et al., Phys. Lett. 91B, 481 (1980).

10) K. Ueno et al., Phys. Rev. Lett. 42, 486 (1979).

11) E.L. Berger and D. Jones, Inelastic photoproduction of J/ψ and T by gluons, preprint ANL-HEP-PR-80-72 (1980).

HADRON STRUCTURE FUNCTIONS

François Martin
LAPP, Annecy-le-Vieux, France

ABSTRACT

The x dependence of hadron structure functions is investigated. If quarks can exist in very low mass states ($\mathcal{O}$(10 MeV) for d and u quarks) the pion structure function is predicted to behave like $(1-x)$ and not $(1-x)^2$ in a x-region around 1. Relativistic and non-relativistic quark bound state pictures of hadrons are considered together with their relation with the Q^2 evolution of structure functions. Good agreement with data is in general obtained.

Hadron structure functions are measured chiefly in deep inelastic scattering of leptons on nuclear matter (proton and neutron structure functions) (fig. 1a) and in lepton pair production in hadron-hadron collisions (so-called Drell-Yan mechanism; proton, neutron, pion, kaon structure functions) (fig. 1b). These

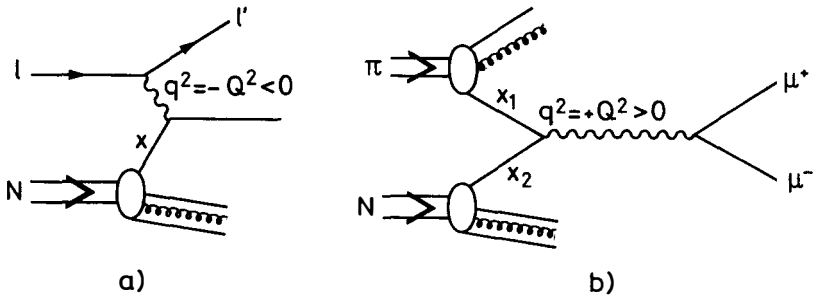

Fig. 1 a) Deep inelastic lepton-nucleon scattering, b) Muon pair production in pion-nucleon collision.

functions, $F(x,Q^2)$, depend on x, the fraction of the hadron longitudinal momentum (light cone variable) carried by the struck or annihilating quark (or antiquark) and on Q^2, which characterizes the scale at which the hadron structure is probed. Perturbative QCD tells something about the Q^2 dependence of those structure functions for large enough $Q^2 (Q^2 \geq 1\ \text{GeV}^2)$. The purpose of this talk is to try to tell something about the x dependence of those structure functions.

Experimental results on nucleon structure functions[1] lead to $x[u_v^p(x) + d_v^p(x)] \sim 3.4\sqrt{x}(1-x)^3$ for $Q^2 \sim 20\ \text{GeV}^2$, where u_v^p and d_v^p are respectively the u and d valence quark distributions inside a proton. For pion structure functions, experimental results are[2),3)] $x\bar{u}_v^{\pi^-}(x) = xd_v^{\pi^-}(x) \sim 0.6\sqrt{x}(1-x)$, also for $Q^2 \sim 20\ \text{GeV}^2$. In the case of the pion structure functions, many theorists have found that $\bar{u}_v^{\pi^-}(x) = d_v^{\pi^-}(x) \sim A(1-x)^2$ when x goes to 1, a prediction which appears to be in contradiction with experimental measurements. Let us discuss the theoretical arguments and how we can explain the disagreement with experiment.

First, there is a perturbative QCD argument[4),5),6)]. The π^- structure functions are measured via $\mu^+\mu^-$ production in π^-N collision. Let k be the 4-momentum of the $\bar{u}$ quark inside the π^-, which annihilates the u quark of the nucleon, and m the mass of the recoiling constituents of the pion. From kinematics, we get

$$k^2 = xm_\pi^2 - \frac{xm^2 + k_T^2}{1 - x}$$

where k_T is the $\bar{u}$ transverse momentum, with respect to the pion momentum. When x goes to 1

$$k^2 \sim -\frac{m^2 + k_T^2}{1 - x} \leq -\frac{m^2}{1 - x} \qquad (1)$$

implying that k^2 gets large and negative. If k^2 gets large the dominant contribution to the Drell-Yan mechanism comes from the diagram of fig. 2, where

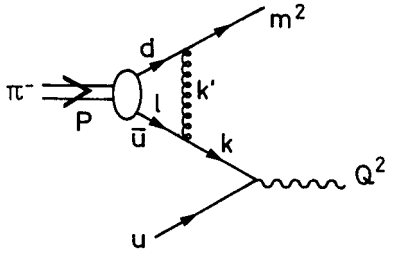

Fig. 2 One gluon exchange contribution to the pion structure function.

m is the recoiling quark mass. The dominant part of this diagram corresponds to the virtualnesses ℓ^2 and $(P-\ell)^2$ remaining small (of order 0.1 GeV^2). In this case, the virtualness of the exchanged gluon is of order k^2 : $k'^2 \sim (1-\xi)k^2$, where ξ is the light cone variable relative to ℓ. For a pion, the most probable value of ξ is 1/2. Since the virtualness of the exchanged gluon is large, the diagram of fig. 2 is a short distance process and the quark-gluon coupling is $\alpha_s(k'^2)$. The computation of this diagram leads to $\bar{u}^{\pi^-}(x) \sim A(1-x)^2$, when x goes to 1. For the nucleon, similar diagrams lead to $u^p(x)$ and $d^p(x)$ behaving like $(1-x)^3$, when x goes to 1[4),7)]. One problem with these results has to do with the recoiling quark mass m [8)]. What is this mass? In the case of the pion, if it is the constituent mass ($\sim$ 340 MeV), (1) reads as $k^2 \leq -0.1$ GeV$^2/(1-x)$. In order to be able to apply perturbative QCD one needs $k'^2 \lesssim -1$ GeV$^2 \Rightarrow k^2 \lesssim -2$ GeV$^2 \Rightarrow x \gtrsim 0.95$. Therefore, in this case, one can justify the $(1-x)^2$ behaviour only in the region $0.95 < x < 1$. Moreover, a quark has also a current mass, which is very small for d and u quarks ($\sim$ 8 MeV for d quark), implying that in a pion some quark state with very low mass can recoil. If m is of order 8 MeV, the x interval where perturbative QCD can be applied (giving the $(1-x)^2$ behaviour) becomes very very small ($x > 0.99...$). In the limit $m = 0$, the $(1-x)^2$ behaviour never shows up because k^2 is never necessarily large and negative. In this case, the non-

perturbative contribution of the pion bound state wave function, corresponding to small values of k^2, always dominates over the large k^2 perturbative QCD contributions of diagram of fig. 2, this even near $x = 1$ [8),9),10)]. In fact, when $m = 0$, and for a large class of bound state wave functions, we find, when x goes to 1, the following behaviours which depend only on kinematical constraints[8)]:

$$\bar{u}^{\pi^-}(x) = d^{\pi^-}(x) \nsim A(1-x)$$

$$u^p(x) \text{ and } d^p(x) \nsim B_{u,d}(1-x)^3 .$$

More generally, for a target with n quark constituents we find

$$\lim_{x \to 1} q_v(x) \propto (1-x)^{2n-3}$$

which directly reflects the number of constituents rather than the related exchanges of large k'^2 gluons.

There exist non-perturbative calculations of the pion structure functions, based on the solution of a Bethe-Salpeter equation for a quark-antiquark bound state with massless gluon exchange[11)]. The kernel of this equation corresponds in fact to the diagram of fig. 2. The result of such calculations exhibits also the $(1-x)^2$ behaviour:

$$\bar{u}_v^{\pi^-}(x) = d_v^{\pi^-}(x) \sim Ax^2(1-x)^2 \text{ for } 0 \leq x \leq 1 . \qquad (2)$$

This result is obtained in the framework of conventional quantum field theory, i.e. using $1/(\not{k} - m_q)$ quark propagator, with $m_q > m_\pi/2$, and $g^{\mu\nu}/k'^2$ gluon propagator. Those propagators are not in agreement with confinement because they lead to free quarks of mass m_q and free massless gluons. Therefore one can have some doubts on result (2).

We propose a quark propagator which is in agreement with quark confinement and gives a meaning to the small current mass of d and u quarks[8),9)]. Our proposed quark propagator is a cut starting at m_o, possibly related to the current quark mass, and does not have the perturbative QCD pole. However, although there is no pole on the real axis, the propagator spectral function is peaked at a mass m, possibly related to the constituent quark mass, with a width γ^2 of the order of the strong interaction scale Λ^2. Explicitly, if in a physical gauge (like an axial gauge), we write the quark propagator as

$$P(k) = \Pi(k^2) \not{k} + M(k^2), \qquad (3)$$

we can choose the absorptive part of $\Pi(k^2)$ as

$$\text{Abs } \Pi(k^2) \sim \frac{\pi^{-1} \gamma^2 \theta(k^2 - m_o^2)}{(k^2 - m^2)^2 + \gamma^4} \frac{}{} \qquad (4)$$

with $\gamma^2 = \mathcal{O}(\Lambda^2)$. For d and u quarks, m_o and m will be respectively of order 10 and 336 MeV, whereas for s quark they will be of order 150 and 540 MeV. Moreover, we can choose the large k^2 behaviour of our propagator to be given by perturbative QCD. Since it does not possess a real pole, this propagator is in agreement with confinement. Using this quark propagator spectral function, together with some realistic bound state wave functions, we find the following results for hadron structure functions: assuming $m_o = 0$ for d and u quarks ($m_o = \mathcal{O}(10 \text{ MeV})$ changes the result only for $0.99 < x < 1$), we find $\bar{u}_v^{\pi^-}(x)$ and $d_v^{\pi^-}(x)$ roughly proportional to $(1-x)$ for $0.45 < x < 1$. On the other hand, using $m_o = 150$ MeV for s quark, we find that $\bar{u}_v^{K^-}(x)$ is roughly a decreasing linear function of x for $0.4 < x < 0.85$ and behaves like $(1-x)^2$ for $0.85 < x < 1$. For the nucleon, we find that $u_v^N(x)$ and $d_v^N(x)$ behaves like $(1-x)^3$ when x goes to 1. Therefore, the pion structure functions that we obtain are in much better agreement with experiment than the ones obtained assuming a finite quark mass (of order 300 MeV for d and u quarks).

It is possible to apply a Drell-Yan-West[12] relation to connect the x near 1 behaviour of the pion structure functions with the resonance channels appearing in deep inelastic scattering of charged lepton on pion[13]: $\gamma(Q^2)\pi \to \rho, A_1, A_2, \ldots$ (the elastic channel $\gamma(Q^2)\pi \to \pi$ contributes only to the longitudinal structure functions, not to the transverse ones). As a result, the $(1-x)$ behaviour of the transverse pion structure functions implies a $1/[Q^2]^{3/2}$ behaviour for the $F_{\pi\rho}^{\gamma}(Q^2)$ form factor (the $\gamma(Q^2)\pi\rho$ coupling is defined as $\epsilon_{\mu\nu\tau\sigma} q^{\mu} \epsilon_{\gamma}^{\nu} r^{\tau} \epsilon_{\rho}^{\sigma} F_{\pi\rho}^{\gamma}(Q^2)$ where q and r are respectively the photon and ρ momenta and ϵ_{γ} and ϵ_{ρ} the photon and ρ polarization vectors). This behaviour leads to a $e^+e^- \to \pi\rho$ cross-section decreasing as $1/s^3$ at large s (e^+e^- invariant mass $\sqrt{s} \gtrsim 1\text{-}2$ GeV).

The quark propagator (3), (4) has a complex pole in the second sheet of the k^2 plane. Can we say something about the related singularities of the quark-antiquark bound state wave function? In conventional quantum field theory, if the quark-antiquark interaction takes place via exchanges of massless gluons, the bound state wave function has the same kind of singularity as the quark propagator. This may also be true in QCD if we assume that the gluon propagator has a cut starting at $k'^2 = 0$. In this case, the bound state wave function possesses also the complex pole of the quark propagator. Moreover, up to an overall phase, the bound state wave function should be real. This is a consequence of unitarity, connected to the fact that, even if the quark and antiquark propagators have cuts

starting at $m_o^2 = \mathcal{O}((10\ \text{MeV})^2)$, the pion propagator should possess only a pole at $m_\pi^2 = 0.02\ \text{GeV}^2$ and a cut starting at $9m_\pi^2$. Therefore, a mechanism must exist, which in the case of color singlet bound states makes the wave function real (this is also related to the stability of the pion in the framework of QCD). This reality can be obtained if we assume, for example, that the bound state wave function possesses also the pole which is complex conjugate of the one of the quark propagator. In this case, an approximation of the quark-antiquark bound state wave function would be

$$\psi(k^2) \sim \frac{A}{(k^2 - m^2)^2 + \gamma^4}$$

Assuming that this kind of wave function is also valid for a heavy quark-antiquark bound state (e.g. J/ψ) and making a non-relativistic approximation, we deduce the following quark-antiquark potential[14]

$$V(r) \sim B \cot \lambda r ,$$

where λ is of the order of the strong interaction scale ($\sim$ 200 MeV). This potential behaves as $1/r$ when r goes to zero, in good agreement with perturbative QCD. It is a confining potential which blows up at $r = \pi/\lambda \sim 4$ fermi. This last point should not be taken too seriously since we believe that our potential is meaningless for $r \gtrsim 3.5$ fermi, a distance at which the D^+D^- threshold will occur. It is not surprising that we do not get a linear potential at large r, as in the case of the gluonic string, because first our quarks and antiquarks are not standard particles, second we have not used precise information on the gluon propagator (we use the fact that it has a cut starting at $k'^2 = 0$, but not the fact that it may behave as $1/k'^4$ in this region).

Going back to our results on pion, kaon and nucleon bound state structure functions, we can ask the following question: at which scale, i.e. at which Q^2, should we compare them with experiment? In particular, so far, our analysis does not include gluon radiation type diagrams (fig. 3) which makes the hadron struc-

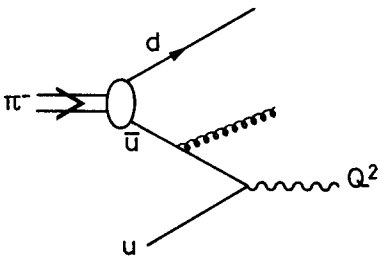

Fig. 3 Gluon radiation contribution to Drell-Yan mechanism.

ture functions vary with Q^2. Some people would say that the bound state structure functions correspond to the experimental ones at the scale for which perturbative QCD starts to be valid, i.e. for $Q^2 \sim 2\text{-}4$ GeV^2. If so, we predict a pion structure function behaving like $(1-x)$ in a x-region near 1, for $Q^2 \sim 3$ GeV^2. In addition, if we include diagrams like the one of fig. 3, in a leading log approximation, the predicted pion structure function behaves like $(1-x)^{1.3}$ for $Q^2 \sim 20$ GeV^2, not in such a good agreement with experiment $[(1-x)]$. But it is possible that, because of non leading log terms of perturbative QCD, the $(1-x)$ behaviour does not change in a sensible way when Q^2 goes from 3 GeV^2 to 20 GeV^2. More dramatic is the fact that in our bound state structure functions almost 100% of the hadron momentum is carried by quarks and antiquarks and none is carried by gluons. This is in contradiction with the experimental result that for $Q^2 \sim 3$ GeV^2, almost 50% of the hadron momentum is carried by gluons. One way out of this difficulty is to introduce gluons by hand, assuming that for $Q^2 \sim 3$ GeV^2 the probability of observing a hadron as a pure bound state of its valence quarks and antiquarks, without gluons and sea quark-antiquark pairs, is much less than 1 (in ref. 10 this probability is estimated to be of order 0.2 to 0.25 in the case of the pion). But in order to have agreement with experiment we have also to assume that the contributions of the states containing gluons and sea pairs, in addition to valence quarks and antiquarks, do not modify in a sensible way the $(1-x)^p$ behaviour corresponding to pure valence quark and antiquark state ($p = 1$ for pion, $p = 3$ for nucleon). Another way of solving the difficulty of gluons, which may be equivalent to the previous one, is to assume that in the leading twist approximation the structure functions associated to pure valence quark and antiquark bound states correspond to a very small momentum scale $Q_o^2 (\sim 0.1$ GeV$^2)$. Then, via perturbative and non-perturbative QCD, they evolve with Q^2, up to $Q^2 = 3$ GeV^2 or 20 GeV^2. In this way we certainly generate gluons, but we have also to assume (or to check) that in doing so the $(1-x)^p$ behaviour corresponding to the pure valence quark and antiquark bound state is not modified (a property which is not satisfied by perturbative QCD in its leading log approximation).

There is a way of taking account of the Q^2 evolution of hadron structure functions in the framework of perturbative QCD without knowing explicitly what this evolution and the starting scale Q_o^2 are. It is to make a comparison between different quark distributions[8),15)]. In the leading twist approximation, the quantum fluctuations relative to a constituent inside a hadron do not depend on the spectator constituents. In particular, if we consider the moments of a non-singlet quark distribution

$$M_{q_{NS}}(n,Q^2) = \int_o^1 x^{n-1} q_{NS}(x,Q^2)dx \ ,$$

in the leading twist approximation and to all orders of perturbative QCD the ratio $M_{q_{NS}}(n,Q^2)/M_{q_{NS}}(n,Q_o^2)$ does not depend on the hadron which is considered. Moreover, if the quark mass squared is negligible as compared to Q_o^2 and Q^2, this ratio does not depend on the flavour of the quark q_{NS}. But this ratio does depend on the process which is probing the structure of the hadron (deep inelastic, lepton pair production, ...). Therefore, one can write

$$M_{\bar{u}_v}\pi^-(n,Q^2) = M_{u_v}p(n,Q^2)\,\frac{M_{\bar{u}_v}\pi^-(n,Q_o^2)}{M_{u_v}p(n,Q_o^2)}\,, \qquad (5)$$

a relation which is true for example for deep inelastic scattering. Taking $M_{u_v}p(n,Q^2)$ from experiment[1] and the ratio $M_{\bar{u}_v}\pi^-(n,Q_o^2)/M_{u_v}p(n,Q_o^2)$ from our relativistic bound state model, we predict $M_{\bar{u}_v}\pi^-(n,Q^2)$ for deep inelastic scattering. Including the corrections necessary to go from deep inelastic scattering to lepton pair production[16),8)] we get the same quantity relative to lepton pair production and then $x\bar{u}_v^{\pi^-}(x,Q^2)$ by an inverse Mellin transformation. Our results[8)] are shown on fig. 4 together with data of the CERN NA3 experiment[3)]. Agreement

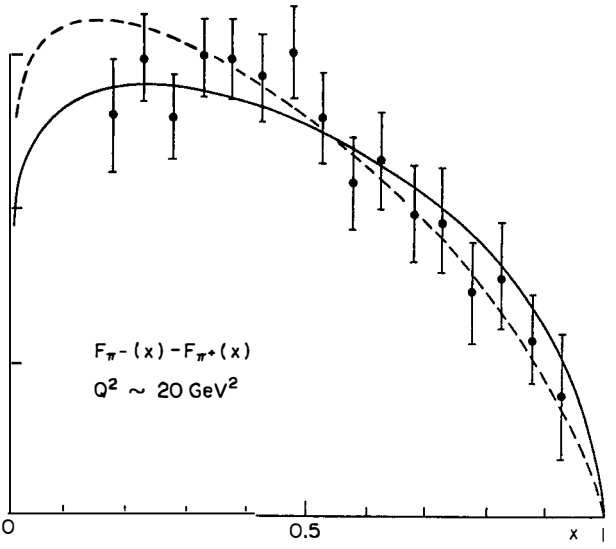

Fig. 4 Comparison of data[3)] on $F_{\pi^-}(x) - F_{\pi^+}(x)$ and theoretical predictions of our relativistic bound state model[8)]. The solid and dashed curves correspond respectively to spin and no spin correlation between the quark and the antiquark inside the pion. Normalization is arbitrary.

between the two is good. Let us note that our analysis does not include possible higher twist effects near $x = 1$. A relation identical to (5), in which we replace $\bar{u}_v^{\pi^-}$ and u_v^p respectively by $\bar{u}_v^{K^-}$ and $\bar{u}_v^{\pi^-}$, can be written for lepton pair production structure functions. Taking $M_{\bar{u}_v}\pi^-(n,Q^2)$ from experiment[3] and the ratio $M_{\bar{u}_v}K^-(n,Q_o^2)/M_{\bar{u}_v}\pi^-(n,Q_o^2)$ from our relativistic bound state model we predict $M_{\bar{u}_v}K^-(n,Q^2)$ and consequently $x\bar{u}_v^{K^-}(x,Q^2)$. The dashed curve of fig. 5 is the prediction of our relativistic bound state model[9] for the ratio $\bar{u}_v^{K^-}(x,Q^2 = 20\ \text{GeV}^2)/\bar{u}_v^{\pi^-}(x,Q^2 = 20\ \text{GeV}^2)$. The data points are from the CERN NA3 experiment[17]. Agreement between the two is not bad. The dashed curve corres-

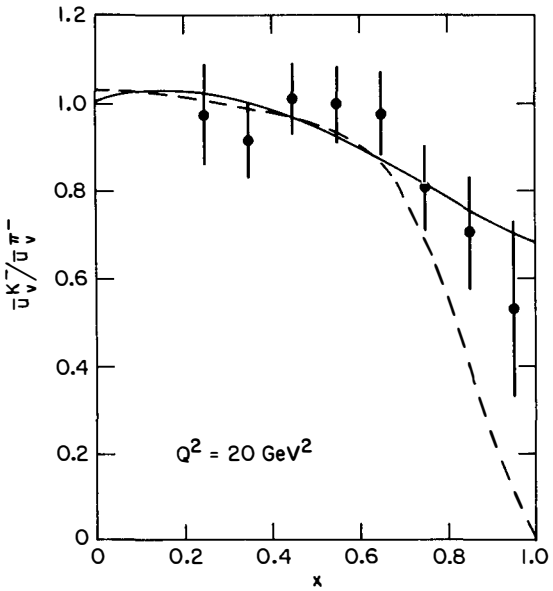

Fig. 5 The ratio of K^-/π^- lepton pair production structure functions versus x, for $Q^2 \sim 20\ \text{GeV}^2$. Data points are from the CERN NA3 experiment[17]. The dashed and solid curves are respectively the predictions of our relativistic and non-relativistic bound state models[9],[15].

ponds to the following values of the parameters: $(m_o, m) = (0, 336\ \text{MeV})$ for d and u quarks and $= (150\ \text{MeV}, 540\ \text{MeV})$ for s quark. Note that our result is very sensitive to those parameters. So, most probably, an adjustement of the parameters can give a better agreement with data. Note also that this curve has

been obtained assuming no spin correlation between the struck quark and the recoiling one. If our relativistic bound state model has something to do with reality, comparison with experiment can give information on the quark (d,u,s,...) propagators in the non-perturbative region. In particular, the kaon structure functions can tell us about the s quark propagator.

In quite a different manner, it is possible to make a non-relativistic approximation to compute $q_v(x,Q_o^2)$. In such an approximation, hadrons are considered as non-relativistic bound states of two or three particles[15),18),19)]. The distributions $q_v(x,Q_o^2)$ obtained are peaked at $x_o = \mu/(m+\mu)$ with a width of order $1/RM$. μ, m and M are respectively the masses of the struck quark or antiquark, the recoiling constituents and the hadron; R^2 is the mass square radius of the hadron. For nucleon, pion and kaon, x_o equals respectively 0.33, 0.5 and 0.38 (this last figure corresponds to the $\bar{u}_v$ distribution inside K^- when using $\mu = m_{\bar{u}} = 336$ MeV and $m = m_s = 540$ MeV) and $1/RM$ equals respectively 0.26, 2.4 and 0.80. The resulting distributions $q_v(x,Q_o^2)$ are quite different from those experimentally measured at $Q^2 \sim 20$ GeV^2 (fig. 6). This means that a large amount of perturbative QCD corrections are needed to obtain $q_v(x,Q^2 = 20\ \text{GeV}^2)$. This is a feasible possibility which in fact is realized when using the leading log approximation for the perturbative QCD corrections[15),18)]. The shapes of the

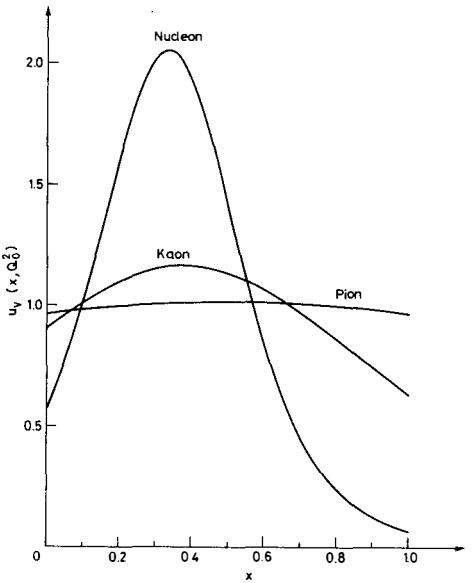

Fig. 6 The three non-relativistic bound state distributions $u_v(x,Q_o^2)$ as functions of x, for nucleon, π^+ and K^+.

distributions $q_v(x,Q_o^2)$ are quite different from the experimental ones, but there are two main features which are not modified by the perturbative QCD corrections and are in fact experimentally observed: i) the nucleon distribution is much more peaked and concentrated at small x than the pion one, ii) the kaon distribution drops faster than the pion one at large x. Using formula (5) in the same way as we did in the case of our relativistic bound state model, we predict[15] the lepton pair production structure function $x\bar{u}_v^{\pi^-}(x,Q^2)$ in the framework of this non-relativistic bound state model (fig. 7). Agreement with CERN NA3 data[3] is good.

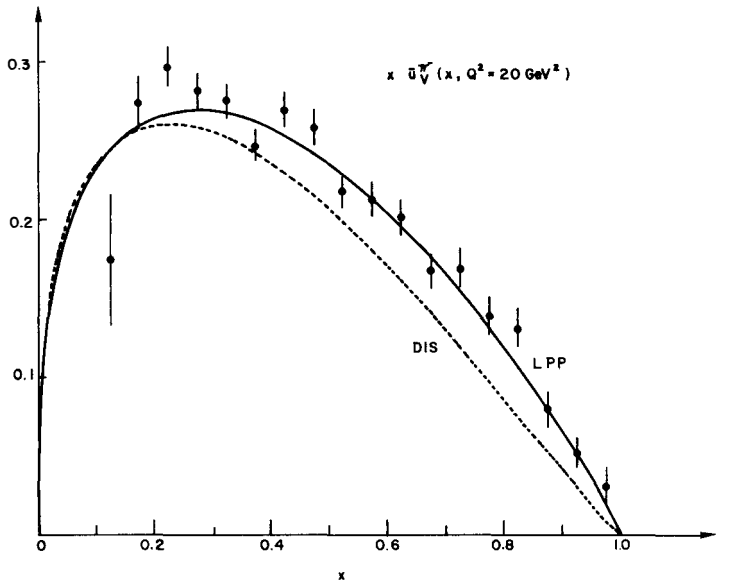

Fig. 7 Comparison between predictions of our non-relativistic bound state model[15] on $x\bar{u}_v^{\pi^-}(x,Q^2 = 20\ GeV^2)$ as a function of x, and data of CERN NA3 experiment[3] on $F_\pi(x)$. Normalization of data is arbitrary. The solid curve corresponds to lepton pair production (LPP) and is the relevant one for comparison with data; the dashed curve corresponds to deep inelastic scattering (DIS). Note that data include some sea contributions at small x ($x < 0.3$).

Similarly, this non-relativistic bound state model predicts a ratio[15] $\bar{u}_v^{K^-}(x,Q^2 = 20\ GeV^2)/\bar{u}_v^{\pi^-}(x,Q^2 = 20\ GeV^2)$, shown as the solid curve on fig. 5. Agreement with data is also quite good.

Even if agreement with experimental data is good, some criticisms of the non-relativistic approximation have to be made. The main one is that it is difficult to consider pion and kaon as non-relativistic bound states. The second criticism is that we do not get an agreement between the non-relativistic bound state picture and the relativistic one. The solution of this contradiction may be the following: the relativistic bound state picture could correspond to the experimental situation at a scale $Q^2 \sim 2\text{-}4$ GeV^2 (note that in this case, we have to add gluons and sea quark-antiquark pairs by hand). On the other hand, the non-relativistic bound state picture could be associated to a very small scale ($Q_o^2 \sim 0.1$ GeV^2). At this scale, a large amount of unknown perturbative and non-perturbative QCD corrections ($1/Q^2$ terms) makes the comparison of the non-relativistic structure functions with experiment meaningless. However, if we let those structure functions evolve with Q^2 via perturbative QCD (mainly leading log terms) the $1/Q^2$ terms disappear at a scale $Q^2 \gtrsim 2\text{-}4$ GeV^2. At this last scale, the quark structure of hadrons shows up and comparison between the model and experiment becomes meaningful. At Q_o^2 the model assumes that there are no glue or sea quark-antiquark pairs. At $Q^2 \gtrsim 2\text{-}4$ GeV^2 it gives the right amount of gluons and sea pairs[20),18)]. This last point is in fact the only justification for considering this model, because it is difficult to understand how we can control perturbative QCD (and moreover the leading log approximation) for $Q^2 \lesssim 1$ GeV^2.

Conclusions are, first of all, that if quarks can exist in very low mass states ($\mathcal{O}$(10 MeV) for d and u) there is no reason to obtain a $(1-x)^2$ behaviour for the pion structure function in a x-region around 1. In fact, in the framework of our relativistic bound state model, we get a $(1-x)$ behaviour which is in agreement with what is experimentally observed. However, our relativistic bound state picture remains to be included in a model taking account of the Q^2 evolution of structure functions. In particular, the 50% of gluons observed at $Q^2 \sim 2\text{-}4$ GeV^2 is not understood. This last point can be understood in a non-relativistic bound state picture used together with a perturbative QCD Q^2 evolution of structure functions (mainly leading log approximation). But this model needs justification, both for the use of a non-relativistic bound state approximation and of perturbative QCD for $Q^2 \lesssim 1$ GeV^2. Agreement between the relativistic and non-relativistic bound state pictures is also needed. Both pictures are in general in good agreement with experimental data, particularly the naive non-relativistic prediction on $\bar{u}^{K^-}/\bar{u}^{\pi^-}$.

I acknowledge useful discussions with R. Blankenbecler, S. Brodsky, A. De Rújula, J. Kaplan, P. Minkowski and R. Stora.

REFERENCES

1) J.G.H. de Groot et al., Phys. Lett. 82B, 456 (1979).

2) C.B. Newman et al., Phys. Rev. Lett. 42, 951 (1979).

3) J. Badier et al., Proceedings of the E.P.S. International Conference on High Energy Physics, Geneva, 27 June - 4 July 1979, (CERN 1980) p. 751; paper presented at the XXth International Conference on High Energy Physics, University of Wisconsin, Madison, U.S.A, July 17-23, 1980, and CERN preprint EP 80-148 (1980); see also S. Weisz, these proceedings.

4) Z.F. Ezawa, Il Nuovo Cimento 23, 271 (1974).

5) G.R. Farrar and D.R. Jackson, Phys. Rev. Lett. 35, 1416 (1975).

6) E.L. Berger and S.J. Brodsky, Phys. Rev. Lett. 42, 940 (1979).

7) R. Blankenbecler and S. Brodsky, Phys. Rev. D10, 2973 (1974).

8) A. De Rújula and F. Martin, Phys. Rev. D22, 1787 (1980).

9) F. Martin, talk given at the XXth International Conference on High Energy Physics, University of Wisconsin, Madison, July 17-23, 1980 and SLAC-PUB-2581 (1980).

10) S.J. Brodsky, T. Huang and G.P. Lepage, SLAC-PUB-2540 (1980).

11) T.N. Pham, Phys. Rev. D19, 707 (1979).

12) S.D. Drell and T.M. Yan, Phys. Rev. Lett. 24, 181 (1970);
G.B. West, Phys. Rev. Lett. 24, 1206 (1970).

13) I am indebted to P. Minkowski for pointing out this connection to me.

14) R. Blankenbecler and F. Martin, unpublished.

15) F. Martin, Proceedings of the XVth Rencontre de Moriond, Vol. 1, edited by TRAN THANH VAN, R.M.I.E.M. Orsay, p. 487.

16) G. Altarelli, R.K. Ellis and G. Martinelli, Nucl. Phys. B143, 521 (1978) and B157, 461 (1979);
J. Kubar-André and F.E. Paige, Phys. Rev. D19, 221 (1979);
B. Humpert and W.L. Van Neerven, Phys. Lett. 84B, 327 and 85B, 293 (1979);
K. Harada, T. Kaneko and N. Sakai, Nucl. Phys. B155, 169 (1979).

17) J. Badier et al., Phys. Lett. 93B, 354 (1980); see also S. Weisz, these proceedings.

18) F. Martin, Phys. Rev. D19, 1382 (1979).

19) G. Altarelli, N. Cabibbo, L. Maiani and R. Petronzio, Nucl. Phys. B69, 531 (1974);
A. Le Yaouanc, L. Oliver, O. Pène and J.C. Raynal, Phys. Rev. D12, 2137 (1975).

20) V.A. Novikov, M.A. Shifman, A.I. Vainshtein and V.I. Zakharov, Annals of Physics 105, 276 (1977);
G. Parisi and R. Petronzio, Phys. Lett. 62B, 331 (1976).

TWO-PHOTON EXCHANGE
IN COMPETITION WITH THE DRELL-YAN PROCESS

B. Schrempp*) and F. Schrempp*)
II. Institut für Theoretische Physik
Universität Hamburg
Hamburg

Abstract: The two-photon exchange mechanism in $p^{(-)}p \to l^+l^-X$ is studied as a function of the dilepton mass M, transverse momentum Q_T and rapidity Y for $27 \leq \sqrt{s} \leq 800$ GeV. It is compared with $pp \to l^+l^-X$ data at ISR and with an "exponentiated" QCD prediction for $pp \to l^+l^-X$ at ISABELLE energies. The $\gamma\gamma$ contribution is found to be important, if not dominant, if at least two of the three kinematical conditions are satisfied: $\sqrt{s}$ very large, $M^2/s \ll 1$, Q_T small. Important clues for a future experimental isolation of the two-photon mechanism are given.

*) Heisenberg foundation fellow

$$\gamma\gamma \;\underset{\tau \ll 1}{\sim}\; \alpha^4 \frac{8}{\pi} \left(\log \frac{s}{0.15\ \mathrm{GeV}^2}\right)^2 \log \frac{\tau s}{m_l^2} \,. \tag{4}$$

The $\gamma\gamma$ formula is a crude approximation for $\tau \ll 1$, obtained[1] in the framework of the equivalent photon approximation. The logarithms in Eq. (4) are responsible for a rather strong rise of the cross section with increasing energy, which at very high energies tends to compensate the relative $O(\alpha^2)$ suppression. Indeed the results of the analyses by Chen et al.[2], Kessler et al.[1] and more recently of Moore[3] for $M^3 d\sigma^{\gamma\gamma}/dM$ and $M^3 d^2\sigma^{\gamma\gamma}/dMdY_{/Y=0}$ show that for $\sqrt{s}$ very large, $\sqrt{s}$ = 600 GeV, say, and $\tau \ll 1$ or $\tau \gtrsim 0.25$, say, the two-photon mechanism becomes a serious competitor to the Drell-Yan process.

ii) Next we turn to the Q_T distributions, which are in fact the main issue in this paper. As we have found in an extensive recent investigation[4], the relative contribution from the $\gamma\gamma$ mechanism is strongly enhanced at small values of Q_T for any $\sqrt{s}$ and τ. This may be seen qualitatively as follows. For the $\gamma\gamma$ contribution we expect a very steep slope at small Q_T due to the combined effect of two photon and one lepton propagator. On the other hand, the $O(\alpha_s)$ QCD predictions for $pp \to l^+l^-X$ - corrected for soft gluon radiation to all orders[5)-10] ("exponentiation") - lead us to expect a strong "radiation damping" at small Q_T resulting in a characteristically flat slope. Thus even for values of $\sqrt{s}$ and τ where the Q_T-integrated $\gamma\gamma$ cross section is small as compared to the Drell-Yan process, it might be the dominant mechanism at small values of Q_T.

Therefore, questions of particular interest are:

1) is the two-photon contribution at small Q_T already important at ISR energies and
2) is it going to swamp the typical signature of "exponentiated" QCD at ISABELLE energies, say?

As a basis for a quantitative discussion let us present in the following the main results from an exact calculation[4] of the triple differential cross section

$$\frac{d^3\sigma}{dM^2 dY dQ_T^2} \quad \left(p\,(\bar{p}) \longrightarrow \gamma\gamma \underset{\hookrightarrow l^+l^-}{\quad} X\right) \tag{5}$$

over the large energy interval $27 \lesssim \sqrt{s} \lesssim 800$ GeV, covering FNAL, ISR, $\bar{p}p$ collider and ISABELLE energies.

Let us finally mention that this whole analysis may be considered as a warming up exercise for the subprocesses $\gamma g \to q\text{-jet} + \bar{q}\text{-jet}$

1. INTRODUCTION

Currently much activity is being devoted to a thorough study of the two-photon exchange mechanism in e^+e^- annihilation. Recently, both the purely electromagnetic subprocess $\gamma\gamma \to l^+l^-$ as well as the subprocess $\gamma\gamma \to$ hadrons, including $\gamma\gamma \to$ q-jet + $\bar{q}$-jet, have been identified in e^+e^- collisions for the first time.

With the advent of very high energy $p(\bar{p})$ machines ($p\bar{p}$ colliders, ISABELLE) in the near future, two-photon physics will gain increasing importance also in hadron collisions. In fact we shall see that it starts to become important already at the ISR.

It is the aim of this contribution to point out that the two-photon exchange mechanism

$$pp \to \gamma\gamma \quad X \qquad (1)$$
$$\hookrightarrow l^+l^-$$

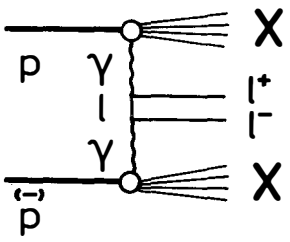

Fig. 1

constitutes an important, if not dominant contribution to $pp \to l^+l^-X$ in particular regions of phase space. More specifically, competition to the Drell-Yan process happens (roughly speaking), if at least two of the three kinematical conditions are satisfied

$$\begin{aligned} &\sqrt{s} \text{ very large} \\ &\tau \ll 1 \text{ (or } \tau \approx 1) \\ &Q_T \text{ small.} \end{aligned} \qquad (2)$$

Our notation is: $\sqrt{s}$ is the cm-energy, M the mass of the lepton pair, Q_T its transverse momentum, Y its rapidity and $\tau = M^2/s$.

Let us first discuss qualitatively, how this is possible even though the $\gamma\gamma$ contribution is an $O(\alpha^4)$ process as compared to the $O(\alpha^2)$ Drell-Yan process ($\alpha = e^2/4\pi$).

i) Consider first the cross section integrated over the dilepton transverse momentum Q_T, $M^3\, d\sigma/dM$ (or $M^3\, d^2\sigma/dMdY_{/Y=0}$) at fixed τ

$$\text{Drell-Yan} \sim \alpha^2 f(\tau) \text{ modulo weak scaling violations} \qquad (3)$$

and $\gamma\gamma \rightarrow q\text{-jet} + \bar{q}\text{-jet}$.

2. RESULTS

2.1 The dominant configuration

The two-photon cross section may be decomposed as

$$d\sigma(p^{(-)}p \rightarrow \gamma\gamma \hookrightarrow l^+l^- \; X) = d\sigma_{el\text{-}el} + d\sigma_{el\text{-}inel} + d\sigma_{inel\text{-}inel} \qquad (6)$$

according to whether the two $p\gamma$ vertices are both elastic, of mixed configuration or both inelastic.

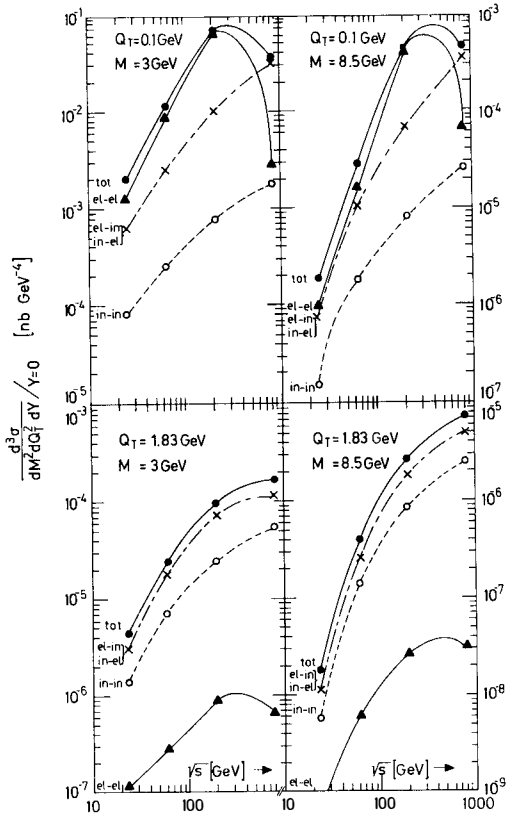

Fig. 2: $p^{(-)}p \rightarrow \gamma\gamma \hookrightarrow \mu^+\mu^- X$ and its decomposition into contributions from both proton vertices being elastic, of mixed configuration and inelastic.

Fig. 2 shows the decomposition into the three different contributions for Y = 0 and fixed (smallish) values of Q_T and M as a function of $\sqrt{s}$. We see that $d\sigma_{el-el}$ dominates only for very small values of $Q_T \lesssim 0.1$ GeV, while the elastic-inelastic contribution $d\sigma_{el-inel}$ dominates for $Q_T \gtrsim 0.5 - 1$ GeV.

In any case we realize that one $p\gamma$ vertex is always elastic. Therefore, triggering on one elastic proton vertex hardly reduces the $\gamma\gamma \to l^+l^-$ rate. This should help enormously with the experimental identification of the two-photon mechanism, since we expect a strong reduction of any (a priori large) "background": The $O(\alpha_s)$ QCD subprocesses

$$q\bar{q} \to \gamma^* g \quad (\hookrightarrow l^+l^-) \qquad \text{and} \qquad qg \to \gamma^* q \quad (\hookrightarrow l^+l^-) \tag{7}$$

are suppressed for colour and triality reasons; only "higher twist" terms of the type as typically calculated in the constituent interchange (CIM) model survive the trigger (see Fig. 3).

Let us finally remark that this trigger applies equally well for the relative enhancement of the subprocesses $\gamma g \to q\text{-jet} + \bar{q}\text{-jet}$ or $\gamma\gamma \to q\text{-jet} + \bar{q}\text{-jet}$.

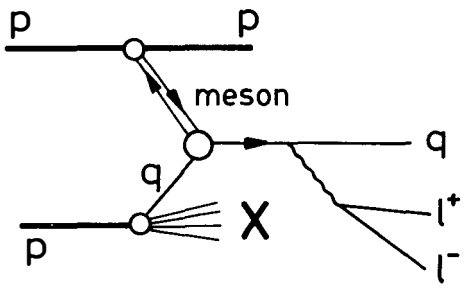

Fig. 3

2.2 $pp \to \gamma\gamma X \ (\hookrightarrow \mu^+\mu^-)$ candidate events at the ISR

Events of the type $pp \to \mu^+\mu^-$ + no hadrons have been measured at the ISR ($\sqrt{s}$ = 62 GeV) and interpreted as candidates for the two-photon mechanism[11]; the missing final state hadrons are lost in the beam pipes; (c.f. Drell-Yan: $pp \to \mu^+\mu^-$ + $\langle 12 \rangle$ charged hadrons). Fig. 4 shows the data in comparison with our exact $\gamma\gamma$ calculation; notice that not only the shape but also the absolute normalization[4] is predicted. Given the fact that the data have not yet been

corrected for Q_T resolution[12], the agreement is quite satisfactory.

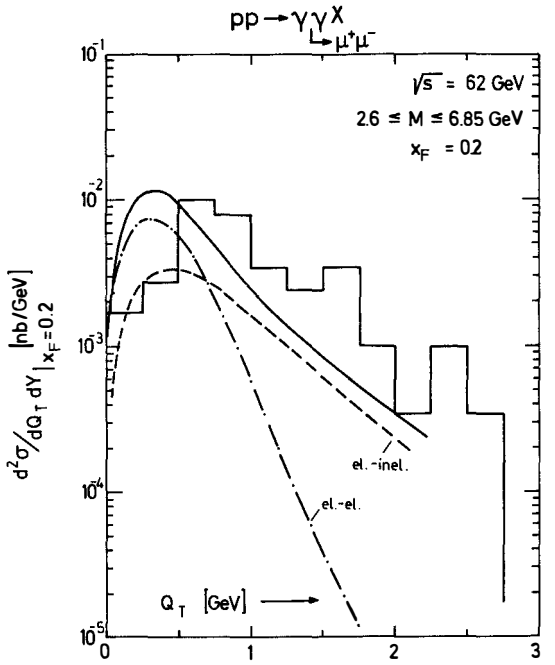

Fig. 4: γγ candidate events from the ISR[11),12)] (histogram) and theoretical prediction[4)] (full line) with decomposition into contributions from both proton vertices being elastic (dashed-dotted line) and from one being elastic and the other one inelastic (dashed line).

2.3 $pp \rightarrow e^+e^-X$ at the ISR and the two-photon mechanism

Even though the ratio of the Q_T-integrated cross sections, γγ/ data, amounts to a few percent only at ISR energies, the situation is different for the ratio of differential cross sections $d\sigma/dQ_T^2$. Fig. 5 shows ISR data[13)] at $\sqrt{s}$ = 63 GeV in two mass intervals in comparison with our calculation of the two-photon contribution. In the mass interval $4 \leq M \leq 4.5$ GeV we find the substantial ratio

$$\frac{pp \to \gamma\gamma \quad X \;(\hookrightarrow e^+e^-)}{pp \to e^+e^-X} \approx \begin{cases} 70\% \text{ for } Q_T \simeq 0, \\ \text{still } 30\% \text{ averaged over the first bin } 0 \leq Q_T \leq 0.5 \text{ GeV} \end{cases} \tag{8}$$

The effect is less important at higher masses M.

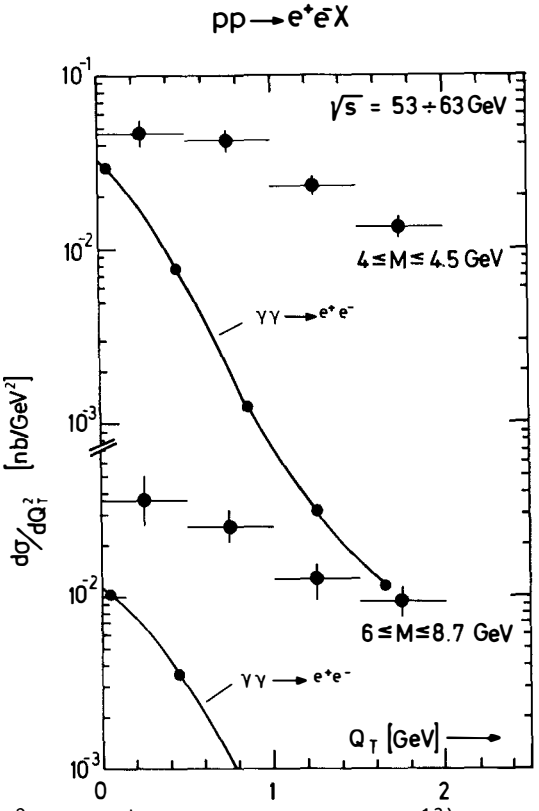

Fig. 5: $d\sigma/dQ_T^2$ ($pp \to e^+e^-X$); data from the ISR[13]; theoretical prediction of the two-photon contribution[4] (full line)

2.4 γγ/QCD expectations at ISABELLE energies

At very high energies we compare our two-photon results with predictions from QCD for $pp \to l^+l^-X$. We expect the ratio γγ/QCD to be largest at small values of Q_T.

In the kinematical range $\Lambda \lesssim Q_T \lesssim M$ of smallish Q_T naive QCD perturbation theory breaks down due to the appearance of two large

logarithms, log (M^2/Q_T^2) and log (M^2/Λ^2). However, as many authors have recently argued[5)-10)] the perturbative QCD predictions may reliably be extended into this regime of small Q_T, if suitable resummation techniques are applied. The recipe is to exponentiate the full $O(\alpha_s)$ result, which amounts to summing both real and virtual gluons to all orders in complete analogy to QED. For small Q_T the resulting "quark form factor" causes a strong "radiation damping" of the Q_T distribution due to the restricted phase space available for gluon radiation.

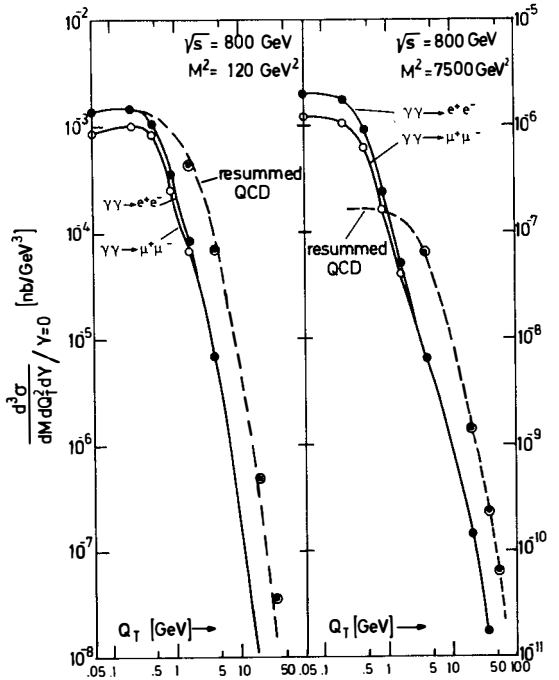

Fig. 6: $pp \rightarrow l^+l^-X$ at $\sqrt{s}$ = 800 GeV: the dashed line is the prediction from "exponentiated" QCD[6)], the full line the prediction for the two-photon contribution[4)]

In our quantitative comparison we take the "exponentiated" QCD predictions of Parisi and Petronzio[6)] at the ISABELLE energy of $\sqrt{s}$ = 800 GeV and two masses M^2 = 120 and 7500 GeV^2 (i.e. $M \simeq 11$ and

87 GeV), properly normalized[4]. The typical signature of "exponentiated" QCD is the flattish slope of the Q_T distribution at small Q_T. Our results for the two-photon contribution are compared with these "exponentiated" QCD predictions in Fig. 6. From this figure we read off the following dramatic ratios

$$\gamma\gamma/\mathrm{QCD}\ (pp \to \underset{(\mu^+\mu^-)}{e^+e^-}\ X),\ \sqrt{s} = 800\ \mathrm{GeV}$$

Q_T \ M	11 GeV	87 GeV
0.3 GeV	1 (0.7)	10 (6.4)
$0 \leq Q_T \leq 1$ GeV	0.77 (0.46)	3.8 (2.4)
all Q_T	0.24 (0.17)	0.25 (0.19)

Table 1

3. CONCLUSIONS

The two-photon mechanism $pp \to \gamma\gamma \underset{\hookrightarrow l^+l^-}{} X$ is an important contribution to $pp \to l^+l^-X$ already at the ISR at small Q_T. This may affect the determination of $\langle Q_T^2 \rangle_{QCD}$ from data.

The two-photon mechanism is important or dominant at ISABELLE energies in an interval $0 \lesssim Q_T \lesssim 1$-2 GeV and sizeable for all Q_T. It swamps the characteristic signature of "exponentiated" QCD (i.e. the flat slope at small Q_T).

Triggering on one elastic proton vertex may be helpful for a future isolation of the two-photon mechnism.

REFERENCES

1) C. Carimalo, P. Kessler and J. Parisi, Phys.Rev. D18, 2443 (1978)
2) M.-S. Chen, I.-J. Muzinich, H. Terazawa and T.P. Cheng, Phys.Rev. D7, 3485 (1973)
3) R. Moore, Z. Physik C, Particles and Fields 5, 351 (1980)
4) B. Schrempp and F. Schrempp, Nucl.Phys. B182, 343 (1981)
5) Yu.L. Dokshitzer, D.I. Dyakonov and S.I. Troyan, Phys.Lett. 78B, 290 (1978); 79B, 269 (1978); Phys.Rep. 58C, 269 (1980)
6) G. Parisi and R. Petronzio, Nucl.Phys. B154, 427 (1979)
7) G. Curci and M. Greco, Phys.Lett. 79B, 406 (1978); G. Curci, M. Greco and Y. Srivastava, Nucl.Phys. B159, 451 (1979)
8) C.L. Basham, L.S. Brown, S.D. Ellis and S.T. Love, Phys.Lett. 85B, 297 (1979)
9) C.Y. Lo and J.D. Sullivan, Phys.Lett. 86B, 327 (1979)
10) S.D. Ellis and W.J. Stirling, Univ. Washington, Seattle Preprint, RLO-1388-821 (1980)
11) CERN-Harvard-MIT-Naples-Pisa Collaboration: F. Vannucci, Proc. of Int. Workshop on $\gamma\gamma$ Collisions, Amiens, Springer-Verlag, p. 238 (1980)
12) F. Vannucci, private communication
13) Athens-BNL-CERN-Syracuse-Yale Collaboration: C. Kourkoumelis et al., Phys.Lett. 91B, 475 (1980)

SIGNATURE FOR INTERMEDIATE VECTOR BOSON PRODUCTION IN PROTON-ANTIPROTON COLLISIONS

M. PERROTTET
Centre de Physique Théorique, Section 2
CNRS - Luminy - Case 907
F-13288 MARSEILLE CEDEX 2 (France)

ABSTRACT

We study the differential cross sections $\frac{d^2\sigma}{d\cos\Theta dp_T^2}$, $\frac{d\sigma}{dp_T}$ and $\frac{d\sigma}{d\cos\Theta}$ for the reaction $p\bar{p} \to B(\to \ell_1 \bar{\ell}_2) + \text{jet}(p_T) + X$, with $B = Z^0, W^{\pm}$ at $\sqrt{s} = 540$ Gev and the same quantities for the pp case (Θ is the scattering angle of ℓ_2 with respect to the proton beam). The corresponding leptonic front-back asymmetry $A(\cos\Theta, p_T^2)$ for these first order QCD processes is then calculated for the $p\bar{p}$ case. $A(\cos\Theta, p_T^2)$ is found to be p_T independent to a very good approximation for $p_T(\text{jet}) \gtrsim 3$ GeV/c, with a magnitude similar to that of the zeroth order process. Since zeroth and first order total cross sections are comparable in magnitude, the first order asymmetry should be an experimentally testable quantity.

I. INTRODUCTION

In a few years, new accelerators like CERN's $p\bar{p}$ collider [1], the Isabelle machine [2], and perhaps forthcoming projects like the LEP [3] will be operable. It is expected that they at last will reveal Nature's comments to one of the more ambitious theories, the SU(2) x U(1) unification of weak and electromagnetic interactions ; namely, whether there are the predicted heavy intermediate bosons which in the simplest version of the theory have masses of the order 90 GeV, or not. Numerous calculations have been done in this theory for the hadronic production of neutral (Z^0) and charged ($W^{\pm}$) bosons, both for the lowest-order $\bar{q}q$ annihilation [4] (the Drell-Yan process) and the QCD-corrected ones [5], where a large-p_T hadronic jet is observed together with a final lepton pair from the intermediate boson ; in the latter one, "Compton scattering" types of diagrams ($qG \to qZ^0$ and $\bar{q}G \to \bar{q}Z^0$, for the neutral case) are also included. There have also been calculations [6] for the case of hadronic jets from the intermediate bosons, where intermediate boson signals were predicted to show up clearly in spin-spin asymmetries. The observation of peaks in spin-spin asymmetries would give a non-trivial signal of the intermediate bosons. A bump in a cross-section would not by itself establish the presence of them ; one is also interested in typical weak interaction effects, which contribute to the asymmetry in a direct way. This is also the case for another type of asymmetry, the front-back (F-B) leptonic asymmetry in

$$\begin{aligned} p\bar{p} &\to Z^\circ \ (\to \ell^+\ell^-) + X \\ p\bar{p} &\quad W^{\pm} \ (\to \ell^{\pm} \overset{(-)}{\nu}_{\ell}) + X \end{aligned} \tag{1.1}$$

To zeroth order in QCD (no large-p_T hadronic jets) this was calculated some time ago [7]. As expected, the asymmetry for the purely weak process was found to be much larger than that involving the Z^0 ; the latter one is roughly proportional to the leptonic vector coupling constant $V_\ell = (+\frac{1}{4} - \sin^2\Theta_W)$ which by recent experimental results for $\sin^2\Theta_W$ is implied to be a small quantity.

However, the first-order QCD-corrected cross-section for $\ell^+\ell^-$ production at the Z^0 peak (one associated large-p_T hadronic jet) is predicted to be sizeable [5], when compared to the lowest order result. Not considering this contribution, as well as the corresponding one with a W, would amount to neglect valuable information when F-B asymmetries are checked.

This talk is dedicated to the study of such first order F-B asymmetries. Denoting the angle in $p\bar{p}$ c.m.s. between a negative lepton and the p beam by Θ , and the transverse jet momentum (= the transverse $\ell^+\ell^-$ momentum) by p_T, we calculate the cross-sections

$$\frac{d^2\sigma}{dz\ dp_T^2}(z) \quad ; \quad z = \cos\theta \tag{1.2}$$

and the asymmetries

$$A(z,p_T^2) = \frac{\frac{d^2\sigma}{dz\ dp_T^2}(z) - \frac{d^2\sigma}{dz\ dp_T^2}(-z)}{\frac{d^2\sigma}{dz\ dp_T^2}(z) + \frac{d^2\sigma}{dz\ dp_T^2}(-z)} \tag{1.3}$$

for the reactions (1.1). Note that for pp reactions there is necessarily a $z \to -z$ symmetry in the cross-section (1.2) and therefore the asymmetry vanishes. Besides this asymmetry we also calculated various distributions such as $\frac{d\sigma}{dz}$ and $\frac{d\sigma}{dp_T^2}$ for $p\bar{p}$ and pp collisions. The quantity $\frac{d\sigma}{dz}$ will be obtained by integrating $\frac{d^2\sigma}{dz dp_T^2}$ from a chosen lower bound p_T^{min} up to the maximal value for the considered s value. With these results at hand one can calculate the fully integrated cross-section with a cut in p_T : σ ($p_T > 3$ GeV/c). The values obtained show that once again gluon corrections give very large effects compared with 0^{th} order or naive Drell-Yan calculations. From $\frac{d\sigma}{dp_T^2}$, we also calculate the averaged transverse momentum $\langle p_T \rangle$ of the hadronic jet, and $\langle p_T^2 \rangle$.

II. A PEDAGOGIC EXAMPLE

Before goint into the study of $p\bar{p}$ collisions it may be useful to recall some known results [7] for the reaction

$$e^+ e^- \to Z^o \to \mu^+ \mu^- \tag{2.1}$$

For obvious reasons, let us call V_ℓ (A_ℓ) the vector (axial vector) coupling of Z^o to muons, and V_q (A_q) the coupling to electrons. The front-back asymmetry of the μ^-, defined by

$$A(z) = \frac{\frac{d\sigma}{dz}(z) - \frac{d\sigma}{dz}(-z)}{\frac{d\sigma}{dz}(z) + \frac{d\sigma}{dz}(-z)} \tag{2.2}$$

is then simply given at the resonance ($\sqrt{s} = M_z$) by

$$A(z) = E\ (s = M_z^2)\frac{2z}{1 + z^2} \tag{2.3}$$

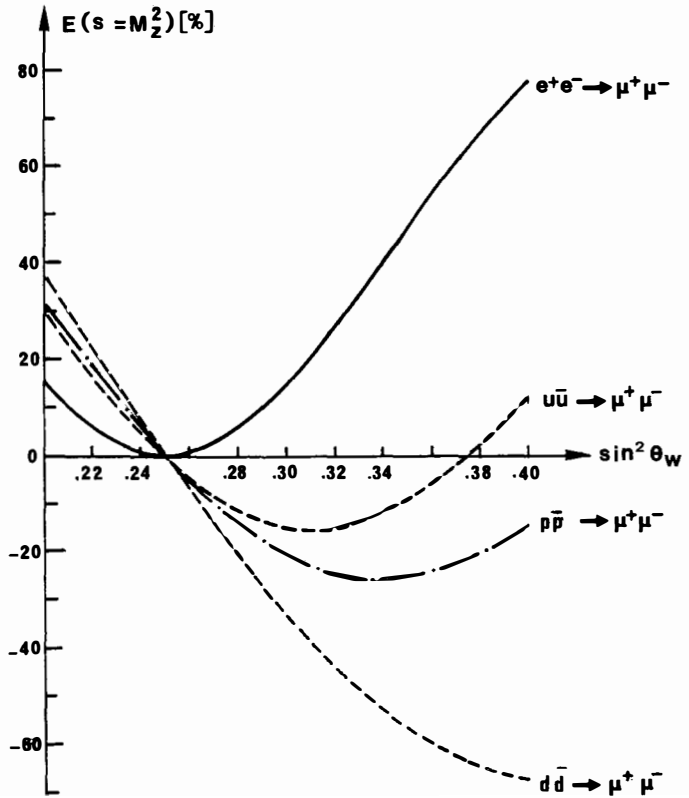

Fig.1 The function E(s = M_z^2) (see Eq. (2.4)) plotted against $\sin^2\theta_W$ for the purely leptonic reaction $e^+e^- \rightarrow \mu^+\mu^-$, the quark reactions $u\bar{u} \rightarrow \mu^+\mu^-$, $d\bar{d} \rightarrow \mu^+\mu^-$ and the combination $\frac{1}{3}(2u\bar{u}+d\bar{d}) \rightarrow \mu^+\mu^-$.

where

$$E\ (s = M_Z^2) = \frac{4\ V_\ell\ A_\ell\ V_q\ A_q}{(V_\ell^2 + A_\ell^2)(V_q^2 + A_q^2)} \qquad (2.4)$$

In the Weinberg-Salam model (that we adopt throughout this paper), the function $E(s = M_Z^2)$ depends only on $\sin^2\Theta_w$. The various coupling constants of interest are given by $V_\ell = \frac{1}{4} - \sin^2\Theta_w$, $A_\ell = \frac{1}{4}$; $V_u = -\frac{1}{4} + \frac{2}{3}\sin^2\Theta_w$, $A_u = -\frac{1}{4}$; $V_d = \frac{1}{4} - \frac{1}{3}\sin^2\Theta_w$, $A_d = \frac{1}{4}$. Fig. 1 shows the variation of $E(s = M_Z^2)$ with $\sin^2\Theta_w$ for the purely leptonic reaction $e^+ e^- \to \mu^+ \mu^-$, the quark reactions $u\bar{u} \to \mu^+ \mu^-$, $d\bar{d} \to \mu^+ \mu^-$ and the combination $\frac{1}{3}(2u\bar{u} + d\bar{d}) \to \mu^+ \mu^-$. The last reaction should provide a first, crude estimate of the μ^- front-back asymmetry in $p\bar{p}$ reactions. It turns out that this first estimate is pretty good in the forward direction, $z = +1$. But the shape of $A(z)$ in $p\bar{p}$ collisions is different from that in e^+e^- annihilation, with $A^{p\bar{p}}(z) < A^{e^+e^-}(z)$. Fig. 1 also shows the sensitivity of the front-back asymmetry to $\sin^2\Theta_w$. In particular, for the present value of $\sin^2\Theta_w \overset{\sim}{=} .23$, $A^{p\bar{p}}(z)$ is positive.

III. THE NAIVE DRELL-YAN MODEL RESULTS

In this Section, we will briefly recall the results obtained in the naive Drell-Yan model, where the only subprocess which is considered is the annihilation $q + \bar{q} \to Z^0 \to \mu^+ \mu^-$ (the $W^\pm$ case is treated in the same way. We just have to change the weak coupling constants to leptons and quarks

($V_{\ell\bar{\nu}_\ell} = A_{\ell\bar{\nu}_\ell} = -\frac{\cos\Theta_w}{2\sqrt{2}}$, $V_{\bar{u}d} = A_{\bar{u}d} = V_{\ell\bar{\nu}_\ell}\cos\Theta_c$, $V_{\bar{u}s} = A_{\bar{u}s} = V_{\ell\bar{\nu}_\ell}\sin\Theta_c$)

and the parton distributions). Quarks are supposed here to possess no primordial transverse momentum so that the intermediate vector boson has no transverse momentum. Explicit formulae for the differential cross section $\frac{d\sigma}{dz}$ and the front-back asymmetry (see Eq. (2.2)) in terms of vector, axial vector coupling constants and parton distributions can be found in the literature [7]. We will not repeat them here, but just give the numerical results for more up to date $\sin^2\Theta_w$ value and parton distributions. A commonly used assumption that we will adopt is the narrow width approximation : the main part of the cross section comes from the vector boson being on the mass shell. For the parton distributions, we used the parametrization of Baier et al. [8]. Thus we ignore charm contributions ; although they may be important at very large Q^2, they should not influence our $\sqrt{s} = 540$ GeV case very much. The distributions are evaluated at

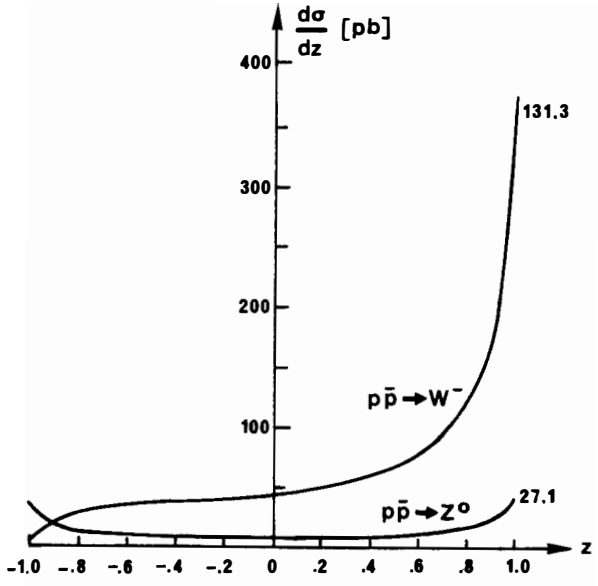

Fig.2 The differential cross section $\frac{d\sigma}{dz}$ for the reactions $p\bar{p} \to Z^0(\to \mu^+\mu^-) + X$ and $p\bar{p} \to W^-(\to \mu^-\bar{\nu}_\mu) + X$ for $\sin^2_W = .23$, at $\sqrt{s} = 540$ GeV.

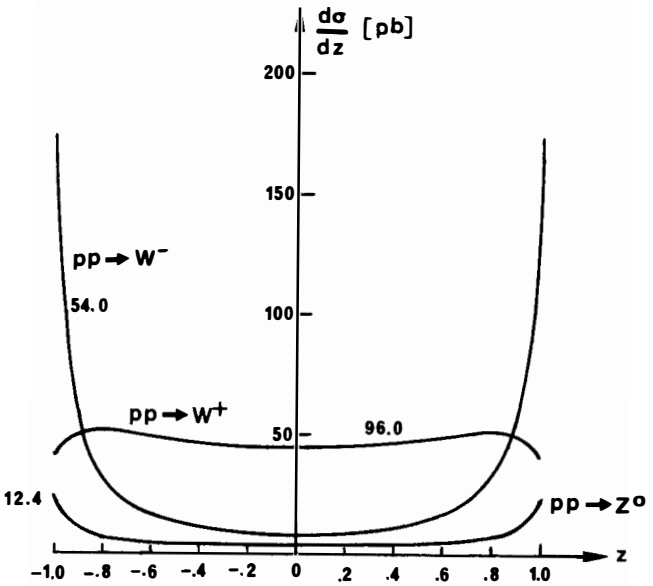

Fig.3 The differential cross section $\frac{d\sigma}{dz}$ for the reactions $pp \to Z^0(\to \mu^+\mu^-) + X$, $pp \to W^-(\to \mu^-\bar{\nu}_\mu) + X$ and $pp \to W^+(\to \mu^+\nu_\mu) + X$ for $\sin^2\theta_W = .23$, at $\sqrt{s} = 600$ GeV.

$Q^2 = M_Z^2$ or M_W^2 . Weak and electromagnetic corrections to vector boson masses [9] have been taken into account, through the relations

$$M_W = \frac{38.5}{\sin\theta_W} \text{ GeV/c}^2 \quad ; \quad M_Z = \frac{M_W}{\cos\theta_W} \text{ GeV/c}^2 \tag{3.1}$$

We have also incorporated QCD corrections to order α_s to hadronic width of Z^0 and $W^{\pm}$ [10] :

$$\Gamma(W^{\pm} \to \text{Hadrons}) = \frac{3G_F}{2\pi\sqrt{2}} M_W^3 \left(1 + \frac{\alpha_s(M_W)}{\pi}\right) \tag{3.2}$$

$$\Gamma(Z^0 \to \text{Hadrons}) = \frac{3G_F}{2\pi\sqrt{2}} M_Z^3 \left(1 - 2\sin^2\theta_W + \frac{20}{9}\sin^4\theta_W\right)\left(1 + \frac{\alpha_s(M_Z)}{\pi}\right)$$

assuming three quark doublets. Let us recall that

$$\alpha_s(M) = \frac{6\pi}{(33 - 2N_F)\ln M/\Lambda} \tag{3.3}$$

where $\Lambda = 0.47$ GeV is taken from Ref. 8). Numerical results are shown on Figs. 2 to 5. We have chosen $\sin^2\theta_W = .23$, $\sqrt{s} = 540$ GeV for $p\bar{p}$ collisions and $\sqrt{s} = 600$ GeV for pp collisions. Fig. 2 shows that the asymmetry will be rather small for the reaction $p\bar{p} \to Z^0(\to \mu^+ \mu^-) + X$, but large for the reaction $p\bar{p} \to W^-(\to \mu^- \bar{\nu}_\mu) + X$. Actually, for the W^- case, a simple helicity argument with the massless valence quarks $\bar{u}$ and d leads to the favoured configuration where the μ^- is emitted in the forward direction. Fig. 3 shows the different behaviour of $\frac{d\sigma}{dz}$ for the reactions $pp \to Z^0(\to \mu^+\mu^-) + X$, $pp \to W^-(\to \mu^- \bar{\nu}_\mu) + X$ and $pp \to W^+(\to \mu^+ \nu_\mu) + X$. We also give on Figs. 2 and 3 the value of the corresponding total cross section σ (not cut over $z = \cos\theta$). The sensitivity of the μ^- front-back asymmetry to $\sin^2\theta_W$ for the reaction $p\bar{p} \to Z^0(\to \mu^+\mu^-) + X$ is displayed on Fig. 4. In the W^- case, the asymmetry is rather insensitive to $\sin^2\theta_W$ (at least over the range considered in Fig. 4) ; we plot it on Fig. 5 for $\sin^2\theta_W = .23$. An experimentally more accessible quantity is the integrated front-back asymmetry A :

$$A = \frac{\int_0^1 dz \frac{d\sigma}{dz} - \int_{-1}^0 dz \frac{d\sigma}{dz}}{\int_0^1 dz \frac{d\sigma}{dz} + \int_{-1}^0 dz \frac{d\sigma}{dz}} \tag{3.4}$$

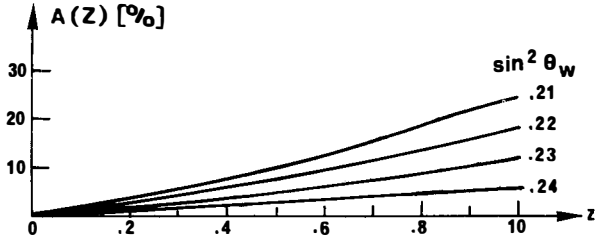

Fig.4 The μ^- front-back asymmetry for the reaction $p\bar{p} \to Z^0(\to \mu^+\mu^-) + X$ at $\sqrt{s}$ = 540 GeV plotted against z =cos θ for various values of $\sin^2\theta_W$: .21, .22, .23, .24 and .25.

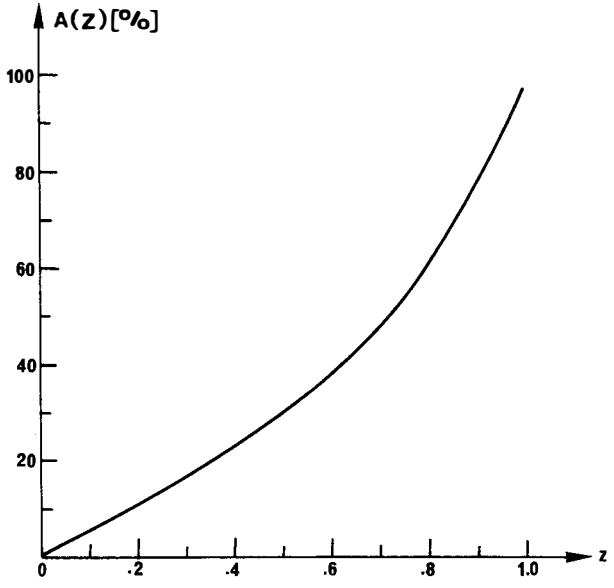

Fig.5 The μ^- front-back asymmetry for the reaction $p\bar{p} \to W^-(\mu^-\bar{\nu}_\mu) + X$ at $\sqrt{s}$ = 600 GeV, for $\sin^2\theta_W$ = .23.

The denominator is nothing but the total cross section σ . Table 1 shows the dependence of σ and A on $\sin^2\theta_W$ at $\sqrt{s}$ = 540 GeV for $p\bar{p}$ reactions. In Table 2 we give the dependence of σ on $\sqrt{s}$ for pp reactions ($\sin^2\theta_W$ = .23). It should be clear that θ is the total cross section for the leptonic decay modes $Z^0 \to \mu^+\mu^-$, $W^- \to \mu^-\bar{\nu}_\mu$ or $W^+ \to \mu^+\nu_\mu$. Thus $p\bar{p} \to Z^0$, $p\bar{p} \to W^-$, etc. are shorthand notations for $p\bar{p} \to Z^0(\to \mu^+\mu^-) + X$, $p\bar{p} \to W^-(\to \mu^-\bar{\nu}_\mu) + X$, etc. ; the same notation is used on the figures too.

Table 1

Reaction \ $\sin^2\theta_W$	.21	.22	.23	.24	.25
$p\bar{p} \to Z^0$ σ[pb]	25.8	26.5	27.1	27.8	28.5
$p\bar{p} \to Z^0$ A[%]	14.0	10.2	6.6	3.1	0.0
$p\bar{p} \to W^-$ σ[pb]	118.8	125.1	131.3	137.4	143.5
$p\bar{p} \to W^-$ A[%]	49.1	48.6	48.0	47.5	47.0

Table 2

Reaction \ $\sqrt{s}$ [GeV]	400	600	800
$pp \to Z^0$	2.3	12.4	29.3
$pp \to W^-$	12.3	54.0	118.6
$pp \to W^+$	24.1	96.0	189.7

IV. FIRST ORDER QCD CORRECTIONS

As explained in the Introduction, it is also interesting to look at the reactions

$$p\bar{p} \to Z^0 (\to \mu^+\mu^-) + \text{jet } (p_T) + X \qquad (4.1)$$

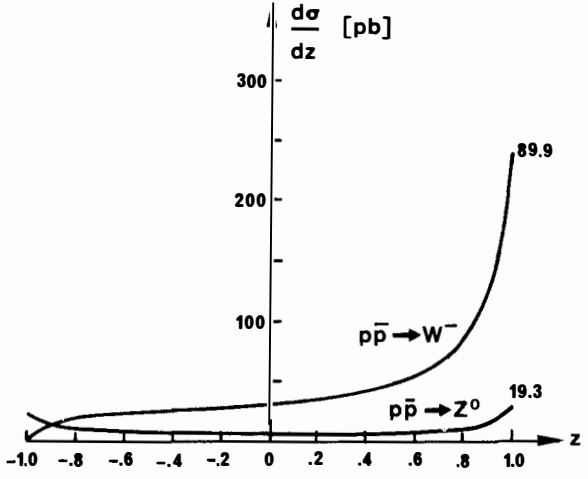

Fig.6 The differential cross section $\frac{d\sigma}{dz}$ for reactions (4.1) and (4.2) at $\sqrt{s}$ = 540 GeV, for $\sin^2\theta_W$ =.23.

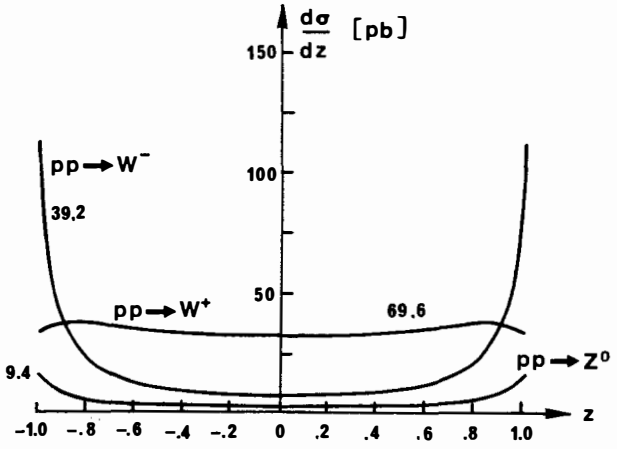

Fig.7 $\frac{d\sigma}{dz}$ for the reaction pp → Z° ($\to \mu^+\mu^-$) + jet(p_T) + x, pp → W^-($\mu^- \bar{\nu}_\mu$) + jet(p_T) + X and pp → W^+ ($\to \mu^- \bar{\nu}_\mu$) + jet(p_T) + X at $\sqrt{s}$ = 600 GeV, for $\sin^2\theta_W$ = .23.

$$p\bar{p} \to W^- \ (\to \mu^- \bar{\nu}_\mu) + \text{jet}\ (p_T) + X \qquad (4.2)$$

whose cross sections are expected to be far from negligible compared to the zeroth order one. As previously, we keep the Drell-Yan model but take as subprocesses reactions implying the presence of gluons $G : q + \bar{q} \to Z^o(\to \mu^+ \mu^-) + G(p_T)$; $q + G \to Z^o(\to \mu^+ \mu^-) + q(p_T)$; $\bar{q} + G \to Z^o(\to \mu^+ \mu^-) + \bar{q}(p_T)$. No primordial transverse momentum is given to the incoming partons of the subprocesses, so that the p_T of the intermediate vector boson is the same as that of the jet formed by hadronization of the outgoing parton. We put all masses but the vector boson mass to zero. As in Section III, radiative corrections to vector boson masses and widths have been incorporated. Withoug going into the technical details of the calculation, which can be found in the paper by J. Finjord et al., let us present the results. We have calculated the twofold differential cross section $\frac{d^2\sigma}{dzdp_T^2}$ for reactions (4.1), (4.2) and the analogous reactions with pp as initial state. To avoid the problem of the infrared divergence at $p_T = 0$, we will impose the cut $p_T \geq p_T^{min} = 3$ GeV/c. It turns out that the front-back asymmetry $A(z, p_T^2)$ (see Eq.(1.3)) is p_T independent to a very good approximation, with a magnitude quite close to that of the zeroth order process plotted on Figs. 4 and 5. Fig. 6 shows the angular distribution $\frac{d\sigma}{dz}$ of the $\mu-$ coming from the Z^o or W^- decay. Here we have integrated $\frac{d^2\sigma}{dzdp_T}$ from $p_T = 3$ GeV/c to the kinematical limit $p_T^{max} = \frac{s - M^2}{2\sqrt{s}}$. The total cross section σ is also indicated on the figure. The asymmetry corresponding to Fig. 6 is just as on Fig. 4 (for $\sin^2\theta_W = .23$) and Fig. 5. Finally we have on Fig. 7 $\frac{d\sigma}{dz}$ for the various pp reactions, together with the corresponding total cross sections, at $\sqrt{s} = 600$ GeV. It is interesting to compare zeroth and first order total cross sections. The ratio σ (first order)/ σ (zeroth order) lies around 0.70 for $p\bar{p}$ reactions at $\sqrt{s} = 540$ GeV, and 0.74 for pp reactions at $\sqrt{s} = 600$ GeV. From $\frac{d^2\sigma}{dzdp_T^2}$ we can also calculate $\frac{d\sigma}{dp_T^2}$ by integrating over z from -1 to $+1$. For $p_T > 2$ or 3 GeV/c, we can nicely represent the curves by

$$\frac{d\sigma}{dp_T} \simeq B\, e^{-b\sqrt{p_T}} \qquad (4.3)$$

This parametrization allows to get an idea of the dependence of σ on p_T^{min}, which is shown in Table 3. Finally we also give in this table $<p_T>$ and $<p_T^2>^{1/2}$ which clearly depend on p_T^{min}. We found that they are very little sensitive to the reaction considered.

TABLE 3

p_T^{min}	2	3	4	
$p\bar{p} \to Z^0$	25.1	19.3	15.2	$\sqrt{s}$ = 540 GeV
$p\bar{p} \to W^-$	117.9	89.9	70.6	
$pp \to Z^0$	12.2	9.4	7.5	$\sqrt{s}$ = 600 GeV
$pp \to W^-$	51.3	39.2	30.8	
$pp \to W^+$	90.7	69.6	54.8	
$<p_T>$ [GeV/c]	7.2	8.7	10.1	
$<p_T^2>^{1/2}$ [GeV/c]	10.0	11.4	12.7	

- REFERENCES -

1) CERN/SPSC/78-06, SPSC/92.

2) BNL report n° BNL 20161 (1975).

3) The LEP Study Group CERN/ISR - LEP/78-17.

4) R.W. Brown, K.O. Mikaelian and M.K. Gaillard, Nucl. Phys. B75 (1974), 112 ;
R.B. Palmer, E.A. Paschos, N.P. Samios and L.-L. Wang, Phys. Rev. D14 (1976), 118 ;
L.B. Okun and M.B. Voloshin, Nucl. Phys. B120 (1977), 459 ;
C. Quigg, Rev. Mod. Phys. 49 (1977), 297 ;
R.F. Peierls, T.L. Trueman and L.-L. Wang, Phys. Rev. D16 (1977), 1397 ;
J. Finjord, Nucl. Phys. B131 (1977), 507 ;
M. Perrottet, Ann. of Phys. 115 (1978), 107 ;
F.E. Paige, T.L. Trueman and T.N. Tudron, Phys. Rev. D19 (1979), 935 ;
and with scaling violations in the structure functions :
I. Hinchliffe and C.H. Llewellyn-Smith, Phys. Lett. 66B (1977), 281 ;
J. Kogut and J. Shigemitsu, Nucl. Phys. B129 (1977), 461.

5) F. Halzen and D.M. Scott, Phys. Lett. 78B (1978), 318 ;
M. Chaichian, O. Dumbrajs and M. Hayashi, Phys. Rev. D20 (1979), 2873 ;
M. Chaichian and M. Hayashi, Phys. Lett. 81B (1979), 53 ;
J. Finjord, G. Girardi and P. Sorba, Phys. Lett. 89B (1979), 99.

6) G. Ranft and J. Ranft, Leipzig preprint KHO-HEP 79-11.

7) M. Perrottet, ref. (4).

8) R. Baier, J. Engels, B. Peterson, Z. Physik C2 (1979), 265.

9) W.J. Marciano, Phys. Rev. D20 (1979), 274 ;
M. Veltman, Phys. Lett. 91B (1980), 95.

10) D. Albert, W.J. Marciano, D. Wyler and Z. Parsa, Nucl. Phys. B166 (1980), 460.

Most of the material of this talk is based on a paper by J. FINJORD, G. GIRARDI, M. PERROTTET and P. SORBA, "Leptonic front-back asymmetry in $p\bar{p} \to Z^0(\to \mu^+\mu^-)$ + jet + X and $p\bar{p} \to W^{\pm}(\to \ell^{\pm} \overset{(-)}{\nu}_{\ell})$ + jet + X", LAPP Preprint, LAPP-TH-25 (1980), where technical details can be found.

LEPTON PAIR PRODUCTION IN HADRONIC COLLISIONS

Tung-Mow Yan
Newman Laboratory of Nuclear Studies
Cornell University, Ithaca, N.Y. 14853
U.S.A.

ABSTRACT

This is a summary talk at the 1981 Moriond Workshop on Lepton Pair Production. We discuss the theoretical and experimental status of high mass lepton pair production in hadronic collisions.

I. INTRODUCTION

Before I begin my talk I would like to express our sincere thanks to our hosts of the Workshop on behalf of all the participants. Professor Tran Thanh Van, the Organizing Committee, and the secretaries have worked more than full time to make the Workshop most enjoyable. It is particularly profitable for me personally. I have learned so much physics in one week's time. From the talks we have heard in the Workshop it is clear that lepton pair production has grown in the last ten years to become a major field of research in high energy physics.

When I was asked to give the summary talk of the Workshop, I was hesitant to accept the task since I have not worked on the subject for a long time. The challenge becomes more apparent as the Workshop progressed: I am the most ignorant person among all the participants. Perhaps I can turn my ignorance into an advantage. As I am not able to absorb all the information presented, a natural filtering mechanism has been working in my mind. What arouse my interest most are: (i) progress made in theoretical issues which Drell and I could not resolve ten years ago; (ii) experiments which have been done but we could only dream of ten years ago; and (iii) surprises which were not foreseen ten years ago. This talk will concentrate on these aspects.[1] I will restrict myself to general remarks. For specifics and technical details, please consult the talks of various speakers in these Proceedings.

Lepton Pair Production began with the pioneering experiment[2] at BNL by Lederman and his group. The results were shown in Fig. 1. A gold mine was hidden in the curve as Ting and his group[3] found out a few years later. Despite the early misfortune, Lederman and his group have achieved remarkably during these years. The culmination of their effort is best illustrated by the data[4] in Fig. 2. This figure touches all important developments in particle physics of last decade. Let me elaborate.

First of all, it contains two distinct types of information: the bumps and the continuum. The constituents of the first bump J/ψ have all the characteristics required to support the GIM mechanism[5], a crucial ingredient for the success of the standard model[6] of electroweak interactions. The subsequent discovery of the T particles[7] opens up, once again, the generation problem--one of the most important puzzles in particle physics. The two families of heavy quarks, c and b, provide also ideal systems to study the quark binding and hadron spectroscopy. We now have a semiquantitative description of these heavy $Q\bar{Q}$ systems in terms of a nonrelativistic potential model, although a fundamental understanding of quark confinement is still lacking. However, the production mechanism of these narrow states in hadronic collisions is very complex, as we have learned in this Workshop.[8,9] This is in contrast to the lepton pairs in the continuum where there is a universal agreement of how the pairs are produced.

1970

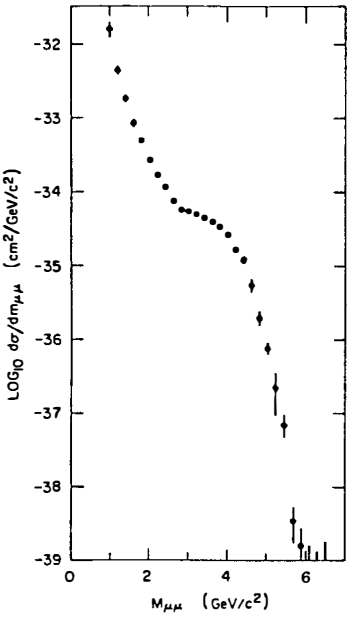

Fig. 1

The dimuon mass spectum from the BNL experiment.

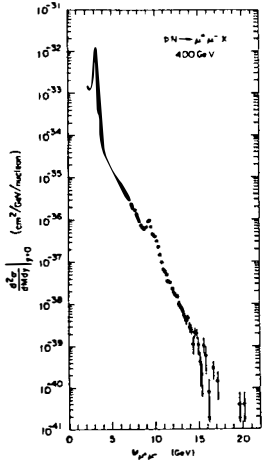

Fig. 2

The dimuon mass spectum from CFS collaboration.

We will come back to the continuum later.

Another reason why I began my talk with the work of Lederman and his group is because it inspired Drell and me to think about the subject. At that time, we asked ourselves the question, "Is the rapid falloff of the μ-pair cross section (Fig. 1) as a function of the pair mass consistent with the idea of point-like constituents in the parton model?" Our innocent inquiry has led to a model[10] which is now the standard reference for this process. In this model the lepton pair is created by quark-antiquark annihilation. Since the model is well known to all of you, I will simply summarize its predictions:

1. The cross section $Q^4 \frac{d\sigma}{dQ^2}$ depends only on the scaling variable $\tau = Q^2/s$;
2. The magnitude and shape of the cross section are determined by the quark and antiquark distributions measured in deep inelastic lepton scatterings;
3. If a photon, pion, kaon, or antiproton is used as the projectile, its structure functions can be measured by lepton pair production. This is the only way I know of to study the quark structure of a particle unavailable as a target;
4. The transverse momentum of the pair should be small (∿300-500 MeV);
5. In the rest system of the lepton pair, the angular distribution is $1 + \cos^2\theta$ with respect to the hadronic collision axis.

The model had at least two difficulties, one fundamental and one practical. We did not have a convincing argument for neglecting the soft interactions between the two hadrons. However, we did conclude that impulse approximation is valid and scaling should hold, although the cross section is not necessarily normalized by deep inelastic lepton scatterings. For all these years Drell and I have always been interested in this question. I believe that this is still an unsettled question.[11] On the practical side, the model did not fit the data[2] that inspired its invention. We were totally puzzled by the shoulder-like structure. We did understand, however, that the rapid decrease of the cross section with the μ-pair mass was related to the behavior of the structure function $F_2(x)$ near $x \to 1$.

During the last ten years, both theory and experiment have made great progress. The agreement between theory and experiment is extremely impressive.[12] As far as the naive model is concerned, there are two surprises. The transverse momentum of the pair is found to be much bigger than expected; and it grows with the center-of-mass energy. The overall normalization of the cross section is about a factor of two larger than predicted. It is interesting that both "surprises" have found an explanation in QCD.

In the next two sections we will discuss the theoretical and experimental developments in the last ten years.

II. THEORETICAL DEVELOPMENTS

Ten years ago many model field theories existed. But there was no reason to favor one over the others. Now, we all accept QCD as the possible true theory for strong interactions. The predictive power of QCD arises from its unique property of asymptotic freedom. Predictions were obtained by combining QCD with modern technology in quantum field theory--renormalization group approach and operator product expansions. The relation of this formal approach to the more intuitive parton model has become clear only after Altarelli and Parisi[13] elucidated the qualitative picture proposed by Kogut and Susskind.[14] Altarelli and Parisi showed that the renormalization group equations and operator product expansions are equivalent to a set of evolution equations in Q^2 for Q^2 dependent quark and gluon distributions. The importance of their contribution is two-fold. First, it describes QCD predictions in a language understandable to everyone. Second, it states that for a deep inelastic process.

$$\text{Real World} = \text{Parton Model} + \text{QCD Corrections} \tag{II.1}$$

It is this ansatz proposed by Politzer[15] that allows lepton pair production to be studied in QCD. It is not possible to show that this is a short distance process. Low order calculations have turned up encouraging and unexpected results. The most important ones are:

1. The leading logarithms in Q^2 can be absorbed by Q^2-dependent quark and anti-quark distribution functions[15] of the hadrons that appear in deep inelastic scatterings with the rule of substitution $Q^2 \to |Q^2|$. Scaling is violated, but only logarithmically and in a way calculable.

2. Analytic continuation from space-like q^2 (deep inelastic scattering) to time-like q^2 (lepton pair production) and the difference in kinematics between the two processes produce[16,17] a nonleading finite correction with a very large coefficient. The result is simplest in terms of moments

$$\sigma_n = \sigma_n^{(o)}\left[1 + \frac{\alpha_s}{2\pi}\cdot\frac{4}{3}\pi^2 + \ldots\right] \tag{II.2}$$

The π^2 term is unusually large. For $\alpha_s \approx 0.2$-0.3, the correction factor is about two. This could be the source of the K factor. The unusually large correction raises the question of convergence of the perturbation expansion. We have heard in the Workshop that the π^2 term might exponentiate[18]:

$$1 + \frac{\alpha_s}{2\pi}\,\frac{4}{3}\pi^2 \to \exp\left(\frac{\alpha_s}{2\pi}\,\frac{4}{3}\pi^2\right) \tag{II.3}$$

Professor Altarelli[19] has called this the "leading π summation". Although the result is plausible, it clearly deserves more study.

3. A large transverse momentum of the lepton pair can be produced by recoil of quarks or gluons.[20] A simple dimensional analysis gives

$$\langle q_T^2 \rangle = a + \alpha_s(Q^2) s f(\tau, \alpha_s) \qquad \text{(II.4)}$$

The constant a is related to the so-called primordial or intrinsic transverse momenta of the quarks. Eq. (II.4) is a very general prediction of QCD. However, the function $f(\tau,\alpha_s)$ depends on quark and gluon distributions, and it is difficult to determine. Furthermore, the constant a is due to non-perturbative effects and is not calculable. Whether there is an analogous K factor for the q_T distribution is now under investigation.[21] This will affect the theoretical determination of $\langle q_T^2 \rangle$. We have also heard schemes[18,22] presented in the Workshop for calculating detailed transverse momentum distributions valid for both large and small q_T. It generalizes the work of Parisi and Petronzio[23] and involves summation of soft gluons. This is an ambitious task since small q_T is outside the domain of conventional perturbative QCD. Again I feel that more theoretical understanding on the subject is desirable.

3. The full angular distributions[17,24] in both θ and ϕ depend on input quark and gluon densities and are rather complicated. For small q_T the θ dependence is close to $1 + \cos^2\theta$ even when high order corrections are taken into account. For large q_T, the θ dependence is expected to be substantially modified.

III. EXPERIMENTAL RESULTS AND COMPARISON WITH THEORY

Most of the quantitative predictions of QCD are difficult to test.[19] In an ideal world where the running coupling constant is small so the calculation is reliable, short distance QCD effects are small corrections to the parton model. What experimentalists actually observe are pure QCD results convoluted with phenomenological inputs of gluon and quark densities. It is then not straightforward to judge whether a confrontation between theory and experiment is a success or not. In practice, the problem is further compounded: the running coupling constant is not small and Q^2 is not infinite. High order corrections could be unusually large as in the case of the K factor mentioned earlier. Higher twist contributions could be significant. We must be careful in distinguishing a general prediction from the specific fit.

Despite the long list of qualifications, there is no question that a great deal has been learned from experiments on lepton pair production. We will mention some of the most impressive experimental results presented in the Workshop:

1. Scaling has now been confirmed by both nucleon[4,25,26] and pion[27,28] data. The CFS data on the proton and the NA3 and Ω result on the pion are shown in Fig. 3. For other evidence of scaling the reader is referred to the talks from different experimental groups in these Proceedings. This is important since it is the first indication that lepton pair production is a hard process, and therefore it is accessible to perturbative QCD treatment. However, scaling

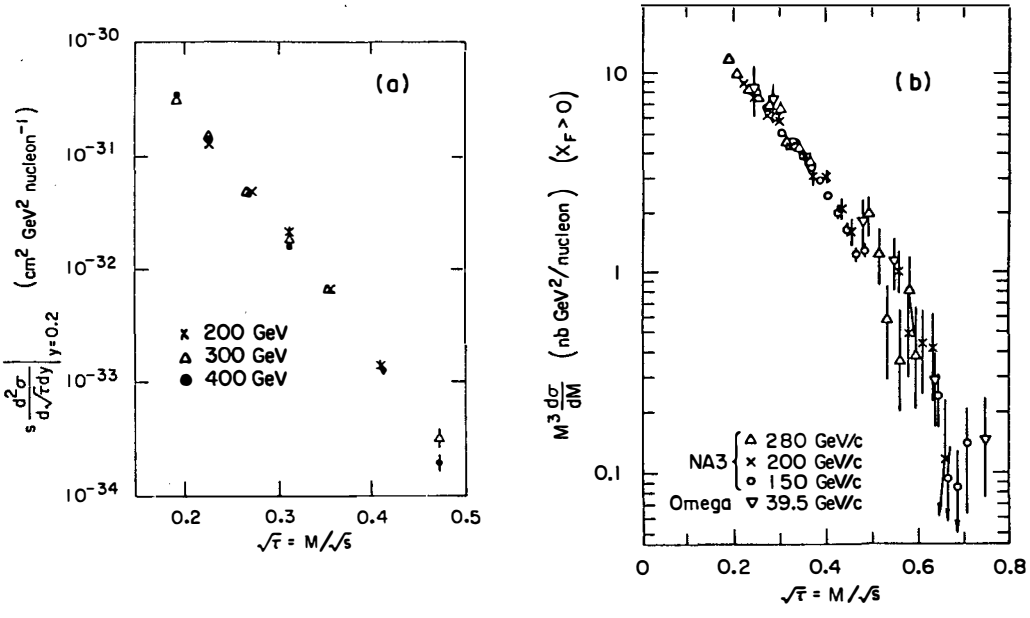

Fig. 3

(a) Test of scaling of the CFS measurements.
(b) Test of scaling for pion produced dimuons.

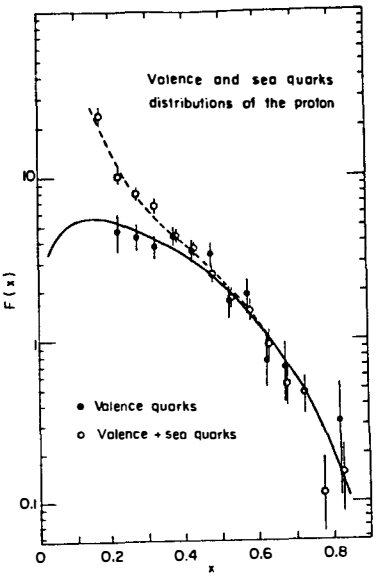

Fig. 4

NA3 measurement on the distribution of valence and sea quarks in the proton. The valence distribution corresponds to the combination $4u(x) + d(x)$. The curves are the CDHS fits multiplied by 2.3.

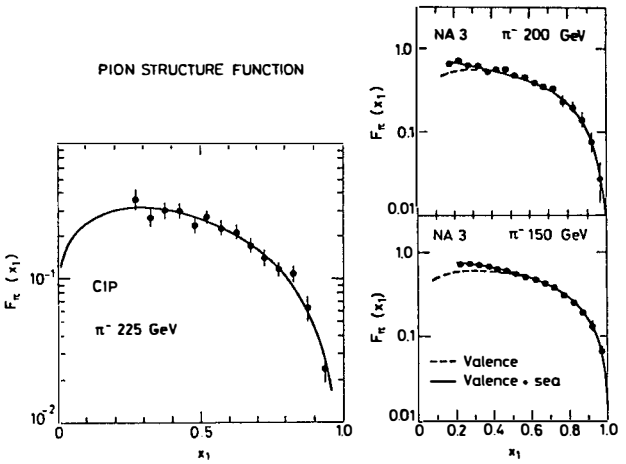

Fig. 5

The CIP and NA3 measurement on the shape of the pion structure.

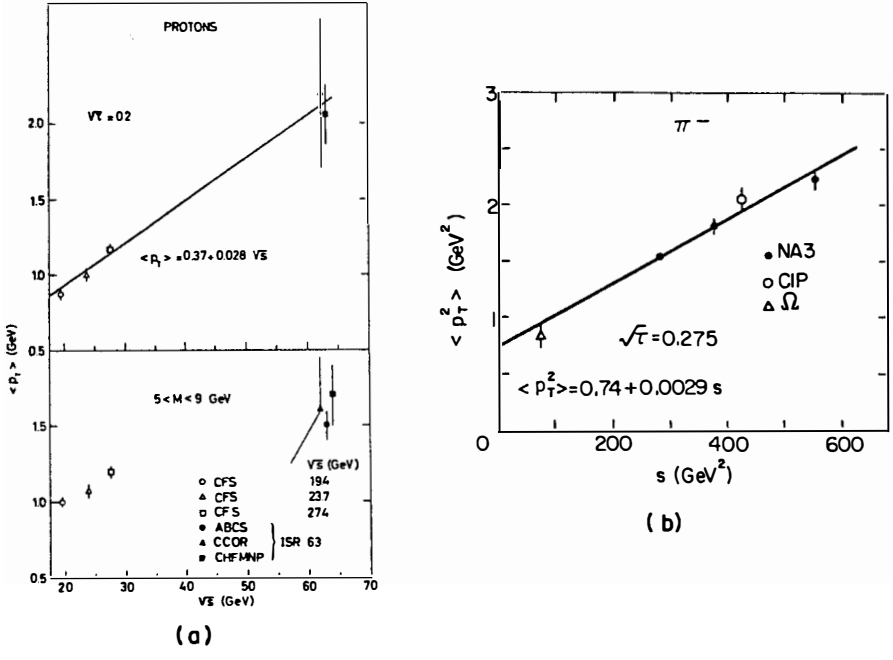

Fig. 6

(a) Energy dependence of the average transverse momentum of dileptons produced in proton collisions.
(b) Energy dependence of $\langle p_T^2 \rangle$ for dimuons produced in π^- collisions.

violation predicted by QCD is not visible in the data.

2. By combining proton and antiproton data[27,29], NA3 is able to separate the valence and sea distribution inside a proton or an antiproton. Comparison between the quark distribution functions from lepton pair production and neutrino scattering is shown in Fig. 4. It is a most remarkable achievement that the shapes agree so well. This is a confirmation of the pair production mechanism of quark-antiquark annihilation. Nevertheless, a factor of K ≈ 2.3 is found necessary to bring the CDHS data to coincide with the NA3 data. A similar K factor was found in other experiments[25,26,30] with the proton beam.

3. For the first time we have gotten a glimpse of how the quarks are distributed inside the unstable particles[27-29,31] π, K and $\bar{p}$. The quark distribution function inside a pion is shown in Fig. 5. The shapes agree very well among data from NA3 and C1P. The normalization is fixed by

$$\int_0^1 [u_{\pi^+}(x) - \bar{u}_{\pi^+}(x)]dx = 1 \qquad \text{(III.1)}$$

Again, it is found that the data exceed by a factor of about two the predicted normalization.

4. Both pN[4,25,26] and N[28,31,32] data show that the transverse momentum of the lepton pair grows with the center-of-mass energy $\sqrt{s}$ (Fig. 6). While this behavior is predicted by QCD on very general grounds, specific attempts to fit the data have not been very satisfactory. A rather large primordial transverse momentum is needed, and the gluon densities needed for input are not known. If we extrapolate the curve in Fig. 6 to $\sqrt{s} \approx 400$ GeV, the lepton pair will have an average transverse momentum larger than 10 GeV. This will make it more difficult to detect the existence of the $W^{\pm}$ boson produced by this process.[20]

5. The electric charges of the annihilating $q\text{-}\bar{q}$ pairs are revealed in the measured cross sections. In the region $\tau \to 1$, where valence quarks dominate, the model predicts

$$\lim_{\tau \to 1} \frac{\sigma(\pi^+ C)}{\sigma(\pi^- C)} = \frac{e_d^2}{e_u^2} = \frac{1}{4} \qquad \text{(III.2)}$$

$$\lim_{\tau \to 1} \frac{\sigma(\pi^+ p)}{\sigma(\pi^- p)} = \frac{e_d^2}{e_u^2} \frac{d}{u} = \frac{1}{8} \qquad (u = 2d) \qquad \text{(III.3)}$$

where d and u are the down and up quark distribution inside a proton, respectively. These trends are clearly visible in the data.[27,28,31] (The NA3 data are shown in Fig. 7.) To me, this is a very visual and direct revelation of the quark charges.

6. The most overwhelming evidence for the $q\text{-}\bar{q}$ annihilation mechanism is offered by the relative yield of the lepton pair production from a proton, an antiproton, and a pion beam. The data[31] are shown in Fig. 8. The ratio

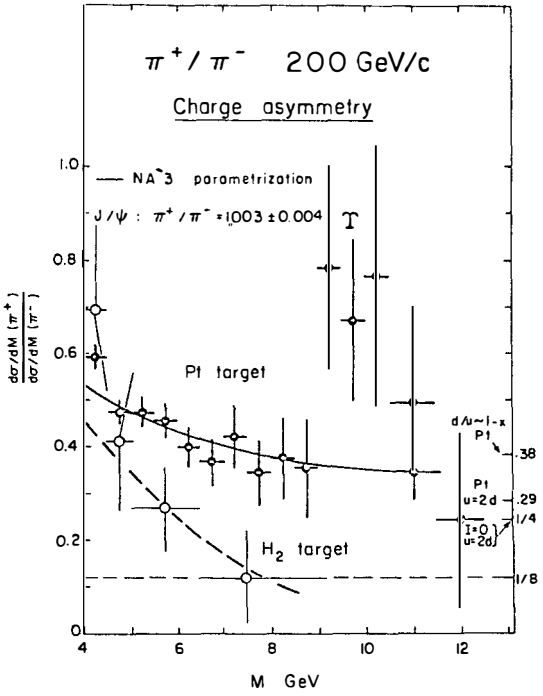

Fig. 7

Ratio of π+ to π- induced dimuon cross section for nuclear and H_2 targets.

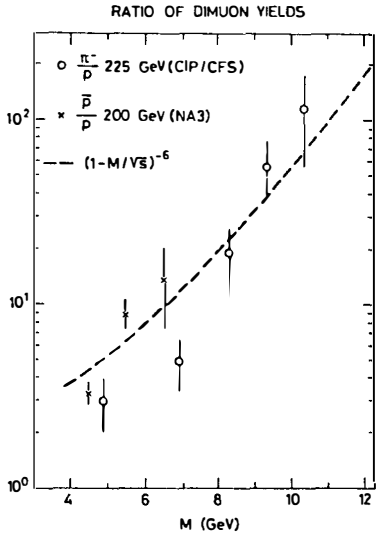

Fig. 8

Ratio of dimuon yields for different beam particles (π-/p) and (p̄/p).

$\sigma(\pi^- p)/\sigma(pp)$ increases steadily with the μ-pair mass and exceeds 100 at Q = 10 GeV. Such a behavior is easily understood if the pair is produced by $q\text{-}\bar{q}$ annihilation. In the πp case the pion is abundant in valence antiquarks, while in the pp case the scarce antiquarks have to come from the sea. It is very difficult for me to imagine an alternative explanation of this dramatic behavior.

7. Angular distributions[25,27,28,31] are found to be consistent with the prediction $1 + \cos^2\theta$. This is another evidence for spin 1/2 quarks. However, the annihilating quarks have substantial transverse momenta. Consequently, the beam axis of the hadrons does not coincide with the colliding axis of participating quarks. Choice of a frame becomes an important issue. The Collins-Soper frame[33] and the Gottfried-Jackson frame are most commonly used for comparison between theory and experiment.

8. The A dependence of the high mass lepton pair production cross section is strikingly different from that of ordinary hadronic processes. For $Q \gtrsim 4$ GeV the cross section does not show any shadowing. The A dependence is commonly parametrized by

$$\sigma_A = A^\alpha \sigma_H \qquad \text{(III.4)}$$

The α parameters from different experiments[4,27,31] are all consistent with $\alpha = 1$. The linear A dependence is intuitively reasonable since to produce a high mass lepton pair the annihilating quarks must be sufficiently off-shell so that they cannot be absorbed on the nuclear surface.

Any item on the list is a great achievement by itself. Together with deep inelastic lepton scatterings they form a coherent and self-consistent picture for electromagnetic and weak current induced processes in terms of the parton model and asymptotic freedom. Of course, they also strongly support the model of $q\text{-}\bar{q}$ annihilation for the lepton pair production. Even the failure of the prediction of a small average q_T for the pair by the naive model should be considered a theoretical triumph. The parton model was constructed to give perfect Bjorken scaling by introducing an artificial transverse momentum cutoff. There is no intrinsic mass scale in QCD and no cutoff exists. Consequently, Bjorken scaling is violated by asymptotic freedom and q_T should grow[34] with $\sqrt{s}$. To me, the most surprising thing is that nonleading corrections (the K factor) have been observed, but the leading corrections (logarithmic scaling violations) have not![35]

IV. DISCUSSION

Based on the talks presented at the Workshop I have briefly summarized the status in theory and experiment of the lepton pair production. Both theorists and experimentalists can be proud of what they have achieved. Not only have we a general understanding of the process itself in terms of a simple model, but

also the process has become an invaluable and only tool to study the short distance structure of the unstable particles π, K and $\bar{p}$. Furthermore, the process has turned out to be a fertile ground for theoretical investigation of various aspects of perturbative QCD. This is an exciting time. Lots have been accomplished; yet lots more remain to be done. To conclude my talk, let me repeat a few important theoretical issues and list some future challenges to the experimentalists.

I will mention only three theoretical issues, all of which are related to soft gluon exchanges:

1. Transverse momentum distributions. Does Compton scattering ($g + q \to \gamma^* + q$) or pair annihilation ($q + \bar{q} \to \gamma^* + g$) dominate? How can primoridal (or intrinsic) transverse momentum be properly incorporated? Is it possible to handle small and large transverse momentum in a uniform framework? We have heard interesting discussions in this week. We hope that lots of progress will be made soon.
2. The K factor. Theorists have found a possible source for the K factor. If indeed it is controlled by $\alpha_s(Q^2)$, the K factor will approach thenaive value of unity as $Q^2 \to \infty$. It appears to be a remnant of soft gluon effects. Is it related to the soft interactions between the two hadrons that Drell and I worried about more than ten years ago? Clearly, we need a better understanding.
3. A dependence. Except for the qualitative argument mentioned earlier, a linear A dependence has not been explicitly demonstrated by the theorists. This particular A dependence indicates that effects of soft interactions between the projectile and a spectator nucleon in the nucleus cancel among different channels. If so, the partial cross section of a specific channel will not exhibit a linear A dependence.

For the experimentalists, the obvious challenges are:

1. Determination of photon structure from the photoproduction of lepton pairs: $\gamma N \to \ell^+\ell^- + X$. The photon structure will also be studied by the two-photon process in e^+e^- annihilation. Imagine the day when we will compare the internal structure of the photon determined by the two different methods!
2. Discovery of Z^0 and $W^\pm$. Several experiments[36] are already under preparation to begin at the $\bar{p}p$ collider at SPS. We wish them the best of luck!
3. Properties of associated hadron final states. Because a $q\text{-}\bar{q}$ pair disappears from the initial state in a lepton pair production, there will be many interesting effects in the associated final hadrons. We have already heard experimental talks on the subject.[37]

ACKNOWLEDGMENT

I would like to thank Professor Tran Thanh Van for inviting me to the Workshop and the warm hospitality extended to me. This work is partially supported by the National Science Foundation.

REFERENCES

1) In preparing this talk I have consulted two excellent reviews on lepton pair production: G. Matthiae, CERN-EP/80-183, and R. Stroynowski, SLAC-PUB-2650. More complete references can be found in these two articles.

2) J. Christenson et al., Phys. Rev. Lett. 25, 1523 (1970); Phys. Rev. D8, 2016 (1973).

3) J. J. Aubert et al., Phys. Rev. Lett. 33, 1404 (1974).

4) C. Brown, these Proceedings and A. S. Ito et al., Phys. Rev. D23, 604 (1981).

5) S. L. Glashow, J. Iliopoulos and L. Maiani, Phys. Rev. D2, 1285 (1970).

6) S. Weinberg, Phys. Rev. Lett. 19, 1264 (1967); A. Salam in Elementary Particle Theory, N. Svartholm, ed. (Almquist and Wilksells, Stockholm, 1969).

7) S. W. Herb et al., Phys. Rev. Lett. 39, 252 (1977); W. R. Innes et al., Phys. Rev. Lett. 39, 1240 (1977).

8) For experiments, see talks by P. Charpentier and A. Romana in these Proceedings.

9) For theory, see talks by Z. Kunszt and R. Rückl in these Proceedings.

10) S. Drell and T. M. Yan, Phys. Rev. Lett. 25, 316 (1970) and Ann. Phys. (N.Y.) 66, 578 (1971).

11) For a recent discussion in QCD see the review by A. Mueller, Columbia Univ. preprint CU-TP-192, and G. Bodwin, S. Brodsky and P. Lepage, in preparation.

12) This was not the case in the early 1970s. the inability of the model to explain the low mass pair data cast doubt on its eventual success. I am glad to hear that the low mass pair data might be understood by a simple but different model, see W. Dunwoodie, these Proceedings.

13) G. Altarelli and G. Parisi, Nucl. Phys. B126, 298 (1977).

14) J. Kogut and L. Susskind, Phys. Rev. D9, 697 (1974).

15) H. D. Politzer, Nucl. Phys. B129, 301 (1977).

16) R. K. Ellis, these Proceedings and references therein.

17) G. Plaut, these Proceedings.

18) M. Greco, these Proceedings and references therein. G. Pancheri Srivastava, these Proceedings and references therein.

19) G. Altarelli, these Proceedings.

20) D. Scott, these Proceedings and references therein; P. Minkowsky, these Proceedings.

21) G. Martinelli, these Proceedings.

22) J. Cleymans, these Proceedings; J. C. Collins, these Proceedings; D. Soper, these Proceedings.

23) G. Parisi and R. Petronzio, Nucl. Phys. B154, 427 (1979). See also Yu. Dokshitzer, D. Dyakanov and S. Trojan, Proceedings of the 13th Winter School of the Leningrad Institute of Nuclear Physics, Leningrad (1978).

24) K. Kajantie et al., Phys. Lett. 74B, 384 (1978); J. Cleymans and M. Kuroda, Phys. Lett. 80B, 385 (1979); J. C. Collins, Phys. Rev. Lett. 42, 291 (1979).

25) C. Kourkoumelis, these Proceedings.

26) F. Vannucci, these Proceedings.

27) O. Callot, these Proceedings.

28) J. D. Dowell, these Proceedings.

29) S. Weisz, these Proceedings.

30) P. Mockett, these Proceedings.

31) A. Smith, these Proceedings; K. J. Anderson et al., Phys. Rev. Lett. 42, 944 (1979); G. E. Hogan et al., Phys. Rev. Lett. 42, 948 (1979); C. B. Newman et al., Phys. Rev. Lett. 42, 951 (1979); K. J. Anderson et al., Phys. Rev. Lett. 43, 1219 (1979).

32) J. Badier, these Proceedings.

33) J. C. Collins and D. Soper, Phys. Rev. D16, 2219 (1979).

34) It should be emphasized that although the observed $\langle q_T \rangle$ is much larger than expected we still have $\langle q_T \rangle \ll Q$, a necessary condition for the validity of impulse approximation used in the naive model.

35) A future experiment will attempt to observe these scaling violation effects; see K. Frendenreich, these Proceedings.

36) See, for example, the talks by V. Hungerb and J. Strauss in these Proceedings.

37) V. Casasinni, these Proceedings; B. Pietrzyk, these Proceedings.

LIST OF PARTICIPANTS

ALBERI Giorgio	Istituto di Fisica Teorica Miramare 34014 TRIESTE Italy
ALTARELLI Guido	Istituto di fisica "G. Marconi" Piazza Aldo Moro 2 00185 ROMA, Italy
ANDERSSON B. A.	Dept. of Theoretical Physics Sölvergatan 14 A 223 62 LUND, Sweden
BADIER Jean	LPNHE Ecole Polytechnique 91128 PALAISEAU Cedex, France
BAUBILLIER Michel	L.P.N.H.E., Tour 32 Univ. P. et M. Curie 75005 PARIS, France
BENSTSSON Hans Uno	Dept. of Theoretical Physics Solvergatan 14 A 223 62 LUND, Sweden
BORDALO Paola	LPNHE Ecole Polytechnique 91128 PALAISEAU Cedex, France
BOUROTTE Jean	LPNHE Ecole Polytechnique 91128 PALAISEAU Cedex, France
BROWN Charles N.	Fermilab P. O. Box 500 BATAVIA, IL 60510 USA
BURNS Alan	CERN EP Division 1211 GENEVA 23, Switzerland
CALLOT Olivier	L.A.L. Bât. 200 Univ. Paris-sud 91405 ORSAY, France
CAVASINNI Vincenzo	INFN, Via Livornese San Piero a Grado 56100 PISA, Italy
CHARPENTIER Philippe	D.Ph.P.E. / S.E.E. CEN Saclay 91191 GIF SUR YVETTE CEDEX, France
CLEYMANS Jean	Univ. Bielefeld, Fak. f. Physik Postfach 8640 4800 BIELEFELD 1, Germany

COLLINS John C.	Physics Dept. Illinois Institute of Tech. CHICAGO, IL 60616, USA
COX Bradley	Fermilab P. O. Box 500 BATAVIA, IL 60510 USA
DE RUJULA Alvaro	CERN TH Division 1211 GENEVA 23, Switzerland
DOWELL John	Dept. of Physics Univ. of Birmingham, BIRMINGHAM, BI5 2TT, United Kingdom
DUNWOODIE William M.	Stanford Linear Acc. Cent. P.O. BOx 4349 STANFORD, CA 94305 USA
ELLIS R.K.	CERN EP Division 1211 GENEVA 23, Switzerland
ESPIGAT Pierre	Lab. de Physique Corpusculaire 11, Place Marcelin-Berthelot 75005 PARIS, France
FREUDENREICH Klaus	CERN EP Division 1211 GENEVA 23, Switzerland
GRECO Mario	Lab. Naz. INFN Casella Postale 13 00044 FRASCATI, Italy
HAGELBERG Ronald	CERN EP Division 1211 GENEVA 23, Switzerland
HUNGERBUHLER Viktor	CERN EP Division 1211 GENEVA 23, Switzerland
JUILLOT Pierre	CERN EP Division 1211 GENEVA 23, Switzerland
KOURKOUMELIS C.	CERN EP Division 1211 GENEVA 23, Switzerland
KUNSZT Zoltan	Dept. of Atomic Physics Eötvös L. University 1088 BUDAPEST, Hungary

LE COULTRE Pierre	ETH - Zürich HPK - Hönggerberg 8093 ZURICH, Switzerland
LINNEMANN James	The Rockefeller University 1230 York Avenue NEW YORK, N.Y. 10023 USA
LYONS Louis	Nuclear Physics Lab. Keble Road OXFORD OX1 3RH United Kingdom
MAILLARD Jacques	Lab. de Physique Corpusculaire 11, Place Marcelin-Berthelot 75005 PARIS, France
MARTINELLI Guido	CERN TH Division 1211 GENEVA 23, Switzerland
MARTIN François	LAPP Chemin de Bellevue, BP 909 74019 ANNECY LE VIEUX CEDEX, France
MATSUDA Takeshi	Dept. of Applied Math. Osaka Univ. Toyonaka, OSAKA, Japan
MELISSINOS Adrian	Dept. of Physics Univ. of Rochester ROCHESTER NY 14627 USA
MINKOWSKI	Inst. f. Theor. Physik Silderstr. 5 30 12 BERN, Switzerland
MOCKETT Paul	Physics Dept. FM-15 Univ. of Washington SEATTLE, Washington 98195 USA
MOLZON William	CERN EP Division 1211 GENEVA 23, Switzerland
MONTANET Lucien	CERN EP Division 1211 GENEVA 23, Switzerland
MOORE Richard	Theoretische Physik IV Postfach 50 05 00 4600 DORTMUND 50, Germany
PANCHERI-SRIVASTAVA Giulia	Physics Dept. Northeastern Univ. BOSTON, MASS. 02115 USA

PERROTTET Michel	C.N.R.S. Luminy, Case 907 13288 MARSEILLE CEDEX 2, France
PIETRZYK Boleslaw	CERN EP Division 1211 GENEVA 23, Switzerland
PLAUT Guy	Centre de Physique Théorique Parc Valrose 06034 NICE CEDEX France
QUERCIGH Emanuele	CERN EP Division 1211 GENEVA 23, Switzerland
RAHAL Ghita	D.Ph.P.E./S.E.E. CEN Saclay 91191 GIF SUR YVETTE CEDEX, France
RUCKL Reinhold	Fak. fur Physik Postfach 8640 4800 BIELEFELD 1, Germany
SCHREMPP Barbara	II Inst. f. Theor. Phy. Luruper Chaussee 149 2000 HAMBURG 50, Germany
SCHREMPP Fridger	II Inst. f. Theor. Phy. Luruper Chausee 149 2000 HAMBURG 50, Germany
SCOTT David	DAMTP Silver Street CAMBRIDGE CB3 9EW, United Kingdom
SIEGRIST Patrice	D.Ph.P.E./S.E.E CEN Saclay 91191 GIF SUR YVETTE CEDEX, France
SMITH A.J.S.	Physics Depts. Univ. of Princeton PRINCETON, NJ 08540 USA
SONDEREGGER Peter	CERN EP Division 1211 GENEVA 23, Switzerland
SOPER Davison	Institute of Theoretical Science University of Oregon EUGENE, OR 97403 USA
STRAUSS Jozko	CERN EP Division 1211 GENEVA 23, Switzerland

SUTER Henry	Lab. f. Hochenergiephys. ETH. Zurich - c/o SIN 5234 VILLIGEN Switzerland
TILQUIN André	Lab. de Physique Corpusculaire 11, Place Marcelin-Berthelot 75231 PARIS, France
TRAN THANH VAN Jean	L.P.T.P.E. Bât 211 - Univ. Paris-Sud 91405 ORSAY, France
TRIPICCIONE Raffaele	Scuola Normale Superiore Piazza dei Cavalieri, 7 56100 PISA, Italy
VAN NEERVEN Wilhelmus	NIKHEF - H P.O. Box 41882 1009 DB AMSTERDAM, Netherland
VANNUCCI François	L.A.P.P. Chemin de Bellevue, B.P. 909 74019 ANNECY-LE-VIEUX CEDEX, France
VARELA Joào	LPNHE Ecole Polytechnique 91128 PALAISEAU, France
WEISZ Sylvain	LPNHE Ecole Polytechnique 91128 PALAISEAU, France
YAN Tung-Mow	Newman Lab. of Nuclear Studies Cornell Univ. ITHACA, NY 14853 USA

27 ELECTROWEAK INTERACTIONS AND UNIFIED THEORIES

CONTENTS

I – ELECTRON-POSITRON PHYSICS

II – MUON AND NEUTRINO PHYSICS

III – GRAND UNIFIED THEORIES AND NUCLEON INSTABILITY

IV – CONCLUSIONS

26 ELEMENTARY CONSTITUENTS AND HADRONIC STRUCTURE

CONTENTS

25 CURRENT HADRON INTERACTIONS

CONTENTS